ILMATIETEEN LAITOS
METEOROLOGISKA INSTITUTET
FINNISH METEOROLOGICAL INSTITUTE

186
CONTRIBUTIONS

EXPERIMENTAL STUDIES ON CLOUD CONDENSATION NUCLEI ACTIVATION AND CLOUD MICROPHYSICAL PROPERTIES

KONSTANTINOS-MATTHAIOS DOULGERIS

FINNISH METEOROLOGICAL INSTITUTE
CONTRIBUTIONS
No. 186

Experimental studies on cloud condensation nuclei activation and cloud microphysical properties

Konstantinos-Matthaios Doulgeris

Doctoral Programme in Atmospheric Sciences
Institute for Atmospheric and Earth system Research/ Physics
Faculty of Science
University of Helsinki
Helsinki, Finland

Academic dissertation presented for the degree of Doctor of Philosophy

To be presented for public examination with the permission of the Faculty of Science of the University of Helsinki in the Auditorium CK112, Pietari Kalmin katu 5, Helsinki, on April 21th, 2023 at 12 o'clock.

Finnish Meteorological Institute
Helsinki, 2023

Author's contact: Atmospheric Composition Research,
Finnish Meteorological Institute,
P.O. Box 503
FI-00101, Helsinki, Finland,
konstantinos.doulgeris@fmi.fi

Supervisors: Professor Veli – Matti Kerminen
Department of Physics
University of Helsinki, Helsinki, Finland

Dr. David Brus
Atmospheric Composition Research,
Finnish Meteorological Institute, Finland

Reviewers: Dr. Radovan Krejci
Department of Environmental Science & Bolin Centre for Climate Research,
University of Stockholm, Stockholm, Sweden

Dr. Scientist Vladimir Zdimal
Department of Aerosols Chemistry and Physics
Institute of Chemical Process Fundamentals of the CAS, Prague, Czech Republic

Custos: Professor Veli – Matti Kerminen
Department of Physics
University of Helsinki, Finland

Opponent: Dr. Ottmar Möhler
Department of Atmospheric Aerosol Research
Institute of Meteorology and Climate Research,
Karlsruhe Institute of Technology, Karlsruhe, Germany

ISBN 978-952-336-170-6 (print)
ISBN 978-952-336-171-3 (online)
ISSN 0782-6117 (print)
ISSN 2814-5658 (online)
https://doi.org/10.35614/isbn.9789523361713

Edita Prima Oy

Helsinki, 2023

ILMATIETEEN LAITOS
METEOROLOGISKA INSTITUTET
FINNISH METEOROLOGICAL INSTITUTE

Published by **Finnish Meteorological Institute**
(Erik Palménin aukio 1), P.O. Box 503
FIN-00101 Helsinki, Finland

Series title, number and report code of public
Finnish Meteorological Institute Contributions 186,
FMI-CONT-186

Date April 2023

Author
Konstantinos-Matthaios Doulgeris

Title
Experimental studies on cloud condensation nuclei activation and cloud microphysical properties

Abstract

Clouds are considered as a major component of the climate system and the hydrological cycle. Their interaction with aerosol particles provides some of the greatest uncertainties in predictions of climate change. The investigation of cloud condensation nucleus (CCN) and cloud microphysical properties contributes to understanding some of the aerosol cloud interactions mechanisms. Experimental laboratory and field observational data sets are crucial as they can be widely used in different phases of aerosol cloud activation; from activating cloud condensation nuclei to cloud evolution and dynamics.

In this thesis, one aim was to investigate CCN in laboratory measurements. Thus, a new experimental laboratory setup, the Finnish Meteorological Institute Aerosol Cloud Interaction Tube (FMI-ACIT) is introduced and its ability to measure CCN is tested. Particularly, the optimal conditions of the experimental set up were found out and presented. Also, for establishing that FMI-ACIT can perform as CCN counter, experiments in several supersaturations and different aerosol sizes were executed. It was shown that FMI-ACIT can measure the activation and the growth of ammonium sulfate particles in supersaturations ranging from 0.18% to 1.25%.

Furthermore, cloud microphysical properties using measurements from a subarctic environment are investigated and new methods to measure cloud properties in an environment where supercooled clouds occur frequently are tested. For this reason, field experiments using ground-based cloud spectrometers were performed. Limitations were set on the performance of three ground-based cloud spectrometer setups and recommendations were made on their usage. One key output is that it is of high importance for the setups to face the wind direction to minimize the sampling losses. Along with a semi long term data set of cloud microphysical properties, new information on how the characteristics and forcing mechanisms of low-level clouds were affected from long transport air masses: mainly from marine (clean areas) and continental (polluted) areas. The classification of the air masses was based on Flexpart calculations. The analysis of the field observations showed that the microphysical properties of the clouds we sampled during Pallas Cloud Experiments and the air mass source region are connected. The higher values of cloud droplet number concentrations were related to air masses coming from the continental areas and the lowest values of number concentration were related to marine air masses.

Publishing unit
Atmospheric composition research

Classification (UDC)	Keywords
551.574.1	cloud condensation nuclei
159.922.25	cloud droplets
211-17	arctic regions

ISSN and series title	ISBN
0782-6117 (print), 2814-5658 (online)	978-952-336-170-6 (print)
Finnish Meteorological Institute Contributions	978-952-336-171-3 (online)

DOI	Language	Pages
https://doi.org/10.35614/isbn.9789523361713	English	47

Acknowledgements

The research in this thesis was carried out at the Finnish Meteorological Institute. I am highly grateful to Dr. Ottmar Möhler for accepting to serve as my opponent. I would like to thank both Dr. Radovan Krejci and Dr. Vladimir Zdimal for reviewing this thesis and for their comments.

I want to thank my supervisors David Brus and Veli Matti Kerminen - without you this thesis would have never happened. Most of my gratitude goes to my main supervisor David. Thanks for being a great mentor and believing in me since the very beginning of my studies and encouraging me during all the difficulties. I learned a lot from you. You were also extremely patient during our discussions and disagreements. Thanks for fun moments and the numerous hours spending with me on the field but also at the sauna. Especially our days at Pallas will be never forgotten. Veli-Matti, thanks for continuous support and hours spent to help, educate me and taking care of many practicalities.

I am deeply grateful to Eija Asmi for taking me in her group in 2014 when I started my PhD work. You were and still are a great group leader but also a good friend that was always supportive to me. Not only to me but also towards my cat, every time I was traveling to Greece. I would also like to thank Antti Hyvärinen who, as a group leader and currently as the head of the atmospheric composition group, supported me and let me focus on my PhD research. You are one of the most charismatic and inspiring leaders someone could have. I thank all my co-authors Tomi Raatikainen, Mika Komppula, Sami Romakkaniemi, Ewan O'Connor, Heikki Lihavainen and Ville Vakkari for all the help and discussions. Also, I would like to thank Michael Todt for the helpful language tips.

I acknowledge KONE foundation for supporting financially my PhD research. In addition, I thank FMI, University of Helsinki, and ACTRIS for the financial support, including many inspiring travels to participate in courses, show my results and meet talented scientists at international conferences.

I sincerely thank my colleagues at FMI for continuous peer-support and for lighting my working days. I would also like to thank all my dear friends who helped me release working stress either by having beers, playing basketball or watching PAOK football games. You have always been one of the most important sources of strength to continue this process.

To my parents, everything I will ever accomplish – and it will always not be enough – is due to you and for you. You provided me the best education I could ever get- to be curious, to work ethically to respect and serve the common good. Ευχαριστώ μαμά, ευχαριστώ μπαμπά. Σας αγαπάω πολύ.
Ευχαριστώ όλη την οικογένεια μου που είναι μακριά. Μου λείπετε όλοι και σας αγαπάω. I want to dedicate this work also to those who are not in life anymore and I am sure that they are continuously watching me from above and are proud of me. Παππού Κώστα, γιαγιά Αναίτ, παππού Ματθαίε, είναι αφιερωμένο και σε εσάς, σας έχω πάντα στην καρδιά μου.

Finally, I do not have enough words for the most important women in my life – my other half Tonia and my two princesses Ariadni and Maida. Everything I do, I do it for you. Tonaki, my magnificent queen, inspiring personality and loving protector, thank you for making me believe that anything is possible. I know you continuously believed in me, no matter what, and even when I did not. Σε αγαπάω! Thank you.

Kostantinos-Matthaios Doulgeris, Helsinki, 2023

List of original publications

I. Doulgeris, K. M., Brus, D., Raatikainen, T., and Kerminen V.-M.: A Finnish Meteorological Institute–Aerosol Cloud Interaction Tube (FMI–ACIT): Experimental setup and tests of proper operation, J. Chem. Phys., 149, 124201, https://doi.org/10.1063/1.5037298, 2018.

II. Doulgeris, K.-M., Komppula, M., Romakkaniemi, S., Hyvärinen, A.-P., Kerminen, V.-M., and Brus, D.: In situ cloud ground-based measurements in the Finnish sub-Arctic: intercomparison of three cloud spectrometer setups, Atmos. Meas. Tech., 13, 5129–5147, https://doi.org/10.5194/amt-13-5129-2020, 2020.

III. Doulgeris, K. M., Lihavainen, H., Hyvärinen, A.-P., Kerminen, V.-M., and Brus, D.: An extensive data set for in situ microphysical characterization of low-level clouds in a Finnish sub-Arctic site, Earth Syst. Sci. Data, 14, 637–649, https://doi.org/10.5194/essd-14-637-2022, 2022.

IV. Doulgeris, K. M., Vakkari, V., O'Connor, E. J., Kerminen, V.-M., Lihavainen, H., and Brus, D.: Influence of air mass origin on microphysical properties of low-level clouds in a subarctic environment, Atmos. Chem. Phys., 23, 2483–2498, https://doi.org/10.5194/acp-23-2483-2023, 2023.

List of Acronyms

AF	Activated fraction
C	Condenser
CAPS	Cloud, Aerosol and Precipitation Spectrometer probe
CAS	Cloud and Aerosol Spectrometer
CCN	Cloud Condensation Nuclei
CIP	Cloud Imaging Probe
CPC	Condensation Particle Counter
D_p	Dry diameter
DMA	Differential Mobility Analyzer
DMT	Droplet Measurement Technologies
ED	Effective Diameter
FMI	Finnish Meteorological Institute
FMI-ACIT	Finnish Meteorological Institute aerosol cloud interaction tube
FEMTUBE2	Finite element method tube2 model
FSSP	Forward-scattering spectrometer probe, model 100
GBCS	Ground based cloud spectrometers
H_S	Humification system
LWC	Liquid Water Content
LWC_{HW}	Hot-wire liquid water content
MVD	Median Volume Diameter
N_c	Cloud droplet number concentration
OPS	Optical Particle Sizer
PaCE	Pallas Cloud Experiment
PES	Potential Emission Sensitivity
PMS	Particle Measurement Systems
PR	Preheater
SS	Supersaturation
SS_{exp}	Experimental supersaturation
UAV	Unmanned Aerial Vehicles

CONTENTS

1. Introduction

The Earth system has been severely altered at unprecedented scale and magnitude by human activity (IPCC, 2021). An important part of earth system are aerosols and clouds. They both play an important role in the atmospheric radiation budget; aerosol reflect sunlight and they have a potential to activate into cloud droplets i.e., act as cloud condensation nuclei (CCN). Clouds also affect climate by scattering and absorbing radiation. Currently, clouds and their interaction with aerosol particles provide some of the greatest uncertainties in predictions of climate change (Boucher et al., 2013; Sherwood et al., 2020). This is, in large part, because the properties of clouds and their formation processes are poorly understood, particularly the properties and formation processes of mixed phase clouds and ice clouds (Penner et al., 2001; McCoy et al.,2016). Specifically, the area of the Arctic exerts a special influence on global change. This happens since the Arctic is warming about twice as fast as the global average, a phenomenon known as arctic amplification effect (Serreze and Barry, 2011; Post et al.,2019). The impacts from this effect are expected to extend well beyond the Arctic region (Wendisch et al., 2019; Shupe at al.,2022). Additionally, low-level clouds are important for the Arctic climate through the warming of near-surface air (Shupe and Intrieri, 2004 ; Zuidema et al., 2005).

Microphysical properties of clouds and dynamics of cloud formation processes are poorly understood and need to be investigated further (Morrison et al., 2020). Some of the essential cloud microphysical parameters in studying aerosol-cloud-climate interactions are the total number concentration and effective radius of cloud droplets, cloud liquid water content and the relative dispersion of a cloud droplet population (Komppula et al., 2005; Lihavainen et al., 2008; Donovan et.al., 2015; Chang et al., 2019; Morrison et al., 2020). Detailed observations of cloud microphysical parameters will lead to a better understanding of the processes that drive sub-Arctic climate and will help to achieve a better representation of clouds in the models to predict the future of the whole region (Grabowski et al., 2019). Currently, existing numerical models poorly reproduce the Arctic cloud cover. This is happening because understanding of clouds representation even on a small scale is low.

The focus of this thesis is on CCN activation and cloud microphysical properties of low-level clouds. The general goal of this thesis has been to increase our knowledge on how to perform CCN activation experiments and *in situ* cloud measurements. Specifically, this work aims to shed new light on how to investigate CCN activation under controlled laboratory conditions, and how to monitor cloud microphysical properties of low-level clouds in a subarctic environment. The general goal is addressed in four research articles, through more specific research questions and aims:

1. **There is a continuous need for new experimental setups that can measure the activation and subsequent growth of aerosol particles under defined laboratory conditions. How can the optimal operational characteristics and the ability to work as a CCN counter of such an experimental setup could be verified?**

In paper I, the aim was to introduce a multi-purpose instrument for investigating atmospherically relevant interactions between aerosol particles and water vapor under defined laboratory conditions. Several simulations and experimental tests were conducted to find out the optimal operational parameters of the experimental setup and to investigate its ability to perform as cloud condensation nuclei (CCN) counter.

2. **There is an increased demand for long-term continuous ground-based in situ cloud measurements. How cloud spectrometer probes can be operated to perform those measurements in harsh (e.g., subarctic) environments?**

In papers II and III, the aim was to test the usage and the operation of cloud ground-based spectrometers (GBCS) for *in situ* cloud measurements (paper II), and to make a semi long-term data set of *in situ* cloud microphysical properties available to the scientific community (paper III). The evaluation the GBSC' performance and their limitations for future studies were set in paper II. In paper III, a semi-long data set of cloud microphysical properties, as monitored by the cloud spectrometers along with several meteorological variables, were published (eight PaCE campaigns conducted during autumns from 2004 to 2019).

3. **How do long-range transport air masses affect cloud microphysical properties?**

After verifying the measurement method (GBSC) and exploring possible limitations, our aim was to investigate differences in the cloud microphysical properties of low-level clouds between air masses originating from different regions (clean vs polluted air) (paper IV). A detailed analysis was made to reveal that the origin of the long-range transport of air masses should be considered as a significant influencing factor, complementary to the local meteorological parameters, when investigating cloud microphysical properties.

This thesis is structured as follows: in section 2 the background of this thesis is discussed. Next, in Section 3, data and methodology used in this thesis are briefly described. Then, the main results are presented in section 4 followed by the review of papers and author's contribution in section 5. Afterwards, the conclusions are presented in section 6. Finally, the four published papers are printed in order of their publication.

2. Theoretical framework and historical background

Several instruments such as cloud condensation nuclei counters and cloud spectrometers are used to measure CCN activation in laboratory and cloud microphysical properties in the field. Here, a short introduction to cloud condensation nuclei, clouds and the role of cloud microphysics is presented (Sect. 2.1). Lastly, the most relevant laboratory CCN counters and ground-based in situ cloud measurements of cloud microphysical properties are presented in Section 2.2.

2.1 CCN and cloud microphysics

2.1.1 Cloud condensation nuclei

Aerosol particles are liquid or solid particles suspended in a gas (Hinds, 1999). They have a large number of different natural and anthropogenic sources, a wide variety of chemical compositions, and sizes that can span over four orders of magnitude. Aerosol particles can absorb or scatter incoming solar radiation, and they have the potential to serve as cloud condensation nuclei (CCN) (Aitken, 1881; Myhre et al., 2013). CCNs are considered as cloud "seeds" in the atmosphere, as water vapor condenses onto them to form a cloud droplet. The number concentration of CCN affects cloud microstructure and precipitation processes, and thereby the radiative properties of clouds, atmospheric circulation and thermodynamics, as well as radiative budgets (Paramonov et al., 2015; Schmale et al., 2017). The ability of aerosol particles to act as CCN is dependent on multiple factors, such as the supersaturation of water vapor, aerosol size (Kelvin effect) (Petters and Kreidenweis, 2007) and its chemical composition (Raoult effect) (Seinfeld and Pandis, 1998). Supersaturation is achieved when the partial pressure of water is higher that it's equilibrium vapor pressure at a given temperature. Aerosol particles with higher CCN activities, such as larger particles, will form cloud droplets at lower supersaturations. Fig. 1 demonstrates a simplified procedure of CCN activation in typical supersaturations for different particle sizes. The CCN sizes are significantly smaller in comparison with a cloud droplet. For example, an aerosol particle to be able to act as CCN needs to be larger than 20-30 nm while a typical cloud droplet ranges from few micrometers to 100 µm, and a typical raindrop would be range from several hundred micrometers to several millimeters.

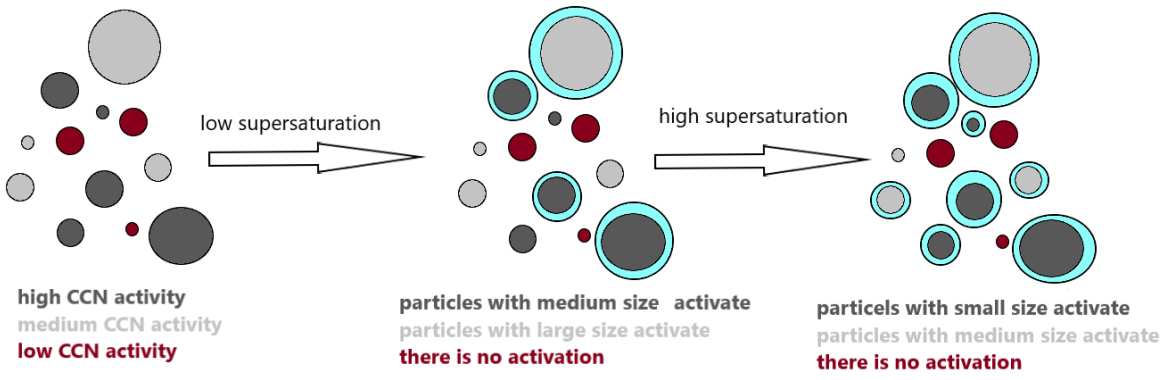

Figure 1. Simplified schematic of CCN activation in typical supersaturations in atmosphere.

2.1.2 Cloud microphysics

The results of CCN activation along with several complex procedures is the formation of clouds. In general, the cloud droplets form when humid air rises and becomes supersaturated with respect to water. Clouds are the most conspicuous and observable aspects of the atmosphere. They consist of millions of water droplets, all so fine that they remain suspended in the air. They transport moisture, heat, and impulse. They are of high interest due to their ability to reflect and absorb radiation (McFarquhar et al., 2020). In the case where cloud formation occurs at or below freezing temperatures, icy crystals can be formed (Korolev et al., 2017). Thus, a cloud can consist of water, ice crystals or both. In general, clouds are classified according to their form and height. (Howard, 1803) (Fig. 2). In papers II-IV, the measurements that were performed related to low level clouds. Low level clouds form near Earth's surface and can be divided into three categories: Stratus low level clouds are uniform fog-like layers of clouds that frequently cover much of the sky. They can also produce light precipitation. Stratocumulus low level clouds have a scalloped bottom that appears as broken globular patches. Last, nimbostratus low level clouds tend to produce precipitation and low visibility.

Investigating cloud microphysics is crucial as the properties of clouds are poorly understood. Detailed information on the size, shape, mass and optical properties of cloud droplets over a broad range of atmospheric conditions is needed to understand the processes of cloud formation. Using the term "cloud microphysics" in the atmosphere, we refer to all the small-scale processes driving the formation and evolution of the cloud and precipitation particles. These processes are extremely complicated due to the huge number of particles present in a cloud, the variety of particle shapes, and complex nonlinear interactions among these processes. Microphysics are important because they influence forecasts of both global (Bodas-Salcedo et al., 2019) and local weather events (Morrison et al., 2020). In addition, one of the main sources of uncertainties in the influence of microphysics on climate is through aerosols on the size and number of cloud particles (Boucher et al.,2013). In this thesis (PAPER II-IV), the clouds that were sampled and investigated were mainly warm and mixed phase clouds.

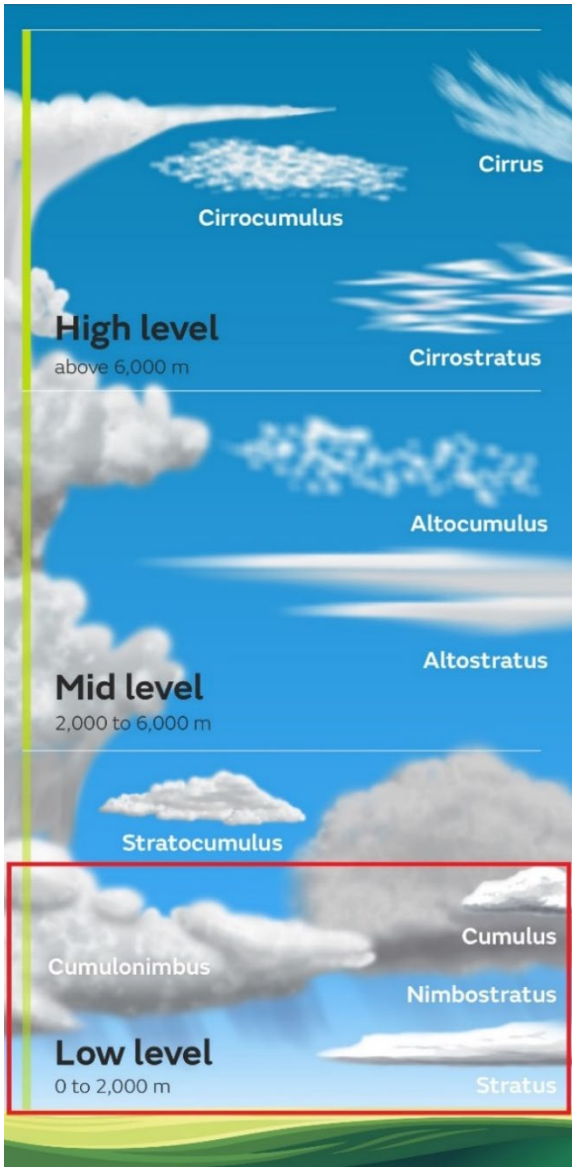

Figure 2. Different form and type of clouds according to Howard classification (Howard, 1803). Cloud types investigated in this thesis (PAPER II-IV) are shown in the red frame. Original figure was adopted from the word meteorological organization.

2.2 History of observations on CCN and clouds microphysics

2.2.1 CCN laboratory counter devices

Several devices with different set ups have been created and used to investigate CCN. Generally, CCN counters can be classified into two categories according to the production of water vapor supersaturation.

1) by using the nonlinear dependence of water vapor pressure upon temperature. This concept is used in static diffusion chambers where they consist of two parallel metal plates, held at different temperatures, with their facing surfaces wetted (e.g., Twomey, 1963; Katz, 1970).
2) by using the difference between water vapor diffusivity and thermal diffusivity. This concept is used in laminar flow chambers where laminar flow is employed between two parallel plates

(e.g., Hudson, 1989; Stratmann et al., 2004; Roberts and Nenes, 2005; Conolly et al., 2012; PAPER I).

The device that was used in this thesis is a laminar flow CCN counter and can be used only for laboratory experiments. Several devices from both categories were widely used in laboratory experiments as well. A theoretical analysis of four different CCN counters from both categories was done by Nenes et al. (2001). The first static diffusion chamber was introduced by Twomey (1963). Sinnarwalla and Alofs (1973) implemented the continuous flow parallel metal plate thermal diffusion chamber to avoid limitations of the static diffusion chamber. Fukuta and Saxena (1979) improved the continuous flow parallel metal plate thermal diffusion chamber, which allowed particles with the same residence time to experience different supersaturations along different streamlines. The Leipzig Aerosol Cloud Interaction Simulator (LACIS) setup and its operation characteristics, which was also based on a laminar flow tube, was introduced by Stratmann et al. (2004). Wex et al. (2006) performed CCN laboratory experiments with the Leipzig Aerosol Cloud Interaction Simulator where it was established that the setup is a CCN detector able to measure hygroscopic growth of atmospheric particles. Snider et al. (2006) derived the maximum steady-state supersaturation within the Wyoming CCN Instrument. In 2005, Robert and Nenes presented a cylindrical continuous-flow thermal-gradient diffusion chamber where different supersaturation values from 0.1 to 3% could be produced by establishing a constant streamwise temperature gradient so that the difference in water vapor and thermal diffusivity yields a quasi-uniform centerline supersaturation. Rose et al. (2008) fully explored the Robert and Nenes (2005) CCN counter by performing calibration experiments using ammonium sulphate and sodium chloride particles and discovered the supersaturation using the Kohler theory (Kohler,1936). For the CCN counter we presented in Paper I, a similar method is utilized as ammonium sulphate particles are used for CCN experiments and the Kohler theory is implemented to calculate the supersaturation value.

2.2.2 In situ cloud measurements

Several instruments have been developed since 1970 to attempt to measure cloud microphysical properties. The approaches that were used for this reason can be split into four categories.

1) Instruments deployed on aircrafts and flights through the cloud (e.g., Heymsfield et al., 2011; Craig et al., 2014; Petäjä et al., 2016; Nguyen et al., 2021),
2) Instruments deployed on unmanned aerial systems (UAVs) (e.g., Girdwood et al., 2020; Brus et al., 2021; Harrison et al., 2021, Girdwood et al., 2022),
3) Cloud chambers used in laboratory under controlled parameters (e.g., Möhler et al., 2003; Stratman et al., 2004; Nichman et al., 2017), and
4) In situ ground-based measurements (e.g., Guyot et al., 2015; Lloyd et al., 2015; Lowenthal et al., 2019; PAPER II, III, IV) when the cloud spectrometers were deployed on ground station that were occasionally inside a cloud.

In this thesis (Papers II-IV), the last method of performing cloud measurements was used. In situ ground-based measurements using cloud spectrometers are considered fundamental as they offer instrumental access to individual hydrometeors within a sampling volume (Wandinger et al., 2018). The instruments we used for in-situ ground-based measurements were the cloud spectrometers (e.g.,

Knollenberg, 1976; Dye and Baumgardner, 1984; Wendish et al., 1996; Baumgardner et al., 2001, 2014; Lance et al., 2010; Smith et al., 2015; Nichman et al., 2017; Lowental et al., 2019). The cloud spectrometers are single particle counters that use forward scattering, usually with the angles between 4 and 12° of a laser beam, to detect and classify individual particles in different size bins. For the particle sizing, the Lorenz–Mie theory (Mie, 1908) is used. The Lorenz–Mie theory is based on the scattering of light from single particles.

Several studies were done both to quantify biases and uncertainties of the ground-based cloud spectrometers (GBSC) (e.g. Gerber et al., 1999; Spiegel et al., 2012; Guyot et al., 2015; PAPER II). Generation of uncertainties is a complicated procedure depending mainly on the different meteorological conditions. Wendish (1998) made a quantitative comparison of ground based forward-scattering spectrometer probe (FSSP) with a particle volume monitor (PVM). He showed that FSSP should be regarded as an excellent microphysical sensor in continental, stratiform or cumuliform clouds with mostly small drops and highlighted discrepancies in the liquid water content for cloud droplets larger than 25 μm. Gerber et al. (1999) evaluated ground-based measurements of liquid water content using an FSSP and a PVM and suggested that the liquid water content overestimated by the FSSP for large droplets due to inertial concentration effect produced by the droplets' inability to follow the curved streamlines of the flow generated by drawing air into the FSSP's sensitive volume at 25 m s^{-1}. Spiegel et al. (2012) compared the fog droplet spectrometer to others instruments for different wind velocity and wind angle impacts and found out that the fog droplet spectrometer experienced several artifacts at temperatures below 0 ^{0}C. Guyot et al. (2015) intercompared seven optical sensors including an FSSP, a fast FSSP, a fog monitor and two CDP probes at the Puy-de-Dôme observatory. It was shown that there was very good correlation in the sizing abilities of the instruments, both in terms of amplitude and variability, but they observed discrepancies in number concentration and the liquid water content values.

Throughout the development and the evaluation of the GBSC as a method to investigate cloud microphysics several studies adopting this method of measurements were performed (e.g., Lihavainen et al., 2008; Romakkaniemi et al., 2017; PAPER III, IV). During Pallas Cloud Experiment 2004, Lihavainen et al. (2008) proved that there was a clear Twomey effect depending on air mass origin. Portin et al. (2009) found clear evidence of the aerosol indirect effects at the Puijo site showing that there was positive correlation between cloud droplet number concentration and aerosol particle number concentration. Asmi et al. (2012) provided evidence on the effects of aerosol particles on maximum cloud supersaturations by showing that the cloud droplet number concentrations increased with accumulation mode particle number, while the real in-cloud supersaturation correspondingly decreased (Puy de Dôme observatory). Lloyd et al. (2015) observed high concentrations of ice particles that exceeded 1000 L^{-1} at temperatures around −15 °C at the Sphinx Laboratory, (Jungfraujoch, Switzerland) and stated that changes in the liquid water content leading to significant changes in ice mass fraction values were occurring over temporal scales of seconds to hours. Romakkaniemi et al. (2017) suggested that when the wind direction aligned with the direction of the steepest slope of the hill close to the Puijo tower, a clear topography effect was observed. Lowenthal et al. (2019) examined microphysical properties of wintertime mixed-phase orographic clouds at the Storm Peak Laboratory (Colorado, USA) and showed that cloud droplet size distribution, number concentration and liquid

water content maintained similar values from 2011 to 2014. Renard et al. (2020) stated that the influence of cloud microphysics remained minor at the Puy de Dôme compared with the impact of the air mass history. Iwamoto et al. (2021) suggested that the cloud droplet number concentrations were significantly higher when continental air masses were arriving to the study site than in air masses arriving from the Pacific Ocean.

3. Material and methods

The main instruments, experiments and modeling work used in this thesis are described in this chapter. It consists of two types of measurements, laboratory studies (PAPER I) and field measurements (PAPERS II-V). For detailed description, kindly refer to the original publications.

3.1 Laboratory studies

3.1.1 The Finnish Meteorological Institute Aerosol Cloud Interaction Tube (FMI-ACIT)

The setup that was introduced in PAPER I, the FMI-ACIT, is based on the principle of a laminar flow diffusion chamber (Lihavainen and Viisanen, 2001) and shares the design of the laminar flow tube that was used in previous studies (Brus et al., 2010; Neitola et al., 2014). A schematic figure is presented in Fig. 3. The setup consists of three main components: the humidification system (H_S), the preheater (PR), and the condenser (C). To adjust and control the temperatures of the humidification system and preheater, two circulating liquid baths (LAUDA RC 6 CS) were used. The temperature of the condenser was controlled by a different circulating liquid bath (LAUDA Proline RP 1845). To monitor the temperature values, six PT100 probes were deployed. To ensure that the environmental temperature will not affect the setup, each part of it was insulated. The polydisperse aerosol was produced by an aerosol generator (Topas, model ATM226) and dried with a silica-gel dryer. Then, the polydisperse aerosol was size selected by a differential mobility analyzer (DMA, Hauke type, length 0.109 m). The concentration of the monodisperse aerosol was monitored by a condensation particle counter (CPC, model 3776, TSI, Inc.). As a counting system of the setup, an Optical Particle Sizer (OPS model 3330, TSI, Inc. USA, 0.3–10 μm) was deployed at the end of the condenser. The OPS was modified to bypass the OPS pump. The tube of the total flow passed through the OPS counting chamber, and the raw counts were corrected accordingly.

The humidification system consists of one saturator and four Nafion humidifiers. The temperature of this part controlled the amount of vapor in the air flow. One humidifier was placed after the aerosol size selection and the remaining three humidifiers were placed in parallel to the saturator to humidify the sheath flow. The saturator was a horizontal iron tube with a Teflon insert having an inner diameter, I.D. = 5 cm and length L = 1 m. A steady flow of purified and particle free air was introduced to the humidification system using ultrapure milli-Q water (resistivity 18.2 MΩ cm at 25 °C). Aerosol enters the preheater from the humidification system through the stainless-steel tube I.D. = 4 mm and length (inside the preheater) L = 5 cm.

The preheater is a stainless-steel cylinder (I.D. = 6 cm, L = 0.5 m). Its temperature was set always higher (∼1°C) than the temperature of the humidification system to stabilize the flow and avoid condensation in the top section of the flow tube. The sheath flow entered the preheater via a Teflon part having ports (I.D. = 1 mm). The total flow inside the flow tube combined aerosol and sheath flow. Those were kept constant with a mass flow controller to within ±3% (MKS type 250). The sheath flow was measured continuously with a mass-flow meter (model 4043, TSI, Inc.) placed before the humidification system and the aerosol flow was measured before and after every run with a bubble flow meter (Gilian Gilibrator2 air flow calibrator, Sensidyne) placed after the DMA and before the flow enters the Nafion humidifier.

The condenser is a stainless-steel cylinder and has I.D. = 6 cm and L = 1 m. It was installed vertically along with the preheater to avoid gravitational settling of the particles. The temperatures were monitored with four PT100 probes. The connection between preheater and condenser was insulated resulted a steep temperature change. Thus, supersaturation was created at well-defined conditions.

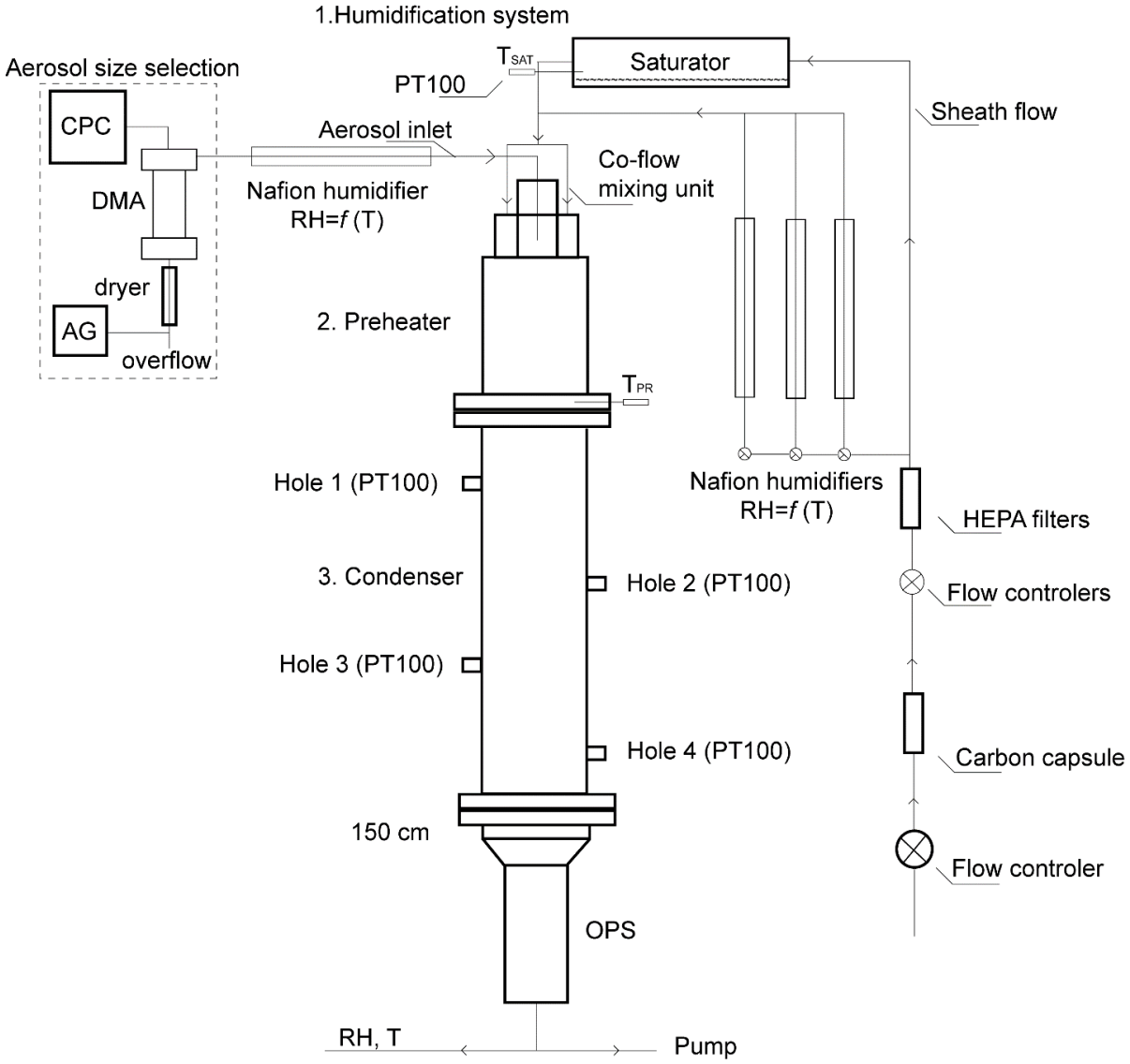

Figure 3. Schematic figure of the FMI-ACIT setup using the OPS as a counter to perform CCN laboratory experiments. Figure from Paper I.

To test the ability of FMI–ACIT (in Paper I) to measure CCN we calculated the activated fraction (AF) of the activated particles. AF was defined as

$C_{A,END}/C_{A,INIT}$, where (1)

$C_{A,END}$ is the concentration of activated aerosol at the end of FMI–ACIT measured by the OPS and $C_{A,INIT}$ is the initial concentration of aerosol before entering the preheater measured by the CPC.

3.1.2 The Finite element method tube2 model (FEMTUBE2)

The saturation ratio and the temperature profiles inside the condenser of the FMI–ACIT cannot be measured directly. For that reason, in PAPER I, an existing finite element method tube 2 (femtube2) model was adopted (Lihavainen, 2000).
The model solves five coupled differential equations, heat and mass transfer, equations of motions, and an equation of continuity to simulate the flows inside the condenser. To simplify these equations, three assumptions were made: 1) the equations can be solved in a steady state, 2) the effect of radial velocity is negligible and set to zero, and 3) the flow is incompressible. The above simplifications of the equations of motion lead to a simple problem that was analytically solved and produced a parabolic lateral velocity profile (Bird et al.,1960).

The boundary conditions for the heat and mass transfer equations are

$$T(r,z = z_0) = T_{PR}, \quad (2)$$

$$T(R_0,z_0 < z \leq 0) = T_{PR}, \quad (3)$$

$$T(R_0,z > 0) = T_C, \quad (4)$$

$$\omega(r,z = z_0) = \omega_{eq}(T_{HS}), \quad (5)$$

$$\omega(R_0,z_0 < z \leq 0) = \omega_{eq}(T_{HS}), \quad (6)$$

$$\omega(R_0,z > 0) = \omega_{eq}(T_C), \quad (7)$$

where T_{PR} is the temperature of the preheater, T_C is the temperature of the condenser, T_{HS} is the temperature of the humidification system, and R_0 is the radius of the tube. $\omega_{eq}(T_{HS})$ is the mass fraction of water vapor defined by the saturation vapor pressure at the temperature T_{HS}, $\omega_{eq}(T_C)$ is the mass fraction of water vapor defined by the saturation vapor pressure at the temperature T_C, $z = 0$ is the boundary point between the preheater and the condenser, and z_0, −10 cm, is a chosen starting point of calculations in the preheater.

The first boundary condition in Eq. (2) sets the temperature at z_0 to that of the preheater. The second boundary condition in Eq. (3) sets the temperature of the wall between the starting point of the calculation, z_0, and the boundary between the preheater and the condenser, $z = 0$. The third boundary condition in Eq. (4) sets the temperature at the wall of the condenser. The fourth boundary condition in Eq. (5) sets the mass fraction profile across the tube at z_0 to the value defined by the equilibrium vapor pressure at the temperature of the saturator. The fifth boundary condition in Eq. (6) sets the mass fraction of the vapor at the wall between z_0 and z to the same value as the fourth boundary condition. The sixth boundary condition in Eq. (7) sets the mass fraction at the wall of the condenser to the value defined by the equilibrium vapor pressure at the temperature of the condenser wall.

3.1.3 The droplet growth model

To describe the growth of the particles inside the flow chamber, we used the droplet growth model as described in detail in Raatikainen et al., (2012).
The rate of the change of the droplet size is described by the differential growth equation (Seinfeld and Pandis, 1998; Fukuta and Walter,1970)

$$D_p \frac{dD_p}{dt} = \frac{S - S_{eq}}{\frac{\rho_w R T_\infty}{4p^0(T_\infty) D_u^{'} M_w} + \frac{\Delta H_u \rho_w}{4\kappa_\alpha^{'} T_\infty R}\left(\frac{\Delta H_u M_w}{T_\infty R} - 1\right)}, \quad (8)$$

where D_p is the droplet diameter,

S and S_{eq} are ambient and droplet water equilibrium saturation ratios,

ρ_w is the water density,

M_w is the molar mass of water,

T_∞ is temperature of the environment,

$p^o(T_\infty)$ is water saturation vapor pressure at temperature of the environment,

$D_u^{'}$ is the diffusivity of water,

$\kappa_\alpha^{'}$ is the thermal conductivity of air that account for non-continuum effects

and ΔH_u is the water vaporization enthalpy.

The initial value problem is in Equation (8) where temperature and water vapor saturation ratio depend on time or on the location of the droplet in the flow tube. The femtube2 model was used to generate supersaturation and temperature profiles inside the flow tube and the droplet velocity was calculated from the total flow rate while assuming a parabolic lateral velocity profile.

For the calculation of the water equilibrium saturation ratio of the growing droplets, Kohler theory is used (Kohler, 1936)

$$S_{eq} = a_w exp\left(\frac{4\sigma M_w}{R T_\infty \rho_w D_p}\right) \quad , \quad (9)$$

where σ is the surface tension and a_w is the Raoult term and it is calculated following the kappa-Kohler approach (Petters and Kreidenweiss, 2007; 2008)

$$a_w = \left(1 + \frac{\kappa}{\left(D_p/D_{dry}\right)^3 - 1}\right)^{-1}, \quad (10)$$

where D_{dry} is the dry diameter of the particle and κ is a single solute hygroscopicity parameter.

3.2 Field experiments

3.2.1 Research area

Measurements of the field work (PAPER II-IV) were conducted in the measuring site - Sammaltunturi station (67°58'N, 24°07'E) at northern Finland (Fig. 4). The Sammaltunturi station, part of the Pallas Atmosphere-System Supersite and the Global Atmospheric Watch, resides on a top of the second southernmost fjeld, a round topped treeless hill, in a 50-km-long north and south chain of fjelds at an elevation of 565 meters above sea level. The surrounding environment is consisting of mixed pine, spruce, and birch and the vegetation on the fjeld top is sparse. Due to its altitude, the Sammaltunturi station is from time to time immersed into a cloud and it is considered as an excellent place to perform in situ low level cloud measurements.

The most suitable time of the year for in situ cloud measurements is autumn when the horizontal visibility drops below 1 km around 40 % of the time (Hatakka et al., 2003). Thus, the field experiments used in this thesis (PAPER II-V) were conducted during Autumn. Particularly, the Pallas Cloud Experiments (PaCE) were, usually, 6 – 8 weeks long and lasted approximately from the beginning of September until the end of November, occasionally extended to the beginning of December.

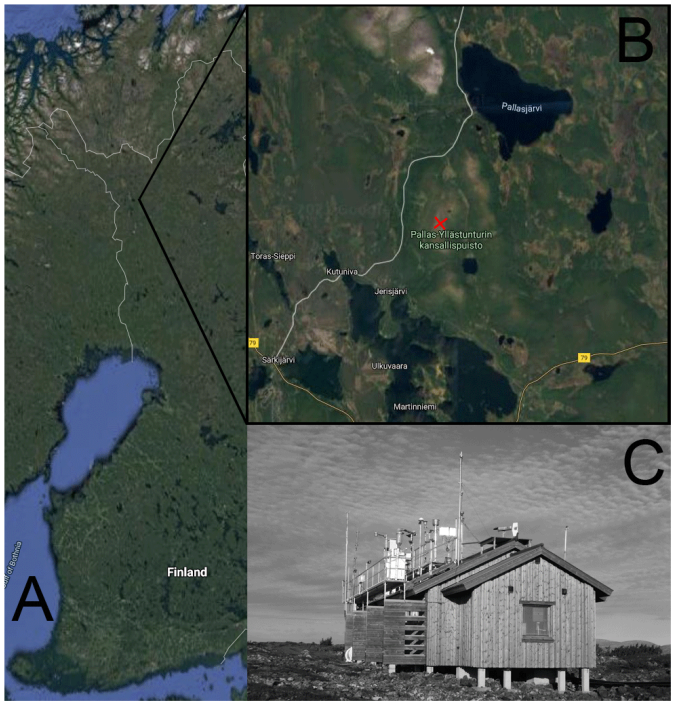

Figure 4. Map of the Sammaltunturi measuring station where the PaCE were conducted. Figure from Paper III.

3.2.2 Field instrumentation

The GBCS are the main instrumentation used for the research presented herein, and the cloud measurements that have been analyzed and presented in this thesis (Papers II-IV). In-situ cloud measurements were conducted at the Sammaltunturi station with three different cloud

spectrometers. In particular, the Cloud, Aerosol and Precipitation Spectrometer probe (CAPS, Droplet Measurement Technologies, Boulder, CO, USA), the forward-scattering spectrometer probe (FSSP) and the cloud droplet probe (CDP, Droplet Measurement Technologies, Boulder, CO, USA), all with tailored inhalation system (Fig. 5). The basic concept of all three instruments is that they use the forward scattering of a laser beam for the detection and sizing of individual particles and then the size of the particle is calculated using Mie theory (Mie, 1908) from the intensity of the scattered light.

CAPS was made by Droplet Measurement Technologies (DMT), Boulder, CO, USA. The CAPS probe includes three instruments: the cloud and aerosol spectrometer (CAS), the cloud imaging probe (CIP), and the hot-wire liquid water content (LWC_{hw}) sensor (Baumgardner et al., 2001,). In this thesis, (papers II and IV) we used only data from the CAS probe except in Paper III where data from the CIP are also provided. CAS (0.51 to 50 μm) relies on light scattering. Particles scatter light from an incident laser at a wavelength of 680 nm and a sample area of 0.24 mm^2, and collecting optics guide the light scattered in the 4 to 12° range into a forward-sizing photodetector. The intensity of light is measured and used to infer the particle size. Backscatter optics also measure light intensity in the 168 to 176° range, which allows the determination of the real component of a particle's refractive index for spherical particles. The droplets are then classified into 30 size bins. The CIP (12.5 to 930 μm) is a single particle optical array probe. Its design is based on optical measurement techniques whereby single particles pass through a collimated laser beam and their shadow is projected onto a linear array of 64 photodetectors. The count of the particle is dependent on the change in the light intensity of each diode. For the ground setup the manufacturer pylon (height 0.3 m) was used. The setup was fixed on a horizontal metallic circle (D = 0.28 m) which was attached to a vertical metallic bar (height 0.3 m), part of a square metallic stand (0.7m × 0.7m). CAPS had its own tailored inhalation system: a high-flow pump (Baldor, Reliance, USA), which worked continuously. The pump was connected with the CAS probe through a 1.14 m long hose with an inner diameter of 0.07 m. The hose was connected to a triple branch (three parts with I.D. = 0.12) through a 0.12 to 0.05 m reducer. The triple branch connected the CAS probe through the hose with the high-flow pump. The other parts of the branch connected the pump with the CIP through two different hoses (L = 1.52 m; I.D. = 0.12 m). In addition, a stepped CAS inlet (funnel shape reducer I.D. = 0.12 to I.D. = 0.05 m) was attached over the CAS inlet tube.

The FSSP (model SPP-100, DMT) was initially manufactured by Particle Measuring Systems (PMS Inc., Boulder CO, USA) and later acquired by DMT. The size range of FSSP-100 is from 0.5 to 47 μm in diameter. FSSP, similarly to CAS, measures the light scattered in the 4 to 12° range with a laser of wavelength 633 nm and a sample area of 0.414 mm^2. The FSSP was installed on a rotating platform (a horizontal metallic base (0.7 × 0.1 × 0.4m) with a metallic fin fixed at the back of it). A vertical metallic bar (L = 0.3 m, D. = 0.6 cm) and two horizontal bars (L = 0.25 m, D = 0.6 cm) were installed (northeast ∼ 60◦) and served as a brake to prevent full rotation of the cloud probe. A custom inhalation system with a high-flow ventilator was employed through the instruments' inlet to ensure that the air speed would remain constant. The droplets then can be classified in 30 or 40 size bins.

The Cloud Droplet Probe (CDP) was used only in Paper II. The CDP is a single optical particle counter manufactured by Droplet Measurement Technologies (DMT) in Boulder, Colorado. It is designed to

detect and classify cloud droplets 3 to 50 µm diameter. Photons forward scattered by particles from within the sample area that fall within an annular cone of 4 to 12° of the incident beam are directed via the second 45° mirror onto an optical beam splitter. The CDP has two arms, 140 mm apart, which house the detecting components of its system. CDP classified droplets into 30 size bins. It was placed on a rotating platform to be continuously directed against the wind direction. The metallic platform covering the instrumental electronics consists of a fixed part (0.4 × 0.4 × 0.3m) at the bottom and on top of that the rotating part (0.4×0.4×0.1m) with the probe itself on top. The rotating part is equipped with a large fin to keep the inlet towards the wind. The instrument had a custom inlet with an external pump to ensure a constant probe air speed.

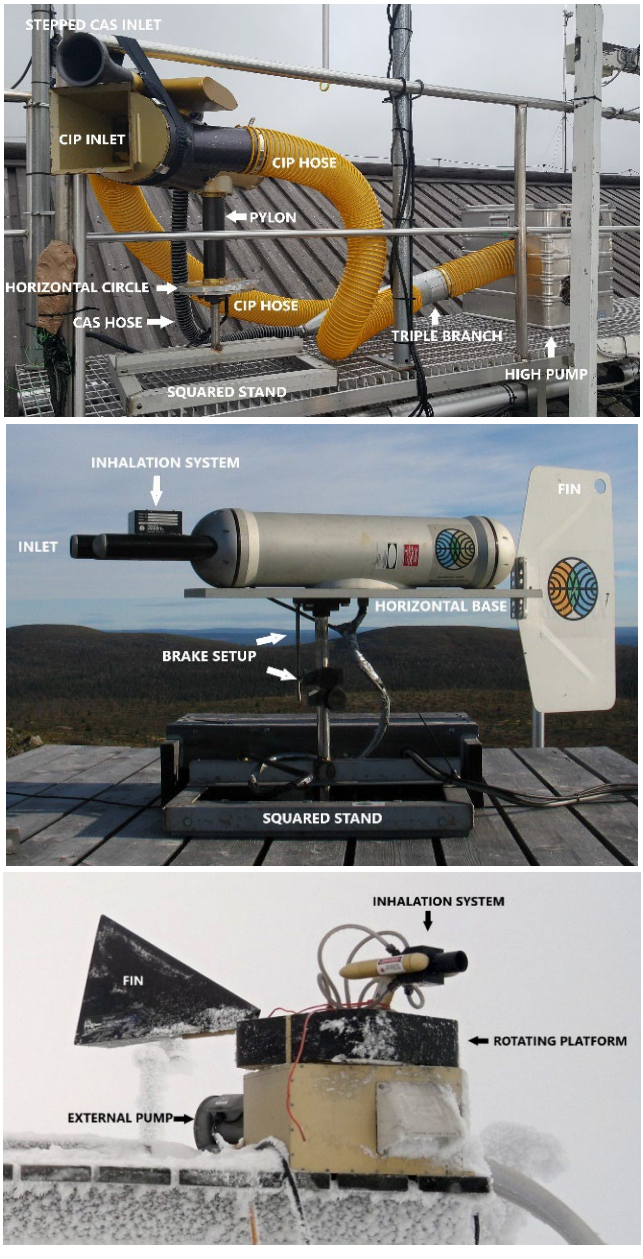

Figure 5. The CAPS, the FSSP, and the CDP ground setups, as they were installed at the Sammaltunturi station during PaCE 2013.

As a result, from the GBCS setups, the cloud droplet size distribution and four derived parameters were obtained: the cloud droplet number concentration, N_c (cm^{-3}), the liquid water content, LWC (g

m^{-3}), the median volume diameter, MVD (μm), and the effective diameter, ED (μm). The description of the three GBCS setups can be found more excessively in Paper II.

The instrument that monitored the cloud base (Paper V) was a Vaisala CT25K (Vaisala users guide, 2002; Emeis et al, 2004) lidar ceilometer, except in 2019 when it was replaced by a Vaisala CL31. The meteorological variables were monitored by an automatic weather station (Milos 500, Vaisala Inc.). All the weather sensors that were used in this work were described in Hatakka et al., (2003). The temperature was measured at 570 meters above sea level by a PT100 sensor, the horizontal visibility by a FDP12P Vaisala weather sensor, the relative humidity by a Vaisala HUMICAP, the barometric pressure by a Vaisala BAROCAP sensor, the wind direction by a heated wind vane and the wind speed by a heated cup. A description of the instrumentation that was used in Paper IV along with their operational parameters and accuracy can be found in table 1.

Table 1: Instrumentation (operational parameters and their accuracy) of the published dataset. Table from paper III.

Instrument	Operating range	Number of bins	Sampling frequency	Air speed range	Accuracy	Uncertainties
Cloud instruments						
CAS, DMT	0.51 μm to 50 μm	10, 20, 30, or 40	0.05 to 40 Hz	10 - 200 ms^{-1}	upper N_c > 1,000 cm^{-3} after corrections for coincidence that are about 25% at 800 and 30% at 1,000 particles/ cm^3 Sizing accuracy: 20%	ambient N_c of 500 cm^{-3}: 27% undercounting and 20%–30% oversizing bias Lance et al. (2012) *LWC*: 40% (DMT Manual)
CIP, DMT	12.5 μm to 1.55 mm	62	0.05 to 40 Hz	10 - 300 ms^{-1}	upper N_c range up to 500 particles/ cm^3 for a CIP with standard tips and arm width sizing accuracy: 1 μm	digitization uncertainty of approximately ±1 size resolution that depends upon where the particle passes across the array Baumgardner et al. (2017)
FSSP, PMS	0.5 μm to 47 μm	15,30 or 40	0.05 to 40 Hz		N_c accuracy: 16% sizing accuracy: ±3 μm	derived *ED*: 3μm derived *LWC*: 30% Febvre et al. (2012)

				LWC accuracy: 30%–50% Baumgardner (1983); Baumgardner et al., (2017)
Meteorological instruments				
	Range	Resolution	Sensitivity	Accuracy
PT100 sensor, Vaisala	-70 – +180 (°C)	0.01 (°C)		±0.1 (°C)
HUMICAP sensor, Vaisala	0 – 100 (%) RH	<0.01 (%) RH		±0.8 (%) RH
BAROCAP sensor, Vaisala	500 – 1000 (hPa)	0.01 (hPa)		±0.15 (hPa)
heated cup and wind vane, Vaisala	0.4 – 75 (ms^{-1}) 0 – 360°	0.1 (ms^{-1}) 1°		±0.17 (ms^{-1}) ±3°
Pyranometer, Vaisala	305 – 2000 (Wm^{-1})		9– 15 ($\mu V\ Wm^{-2}$)	< ±20 Wm^{-2}at 1000 Wm^{-2}
FD12P, Vaisala	10 - 50000 (m)			±10 %, 10 –10000 m ±20 %, 10000 –50000 m

3.2.3 Air mass trajectory model

Air mass origins were analyzed using the Lagrangian particle dispersion model FLEXPART version 10.4 (Seibert and Frank, 2004; Stohl et al., 2005; Pisso et al., 2019). FLEXPART was run backward in time to calculate potential emission sensitivity (PES) fields. PES in a particular grid cell is proportional to the air mass residence time in that cell. Its calculation was done in units of seconds (Seibert and Frank, 2004; Pisso et al., 2019). ERA5 reanalysis by European Centre for Medium-Range Weather Forecasts (ECMWF) was used as meteorological input fields for FLEXPART at 1 hour temporal resolution and 0.25° resolution in latitude and longitude. ERA5 levels 50 to 137 were used in vertical which corresponds approximately to the lowest 20 km above surface. The model domain is from 125° W to 75° E and 10° N to 85° N. This domain was large enough to contain 96 hours simulations backward in time. FLEXPART runs were initiated at an hourly time resolution for the in-cloud measurement periods at Sammaltunturi. The retro plume release height was set to 560-660 meters above sea level, as the terrain height in ERA5 at the site was approximately 300 meters above sea level. The PES output resolution was set to 0.2° latitude and longitude with a 250 meters height resolution up to 5 km and two additional output levels at 10 km and 50 km. However, for the air mass origin analysis here PES was summed up for all output heights at each latitude-longitude grid cell. The air mass source regions for the Sammaltunturi site were divided into five categories: Arctic, Eastern, Southern, Western and Local. Initially, the regions were classified using trajectories cluster analysis, following the method as Eneroth et al. (2003) proposed. The predefined regions were used for different studies and scopes as

atmospheric transport of carbon dioxide (Aalto et.al., 2003), aerosol studies (Tunved et al., 2006; Asmi et al., 2011). In Figure 6, the map of the air mass regions is presented.

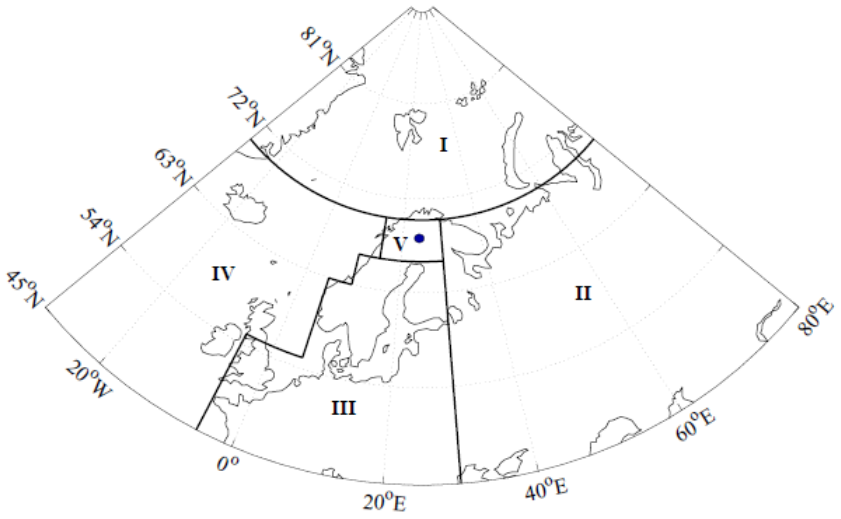

Figure 6. Map of the air mass regions: I (Arctic), II (Eastern), III (Southern), IV (Western) and V (Local). Figure from paper IV.

4. Overview of main results

This chapter present a synopsis of the main results. For detailed results, kindly refer to the original publications.

4.1 Operation of the FMI-ACIT.

In paper I, we introduced a multi-purpose instrument for investigating atmospherically relevant interactions between aerosol particles and water vapor under defined laboratory conditions. The ability of the experimental setup (FMI- ACIT) was tested both for the aerosol activation and droplet growth under supersaturated conditions.

4.1.1 Optimal flow rate

A series of experiments have been conducted to find out what is the most suitable total flow rate, i.e., the sum of the sheath and the aerosol flow rates. Using the femtube2 model, saturation ratio and the temperature profiles along the center line of the condenser were created. For the simulation, constant temperature conditions were set (T_{HS} = 299.00 K, T_{PR} = 300.00 K, and T_C = 281.00 K). The total flows were changed from 0.5 to 1.0 and then up to 10.0 l min^{-1} with steps of 1.0 l min^{-1}. By increasing the total flow rate, the location of the maximum saturation ratio moved further along the centerline of the condenser. For total flow rates higher than 3.0 l min^{-1}, the maximum saturation ratio was observed after 0.4 m along the centerline of the condenser. For flows higher than 2.0 l min^{-1}, there was no change in the maximum saturation ratio along the tube centerline. Maximum saturation ratios were lower than those for 0.5 and 1.0 l min^{-1} flow rates.
Along with the previous simulations, an experimental transmission efficiency test was done to quantify the particle losses using six different total flow rates (1.0, 2.0, 3.0, 5.0, 8.0, and 10 l min^{-1}). During the efficiency test, the temperature conditions were set same as in the simulations. Then, monodisperse ammonium sulfate particles[$(NH_4)_2SO_4$] (sizes of 100, 200, and 300 nm) were injected into the condenser. The number concentration of monodisperse dry aerosols (between 400 and 750 cm^{-3}) was continuously measured at the beginning of the humidification system and droplets were continuously measured at the end of the condenser (between 150 and 745 cm^{-3}). Their ratio produced the counting efficiency for each total flow rate, and it was proved that the investigated setup performs best at total flow rates between 1 and 3 l min^{-1}. At lower total flow rates, the particles grow to bigger sizes, but they could be lost to the wall due to slow flow. At higher flow rates it takes relatively long for the temperature of the flow to stabilize and reach the condenser wall temperature. As a result, the particles do not experience high enough supersaturation to be activated.

4.1.2 FMI ACIT as a CCN counter

As a next step, activation experiments were also performed using the optimal flow rate (2.0 l min^{-1}). Purified, particle free air was used as a carrier gas. Six humidification system and condenser temperature differences (ΔT) were set (18.00, 17.50, 17.25, 17.00, 16.75, and 16.50 K) and produced a different supersaturation inside the condenser. In each scenario, dry ammonium sulfate particles with diameters ranging from 10 to 300 nm were injected into the preheater (10, 15, 20, 25, 30, 40, 50, 60, 70, 80, 90, 100, 150, 200 and 300 nm) and for each size seven minutes measurements were performed. As a result, we obtained the full-size range.

For every set of dry sizes, a sharp increase of the activated fraction occurred, and an activated fraction curve was produced by fitting to our experimental data. In Fig. 7(a), the six obtained activation curves are presented. The higher values of ΔT produced higher values of SS through the centerline of the condenser. For larger particles, the activated fraction increased (average value 0.91 with standard deviation 0.11). To calculate the experimental supersaturation (SS_{exp}), we used the dry diameter from each activated fraction curve for which activated fraction of particles reached 50% (D_{50} diameter) and the temperature of the condenser (through equation 9). A comparison of the model predicted supersaturation and the SS_{exp} is presented in figure 7(b). The linear fit based on six points shown very good agreement between the two supersaturation values (R^2 = 0.98).

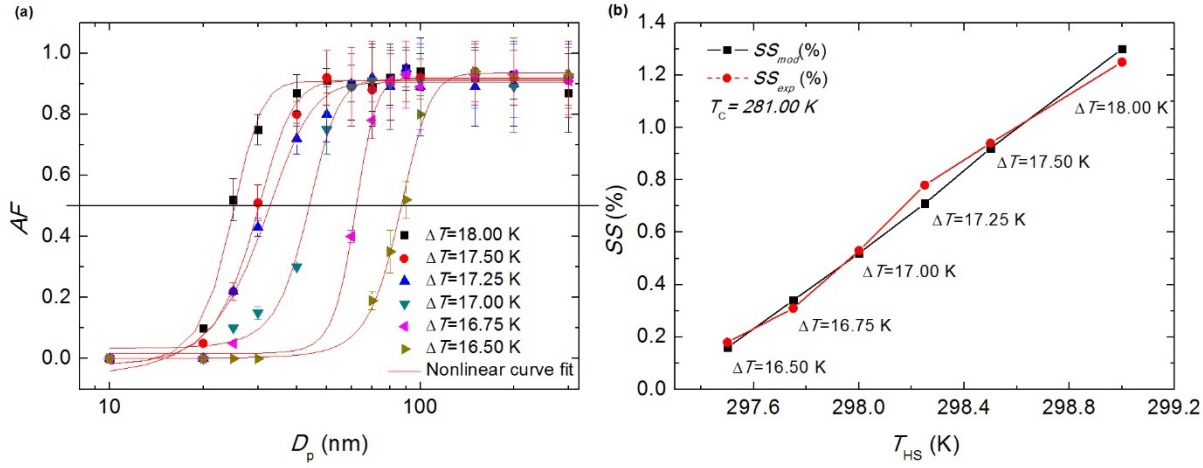

Figure 7. (a) Activated fraction (AF) versus dry diameter (D_p) of ammonium sulfate particles for each ΔT. Nonlinear curve fit was calculated using the sigmoidal dose response function. (b) Maximum supersaturation as it was simulated using the femtube2 model and experimental supersaturation (%) versus the temperature of humidification system. ΔT (difference between the temperature of the humidification system and the condenser) is also provided. Figure from paper I.

Moreover, a comparison of the measured and modeled size distribution for 200 nm ammonium sulfate particles was done to investigate the ability of FMI-ACIT to measure the particle growth. The observed size distributions were wider at supersaturations of 0.18% and 1.25%, which indicates that particles in this experimental setup experienced more variable supersaturations than considered by the modeling. A possible explanation is that an assumption of the model was that all the particles had the same dry size and were travelling in a narrow region close to the centerline of the condenser which resulted in a narrow droplet size distribution. For example, the model predicts that 200 nm particles will grow to 1.4 µm when the supersaturation is 0.18% inside the FMI–ACIT. During the experiments the 200 nm particles grew to different sizes and produced a wider size distribution with the median droplet size of 1.8 µm.

4.2 Ground based cloud spectrometers as a method of in situ cloud measurements.

There is a continuous need for long-term ground-based in situ cloud measurements in environments similar to those of PaCEs (sub-Arctic conditions with frequently occurring supercooled clouds). In paper II, the operation of three GBCS setups to perform continuous ground-based measurements in harsh environments were tested and evaluated.

More specifically, during the Pallas Cloud Experiment (PaCE) in 2013, the performance of the Cloud and Aerosol Spectrometer (CAS), the Cloud Droplet Probe (CDP) and the Forward Scattering Spectrometer Probe (FSSP) were investigated. The focus in this campaign was to reveal how different meteorological parameters affect each instrument's ground-based setup operation and quantify possible biases and discrepancies on deriving different microphysical cloud properties. CAS was intercompared to the FSSP ground setup because their parallel data coverage was the best (∼ 243 hours of common cleaned data set). On the other hand, CDP had a low common data set with the CAS. The reason for this was that from the date that the CAS was installed we were mainly facing subzero temperatures, conditions that proved not to be favorable for the CDP ground setup. During sub-zero conditions, the CDPs' inlet often became clogged because of supercooled cloud drop accumulation. This issue also occurred to both the rotation and inhalation system because the probe's big surfaces were collecting ice, and it had a small opening for the inhalation system.

4.2.1 Intercomparison of CAS and FSSP

The meteorological parameter that was investigated to find out how the droplet counting ability of the instruments was influenced in different sectors of the wind rose was the wind direction. As a benchmark parameter, cloud droplet number concentration (N_c) was adopted as it can clearly represent the count losses in different cases. The wind rose was divided into 12 sectors: 0 to 74, 75 to 94, 95 to 114, 115 to 154, 155 to 184, 185 to 199, 200 to 214, 215 to 235, 236 to 250, 251 to 265, 266 to 295 and 296 to 360°. In the wind rose sector from 200 to 235° (wind iso-axial conditions), agreement was found to be the best according to the N_c ratio (R^2 = 0.78 and 0.62 with slope 0.65 and 0.50 respectively, with maximum difference observed ∼ 30 %). Temperature and wind speed in the range of −11 to −1.4 °C and 1.6 to 13.8 m s^{-1} did not affect the ability of the probes to derive N_c in wind iso-axial conditions. From a similar analysis in each sector of the wind rose a general benchmarking was created (Fig. 8). After the detailed analysis, the 12 sectors were merged into the 4 most representative conditions; wind iso-axial conditions (from 200 to 235°), perpendicular conditions (from 115 to 154 and 296 to 360°), conditions between iso-axial and perpendicular (from 76 to 114, from 155 to 199 and from 236 to 295°) and the area where the performance of FSSP the was influenced by its setup (presence of brake, from 1 to 74°). The loss of cloud droplets at the CAS was obvious when the wind direction was out of the range of the wind iso-axial conditions e.g., in conditions between iso-axial and perpendicular ($0.46 \leq R^2 \leq 0.50$ for 76 to 114, 155 to 199 and 236 to 295°) and in perpendicular conditions (R^2 = 0.32 and 0.11 for 115 to 154 and 296 to 360°). The strong sensitivity to the wind direction suggested that the cloud spectrometers were sampling anisokinetically when the sampling was performed out of the wind iso axial conditions.

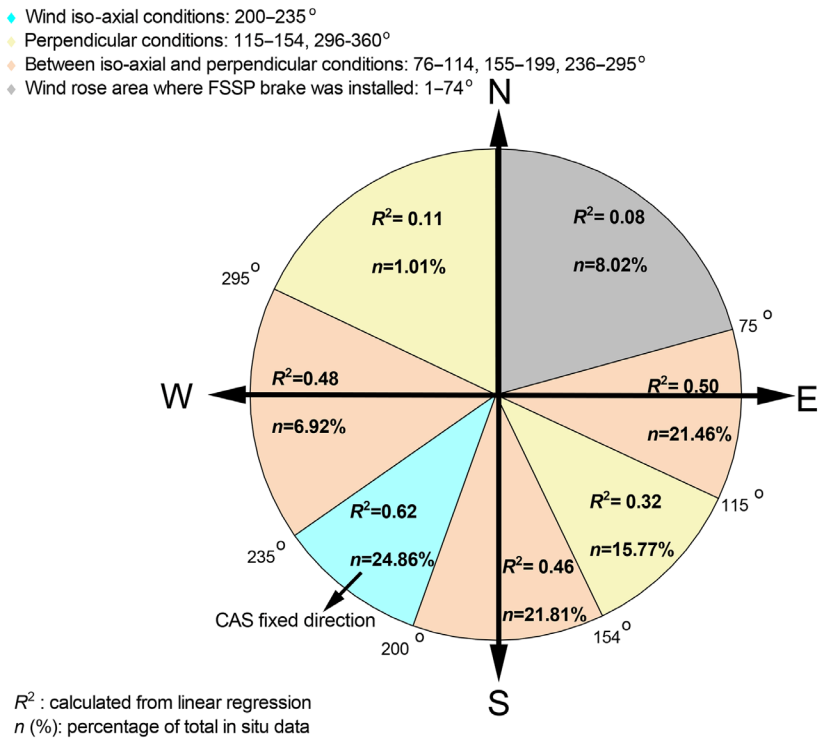

Figure 8. Intercomparison of number concentration (N_c) between the CAS and the FSSP based on the wind direction. The CAS was set and installed in a fixed direction (southwest, ~ 225°); the FSSP was installed on a rotating platform and followed the wind direction. The wind rose was separated into four representative wind direction conditions; wind iso-axial conditions (from 200 to 235°), perpendicular conditions (from 115 to 154 and 296 to 360°), conditions between iso-axial and perpendicular (from 76 to 114, from 155 to 199 and from 236 to 295°) and the case where the brake influenced the performance of FSSP (from 1 to 74°). Figure from Paper II.

As expected, the sampling losses affected the ability of the GBCS to derive the liquid water content (LWC) values. Thus, only LWC values from wind iso-axial conditions should be used. To derive LWC, deployment of another sensor is proposed (e.g., the particle volume monitor) to serve as a reference LWC value. Regarding the ability of the ground setup to derive the effective diameter (ED) and the median volume diameter (MVD), the best agreement was observed when the wind direction was inside the range of iso-axial conditions where all the points were focused along the 1: 1 line. Even though CAS was measuring lower N_c even by a factor of 10 when the wind direction was perpendicular to the CAS fixed direction the maximum observed difference between the two probes was about 20 %. This was happening since even though several cloud droplets were lost, the shape and the position of the peak of the size distribution measured by CAS remained similar. This unexpectable behavior was noticed in the whole available data set, ~ 183 h, (maximum ED and MVD of 35 and 30 μm). We should highlight that the sampled clouds had generally small cloud droplets and this behavior is not expected in clouds with larger cloud droplets. Also, it was noticed that high wind speed values affected the ability of the GBCS to derive ED and MVD as FSSP derived bigger values of ED and MVD when compared to CAS. On the other hand, in case of low wind speeds, FSSP derived smaller values when compared to CAS. A possible explanation was that due to the isokinetic motion of the particles, the

larger particles could not enter the FSSP because the inner diameter necking on the inlet was changing from 3.8 to 2.0 cm.

4.2.2. Intercomparison of CDP and FSSP

As expected, since CDP and FSSP were both following the wind direction, they derived N_c with good agreement (R^2 = 0.84, slope 1.11) (Fig.9). In worst case, N_c difference between them was about 30 %. Regarding the derived sizing parameters ED and MVD the agreement was also acceptable (R^2 = 0.82 and 0.79 with slopes 1.23 and 1.25 for ED and MVD, respectively). In general, the CDP ground setup was operating well in warm liquid clouds however as mentioned in the beginning of the Section 4.2, it had technical problems during subzero conditions. Thus, this setup is not recommended for semi long-term ground-based measurement of clouds during sub-zero conditions.

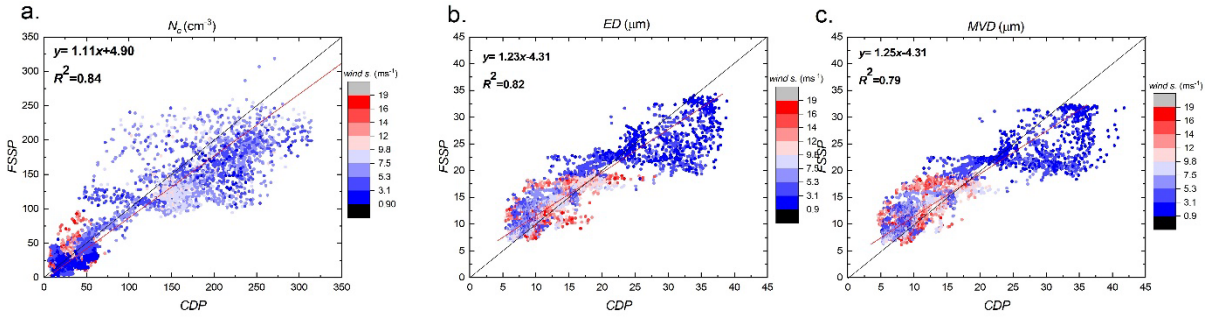

Figure 9. Intercomparison of (a) N_c, (b) ED and (c) MVD as it was derived from the CDP and the FSSP is presented for all wind directions. Color code represents the wind speed. Figure from Paper II.

4.2.3 General recommendations

According to the detailed investigation that was done in Paper II, several recommendations for the future data analysis regarding the GBCS setups in sub-Arctic conditions with frequently occurring supercooled clouds were presented (Table 2).

Table 2: Recommendations for further data analysis of the cloud spectrometers ground-based setups data for future campaigns in subarctic conditions with frequently occurring supercooled clouds.

	N_c	*ED, MVD*	*LWC*	*Comments*
CAS	Only data from wind iso-axial conditions. (± 20° from its fixed direction) should be used	All measurements can be used for further analysis, independent on wind direction in the size range of ED and MVD of 5 - 35 µm	Only data from wind iso-axial conditions and temperatures below – 4 °C should be used	Good data coverage (67%); Operating properly both in non-icy and icy conditions; needs daily cleaning
FSSP	Data from all wind sectors will be used except data from wind sector where brake was installed (± 40° brake direction)	All data can be used for further analysis except data from the wind sector where brake was installed (± 40° from brake direction)	Only data from wind iso-axial conditions and temperatures below – 4 °C should be used	The best data coverage (75%); Operating properly both in non-icy and icy conditions; needs daily cleaning.
CDP	Usable in warm clouds. Limitation in temperature; operational problems at sub-zero temperatures	All data obtained in non-icy conditions can be used for further analysis	Not usable due to temperature range.	Low data coverage (17%), Operating properly in non-icy conditions; not recommended for sub-zero temperatures

4.3 A semi long-term data set of in situ cloud properties and meteorological parameters

In paper III, a unique data set of ground in situ cloud measurements along with several meteorological variables collected in eight PaCE campaigns conducted between 2004 and 2019 was presented. The published data set provides an insight into microphysics of low-level clouds in subarctic conditions over a wide range of temperatures (−25.8 to 8.8 °C). In this temperature range supercooled water droplets were expected mainly at temperatures below 0 °C. For temperatures above 0 °C, the sampled clouds were expected to consist of liquid hydrometeors only.

In paper III, we present only measurements when the station was inside a cloud. Data from the Cloud, Aerosol and Precipitation Spectrometer probe (CAPS), the Forward-Scattering Spectrometer Probe (FSSP) and the weather station were quality controlled and unified in a common format for release and further analysis. To identify the presence of a cloud at the station, three different factors were used: 1) the droplet size distribution was checked as measured in both cloud spectrometer ground setups, 2) droplets counts were crosschecked with two meteorological variables – the relative

humidity at the measurement site which was expected to be ~ 100 % and the horizontal visibility which should be less than 1000 m and 3) a final inspection was done visually using pictures recorded by an automatic weather camera installed on the roof of the station. After the identification of the presence of a cloud at the station, to inspect the measurements of each year the following procedure was followed. The raw data set was checked to eliminate and exclude from further analysis cases in which one of the cloud probes was partially or fully blocked. To detect blocked probes, droplet number concentration (N_c) was carefully investigated. When a sudden decrease just before a sudden increase in N_c was occurring, we had a clear sign of probe inlet freezing. This behavior was caused because the opening of the probe inlet was becoming smaller (from the accumulation of snow/ice) and resulted in a raised probe air speed. During data evaluation we considered that the probe air speed was constant. Thus, this abnormality in the N_c was happening due to the underestimation of the probe air speed. The final data set includes a separate NetCDF and CVS file for each cloud spectrometer and year (example file names are PACE.yyyy.cloud_spectrometer.nc and PACE.yyyy.cloud_spectrometer.cvs).

Each file includes the cleaned timeline data set of the following cloud properties and meteorological variables: year (YYYY), day (DD), month (MM), hour (HH), min (MN), size bin lower limit, size bin higher limit, number concentration (cm^{-3}), liquid water content ($g\ m^{-3}$), effective diameter (μm), median volume diameter (μm), the calculated size distribution (cm^{-3}) values in each bin, temperature at 570 m (°C), dew point (°C), humidity at 570 m (%), pressure (hPa), wind speed ($m\ s^{-1}$), horizontal wind direction (degrees), global solar radiation ($W\ m^{-2}$), photosynthetically active radiation ($\mu mol\ m^{-2}\ s^{-1}$), and the horizontal visibility (m). In addition, the sampling area (mm^2) and the probe air speed (ms^{-1}) that were used to derive each parameter are also provided. Missing data points were marked as −9999.9.

Figure 10 presents the in-situ cloud observation hours of each PaCE campaign. It is visible that the observation hours after PaCE 2013 (PaCE 2013, 2015,2017 and 2019 campaigns had longer duration than PaCE 2004, 2005, 2009 and 2012) are significantly higher. The statistical description of the temperature at 570 meters above sea level for each campaign is provided in Figure 11. In each PaCE year the range and interannual variability were similar (temperature range was ranging approximately from −10.0 to 8 °C) except 2012 when CAPS was also installed for ~ 1 month during winter. Number concentration averaged values were similar for every year of the measurements (around 100 cm^{-3}) even there were some cloud cases during each campaign that number concentration had values around 300 cm^{-3}. The averaged ED and MVD values were ranging approximately from 10 to 20 μm and the liquid water content was in majority of the cases less than 0.2 $g\ m^{-3}$.

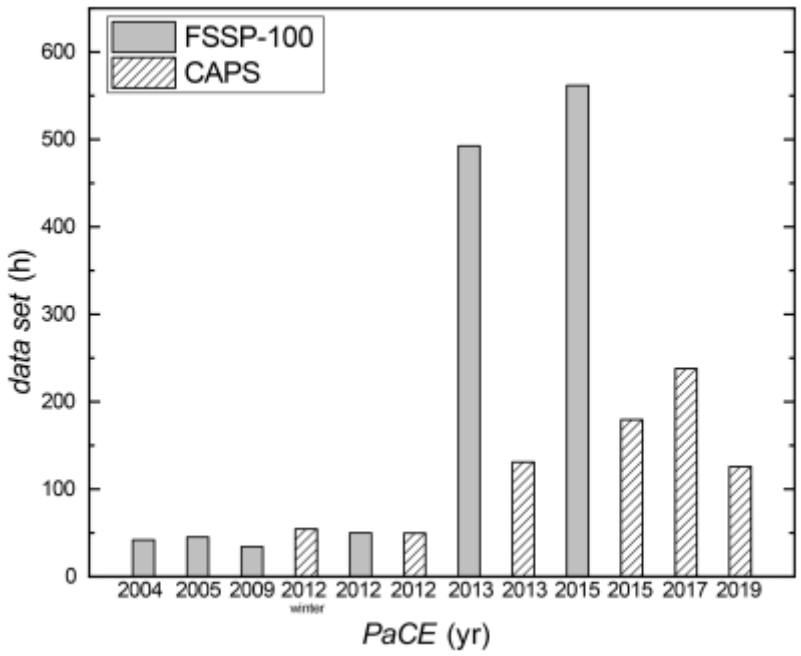

Figure 10. Hours of observation data collected for each PaCE campaign when the FSSP-100 and CAPS ground setups were operational. Figure from paper III.

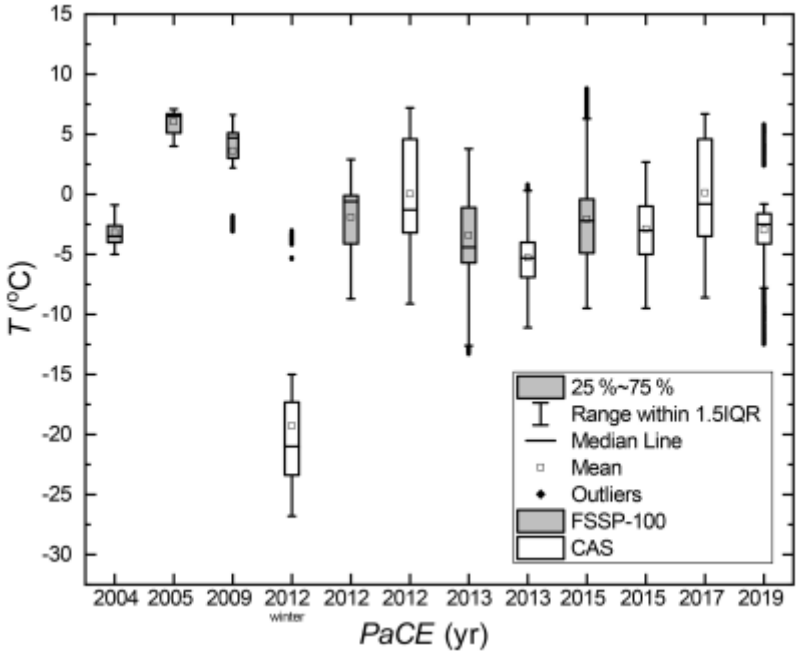

Figure 11. Statistical description of the temperature at 570 meters above sea level for each PaCE campaign when the FSSP-100 and CAS ground setups were operational. Figure from paper III.

The published data set can be used in studies of cloud microphysics, climate change in the subarctic, and performance evaluation and improvement of existing models at higher latitudes. The whole dataset is available in the Finnish Meteorological Institute (FMI) open data repository for each campaign and each cloud spectrometer ground setup individually (Doulgeris et al., 2021).

4.4 Influence of air mass origin on microphysical properties of low-level clouds

After establishing the methodology for performing in situ cloud ground measurements and publishing the dataset from eight PaCEs, a further analysis was done in paper IV using the published data set to investigate how the origin of long-range transport air masses can influence the microphysical properties of low-level clouds. The Sammaltunturi station enables long-term in situ observations of cloud properties in subarctic air. During PaCEs operation time (autumn) the clean, natural Arctic background conditions are significantly increasing (Pernov et al., 2021). Thus, we focused on quantifying the impact of air mass origin (e.g., clean arctic vs. long-range transported air from continental Europe) on low-level clouds and their patterns.

4.4.1 Identification of air mass origin

First, we found out when a region was considered as representative of the air mass type. The potential emission sensitivity (PES) was summed up for the full duration of the 96-hour FLEXPART backward simulations and for all output heights at each latitude-longitude grid cell. Based on those integrated data, hourly values of PES fraction for each source region were calculated. Cloud droplet number concentration (N_c) was used as a benchmark parameter to investigate which was the optimal threshold of PES fraction within one region that should be adopted for this region to be representative of the air mass type. It was shown that when 80 % of the PES fraction was within a region, the observations were representative of that air mass type. Below that threshold, all the air masses were considered as mixed and were excluded from further analysis. Finally, the cloud observation hours related to Arctic, Eastern, Southern, Western and Local air masses were 118, 275, 152, 118 and 43, respectively.

4.4.2. Effect of air mass origin to N_c, size and LWC of the cloud droplets

As a next step, using the optimal threshold (PES>80%), the characteristics of all air mass regions (Arctic, Eastern, Southern and Western as clouds that were related with local air masses were excluded due to relatively small number of observations) were intercompared to reveal any patterns in cloud microphysical properties. In Figure 12, it is shown that the highest values of N_c (approximately 100-200 cm^{-3}) were associated with Southern air masses and the lowest ones (approximately 20 cm^{-3}) were associated with Arctic air masses. In general, it was noticed that marine air masses arriving at the Sammaltunturi station resulted in lower values of N_c and the continental air masses in higher values of N_c. There was not any clear trend in N_c through different years of measurements.

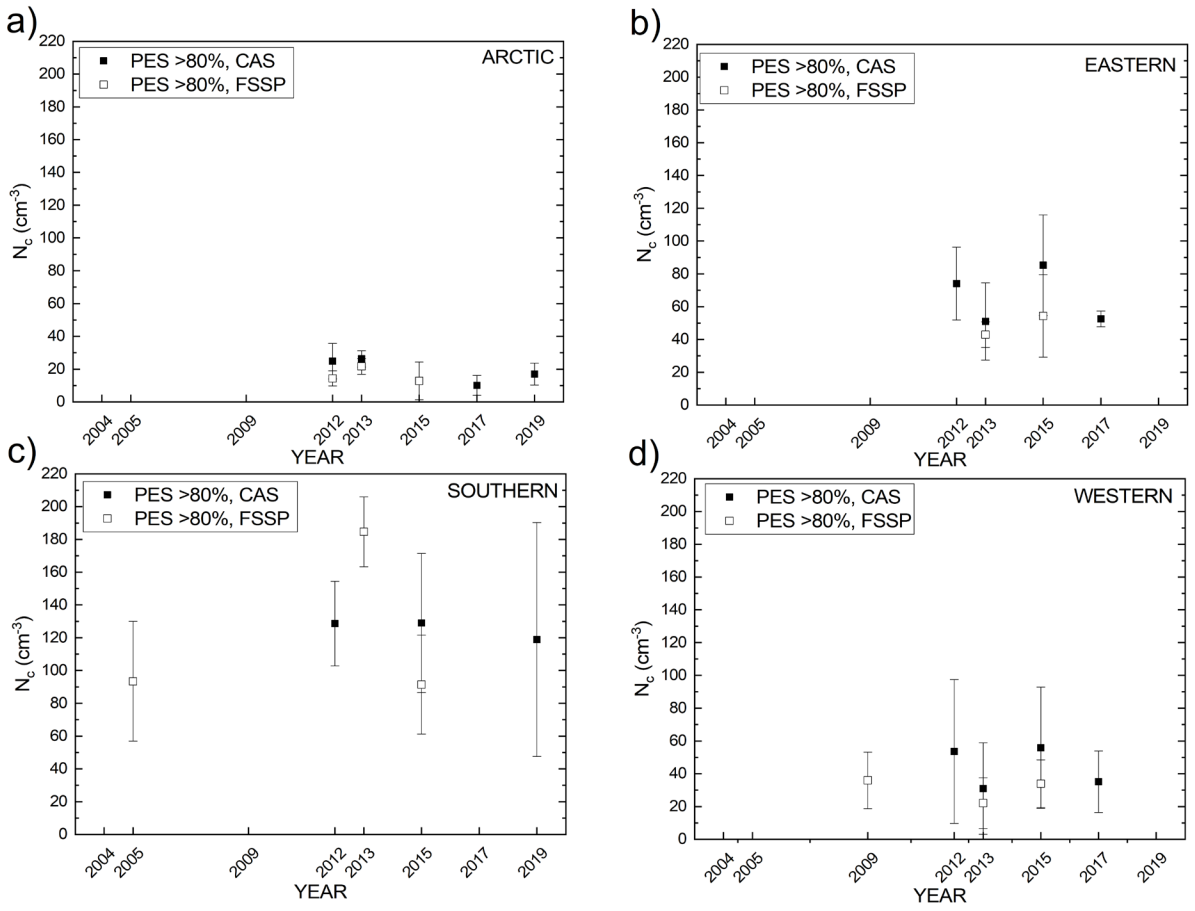

Figure 12. Each single PaCE campaign cloud droplet number concentration (N_c) for (a) Arctic, (b) Eastern, (c) Southern and (d) Western region as they were measured by the cloud and aerosol spectrometer (CAS) and the forward-scattering spectrometer probe (FSSP) where the PES fraction was within one region >80 %. Figure from Paper IV.

The average size distributions of cloud droplets related to each air mass origin for all PaCE campaigns is presented in Figure 13. Marine regions (Arctic, Western) generated cloud droplet size distributions with a relatively broad shape with presence of large (10–20 μm) droplets. On the other hand, continental air masses generated cloud droplet size distributions with lack of large cloud droplets. In all cases, it was noticed that higher number concentrations of cloud droplets are related with smaller cloud droplet effective diameter, result that is consistent with the Twomey effect (Twomey, 1977).

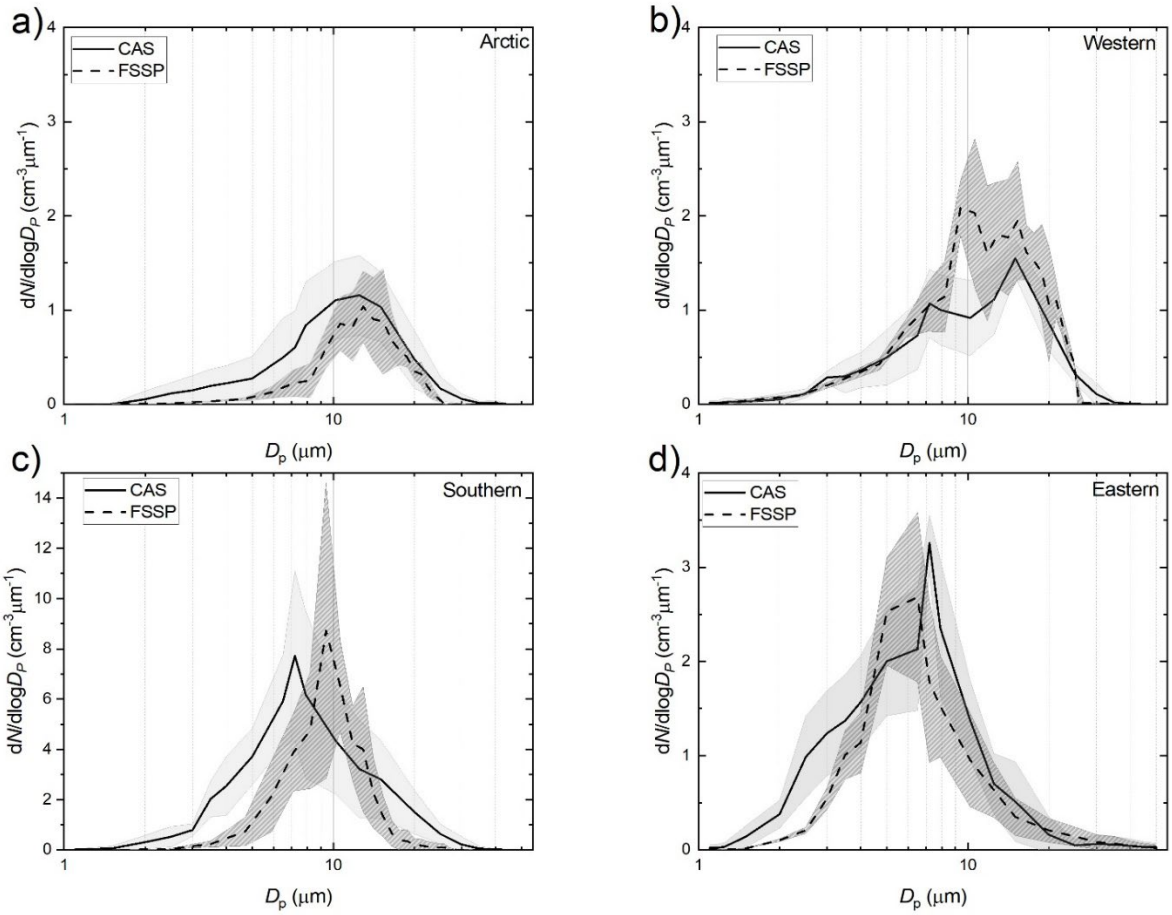

Figure 13. Cloud droplet size distribution associated with the (a) Arctic, (b) Western, (c) Southern and (d) Eastern region as they were measured by the cloud and aerosol spectrometer (CAS) and the forward-scattering spectrometer probe (FSSP) during all PaCEs. Figure from Paper IV.

Along with the air mass origin, the effect of the air temperature to the size of the cloud droplets was also investigated. For that reason, temperature bins of 4 °C range were created (–10 to –6 °C, –6 to –2 °C, –2 to 2 °C and 2 to 6 °C). Cloud droplets appeared to be more prone to grow at temperatures larger than –2 °C. When the clouds were characterized by Arctic air masses, MVD and ED were approximately 15 µm within our temperature spectrum. Clouds related to eastern air masses were approximately 8 µm in majority of cases, however they showed approximately 5 µm larger cloud droplets in temperatures more than 0 °C. More observations on existing and wider temperature ranges are needed to statistically ensure those results.

LWC of low-level clouds for the different air mass types was also investigated. The Arctic air masses were related to the lowest values of LWC (approximately 0.025 g m^{-3}), whereas the Southern air masses were related to the highest values of LWC (> 0.05 g m^{-3}). Western and Eastern air masses were related to LWC values of approximately 0.025 to 0.05 g m^{-3}. In this study, LWC of continental air masses were, on average, larger than those of marine air masses. This is reflected in the higher N_c of continental air masses, as LWC is a function of both N_c and size of cloud droplets.

5. Review of papers and author contribution

The author is responsible for writing the introductory part of the thesis. The publications selected in this dissertation are original research papers on cloud condensation nuclei laboratory experiments and cloud microphysical properties using a laboratory setup and ground-based cloud spectrometer setups respectively. The author was responsible for most of the work in papers I, II, III and IV.

Paper I: The focus of this study was to introduce a new experimental setup for investigating CCN and test the proper operation of setup by performing a series of laboratory tests. The growth modelling data were provided by T. Raatikainen. The author built the experimental setup, post-processed and analyzed the results, and wrote the paper with the help of co-authors.

Paper II: The aim of this paper was the establishment of the methodology that was used for in situ cloud measurements. The author post-processed and analyzed the results and wrote the paper with the help of co-authors. Since, during PaCE 2013, the author was not a part of FMI, the field measurements were carried out by the co-authors.

Paper III: In this study, we made available to the scientific community a semi long term unique data set which was containing in situ cloud data and meteorological observations from eight PaCE campaigns. The author was responsible for most of the work in writing the manuscript, analyzing the data set, and writing the manuscript. PaCE 2004, 2005, 2009, 2012 and 2013 cloud measurements were mostly performed by the co-authors while PaCE 2015,2017 and 2019 cloud measurements were mainly conducted by the author.

Paper IV: The objective of this study was to investigate how different long-range transport air masses can influence the microphysical properties of low-level clouds. The modelling data and the corresponding description of the model was provided by V. Vakkari. The author was responsible for most of the work on post-processing and analyzing the results and wrote the paper with the help of co-authors.

6. Conclusion and future steps

In this thesis, a set of experimental laboratory and field measurements were done to increase our understanding on cloud condensation nuclei activation, cloud microphysics and help on developing methodology to conduct such measurements.

The starting point of this work was to introduce a multi-purpose laboratory setup for investigating atmospherically relevant interactions between aerosol particles and water vapor under defined laboratory conditions, to find its optimal operational parameters, and to discuss its ability to perform as cloud condensation nuclei (CCN) counter (PAPER I). To verify the characteristics of the new introduced setup that can achieve different levels of saturations ratios several simulation and experimental tests were performed. Thus, the behavior of the saturation ratio inside the experimental setup with different flow rates was investigated. The optimal flow rate range (between 1 and 3 l min^{-1}) was find out. Within this flow range, the temperature of the flow inside the CCN counter was stabilized soon enough that the injected particles would experience high enough supersaturation to be activated and at the same time not to be lost to the walls of the setups tube. After completing the characterization of the setup, further tests were made to prove that the setup can measure CCN. Two main values were calculated: the activated fraction and the growth of the activated particles. In this thesis, the experimental setup (FMI-ACIT) that was build was proven that it can operate as a CCN counter and measure the activation and the growth of ammonium sulfate particles in supersaturations ranging from 0.18% to 1.25%. In future work, more tests should be done on low temperatures to test the setups' ability to measure ice nuclei.

The second aim of the thesis was to explore the possibilities to monitor cloud microphysical properties with cloud spectrometer probes in harsh environments (PAPER II). During PaCE 2013 three different ground-based cloud spectrometers (FSSP, CDP and CAPS ground setups) were intercompared. This work was inspired by the increased demand from the scientific community for long-term continuous, ground-based, in-situ cloud measurements. Unfortunately, there is limited instrumentation available to cover such a demand and, moreover, continuous in-situ cloud measurements in conditions of subarctic location are very challenging. Thus, this work is not just merely an instrument comparison but also as an experiment on how to operate the cloud probe spectrometers to perform ground-based measurements in harsh environments. One of the main challenges during ground-based cloud spectrometers measurements is the accumulation of ice or snow on the instruments inlets or on crucial parts of the setups (e.g., rotation system). New upgraded deicing features are needed and can lead to better and longer operation. Also, I would like to highlight the need for development of a new generation of counters designed for ground-based in situ cloud measurements that will give us the possibility to perform all year-round in situ cloud measurements.

Our main conclusion is that cloud spectrometer ground setups can be identified as a potential method for continuous cloud in situ measurements, however the following recommendations for their operation should be followed.

1) It is optimal for the cloud probes to always continuously face the wind direction to minimize the sampling losses.

2) In case that this cannot ensured, for further analysis we recommend that only the measurements that are conducted in wind iso-axial conditions should be used.

3) Deriving the sizing parameters ED and MVD for the whole wind direction spectrum could be done in some cases, but it must be done with insight and prudence.

4) To derive LWC, a deployment of another sensor is proposed (e.g., the particle volume monitor) to serve as a reference LWC value.

After establishing the methodology that was used for monitoring cloud microphysics, eight years of PaCE measurements were made available to the scientific community (PAPER III). The recommendations that were proposed in Paper III were adopted to perform a quality check of the data. In the published dataset, number concentration (cm^{-3}), liquid water content (g cm^{-3}), effective diameter (µm), median volume diameter (µm) and the calculated cloud droplet size distribution (cm^{-3}) values in each bin are available combined with the following meteorological data: temperature at 570 m (°C), dew point (°C), humidity at 570 m (%), pressure (hPa), wind speed (m s^{-1}), horizontal wind direction (degrees), global solar radiation (W m^{-2}), photosynthetically active radiation (µmol m^{-2} s^{-1}), and the horizontal visibility (m). The published data set provides a helpful contribution to cloud microphysics processes on shorter timescales, and it can be used as complementary in model development.

The published dataset was subsequently reanalyzed and combined with air mass back trajectories to reveal the influence of long-range transport air masses to the microphysical properties of low-level clouds (PAPER IV). The origin of the air masses should be considered as an important factor. We proved that the continental air masses (particularly air masses related to the continental Europe) led to the highest cloud droplet number concentrations and marine air masses (especially air masses related to the Artic region that corresponds to clean, natural Arctic background conditions) to the lowest ones. We also noticed that the size of cloud droplets was found to be influenced by the cloud droplet number concentration, result that agrees with the Twomey effect (Twomey, 1977). Furthermore, there was an indication that cloud droplets in clouds in warmer air (from –2 to 6 °C) were more prone to grow. However, more measurements are needed to confirm such temperature dependency of droplet sizes. LWC of continental air masses were, on average, larger than those of marine air masses. From this work, we point out that there is need of considering not only local meteorological parameters but also the air mass origin in investigations of cloud processes. Thus, we need to explore the value of a more dynamical perspective on observational settings in aerosol-cloud interaction area. In future, a quantitative analysis of the relative importance of the various factors using all year-round cloud data should be addressed to determine cloud properties, including both aerosols and meteorological parameters.

References

Aalto, T., Hatakka, J. and Viisanen, Y.: Influence of air mass source sector on variations in CO2 mixing ratio at a boreal site in northern Finland. Boreal Env. Res. 8, 285–393,2003.

Aitken, J.: On Dust, Fogs, and Clouds, Earth Environ. Sci. Trans. R. Soc. Edinburgh, 30, 337, 1881.

Asmi, E., Freney, E., Hervo, M., Picard, D., Rose, C., Colomb, A., and Sellegri, K.: Aerosol cloud activation in summer and winter at puy-de-Dôme high altitude site in France, Atmos. Chem. Phys., 12, 11589–11607, https://doi.org/10.5194/acp-12-11589-2012, 2012.

Asmi, E., Kivekäs, N., Kerminen, V.-M., Komppula, M., Hyvärinen, A.-P., Hatakka, J., Viisanen, Y., and Lihavainen, H.: Secondary new particle formation in Northern Finland Pallas site between the years 2000 and 2010, Atmos. Chem. Phys., 11, 12959–12972, https://doi.org/10.5194/acp-11-12959-2011, 2011.

Baumgardner, D., Abel, S. J., Axisa, D., Cotton, R., Crosier, J., Field, P., Gurganus, C., Heymsfield, A., Korolev, A., Krämer, M., Lawson, P., McFarquhar, G., Ulanowski, Z., and Um, J.: Cloud Ice Properties: In Situ Measurement Challenges, Meteor. Mon., 58, 9.1–9.23, https://doi.org/10.1175/AMSMONOGRAPHS-D16-0011.1, 2017.

Baumgardner, D., Jonsson, H., Dawson, W., O'Connor D., and Newton R.: The cloud, aerosol and precipitation spectrometer (CAPS): A new instrument for cloud investigations, Atmos. Res., 59–60, 251-2-64, https://doi.org/10.1016/S0169- 8095(01)00119-3, 2001.

Baumgardner, D., Newton, R., Krämer, M., Meyer, J., Beyer, A., Wendisch, M., and Vochezer, P.: The Cloud Particle Spectrometer with Polarization Detection (CPSPD): A next generation open-path cloud probe for distinguishing liquid cloud droplets from ice crystals, Atmos. Res., 142, 2–14, https://doi.org/10.1016/j.atmosres.2013.12.010, 2014.

Bird, R. B., Stewart, W. E. and Lightfoot E. N.: Transport Phenomena (John Wiley & Sons, New York, 1960.

Bodas-Salcedo, A., Mulcahy, J. P., Andrews, T., Williams, K. D., Ringer, M. A., Field, P. R., & Elsaesser, G. S.: Strong dependence of atmospheric feedbacks on mixed-phase microhysics and aerosol-cloud interactions. *Journal of Advances in Modeling Earth Systems*, **11**, 1735– 1758, 2019.

Boucher, O., Randall, D., Artaxo, P., Bretherton, C., Feingold, G., Forster, P., Kerminen, V.-M., Kondo, Y., Liao, H., Lohmann, U., Rasch, P., Satheesh, S. K., Sherwood, S., Stevens, B., and Zhang, X. Y.: Clouds and aerosols, in: Climate Change 2013: The Physical Science Basis. Contribution of Working Group I to the Fifth Assessment Report of the Intergovernmental Panel on Climate Change, edited by: Stocker, T. F., Qin, D., Plattner, G.-K., Tignor, M., Allen, S. K., Doschung, J., Nauels, A., Xia, Y., Bex, V., and Midgley, P. M., Cambridge University Press, 571–657, https://doi.org/10.1017/CBO9781107415324.016, 2013.

Brus, D., Hyvärinen, A.-P., Viisanen, Y., Kulmala, M., and Lihavainen, H.: Homogeneous nucleation of sulfuric acid and water mixture: experimental setup and first results, Atmos. Chem. Phys., 10, 2631–2641, https://doi.org/10.5194/acp-10-2631-2010, 2010.

Brus, D., Gustafsson, J., Vakkari, V., Kemppinen, O., de Boer, G., and Hirsikko, A.: Measurement report: Properties of aerosol and gases in the vertical profile during the LAPSE-RATE campaign, Atmos. Chem. Phys., 21, 517–533, https://doi.org/10.5194/acp21-517-2021, 2021.

Chang, Y., Guo, X., Tang, J., and Lu, G.: Aircraft measurement campaign on summer cloud microphysical properties over the Tibetan Plateau, Sci. Rep., 9, 4912, 2019.

Connolly, P. J., Emersic, C., and Field, P. R.: A laboratory investigation into the aggregation efficiency of small ice crystals, Atmos. Chem. Phys., 12, 2055–2076, https://doi.org/10.5194/acp-12-2055-2012, 2012.

Craig, L., Moharreri, A., Rogers, D. C., Anderson, B., and Dhaniyala, S.: Aircraft-Based Aerosol Sampling in Clouds: Performance Characterization of Flow-Restriction Aerosol Inlets, J. Atmos. Ocean. Tech., 31, 2512–2521, https://doi.org/10.1175/JTECH-D-14-00022.1, 2014.

Donovan, D. P., Klein Baltink, H., Henzing, J. S., de Roode, S. R., and Siebesma, A. P.: A depolarisation lidar based method for the determination of liquid-cloud microphysical properties, Atmos. Meas. Tech., 8, 237–266, https://doi.org/10.5194/amt-8-237-2015, 2015.

Doulgeris, K.-M., Lihavainen, H., Hyvärinen, A.-P., Kerminen, V.-M., and Brus, D.: Data set for Doulgeris et al. 2021: In-situ microphysical characterization of low-level clouds in the Finnish sub-Arctic, extensive dataset, Finnish Meteorological Institute [data set], https://doi.org/10.23728/FMIB2SHARE.988739D21B824C709084E88ED6C6D54B, 2021.

Droplet Measurement Technologies Manual: Particle Analysis and Display System (PADS) Image Probe Data Reference Manual DOC-0201 Rev A-2 PADS 2.5.6, DMT, Boulder, Colorado, USA, 2009.

Dye, J. E. and Baumgardner, D.: Evaluation of the forward scattering spectrometer probe, I – Electronic and optical studies, J. Atmos. Ocean. Technol., 1, 329–344, https://doi.org/10.1175/1520-0426(1984)0012.0.CO;2, 1984.

Emeis, S., Münkel, C., Vogt, S., Müller, W.J. and Schäfer, K.: Atmospheric boundary-layer structure from simultaneous SODAR, RASS and ceilometer measurements. Atmos. Environ., 38, 273–286,2004.

Eneroth, K., Kjellström, E. and Holmén, K.: A trajectory climatology for Svalbard; investigating how atmospheric flow patterns influence observed tracer concentrations. Phys. Chem. Earth 28, 1191–1203, doi: DOI: 10.1016/j.pce.2003.08.051., 2003.

Febvre, G., Gayet, J.-F., Shcherbakov, V., Gourbeyre, C., and Jourdan, O.: Some effects of ice crystals on the FSSP measurements in mixed phase clouds, Atmos. Chem. Phys., 12, 8963–8977, https://doi.org/10.5194/acp-12-8963-2012, 2012.

Fukuta, N., and Saxena, V. K. :A Horizontal Thermal Gradient Cloud Condensation Nucleus Spectrometer, Journal of Applied Meteorology and Climatology, 18(10), 1352-1362, 1979.

Fukuta, N., and Walter, L. A. : Kinetics of Hydrometeor Growth from a Vapor-Spherical Model, Journal of Atmospheric Sciences, 27(8), 1160-1172, 1970.

Gerber, H., Frick, G., and Rodi, A.: Ground-based FSSP and PVM measurements of liquid water content, J. Atmos. Ocean. Tech., 16, 1143–1149, https://doi.org/10.1175/1520- 0426(1999)0162.0.CO;2, 1999.

Girdwood, J., Stanley, W., Stopford, C., and Brus, D.: Simulation and field campaign evaluation of an optical particle counter on a fixed-wing UAV, Atmos. Meas. Tech., 15, 2061–2076, https://doi.org/10.5194/amt-15-2061-2022, 2022.

Girdwood, J., Smith, H., Stanley, W., Ulanowski, Z., Stopford, C., Chemel, C., Doulgeris, K.-M., Brus, D., Campbell, D., and Mackenzie, R.: Design and field campaign validation of a multi-rotor unmanned aerial vehicle and optical particle counter, Atmos. Meas. Tech., 13, 6613–6630, https://doi.org/10.5194/amt-13-6613-2020, 2020.

Grabowski, W. W., Morrison H., Shima S., Abade G. C., Dziekan P., and Pawlowska H.: Modeling of Cloud Microphysics: Can We Do Better?, B. Am. Meteorol. Soc., 100, 655–672, https://doi.org/10.1175/BAMS-D-18-0005.1, 2019.

Guyot, G., Gourbeyre, C., Febvre, G., Shcherbakov, V., Burnet, F., Dupont, J.-C., Sellegri, K., and Jourdan, O.: Quantitative evaluation of seven optical sensors for cloud microphysical measurements at the Puy-de-Dôme Observatory, France, Atmos. Meas. Tech., 8, 4347–4367, https://doi.org/10.5194/amt-8-4347-2015, 2015.

Harrison R. G., Nicoll, K. A., Tilley, D. J., Marlton, G. J., Chindea, S., Dingley, G. P., Iravani, P., Cleaver, D. J., du Bois, J. L., and Brus, D.: Demonstration of a remotely piloted atmospheric measurement and charge release platform for geoengineering, J. Atmos. Ocean. Technol, 38, 63–75, https://doi.org/10.1175/JTECH-D-20-0092.1, 2021.

Hatakka, J., Aalto, T., Aaltonen, V., Aurela, M., Hakola, H., Komppula, M., Laurila, T., Lihavainen, H., Paatero, J., Salminen, K., and Viisanen Y., Overview of the atmospheric research activities and results at Pallas GAW station, Boreal Environ. Res., 8, 365– 384, 2003.

Heymsfield, A., Thompsom, G., Morrison, H., Bansemer, A., Rasmussen, R. M., Minnis, P., Wang, Z., and Zhang,D.: Formation and Spread of Aircraft-Induced Holes in Clouds, Science, 33, 77–81, https://doi.org/10.1126/science.1202851, 2011.

Hinds, W.C.: Aerosol Technology, Properties, Behaviour, and Measurement of Airborne Particles. John Wiley & Sons Inc., New York, 1999.

Howard, L.: On the modifications of clouds, and on the principles of their production, suspension, and destruction; being the substance of an essay read before the Askesian Society in the session 1802–3, Phil. Mag. Series 1, 5–11, https://doi.org/10.1080/14786440308676365, 1803.

Hudson, J. G., An instantaneous CCN spectrometer, J. Atmos. Oceanic. Technol., 6, 1055-1065, 1989.

IPCC 2021: Climate Change 2021: The Physical Science Basis- Contribution of Working Group I to the Sixth Assessment Report of the Intergovernmental Panel on Climate Change. Technical Report (2021).

Iwamoto, Y., Watanabe, A., Kataoka, R., Uematsu, M. and Miura, K.: Aerosol–Cloud Interaction at the Summit of Mt. Fuji, Japan: Factors Influencing Cloud Droplet Number Concentrations. Appl. Sci., 11, 8439. https://doi.org/10.3390/ app11188439, 2021.

Katz, J. L., Condensation of a Supersaturated Vapor. I. The Homogeneous Nucleation of the n-Alkanes, J. Chem. Phys., 52, 4733, 1970.

Knollenberg, R. G.: Three new instruments for cloud physics measurements: the 2-D spectrometer probe, the forward scattering spectrometer probe and the active scattering aerosol spectrometer, American Meteorological Society, Int'l Conf. on Cloud Physics, 554–561, 1976.

Köhler, H.: The nucleus in and the growth of hygroscopic droplets, T. Faraday Soc., 32, 1152–1161, 1936.

Komppula, M., Lihavainen, H., Kerminen, V.-M., Kulmala, M., and Viisanen, Y.: Measurements of cloud droplet activation of aerosol particles at a clean subarctic background site, J. Geophys. Res., 110, D06204, https://doi.org/10.1029/2004JD005200, 2005.

Korolev, A., McFarquhar, G., Field, P. R., Franklin, C., Lawson, P., Wang, Z., Williams, E., Abel, S. J., Axisa, D., Borrmann, S., Crosier, J., Fugal, J., Krämer, M., Lohmann, U., Schlenczek, O., Schnaiter, M., and Wendisch, M.: Mixed-Phase Clouds: Progress and Challenges, Meteorological Monographs, 58, 5.1-5.50, 2017.

Lance, S., Brock, C. A., Rogers, D., and Gordon, J. A.: Water droplet calibration of the Cloud Droplet Probe (CDP) and in-flight performance in liquid, ice and mixed-phase clouds during ARCPAC, Atmos. Meas. Tech., 3, 1683–1706, https://doi.org/10.5194/amt-3-1683-2010, 2010.

Lihavainen, H., Finnish Meteorological Institute, in “Laminar flow diffusion chamber for homogeneous nucleation studies,” Report Series in Aerosol Science No. 45 (Finnish Association for Aerosol Research, Helsinki, 2000), ISSN 0784–3496.

Lihavainen, H., Kerminen, V.-M., Komppula, M., Hyvärinen, A.-P., Laakia, J., Saarikoski, S., Makkonen, U., Kivekäs, N., Hillamo, R., Kulmala, M., and Viisanen, Y.: Measurements of the relation between aerosol properties and microphysics and chemistry of low-level liquid water clouds in Northern Finland, Atmos. Chem. Phys., 8, 6925–6938, https://doi.org/10.5194/acp-8-6925-2008, 2008.

Lihavainen and Y. Viisanen: A laminar flow diffusion chamber for homogeneous nucleation studies," J. Phys. Chem. B 105(47), 11619-11629 (2001).

Lloyd, G., Choularton, T. W., Bower, K. N., Gallagher, M. W., Connolly, P. J., Flynn, M., Farrington, R., Crosier, J., Schlenczek, O., Fugal, J., and Henneberger, J.: The origins of ice crystals measured in mixed-phase clouds at the highalpine site Jungfraujoch, Atmos. Chem. Phys., 15, 12953–12969, https://doi.org/10.5194/acp-15-12953-2015, 2015

Lowenthal, D. H., Hallar, A. G., David, R. O., McCubbin, I. B., Borys, R. D., and Mace, G. G.: Mixed-phase orographic cloud microphysics during StormVEx and IFRACS, Atmos. Chem. Phys., 19, 5387–5401, https://doi.org/10.5194/acp-19- 5387-2019, 2019.

McCoy, D. T., Tan, I., Hartmann, D. L., Zelinka, M. D., and Storelvmo, T.: On the relationships among cloud cover, mixed-phase partitioning, and planetary albedo in GCMs, J. Adv. Model. Earth Sy., 8, 650–668, https://doi.org/10.1002/2015MS000589, 2016.

McFarquhar, G. M., Bretherton, C., Marchand, R., Protat, A., DeMott, P. J., Alexander, S. P., Roberts, G. C., Twohy, C. H., Toohey, D., Siems, S., Huang, Y., Wood, R., Rauber, R. M., Lasher-Trapp, S., Jensen, J., Stith, J., Mace, J., Um, J., Järvinen, E., Schnaiter, M., Gettelman, A., Sanchez, K. J., McCluskey, C. S., Russell, L. M., McCoy, I. L., Atlas, R., Bardeen, C. G., Moore, K. A., Hill, T. C. J., Humphries, R. S., Keywood, M. D., 680 Ristovski, Z., Cravigan, L., Schofield, R., Fairall, C., Mallet, M. D., Kreidenweis, S. M., Rainwater, B., D'Alessandro, J., Wang, Y., Wu, W., Saliba, G., Levin, E. J. T., Ding, S., Lang, F., Truong, S. C., Wolff, C., Haggerty, J., Harvey, M. J., Klekociuk, A., and McDonald, A.: Observations of clouds, aerosols, precipitation, and surface radiation over the Southern Ocean: An overview of CAPRICORN, MARCUS, MICRE and SOCRATES, B. Am. Meteorol. Soc., 102, E894–E928, 2020.

Mie, G.: Beiträge zur Optik trüber Medien, speziell kolloidaler Metallösungen, Ann. Phys.-Berlin, 330, 377–445, 1908.

Möhler, O., Stetzer, O., Schaefers, S., Linke, C., Schnaiter, M., Tiede, R., Saathoff, H., Krämer, M., Mangold, A., Budz, P., Zink, P., Schreiner, J., Mauersberger, K., Haag, W., Kärcher, B., and Schurath, U.: Experimental investigation of homogeneous freezing of sulphuric acid particles in the aerosol chamber AIDA, Atmos. Chem. Phys., 3, 211–223, https://doi.org/10.5194/acp-3- 211-2003, 2003.

Morrison, H., van Lier-Walqui, M., Fridlind, A. M., Grabowski, W. W., Harrington, J. Y., Hoose, C., Koroloev, A., Kumjian, M. R., Milbrandt, J. A., Pawlowska, H., Posselt, D. J., Prat, O. P., Reimel, K. J., Shima, S.-I., Van Diedenhoven, B., and Xue, L.: Confronting the challenge of modeling cloud and precipitation microphysics, J. Adv. Model. Earth Sy., 12, e2019MS001689, https://doi.org/10.1029/2019MS001689, 2020.

Myhre, G., Myhre, C. E.L., Samset, B. H. & Storelvmo, T.: Aerosols and their Relation to Global Climate and Climate Sensitivity. *Nature Education Knowledge* 4(5):7, 2013.

Neitola, K., Brus, D., Makkonen, U., Sipila, M., Lihavainen, H., and Kulmala, M.: Effect of addition of four base compounds on sulphuric-acid-water new-particle formation: a laboratory study, Boreal Environment Research, vol. 19, no. suppl. B , pp. 257-274, 2014.

Nenes, A., Chuang, P. Y., Flagan, R. C., and Seinfeld, J. H.: A theoretical analysis of cloud condensation nucleus (CCN) instruments, J. Geophys. Res.-Atmos., 106, 3449–3474, 2001

Nguyen, C. M., Wolde, M., Battaglia, A., Nichman, L., Bliankinshtein, N., Haimov, S., Bala, K., and Schuettemeyer, D.: Coincident in situ and triple-frequency radar airborne observations in the Arctic, Atmos. Meas. Tech., 15, 775–795, https://doi.org/10.5194/amt-15-775-2022, 2022.

Nichman, L., Järvinen, E., Dorsey, J., Connolly, P., Duplissy, J., Fuchs, C., Ignatius, K., Sengupta, K., Stratmann, F., Möhler, O., Schnaiter, M., and Gallagher, M.: Intercomparison study and optical asphericity measurements of small ice particles in the CERN CLOUD experiment, Atmos. Meas. Tech., 10, 3231– 3248, https://doi.org/10.5194/amt-10-3231-2017, 2017.

Paramonov, M., Kerminen, V.-M., Gysel, M., Aalto, P. P., Andreae, M. O., Asmi, E., Baltensperger, U., Bougiatioti, A., Brus, D., Frank, G. P., Good, N., Gunthe, S. S., Hao, L., Irwin, M., Jaatinen, A., Jurányi, Z., King, S. M., Kortelainen, A., Kristensson, A., Lihavainen, H., Kulmala, M., Lohmann, U., Martin, S. T., McFiggans, G., Mihalopoulos, N., Nenes, A., O'Dowd, C. D., Ovadnevaite, J., Petäjä, T., Pöschl, U., Roberts, G. C., Rose, D., Svenningsson, B., Swietlicki, E., Weingartner, E., Whitehead, J., Wiedensohler, A., Wittbom, 705 C., and Sierau, B.: A synthesis of cloud condensation nuclei counter (CCNC) measurements within the EUCAARI network, Atmos. Chem. Phys., 15, 12211–12229, https://doi.org/10.5194/acp-15-12211-2015, 2015.

Penner, J.E., et al.: Aerosols, Their Direct and Indirect Effects. In: Houghton, J.T., et al., Eds., Climate Change 2001: The Scientific Basis, Contribution of Working Group I to the Third Assessment Report of the Intergovernmental Panel on Climate Change, Cambridge University Press, Cambridge and New York, 289-348, 2001.

Petäjä, T., O'Connor, E. J, Moisseev, D., Sinclair, V. A., Manninen, A. J., Väänänen, R., Von Lerber, A., Thornton, J. A., Nicoll, K., Petersen, W., Chandrasekar, V., Smith, J. N., Winkler, P. M., Krüger, O., Hakola, H., Timonen, H., Brus, D., Laurila, T., Asmi, E., Riekkola, M.-L., Mona, L., Massoli, P., Engelmann, R., Komppula, M., Wang, J., Kuang, C., Bäck, J., Virtanen, A., Levula, J., Ritsche, M., and Hickmon, N.: BAECC: A Field Campaign to Elucidate the Impact of Biogenic Aerosols on Clouds and Climate, B. Am. Meteorol. Soc., 97, 1909–1928, https://doi.org/10.1175/BAMS-D-14-00199.1, 2016.

Petters, M. D. and Kreidenweis, S. M.: A single parameter representation of hygroscopic growth and cloud condensation nucleus activity, Atmos. Chem. Phys., 7, 1961–1971, doi:10.5194/acp-7- 1961-2007, 2007.

Petters, M. D. and Kreidenweis, S. M.: A single parameter representation of hygroscopic growth and cloud condensation nucleus activity – Part 2: Including solubility, Atmos. Chem. Phys., 8, 6273–6279, https://doi.org/10.5194/acp-8-6273-2008, 2008.

Portin, H. J., Komppula, M., Leskinen, A. P., Romakkaniemi, S., Laaksonen, A. and Lehtinen, K. E. J.: Observations of aerosol–cloud interactions at the Puijo semi-urban measurement station. Boreal Env. Res. 14: 641–653, 2009.

Post, E., R. B. Alley, T. R. Christensen, M. Macias-Fauria, B. C. Forbes, M. N. Gooseff, A. Iler, J. T. Kerby, K. L. Laidre, M. E. Mann, J. Olofsson, J. C. Stroeve, F. Ulmer, R. A. Virginia, M. Wang, The polar regions in a 2°C warmer world. Sci. Adv. 5, eaaw9883 (2019).

Penner, J.E., et al. (2001) Aerosols, Their Direct and Indirect Effects. In: Houghton, J.T., et al., Eds., Climate Change 2001: The Scientific Basis, Contribution of Working Group I to the Third Assessment Report of the Intergovernmental Panel on Climate Change, Cambridge University Press, Cambridge and New York, 289-348.

Pernov, J.B., Beddows, D., Thomas, D.C. *et al.* Increased aerosol concentrations in the High Arctic attributable to changing atmospheric transport patterns. *npj Clim Atmos Sci* **5**, 62, https://doi.org/10.1038/s41612-022-00286-y, 2022.

Pisso, I., Sollum, E., Grythe, H., Kristiansen, N. I., Cassiani, M., Eckhardt, S., Arnold, D., Morton, D., Thompson, R. L., Groot Zwaaftink, C. D., Evangeliou, N., Sodemann, H., Haimberger, L., Henne, S., Brunner, D., Burkhart, J. F., Fouilloux, A., Brioude, J., Philipp, A., Seibert, P., and Stohl, A.: The Lagrangian particle dispersion model FLEXPART version 10.4, Geosci. Model Dev., 12, 4955–4997, https://doi.org/10.5194/gmd-12-4955-2019, 2019.

Raatikainen, T., Moore, R. H., Lathem, T. L., and Nenes, A.: A coupled observation – modeling approach for studying activation kinetics from measurements of CCN activity, Atmos. Chem. Phys., 12, 4227–4243, https://doi.org/10.5194/acp-12-4227-2012, 2012.

Renard, P., Bianco, A., Baray, J.-L., Bridoux, M., Delort, A.-M. and Deguillaume, L.: Classification of Clouds Sampled at the Puy de Dôme Station (France) Based on Chemical Measurements and Air Mass History Matrices. Atmosphere , 11, 732. https://doi.org/10.3390/atmos11070732, 2020.

Roberts, G. C. and Nenes, A.: A Continuous-Flow Streamwise Thermal-Gradient CCN Chamber for Atmospheric Measurements, Aerosol. Sci. Tech., 39, 206–221, https://doi.org/10.1080/027868290913988, 2005.

Romakkaniemi, S., Maalick, Z., Hellsten, A., Ruuskanen, A., Väisänen, O., Ahmad, I., Tonttila, J., Mikkonen, S., Komppula, M., and Kühn, T.: Aerosol–landscape–cloud interaction: signatures of topography effect on cloud droplet formation, Atmos. Chem. Phys., 17, 7955–7964, https://doi.org/10.5194/acp-17-7955-2017, 2017.

Rose, D., Gunthe, S. S., Mikhailov, E., Frank, G. P., Dusek, U., Andreae, M. O., and Pöschl, U.: Calibration and measurement uncertainties of a continuous-flow cloud condensation nuclei counter (DMT-CCNC): CCN activation of ammonium sulfate and sodium chloride aerosol particles in theory and experiment, Atmos. Chem. Phys., 8, 1153–1179, https://doi.org/10.5194/acp-8-1153-2008, 2008.

Schmale, J., Henning, S., Henzing, B. et al. Collocated observations of cloud condensation nuclei, particle size distributions, and chemical composition. Sci Data 4, 170003. https://doi.org/10.1038/sdata.2017.3, 2017.

Seibert, P. and Frank, A.: Source-receptor matrix calculation with a Lagrangian particle dispersion model in backward mode, Atmos. Chem. Phys., 4, 51–63, SRef-ID: 1680-7324/acp/2004-4-51, 2004

Seinfeld, J. H. and Pandis S. N.: Atmospheric Chemistry and Physics: From Air Pollution to Climate Change (Wiley, New York, USA, 1998).

Serreze, M.C. and Barry, R.G.: Processes and impacts of Arctic amplification: A research synthesis. Global and planetary change. 77 (2011) 85-96, 2011.

Sherwood, S. C., Webb, M. J., Annan, J. D., Armour, K. C., Forster, P. M., Hargreaves, J. C., et al. (2020). An assessment of Earth's climate sensitivity using multiple lines of evidence. Reviews of Geophysics, 58, e2019RG000678. https://doi.org/10.1029/2019RG000678.

Shupe, M. D. and Intrieri, J. M.: Cloud radiative forcing of the Arctic surface: The influence of cloud properties, surface albedo, and solar zenith angle, J. Climate, 17, 616–628, 2004.

Shupe, MD, Rex, M, Blomquist, B, Persson, POG, Schmale, J, Uttal,T, Althausen, D, Angot, H, Archer, S, Bariteau, L, Beck, I, Bilberry, J, Bucci, S, Buck, C, Boyer, M, Brasseur, Z, Brooks, IM, Calmer, R, Cassano, J, Castro, V, Chu, D, Costa, D, Cox, CJ, Creamean, J, Crewell, S, Dahlke, S, Damm, E, de Boer, G, Deckelmann, H, Dethloff, K, Du¨tsch, M, Ebell, K, Ehrlich, A, Ellis, J, Engelmann, R, Fong, AA, Frey, MM,

Gallagher, MR, Ganzeveld, L, Gradinger, R, Graeser, J, Greenamyer, V, Griesche, H, Griffiths, S, Hamilton, J, Heinemann, G, Helmig, D, Herber, A, Heuze´ , C, Hofer, J, Houchens, T, Howard, D, Inoue, J, Jacobi, H-W, Jaiser, R, Jokinen, T, Jourdan, O, Jozef, G, King, W, Kirchgaessner, A, Klingebiel, M, Krassovski, M, Krumpen, T, Lampert, A, Landing, W, Laurila, T, Lawrence, D, Lonardi, M, Loose, B, Lu¨pkes, C, Maahn, M, Macke, A, Maslowski, W, Marsay, C, Maturilli, M, Mech, M, Morris, S, Moser, M, Nicolaus, M, Ortega, P, Osborn, J, Pa¨tzold, F, Perovich, DK, Peta¨ja¨,T, Pilz, C, Pirazzini, R, Posman, K, Powers, H, Pratt, KA, Preußer, A, Que´le´ ver, L, Radenz, M, Rabe, B, Rinke, A, Sachs, T, Schulz, A, Siebert, H, Silva, T, Solomon, A, Sommerfeld, A, Spreen, G, Stephens, M, Stohl, A, Svensson, G, Uin, J,Viegas, J,Voigt, C, von der Gathen, P, Wehner, B, Welker, JM, Wendisch, M, Werner, M, Xie, ZQ, Yue, F. Overview of the MOSAiC expedition: Atmosphere,2022.

Sinnarwalla, A. M., and Alofs, D. J.: A Cloud Nucleus Counter with Long Available Growth Time, Journal of Applied Meteorology and Climatology, 12(5), 831-835, 1973.

Smith, H., Connolly, P., Baran, A., Hesse, E., Smedley, A., and Webb, A.: Cloud chamber laboratory investigations into scattering properties of hollow ice particles, J. Quant. Spectrosc. Ra. Trans., 157, 106–118, https://doi.org/10.1016/j.jqsrt.2015.02.015, 2015.

Snider, J. R., Petters, M. D., Wechsler, P., & Liu, P. S. K.: Supersaturation in the Wyoming CCN Instrument, Journal of Atmospheric and Oceanic Technology, 23(10), 1323-1339, 2006.

Spiegel, J. K., Zieger, P., Bukowiecki, N., Hammer, E., Weingartner, E., and Eugster, W.: Evaluating the capabilities and uncertainties of droplet measurements for the fog droplet spectrometer (FM-100), Atmos. Meas. Tech., 5, 2237–2260, https://doi.org/10.5194/amt-5-2237-2012, 2012.

Stohl, A., Forster, C., Frank, A., Seibert, P., and Wotawa, G.: Technical note: The Lagrangian particle dispersion model FLEXPART version 6.2, Atmos. Chem. Phys., 5, 2461–2474, https://doi.org/10.5194/acp-5- 2461-2005, 2005.

Stratmann, F., Kiselev, A., Wurzler, S., Wendisch, M., Heintzenberg, J., Charlson, R. J., Diehl, K., Wex, H., & Schmidt, S.: Laboratory Studies and Numerical Simulations of Cloud Droplet Formation under Realistic Supersaturation Conditions, Journal of Atmospheric and Oceanic Technology, 21(6), 876-887, 2004.

Tunved P., Hansson H.-C., Kerminen V.-M., Ström J., Dal Maso M., Lihavainen H., Viisanen Y., Aalto P.P., Komppula M. & Kulmala M. 2006. High natural aerosol loading over boreal forests. Science 5771, 261–263.2001–2005.

Twomey, S. (1963). Measurements of natural cloud nuclei. Journal de Recherches Atmospheriques, 1, 101–105

Twomey, S. (1977). The Influence of Pollution on the Shortwave Albedo of Clouds, Journal of Atmospheric Sciences, 34(7), 1149-1152.

Wandinger, U., Apituley, A., Blumenstock, T., Bukowiecki, N., Cammas, J.-P., Connolly, P., De Mazière, M., Dils, B., Fiebig, M., Freney, E., Gallagher, M., Godin-Beekmann, S., Goloub, P., Gysel, M., Haeffelin, M., Hase, F., Hermann, M., Herrmann, H., Jokinen, T., Komppula, M., Kubistin, D., Langerock, B., Lihavainen, H., Mihalopoulos, N., Laj, P., Lund Myhre, C., Mahieu, E., Mertes, S., Möhler, O., Mona, L., Nicolae, D., O'Connor, E., Palm, M., Pappalardo, G., Pazmino, A., Petäjä, T., Philippin, S., Plass-Duelmer, C., Pospichal, B., Putaud, J.-P., Reimann, S., Rohrer, F., Russchenberg, H., Sauvage, S., Sellegri, K., Steinbrecher, R., Stratmann, F., Sussmann, R., Van Pinxteren, D., Van Roozendael M., Vigouroux C., Walden C., Wegene R., and Wiedensohler, A.: ACTRIS-PPP Deliverable D5.1: Documentation on technical concepts and requirements for ACTRIS Observational Platforms, available at: https: //www.actris.eu/sites/default/files/Documents/ACTRISPPP/Deliverables/ACTRISPPP_WP3_D3.1_ACTRISCostBook.pdf (last access: 8 November 2022), 2018.

Wendisch, M., Macke, A., Ehrlich, A., Lüpkes, C., Mech, M., Chechin, D., Dethloff, K., Velasco, C. B., Bozem, H., Brückner, M., Clemen, H.-C., Crewell, S., Donth, T., Dupuy, R., Ebell, K., Egerer, U., Engelmann, R., Engler, C., Eppers, O., Gehrmann, M., Gong, X., Gottschalk, M., Gourbeyre, C., Griesche, H., Hartmann, J., Hartmann, M., Heinold, B., Herber, A., Herrmann, H., Heygster, G., Hoor, P., Jafariserajehlou, S., Jäkel, E., Järvinen, E., Jourdan, O., Kästner, U., Kecorius, S., Knudsen, E. M., Köllner, F., Kretzschmar, J., Lelli, L., Leroy, D., Maturilli, M., Mei, L., Mertes, S., Mioche, G., Neuber, R., Nicolaus, M., Nomokonova, T., Notholt, J., Palm, M., van Pinxteren, M., Quaas, J., Richter, P., Ruiz-Donoso, E., Schäfer, M., Schmieder, K., Schnaiter, M., Schneider, J., Schwarzenböck, A., Seifert, P., Shupe, M. D., Siebert, H., Spreen, G., Stapf, J., Stratmann, F., Vogl, T., Welti, A., Wex, H., Wiedensohler, A., Zanatta, M., and Zeppenfeld, S.: The Arctic Cloud Puzzle: Using ACLOUD/PASCAL Multiplatform Observations to Unravel the Role of Clouds and Aerosol Particles in Arctic Amplification, B. Am. Meteorol. Soc., 100, 841–871, https://doi.org/10.1175/BAMS-D-18-0072.1, 2019.

Wex, H., Kiselev, A., Ziese, M., and Stratmann, F.: Calibration of LACIS as a CCN detector and its use in measuring activation and hygroscopic growth of atmospheric aerosol particles, Atmos. Chem. Phys., 6, 4519–4527, https://doi.org/10.5194/acp-6-4519-2006, 2006.

Zuidema, P., Baker, B., Han, Y., Intrieri, J., Key, J., Lawson, P., Matrosov, S., Shupe, M., Stone, R., and Uttal, T.: An Arctic springtime mixed-phase cloudy boundary layer observed during SHEBA, J. Atmos. Sci., 62, 160–176, 2005.

I

A Finnish Meteorological Institute–Aerosol Cloud Interaction Tube (FMI–ACIT): Experimental setup and tests of proper operation

Konstantinos M. Doulgeris, David Brus, Tomi Raatikainen, and Veli-Matti Kerminen

Citation: The Journal of Chemical Physics **149**, 124201 (2018); doi: 10.1063/1.5037298
View online: https://doi.org/10.1063/1.5037298
View Table of Contents: http://aip.scitation.org/toc/jcp/149/12
Published by the American Institute of Physics

A Finnish Meteorological Institute–Aerosol Cloud Interaction Tube (FMI–ACIT): Experimental setup and tests of proper operation

Konstantinos M. Doulgeris,[1,a)] David Brus,[1] Tomi Raatikainen,[1] and Veli-Matti Kerminen[2]
[1]*Finnish Meteorological Institute, Erik Palménin Aukio 1, P.O. Box 503, FI-00101 Helsinki, Finland*
[2]*Institute for Atmospheric and Earth System Research/Physics, Faculty of Science, University of Helsinki, Helsinki, Finland*

(Received 23 April 2018; accepted 6 September 2018; published online 26 September 2018)

The Finnish Meteorological Institute–Aerosol Cloud Interaction Tube (FMI–ACIT) is a multi-purpose instrument for investigating atmospherically relevant interactions between aerosol particles and water vapor under defined laboratory conditions. This work introduces an experimental setup of FMI–ACIT for investigation of the aerosol activation and the droplet growth under supersaturated conditions. Several simulations and experimental tests were conducted to find out what the proper operational parameters are. To verify the ability of FMI–ACIT to perform as a cloud condensation nuclei (CCN) counter, activation experiments were executed using size selected ammonium sulfate [$(NH_4)_2SO_4$] particles in the size range of 10–300 nm. Supersaturations from 0.18% to 1.25% were tested by experiments with different temperature gradients. Those showed that FMI–ACIT can effectively measure CCN in this range. Measured droplet size distributions at supersaturations 0.18% and 1.25% are in good agreement with those determined by a droplet growth model. *Published by AIP Publishing.*
https://doi.org/10.1063/1.5037298

I. INTRODUCTION

Aerosols play an important role in the atmospheric radiation budget; they can absorb or scatter the incoming or outgoing radiation and they have a potential to activate into cloud droplets, i.e., act as cloud condensation nuclei (CCN). The ability of aerosols to act as CCN is dependent on the supersaturation of water vapor, aerosol size and its chemical composition.[1] Properties of clouds and their formation processes are poorly understood particularly in mixed phase and ice clouds.[2]

Numerous devices with different set ups were built for measuring CCN. Those devices can be classified into two major categories according to the way they produce water vapor supersaturation, first by using the nonlinear dependence of water vapor pressure upon temperature and second by using the difference between water vapor diffusivity and thermal diffusivity. The first mechanism is widely used in static diffusion chambers[3,4] and the second mechanism is used in laminar flow chambers.[5–8]

Nenes *et al.*[9] made a theoretical analysis of basic cloud condensation nucleus devices which involves both static diffusion chambers and laminar flow diffusion chambers. The original design of a static diffusion chamber was presented by Twomey.[3] There, two metal parallel plates, one hot and one cold, were placed with their facing surfaces wetted. Sinnarwalla and Alofs[10] developed the continuous flow parallel metal plate thermal diffusion chamber to avoid some limitations that the static diffusion chamber had. An improvement version of the continuous flow parallel metal plate thermal diffusion chamber was introduced by Fukuta and Saxena[11] where the gradient in temperature was imposed perpendicular to the flow direction so that particles with the same residence time experience different supersaturations along different streamlines. Hudson[5] modified the continuous flow thermal diffusion chamber and built a dynamic spectrometer which could simulate conditions of a warm cloud and it could be used also in airborne measurements. Chuang *et al.*,[12] introduced the Caltech spectrometer which used the Hudson method in a flow tube.

During the last couple of decades several attempts have taken place to construct and introduce CCN counter devices with different possibilities and features. Giebl *et al.*[13] investigated CCN activation of oxalic and malonic test aerosols using the University of Vienna cloud condensation nuclei counter which operated on the principle of a static thermal diffusion chamber and could have supersaturations in the range from 0.1% to 2%. Stratmann *et al.*[6] introduced Leipzig Aerosol Cloud Interaction Simulator (LACIS) which was based on a laminar flow tube. Wex *et al.*[14] proved that LACIS can perform as CCN detector and is able to measure hygroscopic growth of atmospheric particles. Snider *et al.*[15] developed and introduced the Wyoming CCN Instrument, a thermal diffusion cloud chamber. Roberts and Nenes[7] introduced a cylindrical continuous-flow thermal-gradient diffusion chamber that provides *in situ* measurements of CCN and can be operated in airborne measurements for supersaturations from 0.1% to 3%. This instrument produces supersaturation by establishing a constant streamwise temperature gradient so that the difference in water vapor and thermal diffusivity yields a quasi-uniform centerline supersaturation. Later, Lance *et al.*[16] explored fully the possibilities of this instrument by using a

a)Author to whom correspondence should be addressed: konstantinos.doulgeris@fmi.fi

numerical model. Rose *et al.*[17] gave a full description of the measurement uncertainties of the instrument based on calibration experiments CCN counter using ammonium sulphate and sodium chloride particles and determined the supersaturation using Köhler theory.[18]

Both static diffusion chambers and laminar flow chambers have been also used for other purposes except for measuring CCN. Further investigations were made with several different CCN counters which were modified in order to investigate ice nucleation.[19–21] Connolly *et al.*[8] introduced a laminar flow tube with larger dimensions (10 m high, 1 m diameter) with the ability to measure ice crystals.

In 2001, Lihavainen and Viisanen[22] built a laminar flow diffusion chamber for studying homogeneous nucleation of *n*-hexanol. Based on their design, we developed an alternative version of the laminar flow diffusion chamber in order to measure ice and cloud droplet formation under defined laboratory conditions. The relatively large dimensions of the Finnish Meteorological Institute–Aerosol Cloud Interaction Tube (FMI–ACIT) setup allows long (tens of minutes) steady state measurements. Our future work will concentrate on testing FMI–ACITs' ability to investigate ice nuclei formation, but in this paper we focus on CCN. The experimental setup of FMI–ACIT is described in detail in Sec. II A. In Secs. II B and II C, a finite element method (*femtube*2 model) and a droplet growth model that are used for the comparison with our experimental data are presented. Subsequently, in Sec. III A, operational parameters of FMI–ACIT are investigated and chosen based on the *femtube*2 model and several experimental tests. In Sec. III B, experimental CCN activation tests that characterize our setup are presented. Finally, we compare aerosol growth calculated by the model to that from the experimental tests for two different supersaturations.

II. METHODS

A. Experimental setup

FMI–ACIT is based on the principle of a laminar flow diffusion chamber,[22] but it shares the design of a laminar flow tube just as used in our previous studies.[23,24] The experimental setup of FMI–ACIT is presented in Fig. 1. It consists of three main parts: a humidification system (HS), a preheater (PR), and a condenser (C), which are described in the following text. The set values of all the flows and the temperatures of the three main parts were kept constant during each experiment. The temperatures of the humidification system (T_{HS}) and preheater (T_{PR}) are adjustable and controlled by circulating liquid baths (LAUDA RC 6 CS), and the temperature of the condenser (T_C) is adjustable and controlled by another circulating liquid bath (LAUDA Proline RP 1845). The temperatures are measured with six PT100 probes (one in the humidification system, two in the preheater, and four in the condenser). Every part of the FMI–ACIT is insulated from the environment.

Polydisperse aerosol was produced by an aerosol generator (Topas, model ATM226) and subsequently dried with silica-gel dryer. The polydisperse aerosol was then size selected by a differential mobility analyser (DMA, Hauke-type, length 0.109 m). The DMA was operated with 2.0 l min^{-1} aerosol and 10.0 l min^{-1} sheath and excess air flows. The initial concentration of monodisperse aerosol, before entering the humidification system of the FMI–ACIT, was measured

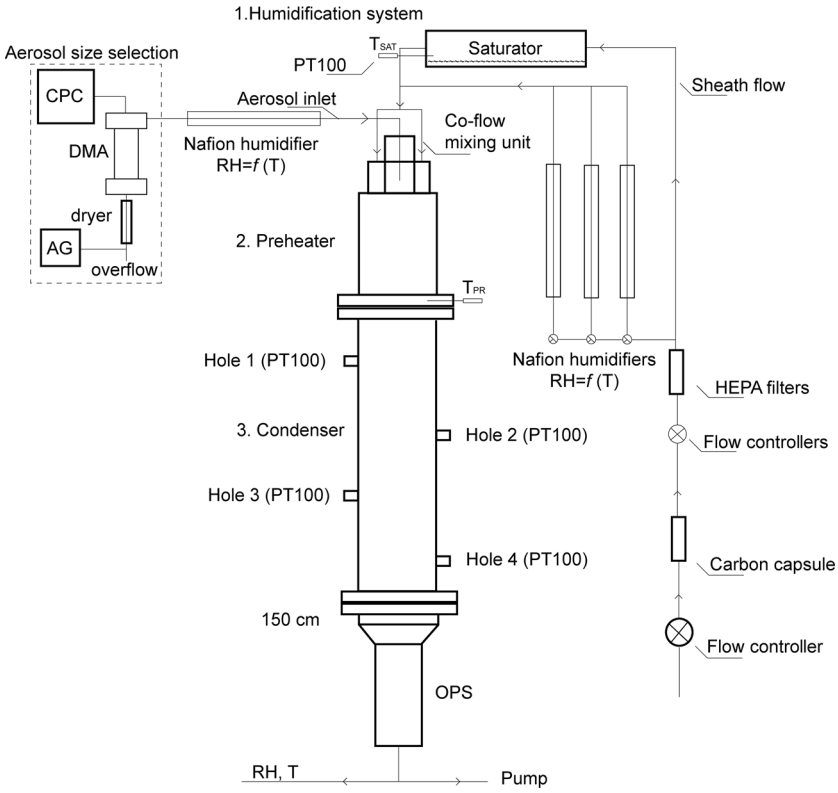

FIG. 1. The experimental setup of FMI–ACIT. AG represents the aerosol generator (Topas, model ATM226), CPC represent the condensation particle counter (CPC, model 3776, TSI, Inc.) and DMA represents the differential mobility analyser (DMA, Hauke-type, length 0.109 m). The temperatures are measured with six PT100 probes (one in the saturator, one in the preheater, and four in the condenser). OPS represent Optical Particle Sizer (OPS model 3330, TSI, Inc. USA) which is used as a counter in this work.

by a condensation particle counter (CPC, model 3776, TSI, Inc.).

The humidification system used in the experimental setup of this work consists of one saturator and four nafion humidifiers. One humidifier was placed after the aerosol size selection and the remaining three humidifiers were placed in parallel to the saturator to humidify the sheath flow. The four nafion humidifiers were used only during initial tests and especially at high flow rates (6–10 l min^{-1}) in order to ensure that desired supersaturation will be achieved inside the condenser. During the activation experiments (Sec. III B), only one humidifier was used (the one after the aerosol size selection). The saturator is a horizontal iron tube with a Teflon insert having an inner diameter, I.D ID = 5 cm and length L = 1 m. A steady flow of purified and particle free air was introduced to the humidification system using ultrapure milli-Q water (resistivity 18.2 MΩ cm@at 25 °C). The air runs through a set of high efficiency particle absorbers (HEPA filters, Pall Corp.) and active carbon capsules (Pall Corp.) before entering the saturator/humidifiers. The temperature of the humidification system controls the amount of vapor in the air flow. All humidifiers and the saturator were set to the same temperature.

Aerosol enters the preheater from the humidification system through the stainless steel tube I.D. ID = 4 mm and length (inside the preheater) = 5 cm. Preheater is a stainless steel cylinder and has I.D. ID = 6 cm and L = 0.5 m. The sheath flow enters the preheater via a Teflon part having ports of I.D. ID = 1 mm. The ports were drilled in as concentric circles with 1 cm gap around the aerosol inlet and 1 cm from the flow tube preheater wall. The total flow inside the flow tube is combined aerosol and sheath flow. Those are kept constant with a mass flow controller to within ±3% (MKS type 250). The sheath flow was measured continuously with a mass-flow meter (model 4043, TSI, Inc.) placed before the humidification system and the aerosol flow was measured before and after every run with a bubble flow meter (Gilian Gilibrator-2 air flow calibrator, Sensidyne) placed after the DMA and before the flow enters the nafion humidifier. The temperature of the preheater was set always higher (∼1°) than the temperature of the humidification system in order to stabilize the flow and avoid condensation in the top section of the flow tube.

The condenser is a stainless steel cylinder and has I.D. ID = 6 cm and L = 1 m. Both the preheater and the condenser are installed vertically to avoid gravitational settling of the particles. The connection between preheater and condenser was insulated to make as steep temperature change as possible and thus create supersaturation at well-defined conditions. Thermal separation was made with a Teflon insulator with a thickness of 2 cm and I.D. ID = 6 cm. Figures 2(a) and 2(b) demonstrate typical profiles of temperature and saturation ratio inside the condenser using conditions from the experimental measurements. The conditions used for the simulations were T_{HS} = 299.00 K, T_{PR} = 300.00 K, T_C = 281.00 K, and Q_{tot} = 2.0 l min^{-1}. The higher saturation ratio was first reached close to the wall since the flow started to cool from the wall toward the centerline. This is because the rate of heat transfer by conduction is lower than the rate of mass transfer by molecular diffusion.[25] Saturation ratios inside the condenser centerline range from 0.94 to 1.1. This is because the rate of heat transfer by conduction is lower than the rate of mass transfer by molecular diffusion.[25] The temperature of the condenser had a drop in its first 20 cm. After the first 20 cm of the condenser, the mixture in the centerline reached the same temperature with the tube walls. Figure 2(c) represents both the saturation ratio and the temperature along the centerline of the condenser. Saturation ratio increased sharply from sub-saturated conditions to supersaturated conditions (saturation ratio higher than 1). After this sharp increase, the saturation ratio reached its maximum value (around 20 cm from the beginning of the condenser) and decreased slowly to the saturation ratio of 1. The saturation ratio during this simulation example reached a maximum value of 1.013 along the centerline. The full description of the model used for the simulation is presented in Sec. II B.

Particles are injected to the preheater close to the centerline so that they have similar relative humidity history and residence time and also to avoid wall losses. Ideally, every single particle would be travelling only along the centerline of the preheater and the condenser, but in reality some particles traveled through regions with different saturation ratios.

An Optical Particle Sizer (OPS model 3330, TSI, Inc. USA) which detects particles in the range 0.3–10 μm was used as a counting system and it was connected to the end of the condenser. The OPS was modified in a way that the OPS pump was bypassed and the flow tube total flow passed through the OPS counting chamber, and the raw counts were corrected accordingly.

B. Finite element method tube2 model description

The saturation ratio and the temperature profiles inside the condenser of the FMI–ACIT cannot be measured experimentally. For that reason, we adopted the existing finite element method tube 2 (*femtube*2) model, which is described in detail in the study of Lihavainen.[26]

The model solves five coupled differential equations, heat and mass transfer, equations of motions, and an equation of continuity to simulate the flows inside the condenser. However, in order to simplify these equations, several assumptions were made. These are that the equations can be solved in a steady state, the effect of radial velocity is negligible and set to zero, and the flow is incompressible. The simplifications of the equations of motion lead to a simple problem that was analytically solved and produced a parabolic lateral velocity profile.[27] The boundary conditions for the heat and mass transfer equations are

$$T(r, z = z_0) = T_{PR}, \tag{1}$$

$$T(R_0, z_0 < z \leq 0) = T_{PR}, \tag{2}$$

$$T(R_0, z > 0) = T_C, \tag{3}$$

$$\omega(r, z = z_0) = \omega_{eq}(T_{HS}), \tag{4}$$

$$\omega(R_0, z_0 < z \leq 0) = \omega_{eq}(T_{HS}), \tag{5}$$

$$\omega(R_0, z > 0) = \omega_{eq}(T_C), \tag{6}$$

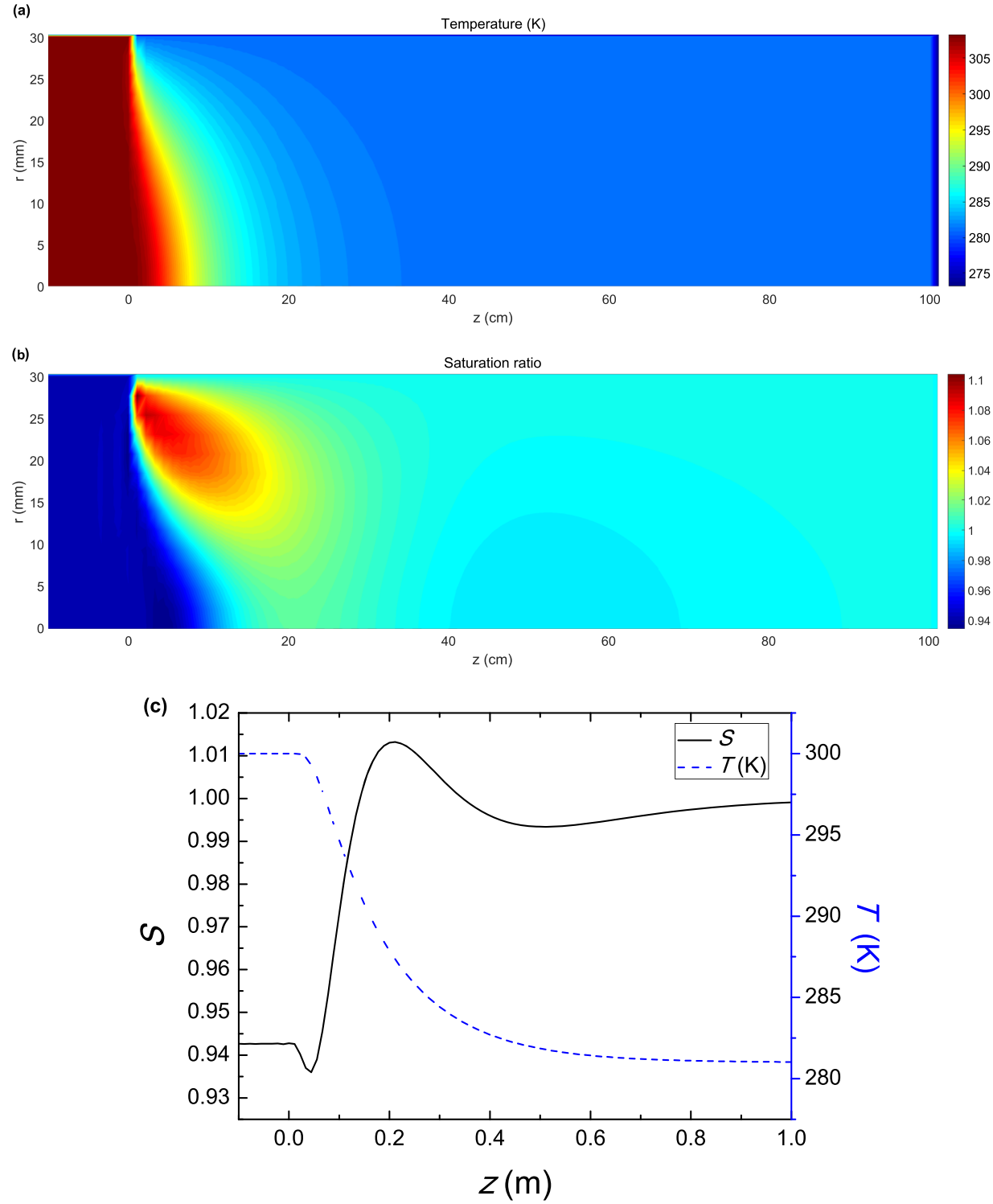

FIG. 2. Simulated profiles of (a) the temperature and (b) the saturation ratio inside the FMI–ACIT where the y-axis and x-axis represents the radial and lateral coordinates of the condenser. (c) Details of temperature (T) and the saturation ratio (S) along the center line of the condenser as calculated with the *femtube*2 model. Temperatures of the humidification system, the preheater, and the condenser were set as 299.00, 300.00, and 281.00 K, respectively. The total flow rate inside the condenser was 2 l min^{-1} and the flow direction is from left to right.

where T_{PR} is the temperature of the preheater, T_{C} is the temperature of the condenser, T_{HS} is the temperature of the humidification system, and R_0 is the radius of the tube. Additionally, $\omega_{\mathrm{eq}}(T_{\mathrm{HS}})$ is the mass fraction of water vapor defined by the saturation vapor pressure at the temperature T_{HS}, $\omega_{\mathrm{eq}}(T_{\mathrm{C}})$ is the mass fraction of water vapor defined by the saturation vapor pressure at the temperature T_C, $z = 0$ is the boundary point between the preheater and the condenser, and z_0, -10 cm, is a chosen starting point of calculations in the preheater. The first boundary condition in Eq. (1) sets the temperature at z_0 to that of the preheater. The second boundary condition in Eq. (2) sets the temperature of the wall between the starting

point of the calculation, z_0, and the boundary between the preheater and the condenser, $z = 0$. The third boundary condition in Eq. (3) sets the temperature at the wall of the condenser. The fourth boundary condition in Eq. (4) sets the mass fraction profile across the tube at z_0 to the value defined by the equilibrium vapor pressure at the temperature of the saturator. The fifth boundary condition in Eq. (5) sets the mass fraction of the vapor at the wall between z_0 and z to the same value as the fourth boundary condition. The sixth boundary condition in Eq. (6) sets the mass fraction at the wall of the condenser to the value defined by the equilibrium vapor pressure at the temperature of the condenser wall. As a binary diffusion coefficient (D_{AB}), we used the most common expression based on both theory and interpolation of experimental data by Hall and Pruppacher.[28]

The simulation based on the Eulerian equations provides us profiles of the temperature (T) and saturation ratio (S) inside the preheater and the condenser. Boundary conditions for the simulations that are presented in this study were set to match the values of the experimental conditions. These parameters are the temperature of the walls of the preheater and the condenser, the temperature of the laboratory which was measured directly, the total flow rate inside the flow tube, the atmospheric pressure and the dimensions of the flow tube.

C. Droplet growth model

To describe the growth of the particles inside the flow chamber, we used the droplet growth model as described in detail in Raatikainen *et al.*[29] The rate of the change of the droplet size is described by the differential growth equation,[30,31]

$$D_p \frac{dD_p}{dt} = \frac{S - S_{eq}}{\frac{\rho_w R T_\infty}{4 p^o(T_\infty) D'_u M_w} + \frac{\Delta H_u \rho_w}{4 k'_a T_\infty}\left(\frac{\Delta H_u M_w}{T_\infty R} - 1\right)}, \tag{7}$$

where D_p is the droplet diameter, S and S_{eq} are ambient and droplet water equilibrium saturation ratios, ρ_w is the water density, M_w is the molar mass of water, T_∞ is temperature of the environment, $p^o(T_\infty)$ is water saturation vapor pressure at temperature of the environment, and ΔH_u is the water vaporization enthalpy. Equation (7) is considered as an initial value problem where temperature and water vapor saturation ratio depend on time or on the location of the droplet in the flow tube. The *femtube*2 model was used to generate supersaturation and temperature profiles inside the flow tube as described in Sec. II B, and the droplet velocity was calculated from the total flow rate while assuming a parabolic lateral velocity profile.

Equation (7) contains D'_u which is the diffusivity of water and the k'_a which is the thermal conductivity of air that account for non-continuum effects,[31]

$$D'_u = \frac{D_u}{1 + \frac{2D_u}{a_c D_p}\sqrt{\frac{2\pi M_w}{R T_\infty}}}, \tag{8}$$

$$k'_a = \frac{k_a}{1 + \frac{2k_a}{a_T D_p \rho_a c_p}\sqrt{\frac{2\pi M_a}{RT}}}, \tag{9}$$

where D_u is the diffusivity of water vapor in air, a_c is the condensation coefficient, M_a is the average molar mass of air, k_a is the thermal conductivity of air, ρ_a is the density of air, c_p is the heat capacity of air, and a_T is the thermal accommodation coefficient.

For the calculation of the water equilibrium saturation ratio of the growing droplets, Köhler theory is used,[17]

$$S_{eq} = a_w \exp\left(\frac{4\sigma M_w}{R T_\infty \rho_w D_p}\right), \tag{10}$$

where σ is the surface tension and a_w is the Raoult term and it is calculated following the kappa-Köhler approach[32,33]

$$a_w = \left(1 + \frac{\kappa}{\left(D_p/D_{dry}\right)^3 - 1}\right)^{-1}, \tag{11}$$

where D_{dry} is the dry diameter of the particle and κ is a single solute hygroscopicity parameter.

All the parameters of the droplet growth model are presented in the supplementary material in Tables SI–SIII.

III. RESULTS

All the FMI–ACIT experiments were made at the Finnish Meteorological Institute, Helsinki, Finland. First, we present which were the best operational parameters (flow rate and temperatures) of the flow tube by modifying initial parameters for *femtube*2 model simulations. To verify the best flow rate found by the simulations, an experimental particle transmission efficiency test was also conducted. All these findings are presented in Sec. III A. Then, to test the functionality of FMI–ACIT as a CCN counter device, several CCN experiments were conducted using the best operational parameters. We injected size-selected ammonium sulfate [$(NH_4)_2SO_4$] particles into the flow tube at different supersaturations. Our experimental results are presented in Sec. III B and show that FMI–ACIT can perform as a CCN counter.

A. Operational characteristics of the FMI–ACIT

The parameters and the conditions of this experimental setup can be modified to achieve different levels of saturation ratios. Several simulations and numerous experimental tests were made to investigate and verify the most suitable operational conditions for the FMI–ACIT.

First, we explored which is the most suitable total flow rate, i.e., the sum of the sheath and the aerosol flow rates. Using the *femtube*2 model, we investigated the behavior of the saturation ratio (S) and the temperature along the center line of the condenser. The following temperature conditions (T_{HS} = 299.00 K, T_{PR} = 300.00 K, and T_C = 281.00 K) were used for the simulations and the total flows were changed from 0.5 to 1.0 and then up to 10.0 l min^{-1} with steps of 1.0 l min^{-1}.

Figures S1 and S2 present the saturation ratio and temperature of the condenser, respectively, for four different flow rates; see the supplementary material for details. Knowing that the aerosol is injected close to the centerline, Figs. 3(a) and 3(b) show these parameters along the centerline of the

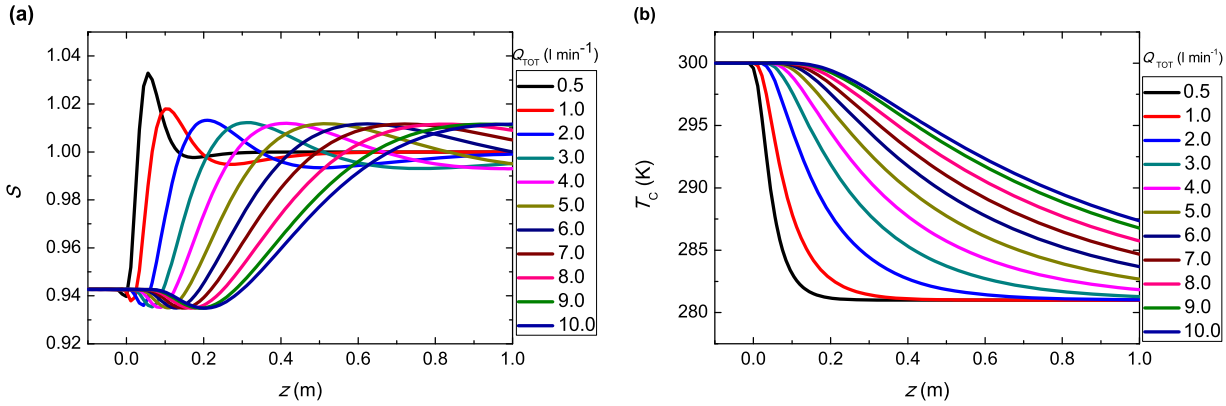

FIG. 3. Details of (a) the saturation ratio (S) and (b) the temperature along the centerline of the condenser (TC) as calculated with the *femtube*2 model for different total flow rates (Q_{TOT}). Conditions for the simulations were T_{HS} = 299.00 K, T_{PR} = 300.00 K, and T_C = 281.00 K.

condenser for all the studied flow rates. Figure 3(a) shows that by increasing the total flow rate, the location of the maximum saturation ratio moved further along the centerline of the condenser. For total flow rates higher than 3.0 l min^{-1}, the maximum saturation ratio was observed after 0.4 m along the centerline of the condenser. For flows higher than 2.0 l min^{-1}, there was no change in the maximum saturation ratio along the tube centerline, but these maximum saturation ratios were lower than those for 0.5 and 1.0 l min^{-1} flow rates. In this particular example, the maximum saturation ratio increases from a value of 1.013 for the total flow rate of 2.0 l min^{-1} to values of 1.017 and 1.030 for total flow rates of 1.0 l min^{-1} and 0.5 l min^{-1}, respectively. Finally, Fig. 3(b) indicates that for total flow rates higher than 3.0 l min^{-1}, the temperature of the condenser along its centerline did not have enough time to reach the temperature of the condenser wall.

In addition to the simulations that were performed, an experimental transmission efficiency test was done to quantify the particle losses using six different total flow rates. During this test, temperatures of the humidification system, preheater, and condenser were kept constant (T_{HS} = 299.00 K, T_{PR} = 300.00 K, and T_C = 281.00 K) and total flow rates of 1.0, 2.0, 3.0, 5.0, 8.0, and 10 l min^{-1} were set inside the condenser. Monodisperse ammonium sulfate particles with the sizes of 100, 200, and 300 nm were used since these particles should be activated at the supersaturations predicted by the *femtube*2 model. The number concentration of monodisperse dry aerosols (between 400 and 750 cm^{-3}) was continuously measured at the beginning of the humidification system and droplets were continuously measured at the end of the condenser (between 150 and 745 cm^{-3}). Their ratio produced the counting efficiency for each total flow rate; the results are presented in Fig. 4 as a penetration through the flow tube as a function of the total flow rate.

Using both simulations and the experimental particle transmission efficiency test, it seems that the FMI–ACIT performs the best at total flow rates between 1 and 3 l min^{-1}. At lower total flow rates (<1 l min^{-1}) the particles grow to bigger sizes, but they could be lost to the wall due to slow flow. At higher total flow rates (>3 l min^{-1}), it takes relatively long for the temperature of the flow to stabilize and reach the condenser wall temperature. As a result, the particles do not experience high enough supersaturation to be activated. The OPS can register particles larger than 300 nm, but its counting efficiency is only ~50% at that size.

Every further operation tests in this work were made using the total flow rate of 2.0 l min^{-1} with the resulting Reynolds number around 30, i.e., the flow inside the flow tube was laminar. Residence time, which is the time for particles to travel through the condenser along the centerline, for total flow of ~2.0 l min^{-1} was ~50 s.

B. FMI-ACIT as a CNN counter

After we completed the characterization of the flow tube, we used the most suitable parameters as Sec. III A suggested and tested the FMI–ACIT setup as a CCN counter by performing a series of experiments. Monodisperse ammonium sulfate [$(NH_4)_2SO_4$] aerosol was produced and used for every test that was conducted. Purified, particle free air was used as a carrier gas and a total flow rate of 2.0 l min^{-1} was used for the experiments as the simulation and the flow rate transmission

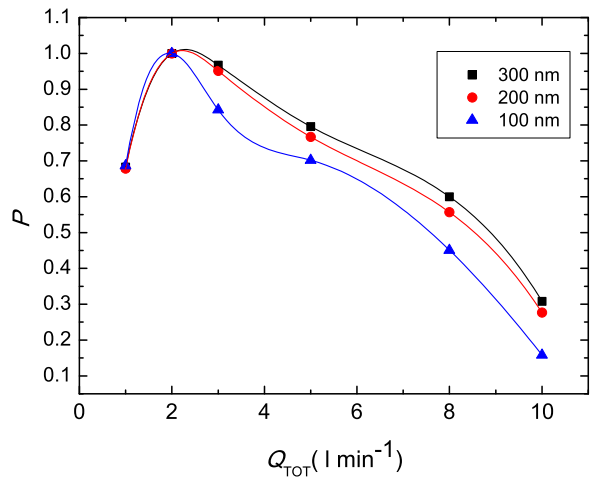

FIG. 4. Particle penetration efficiencies (P) as a function of total flow rate (Q_{TOT}) for 100, 200, and 300 nm particles. Conditions for the tests were THS = 299.00 K, TPR = 300.00 K, and TC = 281.00 K. According to the *femtube*2 model, maximum supersaturation along the centerline of the condenser range from 1.70% to 1.10%. Solid lines are interpolation curves and they were made were made just to lead readers' eyes.

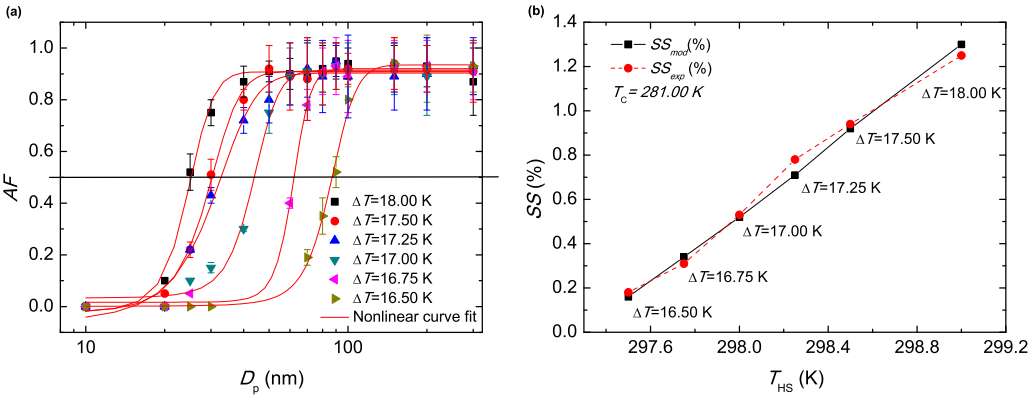

FIG. 5. (a) Activated fraction (*AF*) versus dry diameter (D_p) of ammonium sulfate particles for each ΔT. Nonlinear curve fit was calculated using the sigmoidal dose response function. (b) Maximum supersaturation as it was simulated using the *femtube*2 model and experimental supersaturation (%) versus the temperature of humidification system. ΔT (difference between the temperature of the humidification system and the condenser) is also provided.

efficiency test suggested. All measurements were performed at ambient atmospheric pressure (~1 atm). The sheath flow rate was measured continuously during the experiments using a mass-flow meter (model 4043, TSI, Inc.). The aerosol flow rate was measured and checked both at the beginning and the end of each measurement using a bubble flow meter (Gilian Gilibrator-2 air flow calibrator, Sensidyne). A sheath to aerosol flow ratio of 8(±0.2) inside the condenser was used during all the experimental tests.

Activation of ammonium sulfate particles was measured for six humidification system and condenser temperature differences (ΔT): 18.00, 17.50, 17.25, 17.00, 16.75, and 16.50 K. Every ΔT yielded a different supersaturation inside the condenser as described below.

Dry ammonium sulfate particles with diameters ranging from 10 to 300 nm were used in each measurement. From 10 to 30 nm, we used step of 5 nm, from 30 to 100 nm, step of 10 nm and last three sizes were 150, 200, and 300 nm. Each size that was injected inside the preheater was measured for 7 min. After that, we were waiting until OPS showed zero particle counts and then we were waiting five more minutes to ensure that the tube did not contain any particles. We repeated the same procedure for the following size until we obtained the full size range. Next step was to let the FMI–ACIT dry and purify at elevated temperature (~303 K) overnight. Next day, when the tube was completely dry and clean, we repeated the same cycle for the same conditions to confirm the reproducibility of our measurements.

From these experimental measurements, we calculated two main values to test that FMI–ACIT is able to work as a CCN counter; activated fraction and growth of the activated particles.

First, the *activated fraction* was defined as $C_{A,END}/C_{A,INIT}$, where $C_{A,END}$ is the concentration of activated aerosol at the end of FMI–ACIT measured by the OPS and $C_{A,INIT}$ is the initial concentration of aerosol before entering the preheater measured by the CPC. For the calculation of $C_{A,END}$, we eliminated the first three bins of the OPS counter representing sizes below 0.65 μm. This choice was made due to noisy counts caused by instruments artifacts independent on any flow tube operational parameter. This resulted in slightly underestimated values of $C_{A,END}$. For every set of dry sizes, a sharp increase of the activated fraction occurs and an activated fraction curve was produced by fitting to our experimental data. Figure 5(a) presents the six obtained activation curves. Higher values of ΔT produced higher values of *SS* through the centerline of the condenser. For larger particles, the activated fraction increased

TABLE I. FMI–ACIT temperature gradients along with D_{50} and supersaturation during our experiments. T_{HS} is the temperature of the humidification system, T_{PR} is the temperature of the preheater, and T_C is the temperature of the condenser. D_{50} was determined as the dry diameter for which activated fraction of particles reach 50%. ΔT is the humidification system and condenser temperature difference. SS_{exp} (%) is the experimental supersaturation inside the condenser and SS_{mod} is the maximum supersaturation along the centerline of the condenser as predicted by the *femtube*2 model.

T_{HS} (K)	T_{PR} (K)	T_C (K)	ΔT (K)	D_{50} (nm)	SS_{exp} (%)	SS_{mod} (%)
299.00	300.00	281.00	18.00	25.25	1.25	1.30
298.50	299.50	281.00	17.50	30.35	0.94	0.92
298.25	299.25	281.00	17.25	32.90	0.78	0.71
298.00	299.00	281.00	17.00	43.90	0.53	0.52
297.75	298.75	281.00	16.75	62.30	0.31	0.34
297.50	298.50	281.00	16.50	87.00	0.18	0.16

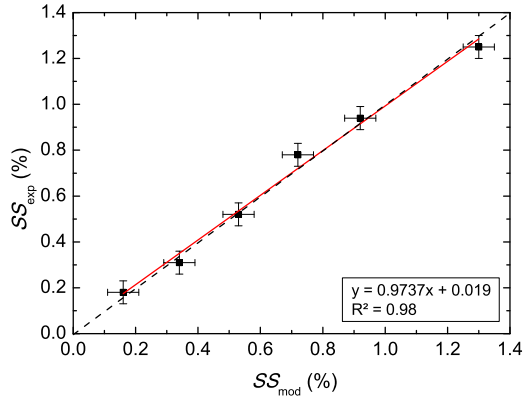

FIG. 6. Experimental supersaturation versus model predicted maximum supersaturation (%). The red line represents a 1-1 line and the blue line represents linear fit to the six points.

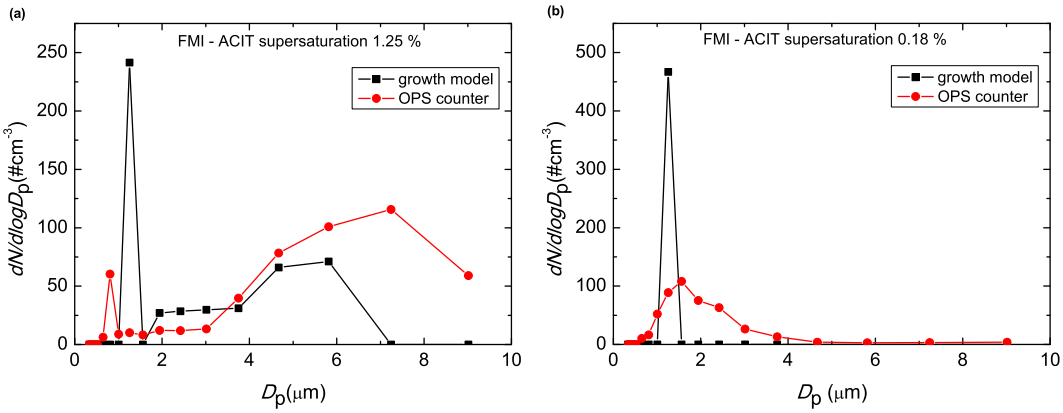

FIG. 7. Predicted and measured droplet size distributions for supersaturation of 1.25% and 0.18%. The difference between predicted and measured sizes indicates that some particles were travelling through different supersaturations.

and approached the average value 0.91 with standard deviation of 0.11. In order to obtain the experimental supersaturation (SS_{exp}),[33] D_{50} diameter was found from each activated fraction curve. D_{50} was determined as the dry diameter for which activated fraction of particles reached 50%. Finally, using the particle size at 50% activated fraction and the temperature of the condenser, the experimental supersaturation inside the condenser was calculated from the Köhler theory,[17,32] as shown in Eq. (10). Table I shows the temperature gradients that were used in this work, D_{50} values, and the six different SS_{mod} and SS_{exp} inside the condenser. SS_{mod} is the maximum supersaturation along the centerline of the condenser as predicted by the *femtube*2 model. Figure 5(b) shows the modeled and the experimental supersaturations for each ΔT. In the text below, we refer to each experiment using the experimental supersaturation (SS_{exp}).

A comparison of the model predicted and experimental supersaturations is presented in Fig. 6. A linear fit based on these six points is presented and shows very good agreement between the two supersaturation values (R^2 = 0.98). Standard deviation for each point is a result of four experiments conducted at the same conditions in order to prove the reproducibility of our results.

At lower supersaturation inside the tube (<0.4%) doubly charged particles were noticed for dry diameters from 10 to 50 nm. Figure S3 shows two activated fraction curves for two different supersaturations lower than 0.4%; see the supplementary material for details. DMA selects particles of one mobility but they are not all singly charged. This leads to the case that there are particles with the same mobility but some of them are slightly larger. Because of their larger diameter, the doubly charged particles activate at a lower supersaturation than the singly charged particles of the same electrical mobility. Doubly charged particles produced a small increase in activated fraction for sizes lower than 50 nm in both cases. For the analysis of the activated fraction curve in order to find the particle size at 50%, counts of doubly charged particles were determined and subtracted from N_{ccn}/N_{cn}, as described in Frank *et al.*[34]

The second factor that was investigated was the growth of activated aerosol. To evaluate the particle growth, a comparison of the measured and modeled (Sec. II C) size distribution for 200 nm ammonium sulfate particles was done. In Figs. 7(a) and 7(b), we present the modeled and measured size distribution for supersaturations 1.25% and 0.18%. We calculated the size of the droplets using the centerline saturation ratio profiles that are shown in Fig. 3(a). Time coordinates that are needed to solve the droplet growth equation was calculated from the lateral coordinate by using the known centerline flow velocity. For simplicity, we refer to those profiles with their maximum supersaturation SS. An assumption of the model is that all the particles have exactly the same dry size and they are travelling in a narrow region close to the centerline of the condenser, which is calculated based on the sheath-to-aerosol flow ratio and the instrument dimensions. This results in a narrow droplet size distribution. However as we can see in both figures, some particles obviously travel through the regions with slightly different supersaturations. This resulted in a wider size distribution counted by the OPS. For example, for supersaturation of 0.18% inside the FMI–ACIT, the model predicts that 200 nm particles will grow to 1.4 μm. However, during measurements the same particles grew to different sizes and produced a wider size distribution with the mode droplet size of 1.8 μm.

IV. CONCLUSIONS

In this work, we have presented and introduced an experimental setup of a laminar flow tube, the Finnish Meteorological Institute–Aerosol Cloud Interaction Tube (FMI–ACIT), that can measure the activation and subsequent growth of aerosols under defined laboratory conditions. FMI–ACIT was built in the Finnish Meteorological Institute and the goal was to find and verify the optimal operational characteristics of this experimental setup. First, a full characterization of the setup was made. The set of optimal working parameters for the proper operation of the FMI–ACIT were chosen using a combination of model simulations and experimental tests. Finally, further experiments were made to test if FMI–ACIT could be operated as a cloud condensation nuclei (CCN) counter.

Model simulations and the experimental tests showed that total flow rates between 1 and 3 l min^{-1} are the best for the operation of the FMI–ACIT. At lower flow rates (<1 l min^{-1}) and at higher flow rates (>3 l min^{-1}), we faced particle losses

(>30%). Therefore, 2.0 l min^{-1} flow rate was used for all further tests that have been made in this study.

In order to test our setups' ability to count CCN, different sizes of monodisperse particles of ammonium sulfate [$(NH_4)_2SO_4$] were used to determine supersaturation inside the flow tube. The comparison of the experimental supersaturation with those from the simulations showed good agreement and proved that FMI–ACIT was able to count activated particles of ammonium sulfate for supersaturations in the range from 0.18% to 1.25%. Finally, we compared the observed droplet size distributions with those predicted by a droplet growth model. Results showed that the observed size distributions are wider at supersaturations of 0.18% and 1.25%, which indicates that particles in this experimental setup experienced a more variable supersaturations than considered by the model.

It can be concluded that FMI–ACIT functionality to measure the activation and the growth of ammonium sulfate particles in supersaturations ranging from 0.18% to 1.25% was tested successfully. Future work will concentrate on low temperature measurements that are needed to test the setups' ability to measure ice nuclei.

SUPPLEMENTARY MATERIAL

See supplementary material for profiles of the saturation ratio and temperature inside the FMI–ACIT condenser as function of different flow rates. Doubly charged particles for low supersaturations are also presented.

ACKNOWLEDGMENTS

This work was financially supported by the Academy of Finland Center of Excellence programme (Grant No. 307331) and the KONE foundation.

[1]U. Dusek, G. P. Frank, L. Hildebrandt, J. Curtius, J. Schneider, S. Walter, D. Chand, F. Drewnick, S. Hings, D. Jung, S. Borrmann, and M. O. Andreae, Science **312**, 1375 (2006).
[2]J. E. Penner, M. Andreae, H. Annegarn, L. Barrie, J. Feichter, D. Hegg, A. Jayaraman, R. Leaitch, D. Murphy, J. Nganga, and G. Pitari, *Report to Intergovernmental Panel on Climate Change From the Scientific Assessment Working Group (WGI)*, edited by J. T. Houghton, Y. Ding, D. J. Griggs, M. Noguer, P. J. Van der Linden, X. Dai, K. Maskell, and C. A. Johnson (Cambridge University Press, 2001), pp. 289–416.
[3]S. Twomey, J. Rech. Atmos. **1**, 101 (1963).
[4]J. L. Katz, J. Chem. Phys. **52**, 4733 (1970).
[5]G. J. Hudson, J. Atmos. Oceanic Technol. **6**, 1055 (1989).
[6]F. Stratmann, A. Kiselev, S. Wurxler, M. Wendisch, and J. Heintzenberg, J. Atmos. Oceanic Technol. **21**, 876 (2004).
[7]G. C. Roberts and A. Nenes, Aerosol Sci. Technol. **39**, 206 (2005).
[8]P. J. Connolly, C. Emersic, and P. R. Field, Atmos. Chem. Phys. **12**, 2055 (2012).
[9]A. Nenes, P. Y. Chuang, R. C. Flagan, and J. H. Seinfeld, J. Geophys. Res. **106**(D4), 3449, https://doi.org/10.1029/2000jd900614 (2001).
[10]A. Sinnarwalla and D. Alofs, J. Appl. Meteorol. **12**, 831 (1973).
[11]N. Fukuta and V. Saxena, J. Appl. Meteorol. **18**, 1352 (1979).
[12]P. Chuang, J. Smith, R. Flagan, and J. Seinfeld, J. Atmos. Sci. Technol. **17**, 1005 (2000).
[13]H. Giebl, A. Berner, G. Reischl, H. Puxbaum, A. Kasper-Giebl, and R. Hitzenberger, J. Aerosol Sci. **33**, 1623 (2002).
[14]H. Wex, A. Kiselev, M. Ziese, and F. Stratmann, Atmos. Chem. Phys. **6**, 4519 (2006).
[15]J. R. Snider, M. D. Petters, P. Wechsler, and P. Liu, J. Atmos. Oceanic Technol. **23**, 1323 (2006).
[16]S. Lance, J. Medina, J. N. Smith, and A. Nenes, Aerosol Sci. Technol. **40**, 242 (2006).
[17]D. Rose, S. Gunthe, E. Mikhailov, G. Frank, U. Dusek, M. Andreae, and U. Poschl, Atmos. Chem. Phys. **8**, 1153 (2008).
[18]H. Köhler, Trans. Faraday Soc. **32**, 1151 (1936).
[19]H. Smith, P. Connolly, A. Baran, E. Hesse, A. Smedley, and A. Webb, J. Quant. Spectrosc. Radiat. Transfer **157**, 106 (2015).
[20]S. Hartmann, D. Niedermeier, J. Voigtländer, T. Clauss, R. A. Shaw, H. Wex, A. Kiselev, and F. Stratmann, Atmos. Chem. Phys. **11**, 1753 (2011).
[21]H. Wex, S. Augustin-Bauditz, Y. Boose, C. Budke, J. Curtius, K. Diehl, A. Dreyer, F. Frank, S. Hartmann, N. Hiranuma, E. Jantsch, Z. A. Kanji, A. Kiselev, T. Koop, O. Möhler, D. Niedermeier, B. Nillius, M. Rösch, D. Rose, C. Schmidt, I. Steinke, and F. Stratmann, Atmos. Chem. Phys. **15**, 1463 (2015).
[22]H. Lihavainen and Y. Viisanen, J. Chem. Phys. B **105**, 11619 (2001).
[23]D. Brus, A.-P. Hyvärinen, Y. Viisanen, M. Kulmala, and H. Lihavainen, Atmos. Chem. Phys. **10**, 2631 (2010).
[24]K. Neitola, D. Brus, U. Makkonen, M. Sipilä, H. Lihavainen, and M. Kulmala, Boreal Environ. Res. **19**(Suppl. B), 257 (2014), http://www.borenv.net/BER/pdfs/ber19/ber19B-257.pdf.
[25]C. Clement, Proc. R. Soc. London, Ser. A **398**, 307 (1985).
[26]H. Lihavainen, Finnish Meteorological Institute, in "Laminar flow diffusion chamber for homogeneous nucleation studies," Report Series in Aerosol Science No. 45 (Finnish Association for Aerosol Research, Helsinki, 2000), ISSN 0784–3496.
[27]R. B. Bird, W. E. Stewart, and E. N. Lightfoot, *Transport Phenomena* (John Wiley & Sons, New York, 1960).
[28]W. D. Hall and H. R. Pruppacher, J. Atmos. Sci. **33**, 1995 (1976).
[29]T. Raatikainen, R. H. Moore, T. L. Lathem, and A. Nenes, Atmos. Chem. Phys. **12**, 4227 (2012).
[30]J. H. Seinfeld and S. N. Pandis, *Atmospheric Chemistry and Physics: From Air Pollution to Climate Change* (Wiley, New York, USA, 1998).
[31]N. Fukuta and L. A. Walter, J. Atmos. Sci. **27**, 1160 (1970).
[32]M. D. Petters and S. M. Kreidenweis, Atmos. Chem. Phys. **7**, 1961 (2007).
[33]M. D. Petters and S. M. Kreidenweis, Atmos. Chem. Phys. **8**, 6273 (2008).
[34]G. P. Frank, U. Dusek, and M. O. Andreae, Atmos. Chem. Phys. Discuss. **6**, 4879 (2006).

II

Atmos. Meas. Tech., 13, 5129–5147, 2020
https://doi.org/10.5194/amt-13-5129-2020

Atmospheric Measurement Techniques
Open Access
EGU

In situ cloud ground-based measurements in the Finnish sub-Arctic: intercomparison of three cloud spectrometer setups

Konstantinos-Matthaios Doulgeris[1], Mika Komppula[2], Sami Romakkaniemi[2], Antti-Pekka Hyvärinen[1], Veli-Matti Kerminen[3], and David Brus[1]

[1]Finnish Meteorological Institute, P.O. Box 503, 00101, Helsinki, Finland
[2]Finnish Meteorological Institute, P.O. Box 1627, 70211, Kuopio, Finland
[3]Institute for Atmospheric and Earth System Research/Physics, Faculty of Science, University of Helsinki, Helsinki, Finland

Correspondence: Konstantinos-Matthaios Doulgeris (konstantinos.doulgeris@fmi.fi)

Received: 7 January 2020 – Discussion started: 20 February 2020
Revised: 20 July 2020 – Accepted: 5 August 2020 – Published: 29 September 2020

Abstract. Continuous, semi-long-term, ground-based in situ cloud measurements were conducted during the Pallas Cloud Experiment (PaCE) in 2013. The measurements were carried out in Finnish sub-Arctic region at Sammaltunturi station (67°58′ N, 24°07′ E; 560 m a.s.l.), part of Pallas Atmosphere – Ecosystem Supersite and Global Atmosphere Watch (GAW) program. The main motivation of the campaign was to conduct in situ cloud measurements with three different cloud spectrometer probes and perform an evaluation of their ground-based setups. Therefore, we mutually compared the performance of the cloud and aerosol spectrometer (CAS), the cloud droplet probe (CDP) and the forward-scattering spectrometer probe (FSSP-100) (DMT; Boulder, CO, USA). We investigated how different meteorological parameters affect each instrument's ground-based setup operation and quantified possible biases and discrepancies of different microphysical cloud properties. Based on the obtained results we suggested limitations for further use of the instrument setups in campaigns where the focus is on investigating aerosol–cloud interactions. Measurements in this study were made by instruments owned by the Finnish Meteorological Institute and results concern their operation in sub-Arctic conditions with frequently occurring supercooled clouds.

The measured parameter from each instrument was the size distribution, and additionally we derived the number concentration, the effective diameter, the median volume diameter and the liquid water content. A complete intercomparison between the CAS probe and the FSSP-100 ground setups and additionally between the FSSP-100 and the CDP probe ground setups was made and presented. Unfortunately, there was not a sufficient amount of common data to compare all three probes together due to operational problems of the CDP ground setup in sub-zero conditions. The CAS probe that was fixed to one direction lost a significant number of cloud droplets when the wind direction was out of wind isoaxial conditions in comparison with the FSSP-100 and the CDP, which were both placed on a rotating platform. We revealed that CAS and FSSP-100 had good agreement in deriving sizing parameters (effective diameter and median volume diameter from 5 to 35 µm) even though CAS was losing a significant amount of cloud droplets. The most sensitive derived parameter was liquid water content, which was strongly connected to the wind direction and temperature.

1 Introduction

Clouds and their interaction with aerosol particles provide some of the greatest uncertainties in predictions of climate change (Boucher et al., 2013). Therefore, in situ measurements of clouds play a key factor for further investigation of the aerosol–cloud interaction area. Many of the climatically important cloud properties (e.g., albedo, precipitation rate and lifetime) depend, among other factors, on the number concentration of aerosol particles and on their chemical composition (Komppula et al., 2005; Lihavainen et al., 2008). Measuring the cloud size distribution is an important parameter for the identification and description of clouds, their microphysical properties (Pruppacher and Klett, 1977; Rosen-

feld and Ulbrich, 2003) and their lifetime (Albrecht 1989; Small et al., 2009).

One major category of instruments that it is commonly used for in situ cloud measurements is known as cloud spectrometers (e.g., Knollenberg, 1976; Dye and Baumgardner, 1984; Wendish et al., 1996; Baumgardner et al., 2001, 2014; Lance et al., 2010). Cloud spectrometers are single particle counters that use forward scattering, usually with the angles between 4 and 12° of a laser beam, to detect and classify individual particles in different size bins. The main theory used for the particle sizing based on the scattering of light from single particles is the Lorenz–Mie theory (Mie, 1908). Several experiments were conducted with these instruments; they mainly cover laboratory (e.g., Wagner et al., 2006; Smith et al., 2015; Nichmann et al., 2017), ground-based (e.g., Mertes et al., 2001; Henning et al., 2002; Eugster et al., 2006; Lihavainen et al., 2008; Guyot et al., 2015; Lloyd et al., 2015; Lowenthal et al. 2019) and airborne measurements (e.g., Knollenberg et al., 1981; Heymsfeld et al., 2004; McFarquhar et al., 2007; Bromwich et al., 2012; Johnson et al., 2012; Jones et al., 2012; Brenguier et al., 2013; Beswick et al., 2014; Luebke et al., 2016; Korolev et al., 2014; Petäjä et al., 2016; Wendish et al., 2016; Voigt et al., 2017; Faber et al., 2018).

In addition to the abovementioned experiments, many studies were done to quantify biases, uncertainties and limitations of cloud spectrometers while they were used in measurement campaigns. Uncertainties were usually a result of different meteorological conditions. Baumgardner (1983) presented a comparison of five water droplet instruments, included the axially scattering spectrometer (ASSP) and the forward-scattering spectrometer probe (FSSP). He concluded that scattering probes had an accuracy of 17 % in number concentration and size measurements. A full description and evaluation of the FSSP was made by Baumgardner et al. (1985) investigating coincidence and dead-time losses and by Baumgardner et al. (1990) investigating time response and laser inhomogeneity limitations. Baumgardner et al. (1989) made a calibration of the FSSP during the airborne Antarctic zone experiment and set further limitations to be applied during the data analysis of this project. A similar study from Baumgardner et al. (1992) was conducted for the FSSP during the airborne Arctic stratospheric expedition where an improved forward-scattering spectrometer probe, the FSSP-300, was developed and introduced. Wendisch (1998) presented a quantitative comparison of ground-based FSSP with a particle volume monitor. He stated that FSSP can be regarded as an excellent microphysical sensor in continental, stratiform or cumuliform clouds with mostly small drops; however he noticed some discrepancies in the liquid water content, especially when cloud droplets larger than 25 µm were considered. Gerber et al. (1999) performed and evaluated ground-based measurements of liquid water content using also an FSSP and a particle volume monitor (PVM). They observed large discrepancies too and stated that the FSSP overestimated liquid water content for large cloud droplets due to the inertial concentration effect. Burnet and Brenguier (1999) validated the droplet spectra and the liquid water content using five instruments including the FSSP, the fast FSSP and the cloud droplet probe (CDP). Burnet and Brenguier (2002) only investigated the FSSP further in detail to address the instrumental uncertainties and their limitations. Coelho et al. (2005a, b) made a detailed discussion for FSSP-100 in low and high droplet concentration measurements with a proposed correction for coincidence effects. Lance et al. (2010) calibrated the CDP and presented a full description of the instrument performance in laboratory and in-flight conditions. Baumgardner et al. (2011) summarized airborne systems for in situ measurements of aerosol particles, clouds and radiation that were currently in use on research aircraft around the world including cloud spectrometer probes. Febvre et al. (2012) highlighted the possible effects of ice crystals in FSSP measurements. Spiegel et al. (2012) made a thoroughly analysis of wind velocity and wind angle impacts at the Junfraujoch comparing the fog droplet spectrometer (FM-100) to others instruments. FM-100 showed several artifacts at temperatures below zero. One more evaluation regarding cloud ground-based measurements which took the wind direction into consideration was made by Guyot et al. (2015) at the Puy-de-Dôme observatory between seven optical sensors including an FSSP, a fast FSSP, a fog monitor and two CDP probes. They placed one FSSP and the fog monitor on the roof of the observatory and the two CDP probes and one FSSP inside a wind tunnel. The authors showed that there was good agreement in the sizing abilities of the instruments but observed possible discrepancies in number concentration values, a fact that also affected the liquid water content values. Lloyd et al. (2015) observed cloud microphysical structures by conducting cloud, aerosol and precipitation spectrometer (CAPS), FSSP, CDP-100, and PVM measurements. They mounted all the instruments on a rotator and wing on the terrace rooftop outside the Sphinx Laboratory, (Jungfraujoch, Switzerland). Several developments of the in situ measurement systems were reviewed and summarized by Baumgardner et al. (2017) with respect to their strengths, weaknesses, limitations and uncertainties. The progress in performing in situ cloud measurements was clearly observed along with other developments. Lowenthal et al. (2019) conducted wintertime mixed-phase orographic cloud measurements at the Storm Peak Laboratory (Colorado, USA). They deployed an FSSP-100 on a rotating wind vane (to orient it into the wind).

In this work, we focused on the intercomparison of three cloud spectrometer probe ground setups as they were used during the Pallas Cloud Experiment (PaCE) 2013. Due to the increased demand for long-term continuous ground-based in situ cloud measurements, we tested and evaluated the operation of three ground setups owned by the Finnish Meteorological Institute (FMI) to perform continuous ground-based measurements in harsh environments. The FMI research sta-

tion (Sammaltunturi) located in northern Finland is regarded as an ideal place to perform in situ low-level cloud measurements, especially during autumn, when the station is usually inside a cloud about 50 % of the time. There, along with the FSSP-100 and the CDP, which are classic instruments for in situ cloud measurements, we also used the CAPS probe (part of this instrument is the cloud and aerosol spectrometer (CAS) probe) with a purchased inhalation system. CAPS' worldwide unique setup allows us to make semi-long-term (in orders of months) observations when compared to short-term (orders of hours) airborne measurement. The exact set of measurement limitations for each cloud probe that are presented in this work will help us to conduct a detailed further analysis of microphysical cloud properties and their interactions with aerosol during all PaCE campaigns. The previous PaCE campaigns already resulted in a series of publications on experimental observations and modeling studies (e.g., Komppula et al., 2005, 2006; Lihavainen et al., 2008, 2010; Kivekas et al., 2009; Anttila et al., 2009, 2012).

A description of the measurement site and the instrumentation as it was installed can be found in Sect. 2.1 and 2.2. Subsequently, in Sect. 2.3, the procedure we followed during data analysis is presented. In Sect. 3, the intercomparison of the instruments and how they were influenced by the meteorological parameters are presented. Finally, in Sect. 4, we summarized our main results and conclusions in order to set limitations and made recommendations for the data analysis of the three instrument ground-based setups during future studies in a sub-Arctic environment.

2 Methods

2.1 Measurement site description

Measurements were conducted during autumn 2013, in the Finnish sub-Arctic region at Sammaltunturi station (67°58′ N, 24°07′ E; 560 m a.s.l.), which is a part of the Pallas Atmosphere – Ecosystem Supersite hosted by the Finnish Meteorological Institute. The station is also part of Global Atmosphere Watch (GAW) program. Sammaltunturi station is located on the top of a treeless hill. A full detailed description of the site can be found in Hatakka et al. (2003). Autumn was chosen as the best period to run the campaign due to the high chances that the station will be inside a cloud. This allows us to conduct in situ cloud measurements. All the meteorological parameters were continuously measured by the Vaisala FD12P weather sensor. During our previous PaCE, cloud microphysical properties and aerosol physicochemical properties and their interactions were measured and investigated (e.g., Lihavainen et al., 2008, 2015; Hyvärinen et al., 2011; Anttila et al., 2012; Collaud Cohen et al., 2013; Jaatinen et al., 2014; Raatikainen et al., 2015; Gérard et al., 2019). During PaCE 2013, our main motivation was to focus on an intercomparison of in situ cloud properties measured with three different cloud probes, their evaluation and mutual benchmarking regarding PaCE campaigns.

2.2 Cloud instrumentation

The atmospheric in situ measurement community has identified cloud droplet probes with surface installation as a potential method for continuous cloud in situ measurements (Wandinger et al., 2018). During PaCE 2013, to perform in situ measurements of cloud droplets, we used three instruments originally developed for airborne measurements, but tailored to ground-based measurements by the manufacturer (DMT, USA): the CAPS, the CDP and the forward-scattering spectrometer probe (FSSP-100; hereafter called FSSP for simplicity). All three of them were installed on the rooftop of the measurement site as described below in detail and share a similar measurement technique. A wind tunnel could be regarded as the optimal choice to utilize these instruments for ground-based setups (e.g., Elk Mountain, Baumgardner, 1983, and Puy de Dôme, Guyot et al., 2015). There are measurement sites like ours in the sub-Arctic which do not have this possibility for both practical and budgetary reasons. However, it was shown that the same quality data could be obtained from rooftop measurements (Guyot et al., 2015). Ground-based measurements with cloud probes that were originally designed to be used for aircraft have already been conducted in several measuring sites without using a wind tunnel (e.g., Jungfraujoch, Lloyd et al., 2015, and Storm Peak, Lowenthal et al., 2019). The basic concept is that they use the forward scattering of a laser beam for the detection and sizing of individual particles. Then, using Mie theory (Mie, 1908), they calculate the size of the particle from the intensity of the scattered light.

Only data of the CAS probe were used for the CAPS. CAS is one part of the CAPS (DMT) (0.51–930 µm), which is an instrument that is widely used in airborne measurements for investigating the microphysical properties of clouds (e.g., Baumgardner, 2001; Baumgardner et al., 2011). The CAPS probe includes two more instruments; however they are not comparable with the FSSP and the CDP probe: the cloud imaging probe (CIP) and the hot-wire liquid water content (hot-wire LWC) sensor. CAS measures smaller particles (0.51 to 50 µm) and relies on light scattering. Particles scatter light from an incident laser at a wavelength of 680 nm and a sample area of 0.24 mm^2, and collecting optics guide the light scattered in the 4 to 12° range into a forward-sizing photodetector. The intensity of light is measured and used to infer the particle size. Backscatter optics also measure light intensity in the 168 to 176° range, which allows the determination of the real component of a particle's refractive index for spherical particles. The droplets are then classified into 30 size bins. CAS was operational from 15 October until 28 November. It was installed and fixed on Sammaltunturi station roof. It was pointing in the main wind direction of the station (southwest, ∼ 225°). For the instrument's installation

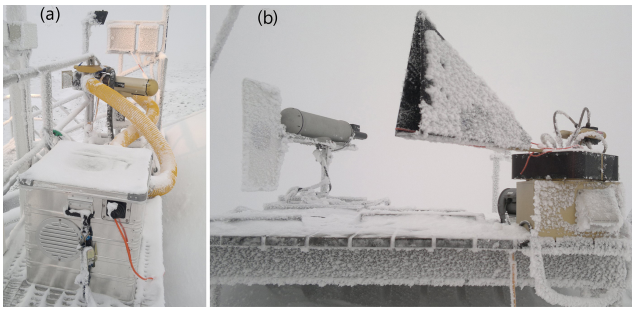

Figure 1. (a) The CAPS probe setup and **(b)** the FSSP-100 and the CDP setups as they were installed on Sammaltunturi station during PACE 2013.

we used the manufacturer pylon (height 0.3 m) (the same as is used for CAPS airborne measurements). The whole system was fixed on a horizontal metallic circle ($D = 0.28$ m). The metallic circle was attached to a vertical metallic bar (height 0.3 m), part of a square metallic stand (0.7 m × 0.7 m) (see Fig. 1a). As a result CAPS had a total height of 0.6 m on the roof where it was installed and a height of 4.5 m from the ground. In our setup, CAPS had its own tailored inhalation system: a high-flow pump (Baldor, Reliance, USA), which worked continuously. The pump was connected with the CAS probe with a 1.14 m long hose with an inner diameter of 0.07 m. The hose was connected to a triple branch (three parts with i.d. = 0.12) through a 0.12 to 0.05 m reducer. The triple branch connected the CAS probe through the hose with the high-flow pump. The other parts of the branch connected the pump with the CIP through two different hoses ($L = 1.52$ m; i.d. = 0.12 m). In addition, a stepped CAS inlet (funnel shape reducer i.d. = 0.12 to i.d. = 0.05 m) was attached over the CAS inlet tube (for detailed description, please see Figs. S1 and S2 in the Supplement).The probe air speed (PAS) inside CAS was checked daily with a digital thermo-anemometer (model 471, Dwyer Inc.) to ensure that the flows inside the instrument remained similar. This was done through a small hole near the end of the CAS probe outlet and the beginning of the 0.05 m hose and in a position such that the anemometer inserted into the hole was just in the middle of the CAS probe outlet (hose diameter). In cases when PAS changed, data were corrected accordingly. During this campaign PAS values ranged from 17 to 23 m s^{-1}. The calibration of the instrument was done at DMT and also at the Finnish Meteorological Institute before and after the campaign using glass beads and polystyrene latex sphere (PSL) standards.

The FSSP (1.2–47 µm, model SPP-100, DMT), initially manufactured by Particle Measuring Systems (PMS Inc., Boulder CO, USA), is a widely used cloud probe for measuring droplet size distribution (Brenquier, 1989). It shares the measurement principle with the CAS probe and measures the light scattered in the 4 to 12° range with a laser of wavelength 633 nm and a sample area of 0.414 mm^2. Droplets were classified into 40 size bins. During PaCE, the FSSP was installed and placed on a rotating platform, so that the inlet was always directed against the wind direction. The rotating platform was a horizontal metallic base (0.7 × 0.1 × 0.4 m) with a metallic fin fixed at the back of it. This setup ensured that the instrument would follow the wind direction continuously. The rotating platform was placed on a similar squared metallic stand we also used in the CAPS setup, but with a higher metallic vertical bar ($L = 0.6$ m, i.d. = 4 cm). Thus, the instrument had a total height of 0.6 m on the roof where it was installed and a height of 5.5 m from the ground. During FSSP installation on the rotating platform, we wanted to prevent the full rotation of the probe, which could be dangerous for the cable wiring and safety of the instrument. For this reason, a vertical metallic bar (0.3 m, D. = 0.6 cm) and two horizontal bars ($L = 0.25$ m, D = 0.6 cm) were installed (northeast ∼ 60°), and they served as a brake (Fig. 1b). A custom inhalation system with a high-flow ventilator was employed through the instruments' inlet to ensure that the air speed would remain constant (for detailed description, please see Fig. S3 in the Supplement). In addition, the PAS inside the FSSP tube was checked daily with the digital thermo-anemometer (model 471, Dwyer Inc.). The PAS during the campaign was ∼ 10 m s^{-1}, which led to an air speed of ∼ 36 m s^{-1} inside the inlet due to the necking inside the inlet's mouth from i.d. = 3.8 cm to i.d. = 2.0 cm. This value was used for further data processing. FSSP was installed and operational from 14 September until 28 November 2013. The instrument was calibrated at DMT, USA, before the campaign and on site after the end of the campaign.

The third instrument that we used was the CDP (3–50 µm, Droplet Measurement Technologies) (Lance et al., 2010). Similar to the previous instruments it uses the same principle and measures the light scattered in the 4 to 12° range. The laser beam had a wavelength of 658 nm and a sample area of 0.3 mm^2. The CDP classified droplets into 30 size bins. It was placed next to the FSSP also on a rotating platform to be continuously directed against the wind direction (Fig. 1b). The metallic platform covering the instrumental electronics consists of a fixed part (0.4 × 0.4 × 0.3 m) at the bottom and on top of that the rotating part (0.4 × 0.4 × 0.1 m) with the probe itself on top. The rotating part is equipped with a large fin to keep the inlet towards the wind (for detailed description, please see Fig. S4). The instrument had a custom inlet with an external pump to ensure a constant PAS (14 ms^{-1}). The CDP was installed and was operational from 25 September 2013 until 28 November 2013. It was calibrated at the Finnish Meteorological Institute, Kuopio unit, before the campaign and after the campaign on site using glass beads and PSL standards.

All three instruments used anti-ice heaters as they were deployed by the manufacturer. The external parts of the setup (rotating platforms and inhalation systems) did not use an additional heating system. The instruments were installed in a horizontal position and placed close to each other on Sammaltunturi roof. The CDP and FSSP were installed next to

Table 1. Instruments, wavelengths (nm), sampling area (mm), number of bins, probe air speed (ms^{-1}), size range (µm), time resolution (s), and operation starting and ending date are presented.

Instrument	Laser wavelength (nm)	Sampling area (mm^2)	Number of bins	Probe air speed ($m\,s^{-1}$)	Size range (µm)	Time resolution (s)	Operation start date	Operation end date
CAPS	680	0.24	30	17–23	0.61–50	1	15 Oct	28 Nov
FSSP	633	0.414	40	10	1.2–47	1	14 Sep	28 Nov
CDP	658	0.3	30	14	3–50	1	25 Sep	28 Nov

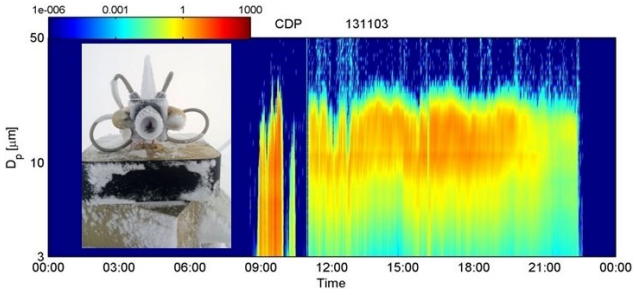

Figure 2. An example case of the CDP probe where its rotational platform and inlet are frozen. The size distribution of the CDP probe on 3 Nov 2013 is depicted. The instrument was out of order from 00:00 to about 11:30 LT (all times in this paper are given as local time), and a CDP cleaning procedure was needed to start operation again.

each other (approx. 0.5 m) and they had a horizontal distance of ∼ 10 m and a vertical distance of ∼ 1 m to the CAS probe. All the probes' parameters are presented in Table 1. During the campaign a routine was consistently followed. The cloud probes functionality was checked visually daily. Ice and snow accumulation could fully or partially block the probes' inlets and affect the flows. In addition, ice and snow could also accumulate in parts of the roof and affect the probe measurements. For this reason, all three cloud probes needed periodical cleaning. When the station was inside a cloud and sub-zero temperatures were observed, the cleaning procedure of the probes during the day was repeated twice or more times per day (if needed).

2.3 Data handling and processing

The presence of a cloud was estimated by the cloud droplet counts measured with all the cloud probes and by the visibility and relative humidity measurements at the site. As a cloud event we defined the situation when there were droplet counts (considering a cleaned data set) measured by the cloud probes for more than 30 continuous minutes, the horizontal visibility was less than 1000 m and the relative humidity was ∼ 100 %.

From each cloud probe we obtained the cloud droplet size distribution. For the intercomparison of the probes we had to eliminate some size bins of the CAS and the FSSP probe in order to use a similar size range in each case. The CAS probe, using the PADS software (Droplet Measurement Technologies Manual, 2011), derives the number concentration (N_c), the LWC, the median volume diameter (MVD) and the effective diameter (ED). The same parameters were derived using the following equations, since we have used old software PACS 2.2 (Droplet Measurement Technologies) for data acquisition of the FSSP-100 and the CDP probe.

N_c (cm^{-3}) was calculated from the division of the total number of sized particles N by the sample volume V_s (cm^{-3}):

$$N_c = \frac{N}{V\,s}, \tag{1}$$

where V_S was defined as

$$V_S = \mathrm{PAS} \times t \times A, \tag{2}$$

where PAS is the probe air speed ($m\,s^{-1}$), t is the time of the sampling interval and A is sample area (mm^2) defined as the height of the laser beam (mm) multiplied by the length of the laser beam within the depth of field (DOF, mm). On an instrument that records probe time, such as CAS and FSSP, the sampling interval is calculated by subtracting the previous instance's probe time from that of the current instance. On the CDP the sampling interval is assumed to be the designated sample rate. All three probes were set up to sample at 1 s (1 Hz).

LWC ($g\,m^{-3}$) is the mass of liquid water per unit volume of air, and it was calculated using the following equation:

$$\mathrm{LWC} = \sum_{i}^{n} \mathrm{LWC}_i, \tag{3}$$

where

$$\mathrm{LWC}_i = c_i 10^{-12} \frac{\pi}{6} m_i^3. \tag{4}$$

m_i is the midpoint of its bin and calculated as

$$m_i = \frac{b_i + b_{i+1}}{2}, \tag{5}$$

and c_i is the droplet concentrations per bin (m^{-3}).

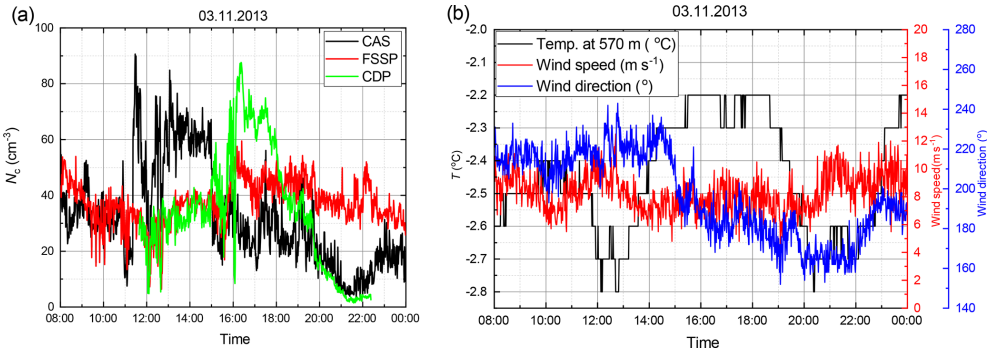

Figure 3. Time series of 1 min averages on 3 Nov 2013; **(a)** N_c of each cloud probe along with **(b)** temperature, wind speed and wind direction are presented. This is a typical example of the cloud probes accumulating ice. From 12:00 we can see a drop in N_c of the CAS. The sudden increase just before was a clear sign of probe inlet freezing. The same behavior could be also seen for the CDP after 16:00. When ice was accumulated, the opening of the probe inlet became smaller, which resulted in a raised PAS. While deriving N_c to evaluate our data set, we considered the PAS to be constant. The underestimation of the PAS explains the abnormality in N_c.

The factor $\frac{\pi}{6}m_i^3$ in the equation indicated that we assume that the particle is a sphere. Another assumption that was made is that water has a density of 1 g cm^{-3}.

MVD (µm) indicates the droplet diameter, which divides the total water volume in the droplet spectrum such that half the water volume is in smaller drops and half is in larger drops; and it is derived by a linear interpolation with respect to the $(i+1)$ bin as

$$\mathrm{MVD} = b_{i^*} + \left(\frac{.5 - \mathrm{cum}_{i^*-1}}{\mathrm{pro}_{i^*}}\right)(b_{i^*+1} - b_{i^*}), \quad (6)$$

where $\mathrm{pro}_{i^*} = \frac{\mathrm{LWC}}{\mathrm{LWC}_i}$ is the proportion of the spectrum LWC that falls in the ith bin and $\mathrm{cum}_{i^*} = \mathrm{pro}_1 + \ldots + \mathrm{pro}_{i^*}$ is the cumulative proportion of the spectrum LWC that falls in the first i bins and i^* is the smallest value of i such that $\mathrm{cum}_{i^*} > 0.5$.

This interpolation gives an accurate estimation in comparison with the half point of b_{i^*} and b_{i+1}. The second component of the equation scales the amount summed to b_{i^*} according to how close b_{i^*} and b_{i+1} each were to 0.5.

ED (µm) is the ratio of LWC to the optical cross-sectional area of droplets of a sample droplet spectrum calculated by the following equation:

$$\mathrm{ED} = \frac{\sum_{i=1}^{n} p_i r_i^3}{\sum_{i=1}^{n} p_i r_i^2} 2, \quad (7)$$

where n is the number of sizing bins, p_i the particle counts for bin i and r_i the mean radius in micrometers of bin i.

All our instruments were calibrated in the laboratory and/or on site. The calibration of all three instruments was done for size measurements but not for N_c measurements. Also, we should take into account the fact that the instruments faced extreme conditions during the whole campaign, in terms of frequent changes in wind direction and speed and sub-zero temperatures. These meteorological conditions could possibly lead to unexpected performance.

The sizing accuracy for cloud spectrometers has been estimated as 20 % and the concentration accuracy as 16 % (Baumgardner, 1983; Dye and Baumgardner, 1984; Baumgardner et al., 2017). The major factors that are usually considered for possible biases in data analysis are coincidence, dead-time losses and changing velocity acceptance ratio (VAR). Coincidence events occur when more than one droplet is registered by an instrument at the same time, resulting in multiple droplets artificially measured as one droplet. A changing VAR is a result of the fact that only part of a laser beam is used to calculate the sampling volume because drops passing the laser beam near the edges are undersized. Lance (2012) showed that at ambient droplet concentrations of 500 cm^{-3}, at least 27 % undercounting and a 20 %–30 % oversizing bias were observed for CAS. However, during PaCE 2013 droplet number concentrations we observed to reach a maximum of 200 cm^{-3}, and in the majority of cases they were less than 100 cm^{-3}. Due to these low number concentration values we do not take coincidence, dead-time losses and VAR uncertainties into consideration in this analysis. LWC as it was derived from the CAS probe has a significant uncertainty of 40 % according to the Droplet Measurement Technologies Manual (2011). FSSP uncertainties, limitations and corrections have been reported in the literature several times (Dye and Baumgardner, 1984; Baumgardner et al., 1985; Baumgardner and Spowart, 1990). Febvre et al. (2012) found out that the uncertainty of the FSSP in derived ED and derived LWC is 3 µm and 30 % regarding mixed-phase clouds. For the CDP probe, Lance et al. (2012) reported the importance of the coincidence errors even if the number concentrations are as low as 200 cm^{-3}, resulting in a 25 % undercounting error and a 30 % oversizing error due to coincidence.

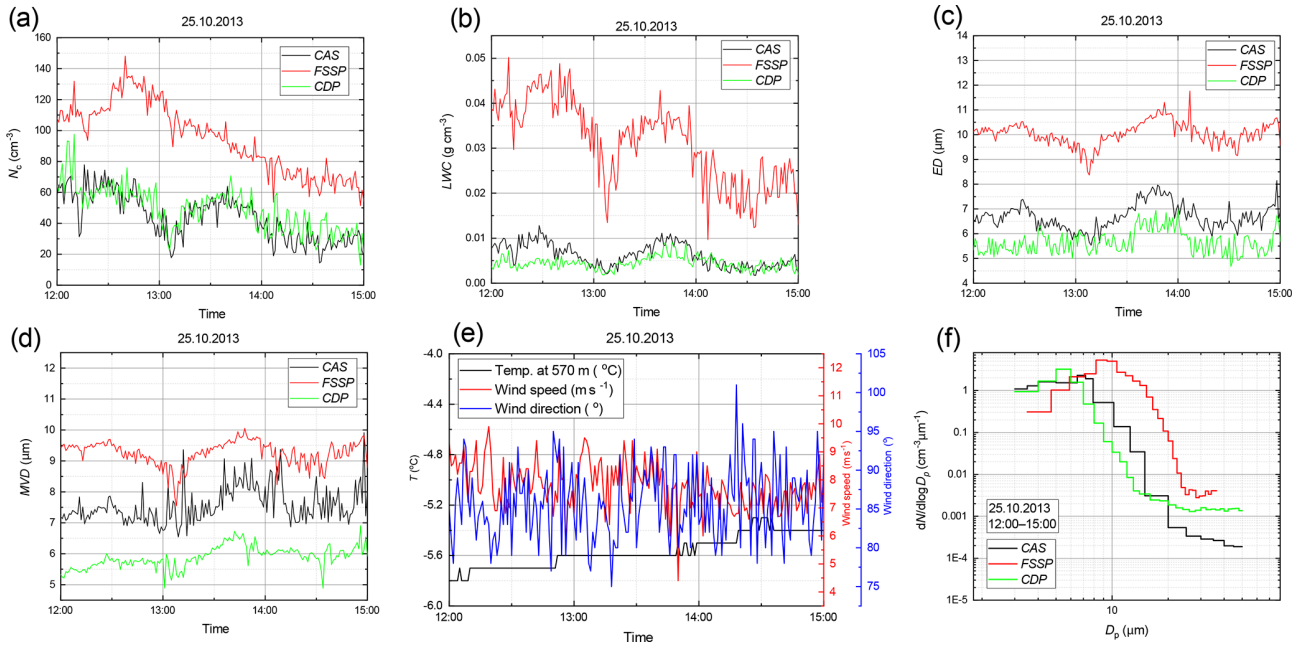

Figure 4. Time series for the 12 November case from 15:00 to 18:00. The main parameters as they were derived/measured from all three cloud probes: **(a)** N_c; **(b)** LWC; **(c)** ED; **(d)** MVD; **(e)** temperature, wind speed, wind direction; and **(f)** size distribution. All three instruments were pointing in the same direction. This resulted in high agreement in N_c for all three probes. In addition, we also noticed good agreement in LWC. The main reason for slight differences in ED and MVD was the different sizing ability of the probes.

During the campaign, measurements were performed with a 1 Hz acquisition frequency for all three probes. During the data analysis, averages per minute from each cloud probe were calculated when the station was inside a cloud. As we previously highlighted, there were cases when the flows of the cloud probes were blocked. This situation was also visible in raw data. Such cases were cleaned out from all data sets for the final analysis. A typical example case of probe freezing was observed on 3 November 2013. The CDP was completely clogged with ice; see Fig. 2, where its size distribution is presented. However, in order to find probe freezing cases a closer look in N_c was carefully undertaken for the whole data set. As an example, Fig. 3 depicts the N_c of each cloud probe on the same day along with the meteorological parameters. There, the sudden decrease in droplet number concentration of the CAS probe from 12:00 onwards and a sudden increase in N_c just before was a clear sign of probe inlet freezing. This behavior in N_c was observed because the opening of the probe inlet becoming smaller (from the accumulation of ice), which resulted in a raised PAS. During data evaluation we considered the PAS to be constant. This led to an underestimation of the PAS, which explains this abnormality in the N_c. The same behavior could be also seen for the CDP after 16:00.

3 Results

3.1 Overview of results for PACE 2013

During PaCE 2013, FSSP, CAS and CDP were installed for a total of 1824, 1080 and 1560 h, respectively; see Table 1 for installation dates. During the campaign, the station was inside a cloud for about 664 h (36.5 %). During this period, the temperature ranged from −12.0 to 10.2 °C with an averaged temperature −1.9 °C (SD 5.1 °C), and the wind speed average was 6.8 (SD 2.9) m s^{-1}. The dominant wind direction was ∼ 220°, but there were winds and clouds from all directions. Regarding data coverage, the FSSP and the CAS probe showed good performance, with ∼ 500 h (75 %) and ∼ 220 h (67 %) cleaned data coverage, respectively. The CDP probe performed significantly worse, with ∼ 108 h (17 %) cleaned data coverage. The worse CDP performance was due to its frozen inlet and/or its rotation system during the night; it encountered frequent operation problems especially at sub-zero temperatures.

3.2 Example cases with all three probes in operation

Firstly, we present example cases when all three probes were operating. These cases correspond to different wind directions. This choice was made since we used two different approaches; two probes were installed on a rotating platform (FSSP, CDP) and one probe was installed in a fixed direction (CAS). We provide the time series of the derived N_c, LWC,

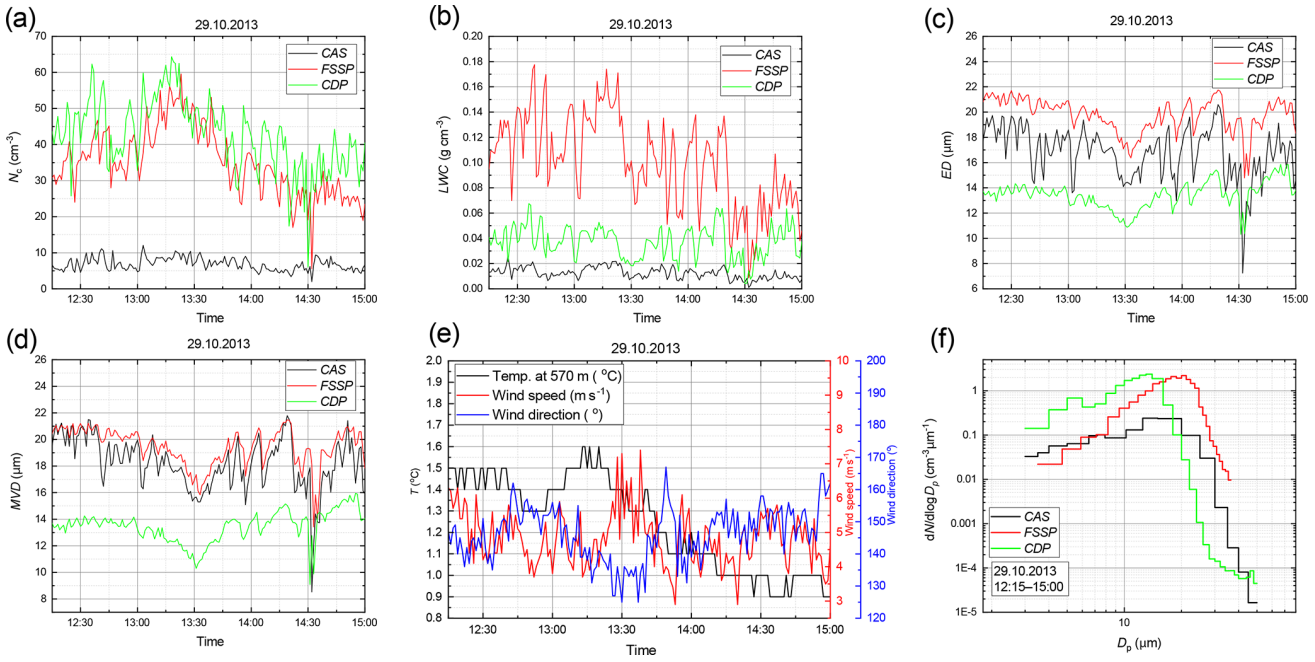

Figure 5. Time series on 29 October from 12:15 to 15:00. The main parameters as they were derived/measured from all three cloud probes: **(a)** N_c; **(b)** LWC; **(c)** ED; **(d)** MVD; **(e)** temperature, wind speed, wind direction; and **(f)** size distribution. The wind direction was perpendicular to the CAS probe. This resulted in CAS significantly underestimating N_c and LWC. The main reason for slight differences in ED and MVD was the different sizing ability of the probes.

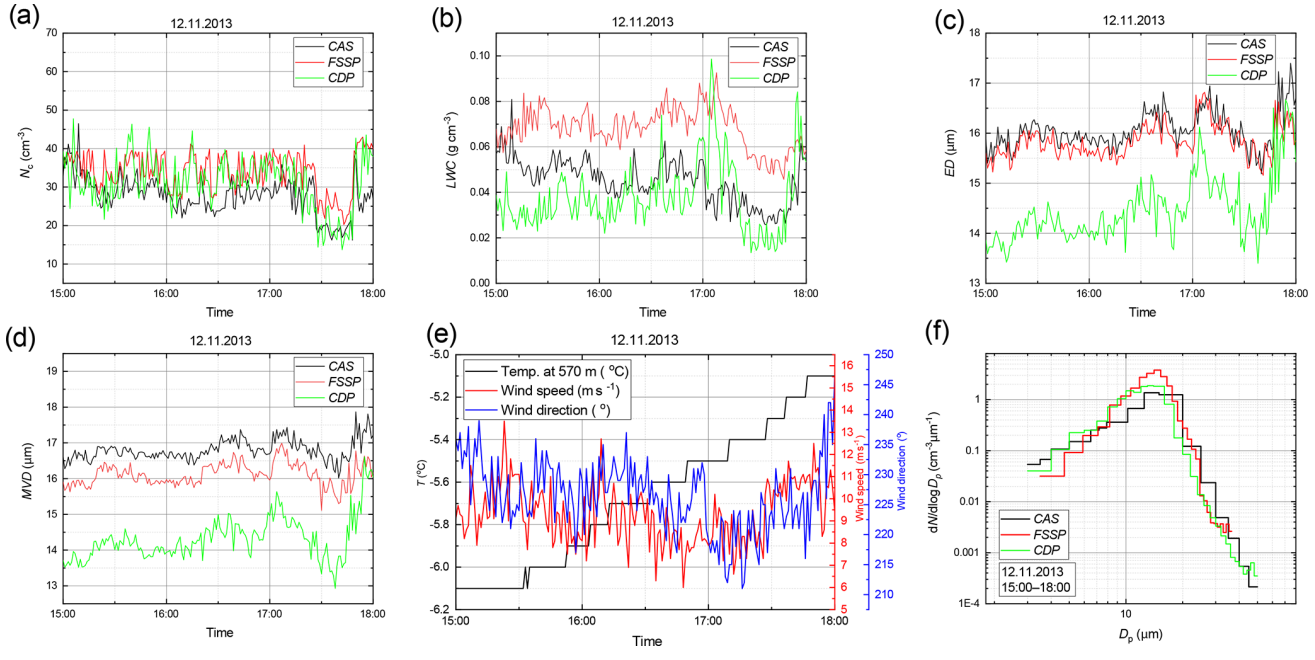

Figure 6. Time series on 25 October from 12:00 to 15:00. The main parameters as they were derived/measured from all three cloud probes: **(a)** N_c; **(b)** LWC; **(c)** ED; **(d)** MVD; **(e)** temperature, wind speed, wind direction; and **(f)** size distribution. During this case the probes were not facing in the same direction. Agreement in N_c between CAS and CDP indicates that the CDP rotation system was frozen and CAS was not facing the wind. Large discrepancies were observed in LWC and slight discrepancies in ED and MVD. The main reason for these discrepancies was the different sizing ability of the probes.

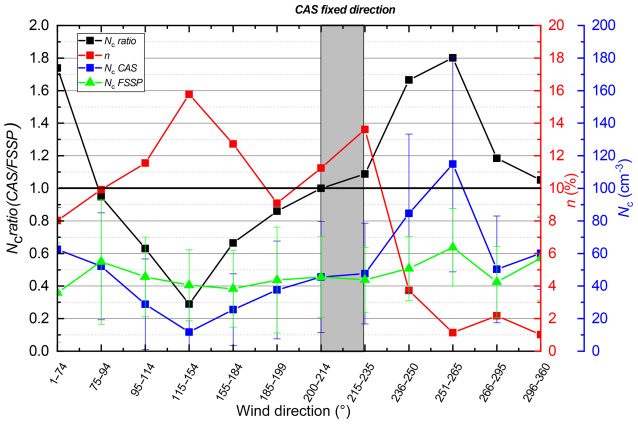

Figure 7. Number concentration ratio ($N_{c\,ratio}$), number of observations (n), and N_c of the CAS probe and the FSSP for each part of the 360° wind rose as it was divided for detailed investigation. The gray rectangle corresponds to wind iso-axial measurements.

ED, MVD and the size distributions as they were measured by all three probes along with selected meteorological parameters (temperature, wind speed and wind direction). For each case, the same size range for each probe was adopted. For this reason, we eliminated 12 bins (ranging from 0.51 to 3 µm) of the CAS probe and two bins (from 1.2 to 3.5 µm) of the FSSP-100. The final size ranges for probe comparison were then as follows: CAS – 3 to 50 µm; FSSP – 3.5 to 47 µm; CDP – 3 to 50 µm.

The abovementioned parameters are presented on 12 November from 15:00 to 18:00; see Fig. 4. The wind speed during this period varied from 6 to 13.5 m s^{-1}, and temperature varied from −6.1 to −5.1 °C. The average wind direction was 226.5 (SD 6.1)°, which means that all three instruments were pointing in the same direction (Fig. 6e). As we noticed in Fig. 4a, this resulted in good agreement among all three probes in deriving N_c. The CDP operated without flaws in both its rotation and inhalation system due to the cleaning procedure of the instrument done just before this measuring period. In this case, the LWC values were in best possible agreement; see Fig. 4b. Derived sizing parameters ED and MVD are presented in Fig. 4c and d, and both of them had good agreement.

The next example case took place on 29 October, from 12:15 to 15:00; see Fig. 5. The wind speed during this period varied from 2.9 to 8.9 m s^{-1}, and temperature varied from −5.4 to 2.9 ° C. Average wind direction was 141.2 (SD 18.4)°, which indicates that the wind direction was perpendicular to the CAS probe (Fig. 5e). Here, the CAS probe significantly undercounted N_c (∼ factor 5) compared to FSSP and CDP (Fig. 5a). The CDP was also operating with no malfunctions in its rotation and inhalation system. LWC as it was derived by the CAS probe was highly affected by a factor of about 7 due to its losses in N_c (Fig. 5b). Furthermore, as we can see in Fig. 5c and d, CAS ability to derive ED and MVD was not affected by N_c. Especially, when we are comparing ED and MVD between CAS and FSSP, their difference is less than 20 %. However, it was also interesting that even though CDP and the FSSP had a good agreement in droplet counts, they present some differences in the other derived parameters. Investigating in detail their size distribution, we found that this was a result of different estimation in sizing. This can be clearly seen in Fig. 5f. In this case there was a shift in CDP sizing when compared with FSSP towards smaller sizes about 5 µm in size range from 15 to 20 µm.

The last example day we present took place on 25 October, from 12:00 to 15:00; see Fig. 6. The wind speed varied during this period from 4.4 to 9.9 m s^{-1} and temperature from −5.8 to −5.3 ° C. The average wind direction was 85.6 (SD 4.8)°, which means that the probes were not facing in the same direction (Fig. 6e). This explains why the N_c of CAS was lower than the N_c of FSSP by a factor of 2. The CDP measured the same N_c of cloud droplets as CAS, something that was not really expected (Fig. 6a). This is a typical example case we faced, which indicates why the CDP counts were not trusted during sub-zero temperatures. Even if the CDP was not obviously clogged, when observed from the raw data, its rotation system was frozen, so it could not follow the wind direction and we were not able to determine where exactly the CDP was pointing. Also, here, we can see that during the period the instruments were not facing in the same wind direction, we observed large discrepancies in derived LWC (Fig. 6b). In Fig. 6c and d we can also see slight discrepancies in the derived sizing parameters ED and MVD. We noticed a slight shift in FSSP sizing towards bigger sizes compared to CAS, about 2.5 µm in size range from 7 to 10 µm, and a slight shift in CDP sizing towards smaller sizes, about 2 µm in size range from 5 to 7 µm, as depicted in Fig. 6f; this clearly explains these differences.

3.3 CAS and FSSP counting performance based on the wind direction

After investigating different example cases, we focused on how the change in the wind direction influenced the droplet counting ability of the instruments in different sectors of the wind rose. In this section, we concentrated only on the intercomparison of the CAS probe (installed in a fixed direction) with the FSSP (was following the wind direction). The decision to first compare only CAS and FSSP setups was made because their parallel data coverage was the best (∼ 243 h of common cleaned data set). CDP was not used in this section due to only few common data with the CAS. The reason for this was that from the date that the CAS was installed the CDP had operation problems. A detailed analysis regarding the CDP and its behavior is presented later in Sect. 3.5. To obtain as close as possible a size range for both instruments we removed the first 10 bins of the CAS and the first bin of the FSSP. As a result, we used the following size ranges: CAS – from 1.25 to 50 µm; FSSP – from 1.2 to 47 µm.

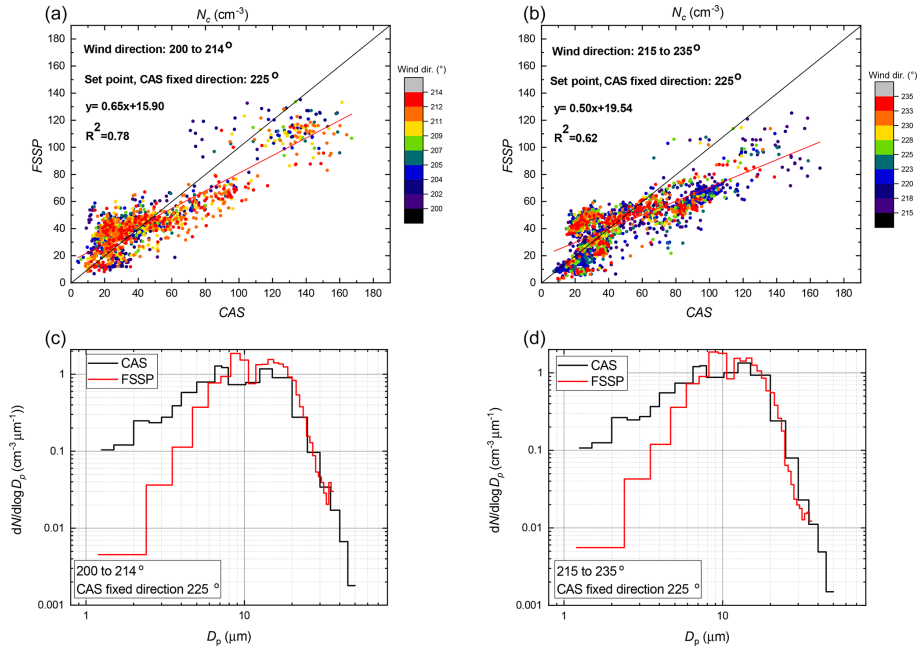

Figure 8. Comparison of number concentration (N_c) as it was derived from the CAS and the FSSP is presented for two sectors of the wind rose while the station was inside a cloud: **(a)** 200 to 214°; **(b)** 215 to 235°. Color code represents the wind direction. In **(c)** and **(d)** the size distribution as it was measured from the CAS probe and the FSSP for the same two wind sectors is presented.

To estimate the possible losses of the cloud droplet counts from each cloud probe we used N_c as a benchmark parameter. Possible CAS sampling losses were investigated by calculating the aspiration efficiency as described in Spiegel et al. (2012). Our expected losses were $\sim 5\,\%$ for 20 µm, $\sim 20\,\%$ for 40 µm and 40 % for 50 µm cloud droplets. Averaged total N_c values of the cleaned data set as they were derived from the CAS probe and the FSSP were 39.8 (SD 35.3) cm^{-3} and 44.1(SD 26.9) cm^{-3}, respectively. We divided the wind rose into 12 parts. This choice was made according to specific factors. First of all, we took into consideration the crucial point orientation of the CAS inlet when compared to actual wind direction since the CAS probe was fixed and installed (southwest of the station, $\sim 225°$). This point helped us to define the areas where the two instruments were performing in wind iso-axial conditions. Secondly, we tried to ensure that we would have enough amount of data in each part to increase the reliability of our results. Accordingly, the 360° wind rose was divided into the following sectors: 0 to 74, 75 to 94, 95 to 114, 115 to 154, 155 to 184, 185 to 199, 200 to 214, 215 to 235, 236 to 250, 251 to 265, 266 to 295 and 296 to 360°. Figure 7 shows the ratio of N_c of the CAS to the FSSP probes along with the percentage of observations in each of these sectors of the wind rose and the averaged N_c values from both instruments. There, we can see that each of the instruments had a different counting performance in each sector. The best counting performance (the ratio is close to 1) was found in two sectors (from 200 to 214° and 215 to 235°), where both probes were facing in a similar direction. On the other hand, when the wind direction was perpendicular (115 to 154°) to the CAS fixed direction, the ratio was found to be lower than 0.4. There the CAS probe undercounted a significant amount of cloud droplets ($\sim 60\,\%$). However, there were also cases where FSSP measured smaller N_c compared to the CAS probe (sectors from 236 to 250° and from 251 to 265°). During these cases, FSSP was not actually freely moving because of the brake setup. Depending on the wind turns, FSSP could be left in the wrong orientation for an unknown amount of time. Inside these two sectors the CAS probe measured relatively high N_c ($\sim 120\,\mathrm{cm}^{-3}$) in comparison with the other parts of the wind rose ($\sim 50\,\mathrm{cm}^{-3}$).

All wind sectors were further investigated to explain the biases in the performance of the two instruments. Firstly, a closer look (see Fig. 8) is presented for two sectors (200–214, 215–235°) where the agreement was found to be the best according to the N_c ratio. For this reason, the wind rose sector from 200 to 235° was adopted as wind iso-axial conditions for the rest of this work. Results indicate that the agreement in both cases was good ($R^2 = 0.78$ and 0.62 with slope 0.65 and 0.50, respectively; Fig. 8a and b), and the maximum difference observed was $\sim 30\,\%$. When N_c as derived from CAS was more than 80 cm^{-3}, FSSP N_c was about 25 % lower. Temperature and wind speed in the range of -11 to -1.4 ° C and 1.6 to 13.8 m s^{-1} were also tested for possible biases in wind iso-axial conditions, and we found that they did not affected the ability of the probes to derive N_c. A more detailed look at how the two cloud probes measured in wind iso-axial conditions when the station was in-

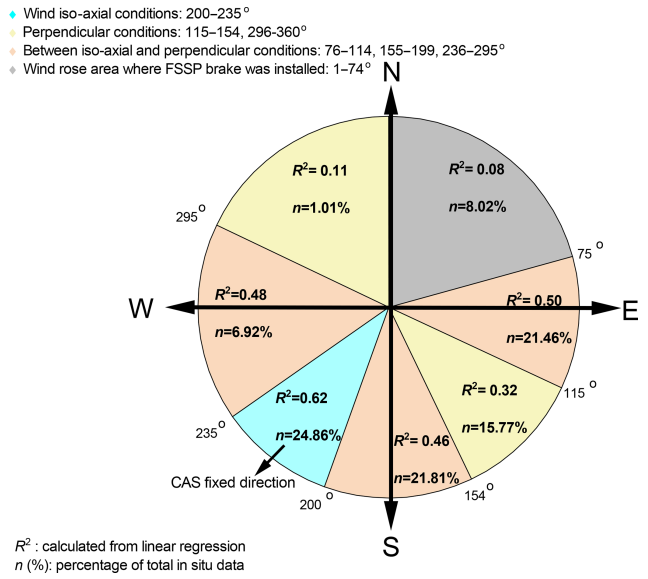

Figure 9. Intercomparison of number concentration (N_c) between the CAS and the FSSP based on the wind direction. The CAS was set and installed in a fixed direction (southwest, ∼ 225°); the FSSP was installed on a rotating platform and followed the wind direction. The wind rose was separated into four representative wind direction conditions; wind iso-axial conditions (from 200 to 235°), perpendicular conditions (from 115 to 154 and 296 to 360°), conditions between iso-axial and perpendicular (from 76 to 114, from 155 to 199 and from 236 to 295°) and the special case where the brake influenced the performance of FSSP (from 1 to 74°).

side a cloud is presented in Fig. 8c and d, where the averaged number size distribution of the cloud droplets is shown. The CAS probe measured more counts in sizes smaller than 7 µm (∼ 3 counts cm^{-3} more than the FSSP at 1.4 µm and ∼ 15 drops cm^{-3} more at 5 µm; in both cases, the difference in counts was less than 30 %). Also, we can see that the FSSP measured no droplets for sizes larger than 35 µm. Within the size range, meaning from 7 to 20 µm (an area which usually represented the peak of the size distribution), the FSSP usually measured higher N_c. This difference could be up to 25 % (∼ 150 more counts cm^{-3}). We have also noticed a slight shift in FSSP sizing towards bigger sizes: about 1.5 µm in the size range from 7 to 10 µm. These differences in the counting efficiency of the two instruments explain the slight discrepancies we observed in N_c even when they were measuring in wind iso-axial conditions. In a similar way, all the remaining sectors of the wind rose were investigated in detail to reveal more biases (for detailed description, please see discussion and Figs. S5, S6).

From the intercomparison of the two instruments in each sector of the wind rose, a general benchmarking was created, and it is presented in Fig. 9. According to our results we merged some of the wind sectors that we had initially created. As a result, we now have four sectors representing the wind rose; wind iso-axial conditions (from 200 to 235°), perpendicular conditions (from 115 to 154 and 296 to 360°), conditions between iso-axial and perpendicular (from 76 to 114, from 155 to 199 and from 236 to 295°) and the special case where the brake influenced the performance of FSSP (from 1 to 74°). To summarize our results, we should highlight that the best agreement between the two cloud spectrometers was obtained in wind iso-axial conditions (from 200 to 235°, $R^2 = 0.60$), and it covered a cleaned data set of ∼ 66 observation hours. The effect of wind direction on the CAS probe's ability to measure N_c was immediately noticed when the wind direction was out of the range of the wind iso-axial conditions. The agreement became slightly worst when the spectrometers were facing conditions in which the wind direction was between iso-axial and perpendicular ($0.46 \leq R^2 \leq 0.50$ for 76 to 114, 155 to 199 and 236 to 295°, respectively; ∼ 50 % of total cleaned data set). The CAS probe performed the worst when the wind direction was perpendicular to the CAS installed direction ($R^2 = 0.32$ and 0.11 for 115 to 154 and 296 to 360°, respectively) and represents ∼ 40 observation hours. Guyot et al. (2015) performed a similar experiment to investigate the sensitivity of the FSSP to meteorological parameters. Even though we conducted the measurements at different temperatures (in Puy-de-Dôme they sampled clouds only above zero), we found that our results were related. The main reason that caused the discrepancies (mainly in deriving N_c and LWC) to the fixed-direction cloud spectrometer ground setups (Pallas – CAPS; Puy-de-Dôme – FSSP) was the wind direction. The strong sensitivity to the wind direction suggested that the cloud spectrometers were sampling anisokinetically in both cases.

3.4 Intercomparison of CAS and FSSP – derived parameters LWC, ED and MVD

In this section, we focus on investigating the derived parameters LWC, ED and MVD. First, a comparison of the LWC for the two probes CAS and FSSP is presented. We only present measurements that were performed in wind iso-axial conditions, since the LWC was very sensitive to both changes in droplet N_c and changes in the shape of the number size distribution. The discrepancies we observed in droplet N_c in sectors outside the wind iso-axial conditions caused a significant difference in total LWC at least by a factor of 5 or even more. We also noticed differences by a factor of 15 especially when the wind direction was perpendicular to the CAS fixed direction. Figure 10a shows that the agreement in LWC ($R^2 = 0.34$ and slope 0.53) between CAS and FSSP in iso-axial conditions was found to be worse than agreement between both probes in N_c. After investigating how different meteorological parameters contribute to apparent biases in more detail, we found that temperature was the main and only factor that affected the instruments' ability to derive LWC. Accordingly, we divided our measurements into two temperature data sets: measurements with a temperature range from −11.1 to −4 and from −3.9 to −1.4 °C. Fig-

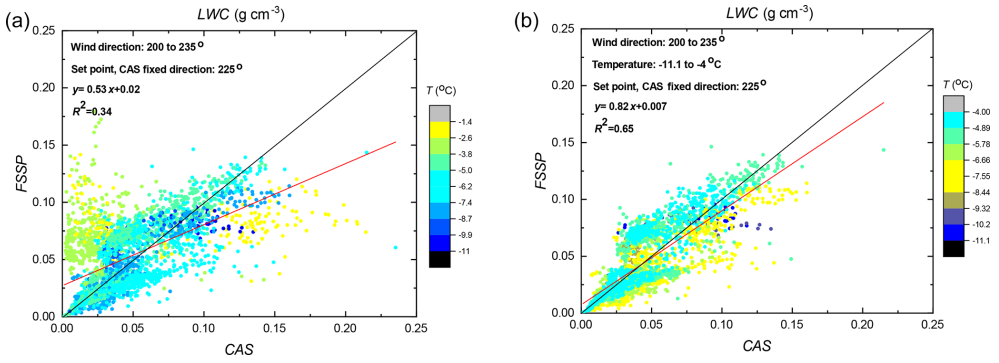

Figure 10. **(a)** Comparison of LWC as it was derived from the CAS and FSSP for wind iso-axial conditions, color code represents full temperature range from −11.1 to −1.4 °C. **(b)** Comparison of LWC as it was derived from the CAS and FSSP is presented for the same conditions but only for the temperature range from −11.1 to −4 °C.

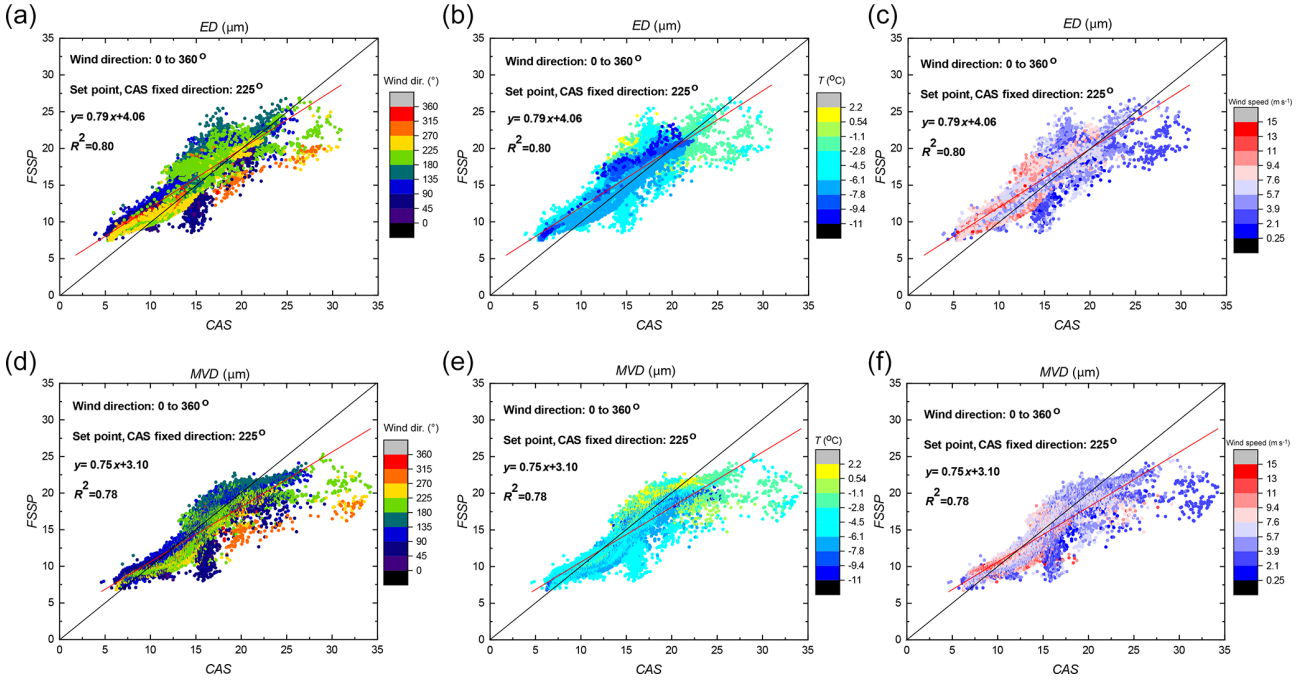

Figure 11. Comparison of ED **(a , b, c)** and MVD **(d, e, f)** as it was derived from the CAS and FSSP is presented for all wind directions. Color code represents wind direction (**a** and **d**), temperature (**b** and **e**), and wind speed (**c** and **f**).

ure 10b presents the agreement for the first set of measurements: temperatures below −4 °C. Excluding the warmer temperature range, we obtained better agreement between the probes ($R^2 = 0.78$ and slope 0.82). On other hand, the second set of temperatures (from −3.9 to −1.4 °C) indicated that the two probes significantly disagreed ($R^2 = 0.02$ and slope 0.07). As we already explained in Sect. 3.3, there was a slight shift in FSSP sizing towards bigger sizes, about 1.5 µm in size range from 7 to 10 µm. However, when the correction to FSSP sizing was applied, the resulting change in LWC was found to be marginal (about 0.7 %).

Our main conclusion regarding the derived LWC was that the main factor affecting LWC, values was the actual difference in the counts in each bin, especially when referring to larger droplets. Taking into account these limitations and biases in deriving LWC, our final proposal is to use only LWC values from wind iso-axial conditions. In addition, the critical parameter should be the temperature of the cloud. This suggests that only derived LWC values for temperatures below −4 ° C will be regarded as acceptable and will be used for further analysis of this data set. However, even when we consider the best agreement, the maximum difference in obtained LWC between CAS and FSSP could still be about 40 %. In addition, we suggest the deployment of another LWC sensor, e.g., the particle volume monitor (PVM-100; Gerber, 1999), during future campaigns in order to obtain

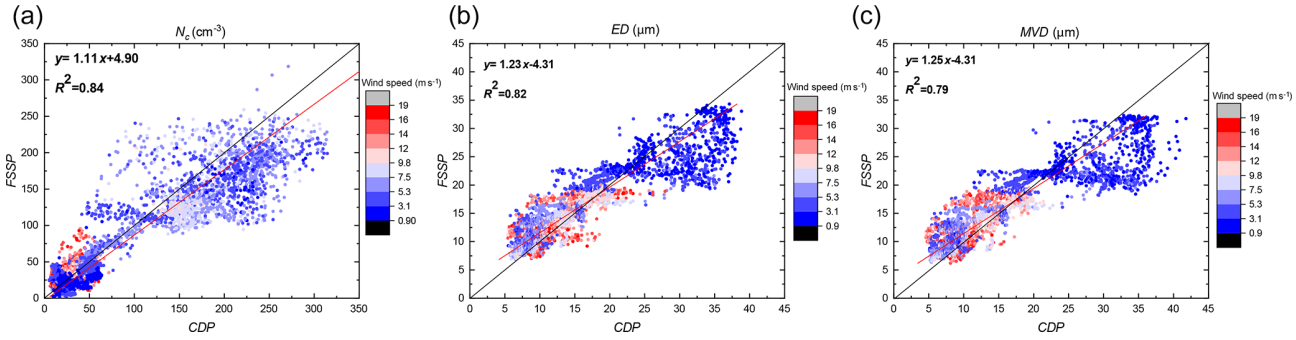

Figure 12. Intercomparison of **(a)** N_c, **(b)** ED and **(c)** MVD as it was derived from the CDP and the FSSP is presented for all wind directions. Color code represents the wind speed.

another reference LWC value for intercomparison in a wide temperature range. In addition, we are continuously pursuing the development of a new generation of counters designed for ground-based in situ cloud measurements. Thus, it is a matter of future deployment during upcoming PaCE campaigns.

The final step to complete the intercomparison between the CAS probe and the FSSP was to investigate their ability to derive two sizing parameters: the ED and the MVD. Both of them are significant to identify and evaluate the sizing performance of the cloud spectrometers (e.g., Stephens, 1978; Slingo and Schencker, 1982; Korolev, 1999; Mitchell et al., 2011). The cleaned data set obtained from the whole wind spectrum plotted in a different color scale for wind directions, temperature and wind speed is presented in Fig. 11a, b and c for ED and in Fig. 11 d, e and f for MVD. The observations when the FSSP did not operate properly due to the installation of the brake were excluded from the intercomparison. The agreement for both sizing parameters was found to be good ($R^2 = 0.80$, slope 0.79 and $R^2 = 0.78$, slope 0.75, respectively). The best agreement was observed when the wind direction (see Fig. 13a, d) was inside the range of isoaxial conditions where all the points were focused along the 1 : 1 line. When the direction was perpendicular the points were spread wider (maximum observed difference between the two probes was about 20 %). Surprisingly, despite the fact that CAS was measuring lower N_c even by a factor of 10 when the wind direction was perpendicular to the CAS fixed direction, the derived ED and MVD were not significantly influenced. Both sizing parameters were derived from the measured size distribution as described in Sect. 2.3. We found that even if a significant number of cloud droplets was lost due to inertia, the shape and the position of the peak of the size distribution measured by CAS remained similar. This behavior was found to be the same through the whole available cleaned data set (∼ 183 h) with the maximum ED and MVD of 35 and 30 µm. It has to be pointed out that this behavior might be exclusive for sub-Arctic conditions with generally small cloud droplets. This fact allows us to use the majority of the data set when investigating these two derived sizing parameters. As a result, it creates a significant and usable data set without the need to disqualify data according to a particular wind direction. Thus we obtain statistically significant size properties of the cloud droplets in a wide range of meteorological conditions. We also investigated the probability that wind speed will affect the sizing parameters (see Fig. 11c, f). When the probes were facing high wind speed, ED and MVD were slightly influenced (FSSP derived bigger values of ED and MVD when compared to CAS). On the other hand, while they were facing low wind speeds, sizing was again influenced in the opposite way (FSSP derived smaller values when compared to CAS). This could happen due to the isokinetic motion of the particles. The larger particles could not enter the FSSP because the inner diameter necking on the inlet was changing from 3.8 to 2.0 cm. Finally, Fig. 11b and d indicate that at lower temperatures we observed smaller ED and MVD values.

According to previous analysis, our main conclusion was that even if there were slight biases and uncertainties, the agreement in intercomparison was considered good as both R^2 and slope were higher than 0.75. As a result, we propose that when deriving the sizing parameters, ED and MVD, all measurements can be used for further research after carefully excluding the FSSP data set that was obtained from the wind rose sector where the brake influenced its performance.

3.5 Evaluation of the CDP during PaCE 2013

After comparing and analyzing discrepancies and biases between the CAS and the FSSP cloud probes, we discuss the performance of the CDP cloud probe separately. To evaluate CDP performance we used only FSSP data. We should remember that during the period that both the CDP and the CAS probe were on site (from 15 October to 27 November), the CDP encountered several malfunctions and operational problems during icy conditions. As a result, there was a lack of common data between the CDP and the CAS probe.

We used CDP and FSSP data from 25 September to 14 October (∼ 70 h of cleaned data set) since it was the only period that the CDP faced fewer operational problems since average ambient temperatures were mostly above 0 °C. During this

Table 2. The table presents the final recommendations for data analysis regarding the cloud spectrometers ground-based setups for future campaigns in sub-Arctic conditions with frequently occurring supercooled clouds.

	N_c	ED, MVD	LWC	Comments
CAS	Only data from wind iso-axial conditions (±20° from its fixed direction) should be used.	All measurements can be used for further analysis, independent of wind direction in the size range of ED and MVD of 5–35 µm.	Only data from wind iso-axial conditions and temperatures below −4 °C should be used.	Good data coverage (67 %); operating properly both in non-icy and icy conditions; needs daily cleaning.
FSSP	Data from all wind sectors will be used except data from the wind sector where the brake was installed (±40° brake direction).	All data can be used for further analysis except data from the wind sector where the brake was installed (±40° from brake direction).	Only data from wind iso-axial conditions and temperatures below – 4 °C should be used.	The best data coverage (75 %); operating properly both in non-icy and icy conditions; needs daily cleaning
CDP	Usable in warm clouds. Limitation in temperature; operational problems at sub-zero temperatures.	All data obtained in non-icy conditions can be used for further analysis.	Not usable due to temperature range.	Low data coverage (17 %); operating properly in non-icy conditions; not recommended for sub-zero temperatures.

intercomparison, a set of data from the FSSP was removed (0 to 74°, where the FSSP had significant malfunctions due to the installation of the brake). For this time period, average temperature at the station was 1.7 (SD 1.6) °C and the averaged wind speed was 6.9 (SD 3.6) m s^{-1}. In order to compare similar size ranges for both cloud probes, the first two bins from the FSSP were removed. This means that the following results depict the size range from 3.5 to 47 µm for the FSSP and from 3 to 50 µm for the CDP probe.

As was already mentioned at the beginning of Sect. 3.2 these two instruments belong to the sub-category of the probes that were installed on a rotating platform during PaCE 2013. Figure 12a shows, as was expected, that the ability of the two instruments to derive N_c was good ($R^2 = 0.84$, slope 1.11). However, there were cases where the difference between them was about 30 %. Additionally, we investigated the derived sizing parameters ED and MVD; see Fig. 12b and c. In a range of temperatures (from −3.9 to 3.8 °C) and wind speeds (0.9 to 19 ms^{-1}) agreement corresponding to the sizing parameters was good ($R^2 = 0.82$ and 0.79 with slopes 1.23 and 1.25 for ED and MVD, respectively). However, when FSSP derived ED and MVD for sizes larger than 22.5 µm, we could see a difference that could even be 15 µm smaller in comparison with CDP. This difference was noticed especially when the wind speeds were low. FSSP had similar behavior (Sect. 3.4) when we were comparing CAS and FSSP due to the isokinetic motion of the particles.

A significant limitation in derived LWC regarding temperature has already been discussed above during the comparison of CAS and FSSP. In this case, the temperature ranged from −3.9 to 3.8 °C. This range that was above −4 °C (the temperature point that was set in Sect. 3.4). As a result, the comparison of CDP- with FSSP-derived LWC did not lead to reasonable correlation, and no LWC data are presented here.

In summary, the CDP was operating well in warm liquid clouds and had good agreement in cloud droplet counts and the sizing derived parameters with FSSP. On the other hand, while we faced sub-zero conditions, the CDP operation was regarded as problematic. Its probe inlet often became clogged because of supercooled cloud drop accumulation. This happened to both the rotation and inhalation system because the probe's big surfaces were collecting ice, and it had a small opening for the inhalation system. In conclusion, even though this CDP setup performed well in warm cloud conditions, it is not a suitable instrument for semi-long-term ground-based measurement of clouds in sub-Arctic conditions when we are facing sub-zero conditions.

4 Conclusions

We conducted ground-based in situ cloud measurements during PaCE 2013 from 14 September until 28 November. We deployed three cloud spectrometer setups (CAS, FSSP and CDP) on the roof of Sammaltunturi station, located in the Finnish sub-Arctic. The obtained data set was analyzed in detail to evaluate the instruments' ground-based setups' performance and to establish limitations for future studies. All cloud spectrometers and their setups are owned by FMI and results could be used in campaigns with similar meteorological conditions: sub-Arctic conditions with frequently occurring supercooled clouds. Although there is a possibility that we sampled ice particles in some cases, it is expected that the number of supercooled liquid droplets greatly exceeds the number of small ice cloud droplets. The CAS was in-

stalled and fixed against the main wind direction of the station ($\sim 225°$), and the other two probes (FSSP and CDP) were installed on rotating platforms. Each probe had its own inhalation system. Their ability to measure the size distribution of cloud droplets along with the derived N_c, the sizing parameters (ED and MVD) and the LWC was tested and the above parameters were mutually compared. In this work, CAS and FSSP ground setups were investigated first because their parallel data coverage was the best (~ 243 h of common cleaned data set). On the other hand, CDP had a low common data set with the CAS. The reason for this was that from the date that the CAS was installed we were mainly facing sub-zero temperatures, conditions that proved not to be favorable for this CDP ground setup.

To estimate the droplet counting performance and possible droplets losses, we used N_c. Results indicated that when we were deriving N_c, the mutual direction of probe heading and the wind direction played the most significant role. From the intercomparison of the CAS (fixed orientation) with FSSP (rotating platform), it was found that the CAS probe had the best agreement ($R^2 = 0.70$) with the FSSP during wind iso-axial conditions (200 to 235°). The CAS probe counting efficiency was strongly dependent on the wind direction; this can be clearly explained by its installation with a fixed orientation. When the station was inside warm clouds, both the CDP and the FSSP had good agreement ($R^2 = 0.82$) as they were both operating on rotating platforms.

The LWC was found to be the most sensitive derived parameter. This is because LWC strongly depends both on size and the number of droplets in each size bin. Thus, the wind direction played the most significant role again. For that reason, we strongly recommend that only CAS- and FSSP-derived LWC values from wind iso-axial conditions should be used. Additionally, LWC values were also found to be temperature dependent. For temperatures lower than $-4\,°C$ the agreement between the CAS and the FSSP in wind iso-axial conditions was high ($R^2 = 0.62$), and that is why temperature $-4\,°C$ was adopted as the critical temperature point regarding LWC estimation. We excluded all LWC values derived from the CDP due to its problematic operation at sub-zero conditions; i.e., close to a temperature of $-4\,°C$, CDP was usually frozen. The CDP probe often accumulated ice in sub-zero condition, both in its rotational platform and inhalation system. This was happening due to the presence of supercooled clouds at the station. The big surfaces of the CDP's rotation platform and the inlet with a small opening collected ice very fast.

The analysis of the derived sizing parameters, ED and MVD, showed good agreement among the three probes during the time they were operating properly. However, our conclusions here concentrate only on CAS and FSSP because only these two instruments operated properly in sub-zero temperatures, temperatures that we usually face during PaCE. The obtained intercomparison results were surprisingly good even though CAS lost a significant amount of cloud droplets due to its orientation. The wind direction did not significantly affect the ED values or the MVD, even though large discrepancies (uncertainty $\sim 85\,\%$) in N_c outside of the wind iso-axial conditions could be found (e.g., when the wind direction was perpendicular to the CAS probe fixed direction, uncertainty for sizing parameters was $\sim 20\,\%$). The ED and MVD were not affected because the shape and the peak position of the CAS size droplet distribution did not change significantly. Such behavior held through ~ 183 h of data set. This result is important as it allows us to use a larger data set without limitations due to wind direction and other meteorological parameters regarding derived ED and MVD. The small differences (about 2 µm) were explained by a closer look at the size distribution of each spectrometer and the differences in sizing during operation in real conditions as they were mentioned above.

At the time of PaCE 2013, the market did not offer any instrumentation fulfilling our requirements on continuous long-term unattended operation at sub-zero conditions. As final suggestions regarding performing continuous ground-based in situ cloud measurements in harsh environments, we would like to highlight two major issues. First, the cloud probes should always continuously face the wind direction to minimize the sampling losses. If this is not ensured, only the measurements that are conducted in wind iso-axial conditions can be used for further analysis. However, deriving the sizing parameters ED and MVD for the whole wind direction spectrum is still possible, but it must be done with insight and prudence. Secondly, deicing features of the ground setups should be upgraded to make possible their long-term unattended operation in sub-zero conditions. Otherwise, the cloud probes need necessary daily or more frequent checkups and cleaning of their inlets. Our final recommendations and our view on the main limitations of each spectrometer ground setup for using and analyzing the obtained data sets during sub-Arctic meteorological conditions with frequently occurring supercooled clouds (including future PaCE campaigns) are summarized and presented in Table 2.

Data availability. The cloud probes and meteorological data used here are available upon request to the corresponding author (konstantinos.doulgeris@fmi.fi).

Supplement. The supplement related to this article is available online at: https://doi.org/10.5194/amt-13-5129-2020-supplement.

Author contributions. K-MD and DB wrote the paper with contributions from all co-authors. K-MD prepared the paper and analyzed data from all cloud probes and meteorological data with contributions from DB. DB installed and operated all the instruments during PACE 2013. MK and SR provided the CDP ground setup and performed its calibration.

Competing interests. The authors declare that they have no conflict of interest.

Acknowledgements. This work was supported by the Koneen Säätiö, NordForsk; the CRAICC Amendment on CRAICC-PEEX Collaboration, the Academy of Finland; the Academy of Finland Center of Excellence program; the Natural Environment Research Council (NERC). This project has received funding from the European Union, Seventh Framework Programme (BACCHUS) and H2020 research and innovation program (ACTRIS-2, the European Research Infrastructure for the observation of Aerosol, Clouds, and Trace gases).

Financial support. This research has been supported by the Koneen Säätiö (grant no. 46-6817), the NordForsk (grant no. 26060), the Academy of Finland (grant no. 269095), the Academy of Finland Center of Excellence program (grant no. 307331) the Natural Environment Research Council (grant no. NE-L011514-1), and the European Union's H2020 research and innovation programme (ACTRIS-2 (grant agreement no. 654109)) and Seventh Framework Programme (FP7/2007–2013) (BACCHUS (grant no. 603445)).

Review statement. This paper was edited by Alexander Kokhanovsky and reviewed by Darrel Baumgardner and two anonymous referees.

References

Albrecht, B. A.: Aerosols, cloud microphysics, and fractional cloudiness, Science, 245, 1227–1230, 1989.

Anttila, T., Vaattovaara, P., Komppula, M., Hyvärinen, A.-P., Lihavainen, H., Kerminen, V.-M., and Laaksonen, A.: Size-dependent activation of aerosols into cloud droplets at a subarctic background site during the second Pallas Cloud Experiment (2nd PaCE): method development and data evaluation, Atmos. Chem. Phys., 9, 4841–4854, https://doi.org/10.5194/acp-9-4841-2009, 2009.

Anttila, T., Brus, D., Jaatinen, A., Hyvärinen, A.-P., Kivekäs, N., Romakkaniemi, S., Komppula, M., and Lihavainen, H.: Relationships between particles, cloud condensation nuclei and cloud droplet activation during the third Pallas Cloud Experiment, Atmos. Chem. Phys., 12, 11435–11450, https://doi.org/10.5194/acp-12-11435-2012, 2012.

Baumgardner, D.: An analysis and comparison of five water droplet measuring instruments, J. Appl. Meteorol., 22, 891–910, https://doi.org/10.1175/1520-0450(1983)022<0891:AAACOF>2.0.CO;2, 1983.

Baumgardner, D. and Spowart, M.: Evaluation of the Forward Scattering Spectrometer Probe. Part III: Time Response and Laser Imhomogeneity Limitations, J. Atmos. Ocean. Technol., 7, 666–672, https://doi.org/10.1175/1520-0426(1990)007<0666:EOTFSS>2.0.CO;2 1990.

Baumgardner, D., Strapp, W., and Dye, J. E.: Evaluation of the Forward Scattering Spectrometer Probe – Part II: Corrections for coincidence and dead-time losses, J. Atmos. Ocean. Technol.,2, 626–632, https://doi.org/10.1175/1520-0426(1985)002<0626:EOTFSS>2.0.CO;2, 1985.

Baumgardner, D., Dye, J. E., and Gandrud, B. W.: Calibration of the forward scattering spectrometer probe used on the ER-2 during the Airborne Antarctic Ozone Experiment, Geophys. Res., 94, 16475–16480, https://doi.org/10.1029/JD094iD14p16475, 1989.

Baumgardner, D., Dye, J. E., Gandrud, B. W., and Knollenberg, R. G.: Interpretation of Measurements Made by the Forward Scattering Spectrometer Probe (FSSP-300) During the Airborne Arctic Stratospheric Expedition, J. Geophys. Res., 97, 8035–8046, https://doi.org/10.1029/91JD02728, 1992.

Baumgardner, D., Jonsson, H., Dawson, W., O'Connor D., and Newton R.: The cloud, aerosol and precipitation spectrometer (CAPS): A new instrument for cloud investigations, Atmos. Res., 59–60, 251-2-64, https://doi.org/10.1016/S0169-8095(01)00119-3, 2001.

Baumgardner, D., Brenguier, J., Bucholtz, A., Coe, H., DeMott, P., Garrett, T., Gayet, J., Hermann, M., Heymsfield, A., Korolev, A., Kramer, M., Petzold, A., Strapp, W., Pilewskie, P., Taylor, J., Twohy, C., Wendisch, M., Bachalo, W., and Chuang, P.: Airborne instruments to measure atmospheric aerosol particles, clouds and radiation: A cook's tour of mature and emerging technology, Atmos. Res., 102, 10–29, https://doi.org/10.1016/j.atmosres.2011.06.021, 2011.

Baumgardner, D., Newton, R., Krämer, M., Meyer, J., Beyer, A., Wendisch, M., and Vochezer, P.: The Cloud Particle Spectrometer with Polarization Detection (CPSPD): A next generation open-path cloud probe for distinguishing liquid cloud droplets from ice crystals, Atmos. Res., 142, 2–14, https://doi.org/10.1016/j.atmosres.2013.12.010, 2014.

Baumgardner, D., Abel, S. J., Axisa, D., Cotton, R., Crosier, J., Field, P., Gurganus, C., Heymsfield, A., Korolev, A., Krämer, M., Lawson, P., McFarquhar, G., Ulanowski, Z., and Um, J.: Cloud Ice Properties: In Situ Measurement Challenges, Meteor. Mon., 58, 9.1–9.23, https://doi.org/10.1175/AMSMONOGRAPHS-D-16-0011.1, 2017.

Beswick, K., Baumgardner, D., Gallagher, M., Volz-Thomas, A., Nedelec, P., Wang, K.-Y., and Lance, S.: The backscatter cloud probe – a compact low-profile autonomous optical spectrometer, Atmos. Meas. Tech., 7, 1443–1457, https://doi.org/10.5194/amt-7-1443-2014, 2014.

Boucher, O., Randall, D., Artaxo, P., Bretherton, C., Feingold, G., Forster, P., Kerminen, V.-M., Kondo, Y., Liao, H., Lohmann, U., Rasch, P., Satheesh, S. K., Sherwood, S., Stevens, B., and Zhang, X. Y.: Clouds and aerosols, in: Climate Change 2013: The Physical Science Basis. Contribution of Working Group I to the Fifth Assessment Report of the Intergovernmental Panel on Climate Change, edited by: Stocker, T. F., Qin, D., Plattner, G.-K., Tignor, M., Allen, S. K., Doschung, J., Nauels, A., Xia, Y., Bex, V., and Midgley, P. M., Cambridge University Press, 571–657, https://doi.org/10.1017/CBO9781107415324.016, 2013.

Brenguier, J. L.: Coincidence and Dead-Time Corrections for Particles Counters. Part II: High Concentration Measurements with an FSSP, J. Atmos. Ocean. Tech., 6, 585–598, https://doi.org/10.1175/1520-0426(1989)006<0585:CADTCF>2.0.CO;2, 1989.

Brenguier, J.-L., Bachalo, W. D., Chuang, P. Y., Esposito, B. M., Fugal, J., Garrett, T., Gayet, J.-F., Gerber, H., Heymsfield, A.,

Kokhanovsky, A., Korolev, A., Lawson, R. P., Rogers, D. C., Shaw, R. A., Strapp, W., and Wendisch, M.: In Situ Measurements of Cloud and Precipitation Particles, in Airborne Measurements for Environmental Research, in: Methods and Instruments, edited by: Wendisch, M. and Brenguier, J.-L., Wiley VCH Verlag GmbH & Co. KGaA, Weinheim, Germany, 225–301, https://doi.org/10.1002/9783527653218.ch5, 2013.

Bromwich, D. H., Nicolas, J. P., Hines, K. M., Kay, J. E., Key, E. L., Lazzara, M. A., Lubin, D., McFarqulah, G. M., Gorodetskaya, I. V., Grosvenor, D. P., Lachnan-Cope, T., and Van Lipzig, N. P. M.: Tropospheric clouds in Antarctica, Rev. Geophys., 50, RG1004, https://doi.org/10.1029/2011RG000363, 2012.

Burnet F. and Brenguier, J. L.: Validation of droplet spectra and liquid water content measurements, Phys. Chem. Earth, 24, 249–254, https://doi.org/10.1016/S1464-1909(98)00046-X, 1999.

Burnet F. and Brenguier, J. L.: Comparison between standard and modified Forward Scattering Spectrometer Probes during the Small Cumulus Microphysics Study, J. Atmos. Ocean. Technol., 19, 1516–1531, https://doi.org/10.1175/1520-0426(2002)019<1516:CBSAMF>2.0.CO;2 ,2002.

Coelho, A., Brenguier, J. L., and Perrin, T.: Droplet spectra measurements with the FSSP-100. Part I: Low droplet concentration measurements, J. Atmos. Ocean. Technol., 22, 1749–1756, https://doi.org/10.1175/JTECH1817.1, 2005a.

Coelho, A., Brenguier, J. L., and Perrin, T.: Droplet spectra measurements with the FSSP-100. Part II: Coincidence Effects, J. Atmos. Ocean. Technol., 22, 1749–1756, https://doi.org/10.1175/JTECH1818.1, 2005b.

Collaud Coen, M., Andrews, E., Asmi, A., Baltensperger, U., Bukowiecki, N., Day, D., Fiebig, M., Fjaeraa, A. M., Flentje, H., Hyvärinen, A., Jefferson, A., Jennings, S. G., Kouvarakis, G., Lihavainen, H., Lund Myhre, C., Malm, W. C., Mihapopoulos, N., Molenar, J. V., O'Dowd, C., Ogren, J. A., Schichtel, B. A., Sheridan, P., Virkkula, A., Weingartner, E., Weller, R., and Laj, P.: Aerosol decadal trends – Part 1: In-situ optical measurements at GAW and IMPROVE stations, Atmos. Chem. Phys., 13, 869–894, https://doi.org/10.5194/acp-13-869-2013, 2013.

Droplet Measurement Technologies Manual: CAPS operator manual, DOC-0066 Revision F, DMT, Boulder, Colorado, USA, 2011

Dye, J. E. and Baumgardner, D.: Evaluation of the forward scattering spectrometer probe, I – Electronic and optical studies, J. Atmos. Ocean. Technol., 1, 329–344, https://doi.org/10.1175/1520-0426(1984)001<0329:EOTFSS>2.0.CO;2, 1984.

Eugster, W., Burkard, R., Holwerda, F., Scatena, F., and Bruijnzeel, L.: Characteristics of fog and fogwater fluxes in a Puerto Rican elfin cloud forest, Agr. Forest. Meteorol., 139, 288–306, https://doi.org/10.1016/j.agrformet.2006.07.008, 2006.

Faber, S., French, J. R., and Jackson, R.: Laboratory and in-flight evaluation of measurement uncertainties from a commercial Cloud Droplet Probe (CDP), Atmos. Meas. Tech., 11, 3645–3659, https://doi.org/10.5194/amt-11-3645-2018, 2018.

Febvre, G., Gayet, J.-F., Shcherbakov, V., Gourbeyre, C., and Jourdan, O.: Some effects of ice crystals on the FSSP measurements in mixed phase clouds, Atmos. Chem. Phys., 12, 8963–8977, https://doi.org/10.5194/acp-12-8963-2012, 2012.

Gérard, V., Noziere, B., Fine, L., Ferronato, C., Singh, D., K., Frossard, A., Cohen, R. C. Asmi, E., Lihavainen, H., Kivekäs, N., Aurela, M., Brus, D., Frka, S., and Cvitešić Kušan, A.: Concentrations and Adsorption Isotherms for Amphiphilic Surfactants in PM1 Aerosols from Different Regions of Europe, Environ. Sci. Technol., 53, 12379–12388, https://doi.org/10.1021/acs.est.9b03386, 2019.

Gerber, H., Frick, G., and Rodi, A.: Ground-based FSSP and PVM measurements of liquid water content, J. Atmos. Ocean. Tech., 16, 1143–1149, https://doi.org/10.1175/1520-0426(1999)016<1143:GBFAPM>2.0.CO;2, 1999.

Guyot, G., Gourbeyre, C., Febvre, G., Shcherbakov, V., Burnet, F., Dupont, J.-C., Sellegri, K., and Jourdan, O.: Quantitative evaluation of seven optical sensors for cloud microphysical measurements at the Puy-de-Dôme Observatory, France, Atmos. Meas. Tech., 8, 4347–4367, https://doi.org/10.5194/amt-8-4347-2015, 2015.

Hatakka, J., Aalto, T., Aaltonen, V., Aurela, M., Hakola, H., Komppula, M., Laurila, T., Lihavainen, H., Paatero, J., Salminen, K., and Viisanen Y., Overview of the atmospheric research activities and results at Pallas GAW station, Boreal Environ. Res., 8, 365–384, 2003.

Henning, S., Weingartner, E., Schwikowski, M., Gäggeler, H. W., Gehrig, R., Hinz, K.-P., Trimborn, A., Spengler, B., and Baltensperger, U: Seasonal variation of water-soluble ions of the aerosol at the high-alpine site Jungfraujoch (3580 m asl), J. Geophys. Res., 108, 4030, https://doi.org/10.1029/2002JD002439, 2003.

Heymsfield, A. J., Bansemer, A., Schmitt, C., Twohy, C., and Poellot, M. R.: Effective Ice Particle Densities Derived from Aircraft Data, J. Atmos. Sci., 61, 982–1003, https://doi.org/10.1175/1520-0469(2004)061<0982:EIPDDF>2.0.CO;2, 2004.

Hyvärinen, A.-P., Kolmonen, P., Kerminen, V.-M., Virkkula, A., Leskinen, A., Komppula, M., Hatakka, J., Burkhart, J., Stohl, A., Aalto, P., Kulmala, M., Lehtinen, K. E. J., Viisanen, Y., and Lihavainen, H.: Aerosol black carbon at five background measurement sites over Finland, a gateway to the Arctic, Atmos. Environ., 45, 4042–4050, https://doi.org/10.1016/j.atmosenv.2011.04.026, 2011.

Jaatinen, A., Romakkaniemi, J., Anttila, T., Hyvärinen, A.-P., Hao, L. Q., Kortelainen, A., Miettinen, P., Mikkonen, S., Smith, J. N., Virtanen, A., and Laaksonen, A.: The third Pallas Cloud Experiment: Consistency between the aerosol hygroscopic growth and CCN activity, Boreal Environ. Res., 19, 368–382, 2014.

Johnson, B., Turnbull, K., Brown, P., Burgess, R., Dorsey, J., Baran, A. J., Webster, H., Haywood, J., Cotton, R., Ulanowski, Z., Hesse, E., Woolley, A., and Rosenberg, P.: In situ observations of volcanic ash clouds from the FAAM aircraft during the eruption of Eyjafjallajökull in 2010, J. Geophys. Res.-Atmos., 117, D00U24, https://doi.org/10.1029/2011JD016760, 2012.

Jones, H. M., Haywood, J., Marenco, F., O'Sullivan, D., Meyer, J., Thorpe, R., Gallagher, M. W., Krämer, M., Bower, K. N., Rädel, G., Rap, A., Woolley, A., Forster, P., and Coe, H.: A methodology for in-situ and remote sensing of microphysical and radiative properties of contrails as they evolve into cirrus, Atmos. Chem. Phys., 12, 8157–8175, https://doi.org/10.5194/acp-12-8157-2012, 2012.

Kivekas, N., Kerminen, V.-M., Raatikainen, T., Vaattovaara, P., and Lihavainen, H.: Physical and chemical characteristics of the activating particles during the Second Pallas Cloud Experiment (Second PaCE), Boreal. Environ. Res., 14, 515–526, 2009.

Knollenberg, R. G.: Three new instruments for cloud physics measurements: the 2-D spectrometer probe, the forward scattering spectrometer probe and the active scattering aerosol spectrometer, American Meteorological Society, Int'l Conf. on Cloud Physics, 554–561, 1976.

Knollenberg, R. G.: Techniques for Probing Cloud Microstructure, in: Clouds, Their Formation, Optical Properties and Effects, edited by: Hobbs, P. V. and Deepak, A., Academic Press, New York, NY, USA, 15–92, 1981.

Komppula, M., Lihavainen, H., Kerminen, V.-M., Kulmala, M., and Viisanen, Y.: Measurements of cloud droplet activation of aerosol particles at a clean subarctic background site, J. Geophys. Res., 110, D06204, https://doi.org/10.1029/2004JD005200, 2005.

Komppula, M., Sihto, S.-L., Korhonen, H., Lihavainen, H., Kerminen, V.-M., Kulmala, M., and Viisanen, Y.: New particle formation in air mass transported between two measurement sites in Northern Finland, Atmos. Chem. Phys., 6, 2811–2824, https://doi.org/10.5194/acp-6-2811-2006, 2006.

Korolev, A. V., Strapp, W. J., and Nevzorov, N. A.: In situ measurements of effective diameter and effective droplet number concentration, J. Geophys. Res., 104, 3993–4003, https://doi.org/10.1029/1998JD200071, 1999.

Korolev, A. V., Shashkov, A., and Barker, H.: Calibrations and Performance of the Airborne Cloud Extinction Probe, J. Atmos. Ocean. Technol., 31, 326–345, https://doi.org/10.1175/JTECH-D-13-00020.1, 2014.

Lance, S.: Coincidence Errors in a Cloud Droplet Probe (CDP) and a Cloud and Aerosol Spectrometer (CAS), and the Improved Performance of a Modified CDP, https://doi.org/10.1175/JTECH-D-11-00208.1, 2012.

Lance, S., Brock, C. A., Rogers, D., and Gordon, J. A.: Water droplet calibration of the Cloud Droplet Probe (CDP) and in-flight performance in liquid, ice and mixed-phase clouds during ARCPAC, Atmos. Meas. Tech., 3, 1683–1706, https://doi.org/10.5194/amt-3-1683-2010, 2010.

Lihavainen, H., Kerminen, V.-M., Komppula, M., Hyvärinen, A.-P., Laakia, J., Saarikoski, S., Makkonen, U., Kivekäs, N., Hillamo, R., Kulmala, M., and Viisanen, Y.: Measurements of the relation between aerosol properties and microphysics and chemistry of low-level liquid water clouds in Northern Finland, Atmos. Chem. Phys., 8, 6925–6938, https://doi.org/10.5194/acp-8-6925-2008, 2008.

Lihavainen, H., Kerminen, V.-M., and Remer, L. A.: Aerosol-cloud interaction determined by both in situ and satellite data over a northern high-latitude site, Atmos. Chem. Phys., 10, 10987–10995, https://doi.org/10.5194/acp-10-10987-2010, 2010.

Lihavainen, H., Hyvärinen, A.-P., Asmi, E., Hatakka, J., and Viisanen, Y.: Long term variability of aerosol optical properties in northern Finland, Boreal Environ. Res., 20, 526–541, 2015.

Lloyd, G., Choularton, T. W., Bower, K. N., Gallagher, M. W., Connolly, P. J., Flynn, M., Farrington, R., Crosier, J., Schlenczek, O., Fugal, J., and Henneberger, J.: The origins of ice crystals measured in mixed-phase clouds at the high-alpine site Jungfraujoch, Atmos. Chem. Phys., 15, 12953–12969, https://doi.org/10.5194/acp-15-12953-2015, 2015.

Lowenthal, D. H., Hallar, A. G., David, R. O., McCubbin, I. B., Borys, R. D., and Mace, G. G.: Mixed-phase orographic cloud microphysics during StormVEx and IFRACS, Atmos. Chem. Phys., 19, 5387–5401, https://doi.org/10.5194/acp-19-5387-2019, 2019.

Luebke, A. E., Afchine, A., Costa, A., Grooß, J.-U., Meyer, J., Rolf, C., Spelten, N., Avallone, L. M., Baumgardner, D., and Krämer, M.: The origin of midlatitude ice clouds and the resulting influence on their microphysical properties, Atmos. Chem. Phys., 16, 5793–5809, https://doi.org/10.5194/acp-16-5793-2016, 2016.

McFarquhar, G. M., Um, J., Freer, M., Baumgardner, D., Kok, G. L., and Mace, G.: Importance of small ice crystals to cirrus properties: Observations from the Tropical Warm Pool International Cloud Experiment (TWP-ICE), Geophys. Res. Lett., 34, L13803, https://doi.org/10.1029/2007GL029865, 2007.

Mertes, S., Schwarzenböck, A., Laj, P., Wobrock, W., Pichon, J. M., Orsi, G., and Heintzenberg, J.: Changes of cloud microphysical properties during the transition from supercooled to mixed-phase conditions during CIME, Atmos. Res., 58, 267–294, https://doi.org/10.1016/S0169-8095(01)00095-3, 2001

Mie, G.: Beiträge zur Optik trüber Medien, speziell kolloidaler Metallösungen, Ann. Phys.-Berlin, 330, 377–445, 1908.

Mitchell, D. L., Lawson, R. P., and Baker, B.: Understanding effective diameter and its application to terrestrial radiation in ice clouds, Atmos. Chem. Phys., 11, 3417–3429, https://doi.org/10.5194/acp-11-3417-2011, 2011.

Nichman, L., Järvinen, E., Dorsey, J., Connolly, P., Duplissy, J., Fuchs, C., Ignatius, K., Sengupta, K., Stratmann, F., Möhler, O., Schnaiter, M., and Gallagher, M.: Intercomparison study and optical asphericity measurements of small ice particles in the CERN CLOUD experiment, Atmos. Meas. Tech., 10, 3231–3248, https://doi.org/10.5194/amt-10-3231-2017, 2017.

Petäjä, T., O'Connor, E.J, Moisseev, D., Sinclair, V.A., Manninen, A.J., Väänänen, R., Von Lerber, A., Thornton, J.A., Nicoll, K., Petersen, W., Chandrasekar, V., Smith, J.N., Winkler, P.M., Krüger, O., Hakola, H., Timonen, H., Brus, D., Laurila, T., Asmi, E., Riekkola, M.-L., Mona, L., Massoli, P., Engelmann, R., Komppula, M., Wang, J., Kuang, C., Bäck, J., Virtanen, A., Levula, J., Ritsche, M., and Hickmon, N.: BAECC: A Field Campaign to Elucidate the Impact of Biogenic Aerosols on Clouds and Climate. B. Am. Meteorol. Soc., 97, 1909–1928, https://doi.org/10.1175/BAMS-D-14-00199.1, 2016.

Pruppacher, H. R. and Klett, J. D.: Microphysics of Clouds and Precipitation, Kluwer Academic Publishers, Dordrecht, 1997.

Raatikainen, T., Brus, D., Hyvärinen, A.-P., Svensson, J., Asmi, E., and Lihavainen, H.: Black carbon concentrations and mixing state in the Finnish Arctic, Atmos. Chem. Phys., 15, 10057–10070, https://doi.org/10.5194/acp-15-10057-2015, 2015.

Rosenfeld, D. and Ulbrich, C. W.: Cloud Microphysical Properties, Processes, and Rainfall Estimation Opportunities, Meteor. Mon., 30, 237–237, https://doi.org/10.1175/0065-9401(2003)030<0237:CMPPAR>2.0.CO;2, 2003.

Small, J. D., Chuang, P. Y., Feingold, G., and Jiang, H.: Can aerosol decrease cloud lifetime?, Geophys. Res. Lett., 36, L16806, https://doi.org/10.1029/2009GL038888, 2009.

Smith, H., Connolly, P., Baran, A., Hesse, E., Smedley, A., and Webb, A.: Cloud chamber laboratory investigations into scattering properties of hollow ice particles, J. Quant. Spectrosc. Ra. Trans., 157, 106–118, https://doi.org/10.1016/j.jqsrt.2015.02.015, 2015.

Slingo, A. and Schencker, H. M.: On the shortwave radiative properties of stratiform water clouds, Q. J. Roy. Meteorol. Soc., 108, 407–426, https://doi.org/10.1002/qj.49710845607, 1982.

Spiegel, J. K., Zieger, P., Bukowiecki, N., Hammer, E., Weingartner, E., and Eugster, W.: Evaluating the capabilities and uncertainties of droplet measurements for the fog droplet spectrometer (FM-100), Atmos. Meas. Tech., 5, 2237–2260, https://doi.org/10.5194/amt-5-2237-2012, 2012.

Stephens, G. L.: Radiation profiles in extended water clouds, II, Parameterization scheme, J. Atmos. Sci., 35, 2123–2132, https://doi.org/10.1175/1520-0469(1978)035<2123:RPIEWC>2.0.CO;2, 1978.

Voigt, C., Schumann, U., Minikin, A., Abdelmonem, A., Afchine, A., Borrmann, S., Boettcher, M., Buchholz, B., Bugliaro, L., Costa, A., Curtius, J., Dollner, M., Dörnbrack, A., Dreiling, V., Ebert, V., Ehrlich, A., Fix, A., Forster, L., Frank, F., Fütterer, D., Giez, A., Graf, K., Grooß, J.-U., Groß, S., Heimerl, K., Heinold, B., Hüneke, T., Järvinen, E., Jurkat, T., Kaufmann, S., Kenntner, M., Klingebiel, M., Klimach, T., Kohl, R., Krämer, M., Krisna, T. C., Luebke, A., Mayer, B., Mertes, S., Molleker, S., Petzold, A., Pfeilsticker, K., Port, M., Rapp, M., Reutter, P., Rolf, C., Rose, D., Sauer, D., Schäfler, A., Schlage, R., Schnaiter, M., Schneider, J., Spelten, N., Spichtinger, P., Stock, P., Walser, A., Weigel, R., Weinzierl, B., Wendisch, M., Werner, F., Wernli, H., Wirth, M., Zahn, A., Ziereis, H., and Zöger, M.: ML-CIRRUS: The Airborne Experiment on Natural Cirrus and Contrail Cirrus with the High-Altitude Long-Range Research Aircraft HALO, B. Am. Meteorol. Soc., 98, 271–288, https://doi.org/10.1175/bams-d-15-00213.1, 2017.

Wagner, R., Bunz, H., Linke, C., Möhler, O., Naumann, K. H., Saathoff, H., Schnaiter, M., and Schurath, U.: Chamber simulations of cloud chemistry: the AIDA Chamber, in: NATO Adv. Res. Work. Environ. Simul. Chambers Appl. to Atmos. Chem. Process. (2004 Zakopane, Poland), edited by: Barnes, I. and Rudzinski, K. J., Springer, Dordrecht, the Netherlands, 2006.

Wandinger, U., Apituley, A., Blumenstock, T., Bukowiecki, N., Cammas, J.-P., Connolly, P., De Mazière, M., Dils, B., Fiebig, M., Freney, E., Gallagher, M., Godin-Beekmann, S., Goloub, P., Gysel, M., Haeffelin, M., Hase, F., Hermann, M., Herrmann, H., Jokinen, T., Komppula, M., Kubistin, D., Langerock, B., Lihavainen, H., Mihalopoulos, N., Laj, P., Lund Myhre, C., Mahieu, E., Mertes, S., Möhler, O., Mona, L., Nicolae, D., O'Connor, E., Palm, M., Pappalardo, G., Pazmino, A., Petäjä, T., Philippin, S., Plass-Duelmer, C., Pospichal, B., Putaud, J.-P., Reimann, S., Rohrer, F., Russchenberg, H., Sauvage, S., Sellegri, K., Steinbrecher, R., Stratmann, F., Sussmann, R., Van Pinxteren, D., Van Roozendael M., Vigouroux C., Walden C., Wegene R., and Wiedensohler, A.: ACTRIS-PPP Deliverable D5.1: Documentation on technical concepts and requirements for ACTRIS Observational Platforms, available at: https://www.actris.eu/Portals/46/Documentation/ACTRISPPP/Deliverables/Public/WP5_D5.1_M18.pdf?ver=2018-06-28-125343-273 (last access: 21 September 2020), 2018.

Wendisch, M.: A quantitative comparison of ground-based FSSP and PVM measurements, J. Atmos. Ocean. Tech., 15, 887–900, https://doi.org/10.1175/1520-0426(1998)015<0887:AQCOGB>2.0.CO;2, 1998.

Wendisch, M., Keil, A., and Korolev, A. V.: FSSP Characterization with Monodisperse Water Droplets, J. Atmos. Ocean. Tech., 13, 1152–1165, https://doi.org/10.1175/1520-0426(1996)013<1152:FCWMWD>2.0.CO;2, 1996.

Wendisch, M., Pöschl, U., Andreae, M. O., Machado, L. A. T., Albrecht, R., Schlager, H., Rosenfeld, D., Martin, S. T., Abdelmonem, A., Afchine, A., Araùjo, A., Artaxo, P., Aufmhoff, H., Barbosa, H. M. J., Borrmann, S., Braga, R., Buchholz, B., Cecchini, M. A., Costa, A., Curtius, J., Dollner, M., Dorf, M., Dreiling, V., Ebert, V., Ehrlich, A., Ewald, F., Fisch, G., Fix, A., Frank, F., Fütterer, D., Heckl, C., Heidelberg, F., Hüneke, T., Jäkel, E., Järvinen, E., Jurkat, T., Kanter, S., Kästner, U., Kenntner, M., Kesselmeier, J., Klimach, T., Knecht, M., Kohl, R., Kölling, T., Krämer, M., Krüger, M., Krisna, T. C., Lavric, J. V., Longo, K., Mahnke, C., Manzi, A. O., Mayer, B., Mertes, S., Minikin, A., Molleker, S., Münch, S., Nillius, B., Pfeilsticker, K., Pöhlker, C., Roiger, A., Rose, D., Rosenow, D., Sauer, D., Schnaiter, M., Schneider, J., Schulz, C., de Souza, R. A. F., Spanu, A., Stock, P., Vila, D., Voigt, C., Walser, A., Walter, D., Weigel, R., Weinzierl, B., Werner, F., Yamasoe, M. A., Ziereis, H., Zinner, T., and Zöger, M.: The ACRIDICON-CHUVA campaign: studying tropical deep convective clouds and precipitation over Amazonia using the new german research aircraft HALO, B. Am. Meteorol. Soc., 97, 1885–1908, https://doi.org/10.1175/BAMS-D-14-00255.1, 2016.

III

Earth Syst. Sci. Data, 14, 637–649, 2022
https://doi.org/10.5194/essd-14-637-2022

Open Access Earth System Science Data

An extensive data set for in situ microphysical characterization of low-level clouds in a Finnish sub-Arctic site

Konstantinos Matthaios Doulgeris[1], Heikki Lihavainen[1,3], Anti-Pekka Hyvärinen[1], Veli-Matti Kerminen[2], and David Brus[1]

[1]Atmospheric Composition Research, Finnish Meteorological Institute, Erik Palménin aukio 1, P.O. Box 503, 00100 Helsinki, Finland
[2]Institute for Atmospheric and Earth System Research/Physics, Faculty of Science, University of Helsinki, Helsinki, Finland
[3]Svalbard Integrated Arctic Earth Observing System (SIOS), SIOS Knowledge Centre, Svalbard Science Centre, P.O. Box 156, 9171 Longyearbyen, Norway

Correspondence: Konstantinos Matthaios Doulgeris (konstantinos.doulgeris@fmi.fi)

Received: 6 September 2021 – Discussion started: 13 September 2021
Revised: 29 December 2021 – Accepted: 6 January 2022 – Published: 11 February 2022

Abstract. Continuous, semi-long-term, ground-based in situ cloud measurements were conducted during eight Pallas Cloud Experiments (PaCEs) held in autumn between 2004 and 2019. Those campaigns were carried out in the Finnish sub-Arctic region at the Sammaltunturi station (67°58′24″ N, 24°06′58″ E; 560 m a.m.s.l.), the part of the Pallas Atmosphere–Ecosystem Supersite and Global Atmosphere Watch (GAW) program. Two cloud spectrometer ground setups and a weather station were installed on the roof of the station to measure in situ cloud properties and several meteorological variables. Thus, the obtained data sets include the size distribution of cloud droplets as a measured cloud parameter along with the air temperature, dew point temperature, humidity, pressure, horizontal wind speed and direction, (global solar) sun radiation, and visibility at the station. Additionally, the number concentration, effective diameter, median volume diameter, and liquid water content from each instrument were derived. The presented data sets provide a insight into microphysics of low-level clouds in sub-Arctic conditions over a wide range of temperatures (−25.8 to 8.8 °C). The data are available in the Finnish Meteorological Institute (FMI) open data repository for each campaign and each cloud spectrometer ground setup individually: https://doi.org/10.23728/FMI-B2SHARE.988739D21B824C709084E88ED6C6D54B (Doulgeris et al., 2021).

1 Introduction

Clouds are considered a major component of both the climate system and the hydrological cycle. Nevertheless, our level of understanding of the fundamental details of the cloud microphysical processes is still very limited (Boucher et al., 2013). To gain a deeper knowledge of the formation and development of the clouds, more in situ measurements are needed (Morrison et al., 2019). In addition, a correct representation of cloud microphysics in general circulation models for numerical weather and climate prediction is of great importance (Guichard and Couvrex, 2017; Morrison et al., 2020). Despite the fact that cloud processes can now be studied with much more confidence (Bony et al., 2015), representing the formation and evolution of cloud droplets and the effects of aerosols on clouds at various meteorological conditions remains a challenge (Grabowski et al., 2019). The number concentration and size distribution of cloud droplets are considered key parameters for a quantitative microphysical description of clouds (e.g., Rosenfeld and Ulbrich, 2003; Komppula et al., 2005; Lihavainen et al., 2008; Pruppacher and Klett, 2010; Chang et al., 2019) and are connected with the cloud

lifetime and radiative effects as well as precipitation (e.g., Albrecht, 1989; Devenish et al., 2012; McFarquhar et al., 2020).

Three general approaches were used in previous studies of cloud microphysical properties: in situ sampling through airborne measurements by aircraft (e.g., Heymsfield et al., 2011; Craig et al., 2014; Petäjä et al., 2016; Nguyen et al., 2021) and recently by unmanned aerial systems (UASs) (e.g., Girdwood et al., 2020; Brus et al., 2021; Harrison et al., 2021), in situ sampling by using laboratory cloud chambers (e.g., Möhler et al., 2003; Stratmann et al., 2004; Nichman et al., 2017; Doulgeris et al., 2018), and in situ ground-based measurements (e.g., Guyot et al., 2015; Lloyd et al., 2015; Lowenthal et al., 2019; Doulgeris et al., 2020). In situ airborne and ground measurements (Wandinger et al., 2018) using cloud spectrometers are considered fundamental as they offer instrumental access to individual hydrometeors within a sampling volume. Unfortunately, each of the aforementioned approaches has inherent limitations.

Data sets that have been obtained from measurements in sub-Arctic clouds are significant as cloud processes are of high value since cloud processes are considered an important component of climate change in the Arctic region (Wendisch et al., 2019). Pallas Cloud Experiments (PaCEs) took place in the Finnish sub-Arctic. The main objective during PaCE was to study low-level clouds and their microphysical properties in a background sub-Arctic environment. In this work, we present a unique data set of ground in situ cloud measurements along with several meteorological variables collected at the Sammaltunturi station in eight autumn campaigns conducted between 2004 and 2019. This data set can be used in studies of cloud microphysics, climate change in the sub-Arctic, and performance evaluation and improvement of existing models, in particular at higher altitudes. In the next section, we provide a description of the sampling location, instrumentation, and the measurement methodology we used for sampling, data processing, and quality control.

2 Methods

2.1 Measurement site and PaCE campaigns overview

The Sammaltunturi station (67°58′24″ N, 24°06′58″ E) is hosted by the Finnish Meteorological Institute (FMI) and is located on a top of an arctic fell (560 m a.m.s.l.) in the Finnish sub-Arctic region inside the Pallas–Yllästunturi National Park (Fig. 1). The Pallas area is located around 180 km above the Arctic circle, and it has no significant local or regional air pollution sources. Thus, the Sammaltunturi station provides an excellent location for the monitoring of background air composition in northern Europe. The station is about 100 m above the tree line, and the vegetation around it consists mainly of low vascular plants, mosses, and lichen. There is a long history of atmospheric data collection in the area (see Lohila et al., 2015). Monitoring activities of atmospheric composition at Sammaltunturi started in 1991 in a building that originally served the Finnish Broadcasting Company. The new station (102 m^2) opened in July 2001. Since 1994, Sammaltunturi has been established as a node of the Pallas–Sodankylä supersite that contributes to the GAW program of the World Meteorological Organization. The site was described in detail in Hatakka et al. (2003). The main research measurements focus on greenhouse gas concentration, climate effects of atmospheric aerosols, aerosol cloud interaction, and air quality (e.g., Komppula et al., 2005; Lihavainen et al., 2008; Asmi et al., 2011; Backman et al., 2017; Doulgeris et al., 2020). The predominant origin of air masses arriving at Sammaltunturi is from the Arctic (Asmi et al., 2011).

The main motivation to perform in situ cloud measurements at the Sammaltunturi was that the station was occasionally immersed in a cloud. Based on analytical data the most suitable time of the year for in situ cloud measurements was autumn when the horizontal visibility drops below 1 km around 40 % of the time (Hatakka et al., 2003). Once the preferable time of the year was identified, we started to conduct ground-based in situ measurements and study cloud formation. The Pallas Cloud Experiments were, usually, 6–8 weeks long and lasted approximately from the beginning of September until the end of November, occasionally extended to the beginning of December. The first attempt at measuring in situ cloud properties was made in 2004 using the forward-scattering spectrometer probe (FSSP-100) ground setup that was the only available cloud spectrometer at that time. The next campaigns, in 2005 and 2009, were done using the same instrument setup (Lihavainen et al., 2008). Later, in 2011 the cloud, aerosol, and precipitation spectrometer (CAPS) ground setup was added. In January and February 2012, it was tested for the first time for two short periods during winter at the Sammaltunturi site. In 2012, 2013, and 2015 both instruments were installed and used during PaCE (Doulgeris et al., 2020). In 2017 and 2019, only CAPS was used (Girdwood et al., 2020). An overview of each year's campaign duration and the cloud spectrometer ground setups' availability is presented in Fig. 2. Instruments that were used for measuring the meteorological variables and the solar radiation were operating continuously during all PaCE years. The instrumentation used during PaCE campaigns is described in detail in the following section.

2.2 Instrumentation

In order to monitor meteorological variables, the station was equipped with an automatic weather station (Milos 500, Vaisala Inc.). A weather sensor (model FD12P, Vaisala Inc.) was used for measuring the horizontal visibility, the Vaisala HUMICAP was used for measuring the relative humidity, BAROCAP sensors were used for measuring the barometric pressure, and PT100 sensors were used to measure temperature at 570 m. Global radiation and photosynthetically active radiation were measured with a pyranometer and a photo-

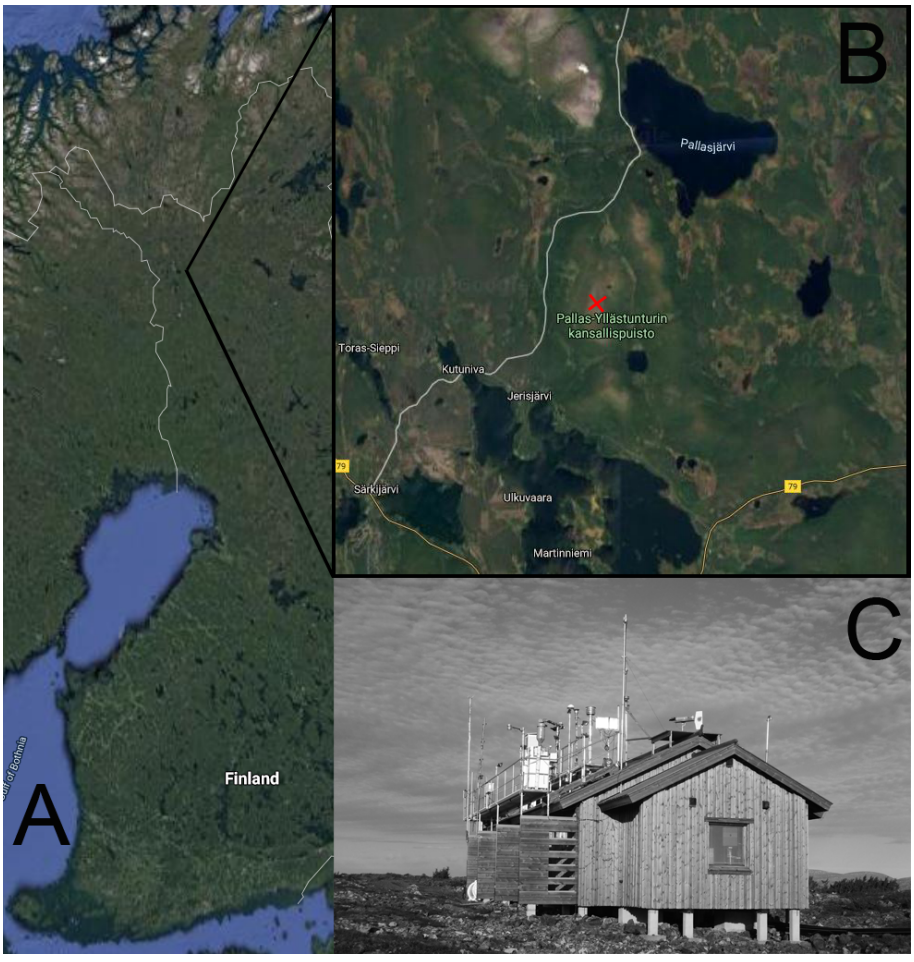

Figure 1. **(a)** Map of Finland showing the location of the field station, and **(b)** map of the wider Pallas area showing the location of the Sammaltunturi station (red cross) (© Google Maps). **(c)** The Sammaltunturi measuring station during PaCE.

voltaic detector, respectively. Additionally, the wind speed was measured with a heated cup and the wind direction with a heated wind vane. All the above meteorological variables were saved as 1 min averages. A detailed description of the weather sensors can be found in Hatakka et al. (2003).

In order to conduct in situ cloud ground-based measurements, we deployed two instruments. The cloud, aerosol, and precipitation spectrometer (CAPS) and the forward-scattering spectrometer probe (FSSP-100; Droplet Measurement Technologies (DMT), Boulder, CO, USA) (Fig. 3). The FSSP (model SPP-100, DMT) was originally manufactured by Particle Measuring Systems (PMS Inc., Boulder CO, USA). Both instruments were originally developed for airborne measurements but modified as ground setups by the manufacturer (DMT, USA). They were installed on the rooftop of the Sammaltunturi station. The CAPS was fixed with a heading always to the main wind direction of the station southwest, $\sim 225°$, while the FSSP-100 was installed on a rotating platform to continuously face the wind. The CAPS had a total height of 0.6 m above the roof where it was installed and a height of 4.5 m from the ground. FSSP had a total height of 0.6 m above the roof where it was installed and a height of 5.5 m from the ground. The two setups had a horizontal distance of ~ 10 m and vertical distance of ~ 1 m between them. From 2004 until 2012 a flow laminator was used inside the FSSP inlet (Lihavainen et al., 2008). However, the flow laminator was often blocked by freezing or supercooled cloud droplets at sub-zero temperatures, and for this reason it was cleaned every hour if occurrence of subcooled water was detected. The laminator blockage was evident both during everyday instrument inspection and from the raw data. Only data cleaned of this artifact were used in the FSSP data set. However, even without placing the laminator, the Reynolds number indicated that the flow inside the inlet was still laminar. As a result, in 2012 we decided that the laminator would not be used in the FSSP setup anymore. Thus, the number of data after 2012 were more extensive, and the number of cases when the FSSP would have been blocked was significantly reduced. A detailed description of both ground setups and the methodology we used for obtain-

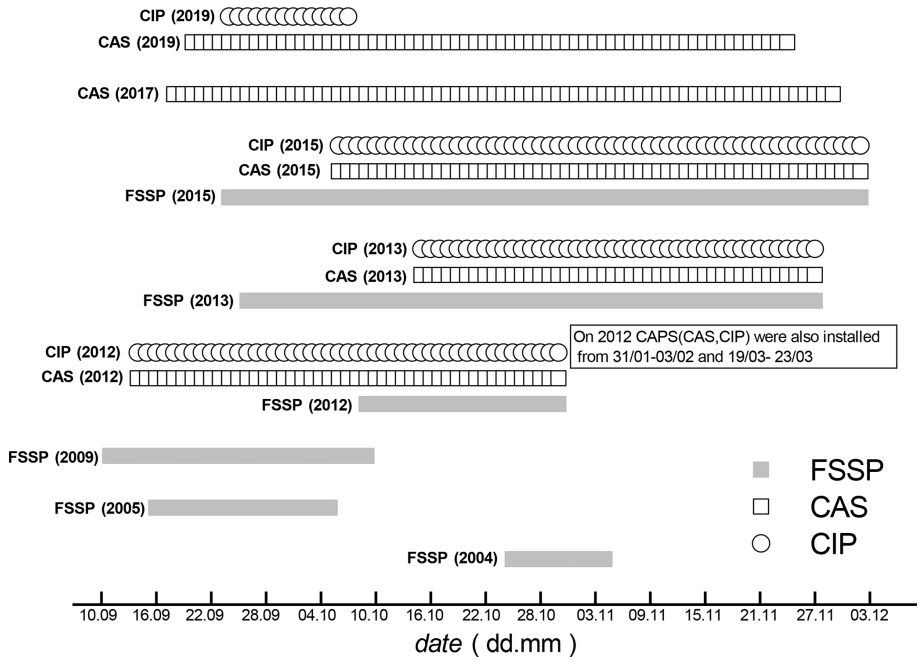

Figure 2. Cloud spectrometer ground setups' availability during PaCE is presented for each year.

ing the ground-based cloud microphysical properties with in situ method was documented in Doulgeris et al. (2020). Only a short overview is given here.

The CAPS has been widely used in airborne measurements of the microphysical properties in clouds (e.g., Baumgardner et al., 2001, 2011; Droplet Measurement Technologies Manual, 2011; Lachlan-Cope et al., 2016). The CAPS probe includes three instruments: the cloud and aerosol spectrometer (CAS) which measures smaller particles, the cloud imaging probe (CIP), and the hot-wire liquid water content (LWC_{hw}) sensor. For the ground setup we deployed, the hot-wire LWC faced difficulties operating in such extreme conditions; after operating in supercooled liquid clouds (even for a short time) the sensor was accreting ice. In addition, the lifetime of the sensor is limited and significantly shorter than the duration of the campaign. The FSSP-100 was widely used for measuring droplet size distribution (e.g., Brenguier, 1989; Lihavainen et al., 2008; Lloyd et al., 2015; Doulgeris et al., 2020). CAS and FSSP-100 derive the size of the particle from the intensity of the scattered light, using the Mie theory (Mie, 1908). Furthermore, backscatter optics measure light intensity in the 168 to 176° range. This allows the determination of the real component of a particle's refractive index for spherical particles. The CIP is a single particle optical array probe. Its design is based on optical measurement techniques whereby single particles pass through a collimated laser beam and their shadow is projected onto a linear array of 64 photodetectors. The count of the particle is dependent on the change in the light intensity of each diode.

All the instruments were calibrated before and after each campaign. Until 2011, we relied on the manufacturer calibration that was done at DMT. After 2011, we also started to perform calibration at the FMI, on top of manufacturer calibration, to ensure the quality of the collected data. For the calibration of the CAS and FSSP-100, glass beads in the diameter size range 2–40 µm and polystyrene latex sphere (PSL) standards in the diameter size range 0.74–2 µm were used. Cloud spectrometers (in our case CAS and FSSP-100) are calibrated for size measurements but not for number concentration measurements. The instruments faced extreme conditions during the whole campaign, in terms of frequent changes in wind direction, wind speed and sub-zero temperatures. Despite the calibration procedures we should always keep in mind that extreme meteorological conditions could possibly lead to unexpected performance. To calibrate the CIP, a spinning glass disk with opaque dots of known size was used.

The CAPS ground setup included a high-flow pump (Baldor, Reliance, USA) which worked as an aspiration system. The aspiration system was made and provided by the manufacturer (DMT). A custom aspiration system with a high-flow ventilator was also made by the manufacturer (PMS) and employed through FSSP-100 inlet to ensure constant flow through it. A digital thermo-anemometer (model 471, Dwyer Inc.) was used in each campaign for checks of daily cloud spectrometers' air speed. The FSSP air speed inside the inlet was calculated from the measured air speed in front of the inlet, except in 2004 and 2005 when the air speed was calculated with measured volume flow rate through the in-

Figure 3. CAPS **(a)** and FSSP-100 **(b)** ground setups as installed on the roof of Sammaltunturi station.

let. A necking inside the inlet led the flow from inner diameter 3.8 to 2.0 cm. Both spectrometers were equipped with anti-ice systems as they were modified by the manufacturers (DMT for CAPS and PMS for FSSP-100) for ground-based use. Despite the existing anti-ice features, due to the subzero temperatures that they were facing, snow or ice could accrete and affect the air speed inside the probe inlets. For this reason, to ensure the proper operation of the instruments, they were inspected and cleaned twice per day, every morning and evening (approximately every 12 h).

The ground-based in situ cloud measurements provided the cloud and precipitation size distribution. The PADS 2.5.6 software that was used for the data acquisition of CAPS measurements (Droplet Measurement Technologies Manual, 2009) provided the number concentration (N_c, cm^{-3}), liquid water content (LWC, $g\,cm^{-3}$), median volume diameter (MVD, µm), and effective diameter (ED, µm). For the FSSP-100, N_c, LWC, MVD, and ED were also derived using the same equations (Doulgeris et al., 2020), since we used an older software for data acquisition (PACS 2.2, DMT).

The major sources of uncertainties of the cloud spectrometers can be coincidence, dead-time losses, and changing velocity ratio (Guyot et al., 2015). The uncertainty of estimation of sizing at the cloud spectrometers was 20 % and that of the number concentration was 16 % (Baumgardner, 1983; Dye and Baumgardner, 1984; Baumgardner et al., 2017). According to Lance (2012), it was observed that for CAS at ambient droplet concentrations of 500 cm^{-3} there was 27 % undercounting and a 20 %–30 % oversizing bias. In our case, during PaCE campaigns the droplet number concentration values we monitored were in the majority of cases less than 300 cm^{-3}. These number concentration values lead us not to take coincidence, dead-time losses, and velocity acceptance ratio (VAR) uncertainties into consideration in this analysis. LWC has a significant uncertainty of 40 % (Droplet Measurement Technologies Manual, 2009). The FSSP-derived ED and LWC had an uncertainty of 3 µm and 30 % in mixed-phase clouds (Febvre et al., 2012). An overview of the instrumentation and their operational characteristics we used for cloud measurements are summarized in Table 1.

3 Overview of data set and quality control description

The current data set contains only in-cloud measurements when the station was immersed in a cloud. Data from each cloud probe and the weather station were quality controlled and unified in a common format for release and further analysis. The presence of a cloud at the station was identified with three different factors. First, we checked the droplet size distribution measured in both of the cloud spectrometers. This was the main parameter to consider that the station was inside a cloud. Then, to confirm this assumption, we cross-checked the droplets counts with two meteorological variables – the relative humidity at the measurement site which was expected to be ~ 100 % and the horizontal visibility which should be less than 1 km, when the Sammaltunturi station is in the cloud. In the event that one of the factors was not fulfilled, a final inspection was done visually using pictures recorded by an automatic weather camera installed on the roof of the station.

During PaCE 2004 and 2005 the sampling time of the FSSP-100 was 15 s. During PaCE 2009 the instrument was set to sample at 10 s. From 2009 until 2019 the sampling time was set to sample each 1 s (1 Hz) for both instruments. The PT100 sensor, Vaisala HUMICAP and BAROCAP sensors, the pyranometer, and the heated cup and wind vane were also set to sample to 1 s. The FD12P Vaisala weather sensor sampling time was 15 s. For every year, 1 min averages were calculated for each cloud spectrometer and each meteorological variable. As a result, we obtained the cloud droplet size distribution and several meteorological variables for each minute and as derived parameters the N_c (cm^{-3}), LWC ($g\,cm^{-3}$), MVD (µm), and ED (µm). All data sets were converted to NetCDF format. All times in this work are given in UTC time. Our data set includes a separate NetCDF and CVS file for each cloud spectrometer and for each year under the file name PACE.yyyy.cloud_spectrometer.nc and PACE.yyyy.cloud_spectrometer.cvs (example names). For every file, the sampling area (mm^2) and the probe air speed (ms^{-1}) that were used to derive each parameter are provided. In addition, it includes the cleaned timeline data set of the fol-

https://doi.org/10.5194/essd-14-637-2022

Table 1. An overview of instrumentation and their operational characteristics provided by manufacturer.

Instrument	Operating range	Number of bins	Sampling frequency	Air speed range	Accuracy	Uncertainties
Cloud instruments						
CAS, DMT	0.51 to 50 µm	10, 20, 30, or 40	0.05 to 40 Hz	10–200 ms^{-1}	upper $N_c > 1000\,cm^{-3}$ after corrections for coincidence that are about 25 % at 800 particles cm^{-3} and 30 % at 1000 particles cm^{-3} sizing accuracy: 20 %	ambient N_c of 500 cm^{-3}: 27 % undercounting and 20 %–30 % oversizing bias Lance (2012) LWC: 40 % (DMT Manual)
CIP, DMT	12.5 µm to 1.55 mm	62	0.05 to 40 Hz	10–300 ms^{-1}	upper N_c range up to 500 particles cm^{-3} for a CIP with standard tips and arm width sizing accuracy: 1 µm	digitization uncertainty of approximately ±1 size resolution that depends upon where the particle passes across the array Baumgardner et al. (2017)
FSSP-100, PMS	0.5 to 47 µm	15, 30 or 40	0.05 to 40 Hz		N_c accuracy: 16 % sizing accuracy: ±3 µm LWC accuracy: 30 %–50 % Baumgardner (1983); Baumgardner et al. (2017)	derived ED: 3 µm derived LWC: 30 % Febvre et al. (2012)
Meteorological instruments						
	Range	Resolution	Sensitivity	Accuracy		
PT100 sensor, Vaisala	−70 to +180 (°C)	0.01 (° C)		±0.1 (°C)		
HUMICAP sensor, Vaisala	0–100 (%) RH	<0.01 (%) RH		±0.8 (%) RH		
BAROCAP sensor, Vaisala	500–1000 (hPa)	0.01 (hPa)		±0.15 (hPa)		
heated cup and wind vane, Vaisala	0.4–75 (ms^{-1}) 0 – 360°	0.1 (ms^{-1}) 1°		±0.17 (ms^{-1}) ±3°		
Pyranometer, Vaisala	305–2000 ($W\,m^{-1}$)		9–15 ($\mu V\,W\,m^{-2}$)	$< \pm 20\,W\,m^{-2}$ at 1000 $W\,m^{-2}$		
FD12P, Vaisala	10–50 000 (m)			±10 %, 10–10 000 m ±20 %, 10 000–50 000 m		

lowing cloud properties and meteorological variables: year (YYYY), day (DD), month (MM), hour (HH), min (MN), size bin lower limit, size bin higher limit, number concentration (cm^{-3}), liquid water content ($g\,cm^{-3}$), effective diameter (µm), median volume diameter (µm), the calculated MSD (cm^{-3}) values in each bin, temperature at 570 m (°C), dew point (°C), humidity at 570 m (%), pressure (hPa), wind speed ($m\,s^{-1}$), horizontal wind direction (degrees), global solar radiation ($W\,m^{-2}$), photosynthetically active radiation ($\mu mol\,m^{-2}\,s^{-1}$), and the horizontal visibility (m). The derived cloud parameters – number concentration (cm^{-3}), liquid water content ($g\,cm^{-3}$), effective diameter (µm), and median volume diameter (µm) – were not included in the CIP files. The number of cloud droplets per minute in CIP size range leads to statistically biased values, and for this reason we decided to exclude them. The variables, naming abbreviations, and units are summarized in Table 2.

The CAS contains 30 size bins with a forward-scattering upper bin size of 0.61, 0.68, 0.75, 0.82, 0.89, 0.96, 1.03, 1.1, 1.17, 1.25, 1.5, 2, 2.5, 3, 3.5, 4, 5, 6.5, 7.2, 7.9, 10.2, 12.5, 15, 20, 25, 30, 35, 40, 45, and 50 µm, and the CIP contains 62 size bins with a bin size of 15, 30, 45, 60, 75, 90, 105, 120, 135, 150, 165, 180, 195, 210, 225, 240, 255, 270, 285, 300, 315, 330, 345, 360, 375, 390, 405, 420, 435, 450, 465, 480, 495, 510, 525, 540, 555, 570, 585, 600, 615, 630, 645, 660, 675, 690, 705, 720, 735, 750, 765, 780, 795, 810, 825, 840, 855, 870, 885, 900, 915, and 930 µm. For the FSSP-100 two different bin size ranges were used. During 2004 and 2005 the instrument was set up to use 30 size bins with a forward-scattering upper bin size of 3.0, 4.5, 6.0, 7.5, 9.0, 10.5, 12.0, 13.5, 15.0, 16.5, 18.0, 19.5, 21.0, 22.5, 24.0, 25.5, 27, 28.5, 30.0, 31.5, 33.0, 34.5, 36.0, 37.5, 39.0, 40.5, 42.0, 43.5, 45.0, and 47.0. From 2009 until 2015, the FSSP was set up to use 40 size bins with a forward-scattering upper bin size of 1.2, 2.4, 3.5, 4.7, 5.9, 7.1, 8.2, 9.4, 10.6, 11.8, 12.9, 14.1, 15.3, 16.5, 17.6, 18.8, 20, 21.2, 22.3, 23.5, 24.7, 25.9, 27, 28.2, 29.4, 30.6, 31.7, 32.9, 34.1, 35.3, 36.4, 37.6, 38.8, 40, 41.1, 42.3, 43.5, 44.7, 45.8, and 47 µm.

Measurements of each year were inspected to ensure a good quality of the data set. First, the raw data set was checked in order to eliminate and exclude from further analysis cases in which one of the cloud probes was partially or fully blocked. Partially or fully blocked probes were also visible in raw data. To detect blocked probes, N_c was carefully investigated for the whole data set. When a sudden decrease just before a sudden increase in droplet number concentration was occurring, we had a clear sign of probe inlet freezing. This behavior was observed due to the opening of the probe inlet becoming smaller (from the accumulation of snow/ice) and resulted in a raised probe air speed. During data evaluation we considered that the probe air speed was constant. This abnormality in the N_c was happening due to the underestimation of the probe air speed. Then, we applied the suggested corrections due to limitations (Doulgeris et al., 2020) for the data analysis of the CAS and FSSP-100 ground setups. Doulgeris et al. (2020) demonstrated that the CAPS (that was fixed to one direction) showed significant sampling losses when it was not facing the wind direction since it was not sampling isokinetically. For this reason, the data that were obtained in the wind iso-axial conditions were considered to have the best quality. Thus, regarding CAPS, only the measurements when the instrument was facing the wind direction were included. The FSSP-100 ground setup was always directed against the wind direction, and as a result we provided measurements from all wind sectors. Missing data points were marked as −9999.9.

As it is shown in Fig. 4, the observation hours after PaCE 2013 when the campaigns had longer duration are significantly higher. The number of data in these years is excessive, serving as an important source of information for Arctic studies. An overview of meteorological variables is presented for each campaign when the FSSP-100 and CAPS ground setups were operational. In Fig. 5, a statistical description of the temperature at 570 m a.m.s.l. for each campaign is illustrated. Each PaCE year the temperature trends and ranges were similar (around −10.0 to 8 °C). In Fig. 6, we show the percentage of the data set for each year in which the global solar radiation was higher than 0. It was used to estimate the number of data collected in each campaign in daylight. In addition, an overview of the microphysical derived cloud properties data from each campaign is presented. Thus, in Figs. 7, 8, and 9, the number concentration, the effective diameter, the medium volume diameter, and the liquid water content are presented for each campaign and for the FSSP-100 and CAS ground setups, respectively. Number concentration averaged values were similar for every year of the measurements and reach scales around $100\,cm^{-3}$. However, there were some cloud cases during each campaign that number concentration had values around $300\,cm^{-3}$. The averaged ED and MVD values were ranging approximately from 10 to 20 µm. The liquid water content was less than $0.2\,g\,cm^{-3}$ in most cases.

4 Code availability

Software developed to process and display the data from the cloud ground-based spectrometers is not publicly available and leverages licensed data analysis software (MATLAB). This software contains intellectual property that is not meant for public dissemination.

5 Data availability

Each described data set was collected by Finnish Meteorological Institute during PaCE campaigns and was published in the described form at the FMI open data repository. All data sets have undergone thorough quality control, and false readings were eliminated. Data sets can be all found at https://doi.org/10.23728/FMI-B2SHARE.988739D21B824C709084E88ED6C6D54B (Doulgeris et

Table 2. Cloud properties and meteorological variables along with abbreviations and units as they are included in each data set.

Variable name	Abbreviations	Units	Comments
Cloud properties			
Number concentration	N_c	cm^{-3}	derived parameter
Liquid water content	LWC	$g\,cm^{-3}$	derived parameter
Effective diameter	ED	µm	derived parameter
Median volume diameter	MVD	µm	derived parameter
Size distribution	MSD	$cm^{-3}\,\mu m^{-1}$	calculated from min averages counts per bin
Meteorological variables			
Temperature at 570 m	T	°C	PT100 sensor
Dew point temperature	T_{DP}	°C	
Relative humidity at 570 m	RH	%	Vaisala HUMICAP sensor
Pressure	P	hPa	Vaisala BAROCAP sensor
Wind speed	W_s	ms^{-1}	measured with a heated cup
Wind direction	W_{dir}	°	measured with a heated wind vane
Global solar radiation	S_{rad}	$W\,m^{-2}$	Pyranometer
Photosynthetically active radiation	PAR	$\mu mol\,m^{-2}\,s^{-1}$	Photovoltaic detector
Horizontal visibility	V	m	FD12P Vaisala weather station

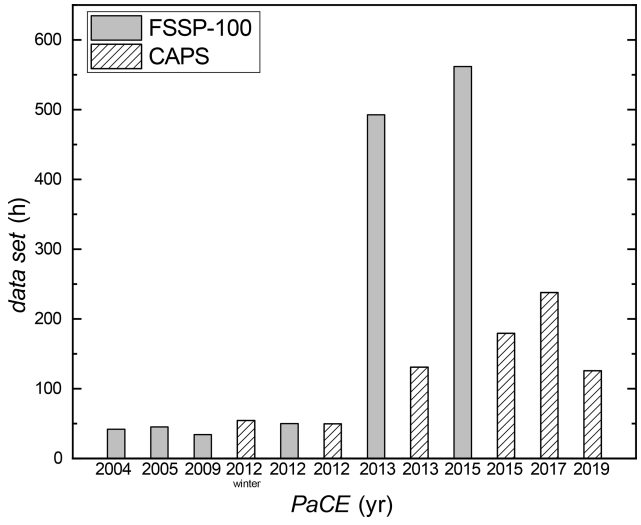

Figure 4. Hours of observation data collected for each PaCE campaign when the FSSP-100 and CAPS ground setups were operational.

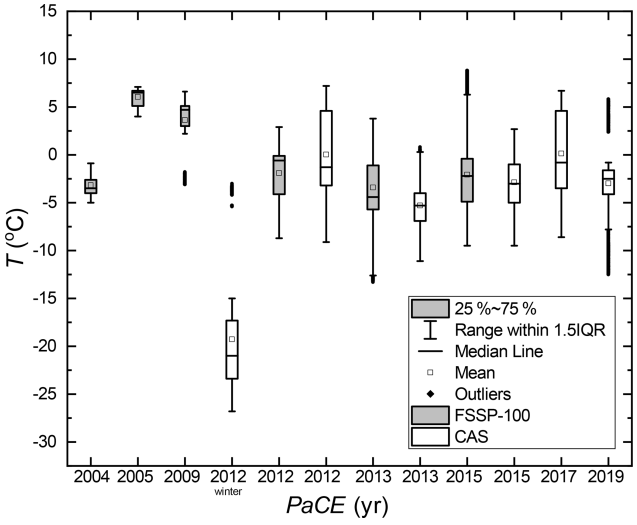

Figure 5. Statistical description of the temperature at 570 m a.m.s.l. for each PaCE campaign when the FSSP-100 and CAS ground setups were operational.

al., 2021). When the CIP was operational, we also collected the CIP images. However, we did not include the raw images in the data set for two reasons. First, they were in binary format. To read them, we used a proprietary image analysis software that was provided by DMT. Secondly, the upper limit of the open data repository is 10 GB, which was not enough to include the CIP raw images which were approximately 0.5 GB per case per day. However, RAW CIP images could be provided by the authors upon request.

6 Summary

In this study we produced and summarized data sets obtained from two cloud ground-based spectrometers (CAPS and FSSP-100 ground setups) owned by the FMI during 8 years of PaCE campaigns conducted in autumn from 2004 until 2019 along with several meteorological variables. PaCE campaigns took place in the Finnish sub-Arctic region in a clear environment in temperatures that were usually below zero. In Sect. 2, we describe the measuring site where PaCE campaigns took place and the cloud ground spectrometers

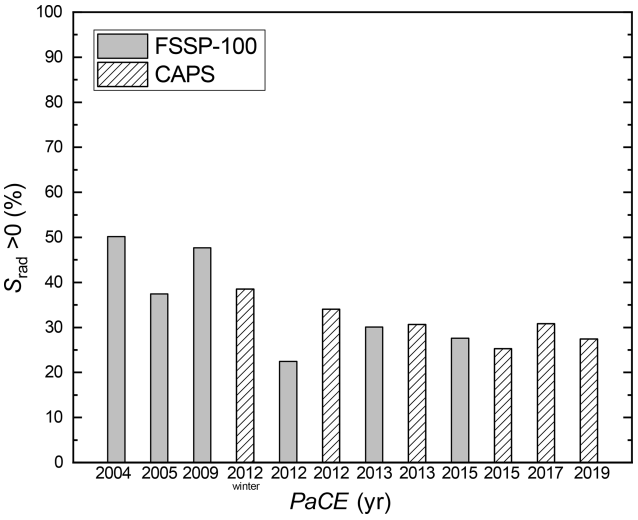

Figure 6. The percentage of the global solar radiation that was higher than 0 during each campaign when the FSSP-100 and CAS ground setups were operational.

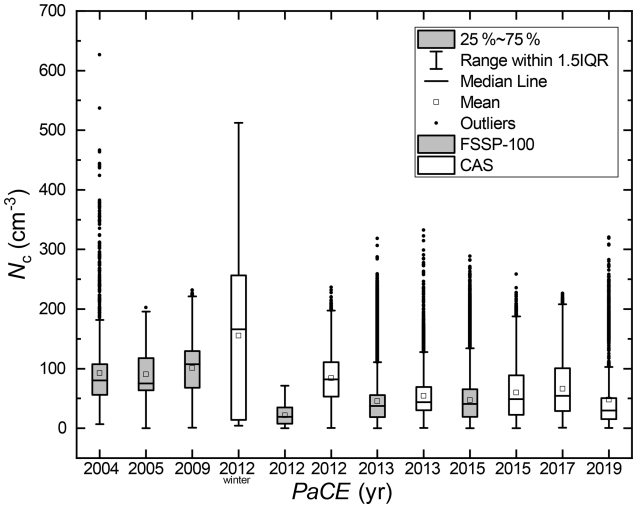

Figure 7. Statistical description of N_c for each PACE campaign during which the FSSP-100 and CAS ground setups were operational.

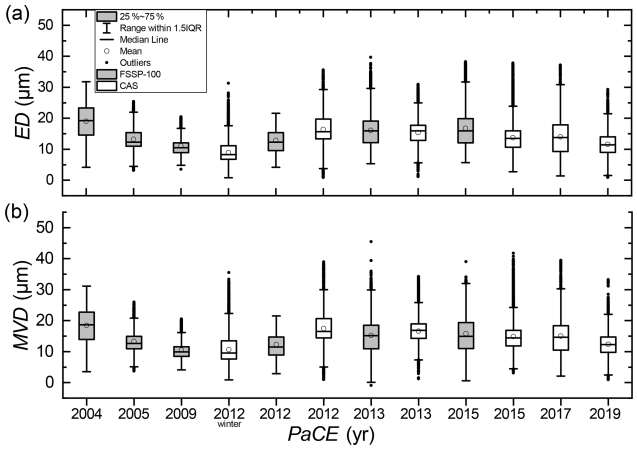

Figure 8. Statistical description of ED **(a)** and MVD **(b)** for each PACE campaign during which the FSSP-100 and CAS ground setups were operational.

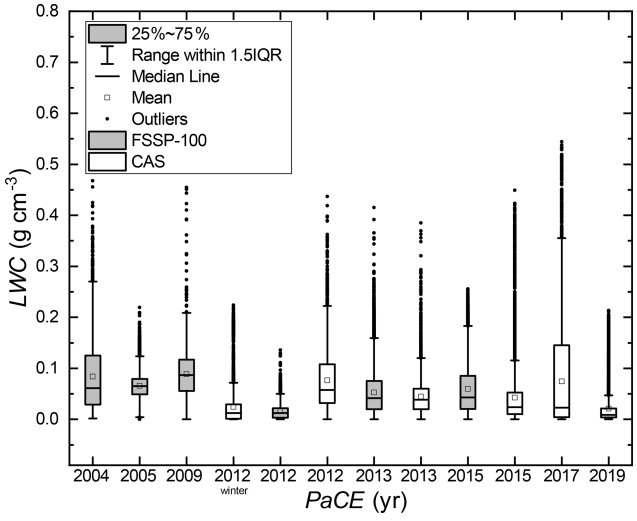

Figure 9. Statistical description of LWC for each PaCE campaign when the FSSP-100 and CAS ground setups were operational.

setups that were used to obtain the cloud data along with the instrumentation that was used to monitor the weather conditions. In Sect. 3 an overview of the data set is presented.

These observations gathered in sub-Arctic conditions are a unique source of in situ cloud measurements, which can contribute to the understanding of the cloud dynamics and formation in a sub-Arctic environment in different meteorological conditions. Such semi-long observations are difficult to obtain in similar environments due to current lack of instrumentation which would allow continuous unattended operation at temperatures below 0 °C. Cloud droplet spectrometers with surface installation has been identified as a potential method for continuous cloud in situ measurements (Wandinger et al., 2018). Thus, due to the increased demand for long-term continuous ground-based in situ cloud measurements, we provide a data set of in situ cloud measurements in a harsh sub-Arctic environment. Each data set includes a combination of cloud microphysical properties along with several meteorological variables. Even though the data set includes measurements from eight campaigns, we would propose a case-by-case cloud investigation. Due to the inhomogeneity of the presented cloud cases, it is challenging to retrieve any trend that can be unambiguously connected to changes in the atmosphere. Also, the quality of data set may differ for each campaign due to the different number of observations per year and operators' experience running the ground-based spectrometers through the years. In addition,

each cloud case could be of different mass origin. We therefore discourage from any trend analysis based only on the presented data set. At least thorough back-trajectory analysis and subsequent segregation of data set according to air mass origin is recommended. However, this was not an objective of this paper. The data set in current form provides a helpful contribution to cloud microphysics processes on shorter timescales. Microphysical processes can strongly influence cloud–climate feedbacks in global climate models (Bodas-Salcedo et al., 2019). Furthermore, it can be used as complementary in model development. Representation of cloud microphysics is considered significant for large eddy simulation (LES) models (Morrison et al., 2020). There is a need for in situ cloud data sets due to two significant problems that the modeling community is facing: the representation of the population of the cloud and precipitation particles and the uncertainties due to fundamental gaps in knowledge of cloud physics (Morrison et al., 2020). In this data set, the cloud size distribution was monitored in different stages of its evolution.

Appendix A: Abbreviations

PaCE	Pallas Cloud Experiment
GAW	Global Atmosphere Watch
UAS	Unmanned aerial system
FMI	Finnish Meteorological Institute
CAPS	Cloud, aerosol, and precipitation spectrometer
CAS	Cloud and aerosol spectrometer
CIP	Cloud imaging probe
LWC_{hw}	Hot-wire liquid water content sensor
FSSP-100	Forward-scattering spectrometer probe
DMT	Droplet Measurement Technologies
PMS	Particle Measuring Systems
PSL	Polystyrene latex sphere
N_c	Number concentration
LWC	Liquid water content
ED	Effective diameter
MVD	Median volume diameter
T	Temperature at 570 m a.m.s.l.
T_{DP}	Dew point temperature
RH	Relative humidity at 570 m a.m.s.l.
P	Pressure
W_s	Wind speed
W_{dir}	Wind direction
S_{rad}	Global solar radiation
PAR	Photosynthetically active radiation
V	Horizontal visibility

Author contributions. KMD wrote the paper with contributions from all co-authors. HL planned and coordinated PaCE 2004, 2005, and 2009. HL and DB planned and coordinated PaCE 2012 and 2013. KMD and DB planned and coordinated PaCE 2015, 2017, and 2019. KMD and DB processed, analyzed, and quality controlled the data set. VMK and APH reviewed and edited the manuscript.

Competing interests. The contact author has declared that neither they nor their co-authors have any competing interests.

Disclaimer. Publisher's note: Copernicus Publications remains neutral with regard to jurisdictional claims in published maps and institutional affiliations.

Acknowledgements. This work was supported by the Koneen Säätiö (grant no. 46-6817), NordForsk (grant no. 26060), the Academy of Finland (grant no. 269095), the Academy of Finland Center of Excellence program (grant no. 307331), Academy of Finland Flagship funding (grant no. 337552), and the Natural Environment Research Council (NERC, grant no. NE-L011514-1). This project has received funding from the European Union Seventh Framework Programme (BACCHUS) (grant no. 603445)) and the Horizon 2020 (H2020) research and innovation program (ACTRIS-2, the European Research Infrastructure for the observation of Aerosol, Clouds, and Trace gases) (grant agreement no. 654109).

Financial support. This research has been supported by the Koneen Säätiö (grant no. 46-6817), NordForsk (grant no. 26026), the Academy of Finland Center of Excellence program (grant nos. 269095 and 307331), Academy of Finland Flagship funding (grant no. 337552), Horizon 2020 (ACTRIS-2, grant no. 654109), the European Union Seventh Framework Programme (BACCHUS (grant no. 603445)), and the Natural Environment Research Council (grant no. NE-L011514-1).

Review statement. This paper was edited by Nellie Elguindi and reviewed by two anonymous referees.

References

Albrecht, B. A.: Aerosols, cloud microphysics, and fractional cloudiness, Science, 245, 1227–1230, 1989.

Asmi, E., Kivekäs, N., Kerminen, V.-M., Komppula, M., Hyvärinen, A.-P., Hatakka, J., Viisanen, Y., and Lihavainen, H.: Secondary new particle formation in Northern Finland Pallas site between the years 2000 and 2010, Atmos. Chem. Phys., 11, 12959–12972, https://doi.org/10.5194/acp-11-12959-2011, 2011.

Backman, J., Schmeisser, L., Virkkula, A., Ogren, J. A., Asmi, E., Starkweather, S., Sharma, S., Eleftheriadis, K., Uttal, T., Jefferson, A., Bergin, M., Makshtas, A., Tunved, P., and Fiebig, M.: On Aethalometer measurement uncertainties and an instrument correction factor for the Arctic, Atmos. Meas. Tech., 10, 5039–5062, https://doi.org/10.5194/amt-10-5039-2017, 2017.

Baumgardner, D.: An analysis and comparison of five water droplet measuring instruments, J. Appl. Meteorol., 22, 891–910, https://doi.org/10.1175/1520-0450(1983)022<0891:AAACOF>2.0.CO;2, 1983.

Baumgardner, D., Jonsson, H., Dawson, W., O'Connor D., and Newton R.: The cloud, aerosol and precipitation spectrometer (CAPS): A new instrument for cloud investigations, Atmos. Res.,

59–60, 251–264, https://doi.org/10.1016/S0169-8095(01)00119-3, 2001.

Baumgardner, D., Brenguier, J., Bucholtz, A., Coe, H., DeMott, P., Garrett, T., Gayet, J., Hermann, M., Heymsfield, A., Korolev, A., Kramer, M., Petzold, A., Strapp, W., Pilewskie, P., Taylor, J., Twohy, C., Wendisch, M., Bachalo, W., and Chuang, P.: Airborne instruments to measure atmospheric aerosol particles, clouds and radiation: A cook's tour of mature and emerging technology, Atmos. Res., 102, 10–29, https://doi.org/10.1016/j.atmosres.2011.06.021, 2011.

Baumgardner, D., Abel, S. J., Axisa, D., Cotton, R., Crosier, J., Field, P., Gurganus, C., Heymsfield, A., Korolev, A., Krämer, M., Lawson, P., McFarquhar, G., Ulanowski, Z., and Um, J.: Cloud Ice Properties: In Situ Measurement Challenges, Meteor. Mon., 58, 9.1–9.23, https://doi.org/10.1175/AMSMONOGRAPHS-D-16-0011.1, 2017.

Bodas-Salcedo, A., Mulcahy, J. P., Andrews, T., Williams, K. D., Ringer, M. A., Field, P. R., and Elsaesser, G. S.: Strong dependence of atmospheric feedbacks on mixed-phase microhysics and aerosol-cloud interactions, J. Adv. Model. Earth Sy., 11, 1735–1758, https://doi.org/10.1029/2019MS001688, 2019.

Bony, S., Stevens, B., Frierson, D., Jakob, C., Kageyama, M., Pincus, R., Shepherd, T. G., Sherwood, S. C., Siebesma, A. P., Sobel, A. H., Watanabe, M., and Webb, M. J.: Clouds, circulation and climate sensitivity, Nat. Geosci., 8, 261–268, https://doi.org/10.1038/ngeo2398, 2015.

Boucher, O., Randall, D., Artaxo, P., Bretherton, C., Feingold, G., Forster, P., Kerminen, V.-M., Kondo, Y., Liao, H., Lohmann, U., Rasch, P., Satheesh, S. K., Sherwood, S., Stevens, B., and Zhang, X. Y.: Clouds and aerosols, in: Climate Change 2013: The Physical Science Basis. Contribution of Working Group I to the Fifth Assessment Report of the Intergovernmental Panel on Climate Change, edited by: Stocker, T. F., Qin, D., Plattner, G.-K., Tignor, M., Allen, S. K., Doschung, J., Nauels, A., Xia, Y., Bex, V., and Midgley, P. M., Cambridge University Press, 571–657, https://doi.org/10.1017/CBO9781107415324.016, 2013.

Brenguier, J. L.: Coincidence and Dead-Time Corrections for Particles Counters. Part II: High Concentration Measurements with an FSSP, J. Atmos. Ocean. Tech., 6, 585–598, https://doi.org/10.1175/1520-0426(1989)006<0585:CADTCF>2.0.CO;2, 1989.

Brus, D., Gustafsson, J., Vakkari, V., Kemppinen, O., de Boer, G., and Hirsikko, A.: Measurement report: Properties of aerosol and gases in the vertical profile during the LAPSE-RATE campaign, Atmos. Chem. Phys., 21, 517–533, https://doi.org/10.5194/acp-21-517-2021, 2021.

Chang, Y., Guo, X., Tang, J., and Lu, G.: Aircraft measurement campaign on summer cloud microphysical properties over the Tibetan Plateau, Sci. Rep., 9, 4912, https://doi.org/10.1038/s41598-019-41514-5, 2019.

Craig, L., Moharreri, A., Rogers, D. C., Anderson, B., and Dhaniyala, S.: Aircraft-Based Aerosol Sampling in Clouds: Performance Characterization of Flow-Restriction Aerosol Inlets, J. Atmos. Ocean. Tech., 31, 2512–2521, https://doi.org/10.1175/JTECH-D-14-00022.1, 2014.

Devenish, B. J., Bartello, P., Brenguier, J.-L., Collins, L. R., Grabowski, W. W., Jzermans, R. H. A., Malinowski, S. P., Reeks, M. W., Vassilicos, J. C., Wang, L.-P., and Warhaft, Z.: Droplet growth in warm turbulent clouds, Q. J. Roy. Meteor. Soc., 138, 1401–1429, https://doi.org/10.1002/qj.1897, 2012.

Doulgeris, K. M., Brus, D., Raatikainen, T., and Kerminen V.-M.: A Finnish Meteorological Institute–Aerosol Cloud Interaction Tube (FMI–ACIT): Experimental setup and tests of proper operation, J. Chem. Phys., 149, 124201, https://doi.org/10.1063/1.5037298, 2018.

Doulgeris, K.-M., Komppula, M., Romakkaniemi, S., Hyvärinen, A.-P., Kerminen, V.-M., and Brus, D.: In situ cloud ground-based measurements in the Finnish sub-Arctic: intercomparison of three cloud spectrometer setups, Atmos. Meas. Tech., 13, 5129–5147, https://doi.org/10.5194/amt-13-5129-2020, 2020.

Doulgeris, K.-M., Lihavainen, H., Hyvärinen, A.-P., Kerminen, V.-M., and Brus, D.: Data set for Doulgeris et al. 2021: In-situ microphysical characterization of low-level clouds in the Finnish sub-Arctic, extensive dataset, Finnish Meteorological Institute [data set], https://doi.org/10.23728/FMI-B2SHARE.988739D21B824C709084E88ED6C6D54B, 2021.

Droplet Measurement Technologies Manual: Particle Analysis and Display System (PADS) Image Probe Data Reference Manual DOC-0201 Rev A-2 PADS 2.5.6, DMT, Boulder, Colorado, USA, 2009.

Droplet Measurement Technologies Manual: CAPS operator manual, DOC-0066 Revision F, DMT, Boulder, Colorado, USA, 2011.

Dye, J. E. and Baumgardner, D.: Evaluation of the forward scattering spectrometer probe, I – Electronic and optical studies, J. Atmos. Ocean. Technol., 1, 329–344, https://doi.org/10.1175/1520-0426(1984)001<0329:EOTFSS>2.0.CO;2, 1984.

Febvre, G., Gayet, J.-F., Shcherbakov, V., Gourbeyre, C., and Jourdan, O.: Some effects of ice crystals on the FSSP measurements in mixed phase clouds, Atmos. Chem. Phys., 12, 8963–8977, https://doi.org/10.5194/acp-12-8963-2012, 2012.

Girdwood, J., Smith, H., Stanley, W., Ulanowski, Z., Stopford, C., Chemel, C., Doulgeris, K.-M., Brus, D., Campbell, D., and Mackenzie, R.: Design and field campaign validation of a multi-rotor unmanned aerial vehicle and optical particle counter, Atmos. Meas. Tech., 13, 6613–6630, https://doi.org/10.5194/amt-13-6613-2020, 2020.

Grabowski, W. W., Morrison H., Shima S., Abade G. C., Dziekan P., and Pawlowska H.: Modeling of Cloud Microphysics: Can We Do Better?, B. Am. Meteorol. Soc., 100, 655–672, https://doi.org/10.1175/BAMS-D-18-0005.1, 2019.

Guichard F. and Couvreux F.: A short review of numerical cloud-resolving models, Tellus A, 69, 1373578, https://doi.org/10.1080/16000870.2017.1373578, 2017.

Guyot, G., Gourbeyre, C., Febvre, G., Shcherbakov, V., Burnet, F., Dupont, J.-C., Sellegri, K., and Jourdan, O.: Quantitative evaluation of seven optical sensors for cloud microphysical measurements at the Puy-de-Dôme Observatory, France, Atmos. Meas. Tech., 8, 4347–4367, https://doi.org/10.5194/amt-8-4347-2015, 2015.

Harrison R. G., Nicoll, K. A., Tilley, D. J., Marlton, G. J., Chindea, S., Dingley, G. P., Iravani, P., Cleaver, D. J., du Bois, J. L., and Brus, D.: Demonstration of a remotely-piloted atmospheric measurement and charge release platform for geoengineering, J. Atmos. Ocean. Technol, 38, 63–75, https://doi.org/10.1175/JTECH-D-20-0092.1, 2021.

Hatakka, J., Aalto, T., Aaltonen, V., Aurela, M., Hakola, H., Komppula, M., Laurila, T., Lihavainen, H., Paatero, J., Salminen, K., and Viisanen Y.: Overview of the atmospheric research activities and results at Pallas GAW station, Boreal Environ. Res., 8, 365–384, 2003.

Heymsfield, A., Thompsom, G., Morrison, H., Bansemer, A., Rasmussen, R. M., Minnis, P., Wang, Z., and Zhang,D.: Formation and Spread of Aircraft-Induced Holes in Clouds, Science, 33, 77–81, https://doi.org/10.1126/science.1202851, 2011.

Komppula, M., Lihavainen, H., Kerminen, V.-M., Kulmala, M., and Viisanen, Y.: Measurements of cloud droplet activation of aerosol particles at a clean subarctic background site, J. Geophys. Res., 110, D06204, https://doi.org/10.1029/2004JD005200, 2005.

Lachlan-Cope, T., Listowski, C., and O'Shea, S.: The microphysics of clouds over the Antarctic Peninsula – Part 1: Observations, Atmos. Chem. Phys., 16, 15605–15617, https://doi.org/10.5194/acp-16-15605-2016, 2016.

Lance, S.: Coincidence Errors in a Cloud Droplet Probe (CDP) and a Cloud and Aerosol Spectrometer (CAS), and the Improved Performance of a Modified CDP, J. Atmos. Ocean. Tech., 29, 1532–1541, https://doi.org/10.1175/JTECH-D-11-00208.1, 2012.

Lihavainen, H., Kerminen, V.-M., Komppula, M., Hyvärinen, A.-P., Laakia, J., Saarikoski, S., Makkonen, U., Kivekäs, N., Hillamo, R., Kulmala, M., and Viisanen, Y.: Measurements of the relation between aerosol properties and microphysics and chemistry of low level liquid water clouds in Northern Finland, Atmos. Chem. Phys., 8, 6925–6938, https://doi.org/10.5194/acp-8-6925-2008, 2008.

Lloyd, G., Choularton, T. W., Bower, K. N., Gallagher, M. W., Connolly, P. J., Flynn, M., Farrington, R., Crosier, J., Schlenczek, O., Fugal, J., and Henneberger, J.: The origins of ice crystals measured in mixed-phase clouds at the high-alpine site Jungfraujoch, Atmos. Chem. Phys., 15, 12953–12969, https://doi.org/10.5194/acp-15-12953-2015, 2015.

Lohila, A., Penttilä, T., Jortikka, S., Aalto, T., Anttila, P., Asmi, E., Aurela, M., Hatakka, J., Hellén, H., Henttonen, H., Hänninen, P., Kilkki, J., Kyllönen, K., Laurila, T., Lepistö, A., Lihavainen, H., Makkonen, U., Paatero, J., Rask, M., Sutinen, R., Tuovinen, J.-P., Vuorenmaa, J., and Viisanen, Y.: Preface to the special issue on integrated research of atmosphere, ecosystems and environment at Pallas, Boreal Env. Res., 20, 431–454, 2015.

Lowenthal, D. H., Hallar, A. G., David, R. O., McCubbin, I. B., Borys, R. D., and Mace, G. G.: Mixed-phase orographic cloud microphysics during StormVEx and IFRACS, Atmos. Chem. Phys., 19, 5387–5401, https://doi.org/10.5194/acp-19-5387-2019, 2019.

McFarquhar, G. M., Bretherton, C., Marchand, R., Protat, A., DeMott, P. J., Alexander, S. P., Roberts, G. C., Twohy, C. H., Toohey, D., Siems, S., Huang, Y., Wood, R., Rauber, R. M., Lasher-Trapp, S., Jensen, J., Stith, J., Mace, J., Um, J., Järvinen, E., Schnaiter, M., Gettelman, A., Sanchez, K. J., McCluskey, C. S., Russell, L. M., McCoy, I. L., Atlas, R., Bardeen, C. G., Moore, K. A., Hill, T. C. J., Humphries, R. S., Keywood, M. D., Ristovski, Z., Cravigan, L., Schofield, R., Fairall, C., Mallet, M. D., Kreidenweis, S. M., Rainwater, B., D'Alessandro, J., Wang, Y., Wu, W., Saliba, G., Levin, E. J. T., Ding, S., Lang, F., Truong, S. C., Wolff, C., Haggerty, J., Harvey, M. J., Klekociuk, A., and McDonald, A.: Observations of clouds, aerosols, precipitation, and surface radiation over the Southern Ocean: An overview of CAPRICORN, MARCUS, MICRE and SOCRATES, B. Am. Meteorol. Soc., 102, E894–E928, https://doi.org/10.1175/BAMS-D-20-0132.1, 2020.

Mie, G.: Beiträge zur Optik trüber Medien, speziell kolloidaler Metallösungen, Ann. Phys.-Berlin, 330, 377–445, 1908.

Möhler, O., Stetzer, O., Schaefers, S., Linke, C., Schnaiter, M., Tiede, R., Saathoff, H., Krämer, M., Mangold, A., Budz, P., Zink, P., Schreiner, J., Mauersberger, K., Haag, W., Kärcher, B., and Schurath, U.: Experimental investigation of homogeneous freezing of sulphuric acid particles in the aerosol chamber AIDA, Atmos. Chem. Phys., 3, 211–223, https://doi.org/10.5194/acp-3-211-2003, 2003.

Morrison, A. L., Kay, J. E., Frey, W. R., Chepfer, H., and Guzman, R.: Cloud response to Arctic sea ice loss and implications for future feedback in the CESM1 climate model, J. Geophys. Res.-Atmos., 124, 1003–1020, https://doi.org/10.1029/2018jd029142, 2019.

Morrison, H., van Lier-Walqui, M., Fridlind, A. M., Grabowski, W. W., Harrington, J. Y., Hoose, C., Koroloev, A., Kumjian, M. R., Milbrandt, J. A., Pawlowska, H., Posselt, D. J., Prat, O. P., Reimel, K. J., Shima, S.-I., Van Diedenhoven, B., and Xue, L.: Confronting the challenge of modeling cloud and precipitation microphysics, J. Adv. Model. Earth Sy., 12, e2019MS001689, https://doi.org/10.1029/2019MS001689, 2020.

Nguyen, C. M., Wolde, M., Battaglia, A., Nichman, L., Bliankinshtein, N., Haimov, S., Bala, K., and Schuettemeyer, D.: Coincident In-situ and Triple-Frequency Radar Airborne Observations in the Arctic, Atmos. Meas. Tech. Discuss. [preprint], https://doi.org/10.5194/amt-2021-148, in review, 2021.

Nichman, L., Järvinen, E., Dorsey, J., Connolly, P., Duplissy, J., Fuchs, C., Ignatius, K., Sengupta, K., Stratmann, F., Möhler, O., Schnaiter, M., and Gallagher, M.: Intercomparison study and optical asphericity measurements of small ice particles in the CERN CLOUD experiment, Atmos. Meas. Tech., 10, 3231–3248, https://doi.org/10.5194/amt-10-3231-2017, 2017.

Petäjä, T., O'Connor, E. J, Moisseev, D., Sinclair, V. A., Manninen, A. J., Väänänen, R., Von Lerber, A., Thornton, J. A., Nicoll, K., Petersen, W., Chandrasekar, V., Smith, J. N., Winkler, P. M., Krüger, O., Hakola, H., Timonen, H., Brus, D., Laurila, T., Asmi, E., Riekkola, M.-L., Mona, L., Massoli, P., Engelmann, R., Komppula, M., Wang, J., Kuang, C., Bäck, J., Virtanen, A., Levula, J., Ritsche, M., and Hickmon, N.: BAECC: A Field Campaign to Elucidate the Impact of Biogenic Aerosols on Clouds and Climate, B. Am. Meteorol. Soc., 97, 1909–1928, https://doi.org/10.1175/BAMS-D-14-00199.1, 2016.

Pruppacher, H. R. and Klett, J. D.: Microphysics of Clouds and Precipitation, edn. number 2, Springer, Dordrecht, Netherlands, ISBN 978-0-7923-4211-3, ISBN 978-0-306-48100-0, https://doi.org/10.1007/978-0-306-48100-0, 2010.

Rosenfeld, D. and Ulbrich, C. W.: Cloud Microphysical Properties, Processes, and Rainfall Estimation Opportunities, Meteor. Mon., 30, 237–237, https://doi.org/10.1175/0065-9401(2003)030<0237:CMPPAR>2.0.CO;2, 2003.

Stratmann, F., Kiselev, A., Wurzler, S., Wendisch, M., Heitzenberg, J., Charlson, R. J., Diehl, K., Wex, H., and Schmidt, S.: Laboratory Studies and Numerical Simulations of Cloud Droplet Formation under Realistic Supersaturation Conditions, J. Atmos. Oceanic Technol., 21, 876–887, https://doi.org/10.1175/1520-0426(2004)021<0876:LSANSO>2.0.CO;2, 2004.

Wandinger, U., Apituley, A., Blumenstock, T., Bukowiecki, N., Cammas, J.-P., Connolly, P., De Mazière, M., Dils, B., Fiebig, M., Freney, E., Gallagher, M., Godin-Beekmann, S., Goloub, P., Gysel, M., Haeffelin, M., Hase, F., Hermann, M., Herrmann, H., Jokinen, T., Komppula, M., Kubistin, D., Langerock, B., Lihavainen, H., Mihalopoulos, N., Laj, P., Lund Myhre, C., Mahieu, E., Mertes, S., Möhler, O., Mona, L., Nicolae, D., O'Connor, E., Palm, M., Pappalardo, G., Pazmino, A., Petäjä, T., Philippin, S., Plass-Duelmer, C., Pospichal, B., Putaud, J.-P., Reimann, S., Rohrer, F., Russchenberg, H., Sauvage, S., Sellegri, K., Steinbrecher, R., Stratmann, F., Sussmann, R., Van Pinxteren, D., Van Roozendael M., Vigouroux C., Walden C., Wegene R., and Wiedensohler, A.: ACTRIS-PPP Deliverable D5.1: Documentation on technical concepts and requirements for ACTRIS Observational Platforms, available at: https://www.actris.eu/sites/default/files/Documents/ACTRISPPP/Deliverables/ACTRISPPP_WP3_D3.1_ACTRISCostBook.pdf (last access: 4 February 2022), 2018.

Wendisch, M., Macke, A., Ehrlich, A., Lüpkes, C., Mech, M., Chechin, D., Dethloff, K., Velasco, C. B., Bozem, H., Brückner, M., Clemen, H.-C., Crewell, S., Donth, T., Dupuy, R., Ebell, K., Egerer, U., Engelmann, R., Engler, C., Eppers, O., Gehrmann, M., Gong, X., Gottschalk, M., Gourbeyre, C., Griesche, H., Hartmann, J., Hartmann, M., Heinold, B., Herber, A., Herrmann, H., Heygster, G., Hoor, P., Jafariserajehlou, S., Jäkel, E., Järvinen, E., Jourdan, O., Kästner, U., Kecorius, S., Knudsen, E. M., Köllner, F., Kretzschmar, J., Lelli, L., Leroy, D., Maturilli, M., Mei, L., Mertes, S., Mioche, G., Neuber, R., Nicolaus, M., Nomokonova, T., Notholt, J., Palm, M., van Pinxteren, M., Quaas, J., Richter, P., Ruiz-Donoso, E., Schäfer, M., Schmieder, K., Schnaiter, M., Schneider, J., Schwarzenböck, A., Seifert, P., Shupe, M. D., Siebert, H., Spreen, G., Stapf, J., Stratmann, F., Vogl, T., Welti, A., Wex, H., Wiedensohler, A., Zanatta, M., and Zeppenfeld, S.: The Arctic Cloud Puzzle: Using ACLOUD/PASCAL Multiplatform Observations to Unravel the Role of Clouds and Aerosol Particles in Arctic Amplification, B. Am. Meteorol. Soc., 100, 841–871, https://doi.org/10.1175/BAMS-D-18-0072.1, 2019.

IV

Atmos. Chem. Phys., 23, 2483–2498, 2023
https://doi.org/10.5194/acp-23-2483-2023

Atmospheric Chemistry and Physics
Open Access
EGU

Influence of air mass origin on microphysical properties of low-level clouds in a subarctic environment

Konstantinos Matthaios Doulgeris[1], Ville Vakkari[1,2], Ewan J. O'Connor[1], Veli-Matti Kerminen[4], Heikki Lihavainen[1,3], and David Brus[1]

[1]Finnish Meteorological Institute, Erik Palménin aukio 1, P.O. Box 503, 00100 Helsinki, Finland
[2]Atmospheric Chemistry Research Group, Chemical Resource Beneficiation, North-West University, Potchefstroom, South Africa
[3]Svalbard Integrated Arctic Earth Observing System (SIOS), SIOS Knowledge Centre, Svalbard Science Centre, P.O. Box 156, 9171 Longyearbyen, Norway
[4]Institute for Atmospheric and Earth System Research/Physics, Faculty of Science, University of Helsinki, 00014 Helsinki, Finland

Correspondence: Konstantinos Matthaios Doulgeris (konstantinos.doulgeris@fmi.fi)

Received: 25 August 2022 – Discussion started: 15 September 2022
Revised: 24 January 2023 – Accepted: 3 February 2023 – Published: 22 February 2023

Abstract. In this work, an analysis was performed to investigate how different long-range transport air masses can affect the microphysical properties of low-level clouds in a clean subarctic environment. The cloud measurements included in situ and remote sensing ground-based techniques and were conducted during eight Pallas Cloud Experiments (PaCEs) held in the autumn between 2004 and 2019. Each PaCE was carried out at the Pallas Atmosphere-Ecosystem Supersite, located in the Finnish subarctic region. Two cloud spectrometer ground setups were installed on the roof of the station to measure cloud microphysical properties: the cloud, aerosol and precipitation spectrometer (CAPS) and the forward-scattering spectrometer probe (FSSP). Air mass histories were analyzed using the Lagrangian FLEXible PARTicle dispersion model (FLEXPART) in order to investigate the differences between five distinct source regions ("Arctic", "Eastern", "Southern", "Western" and "Local"). We observed clear differences in the cloud microphysical properties for the air mass source regions. Arctic air masses were characterized by low liquid water content (LWC), low cloud droplet number concentration (N_c) and comparatively large median volume and effective droplet diameter. The Western region (marine North Atlantic) differed from the Arctic by both higher N_c and LWC. The Eastern region (continental Eurasia) only had a little higher LWC than the Arctic but substantially higher N_c and a smaller droplet diameter. The Southern region (continental Europe) had high N_c and LWC and a very similar droplet diameter to the Eastern region. Finally, the relationship between N_c and droplet size (i.e., the Twomey effect) was characterized for the different source regions, indicating that all region clouds were sensitive to increases in N_c.

1 Introduction

Uncertainties in cloud processes and feedbacks are key challenges when developing climate projections (e.g., Boucher et al., 2013; Sherwood et al., 2020). Cloud microphysics and their dynamics are considered a fundamental challenge (Morrison et al., 2020) due to their connection to the cloud radiative effect (e.g., Devenish et al., 2012; McFarquhar et al., 2020). Thus, it is necessary to distinguish between the effects of aerosol and varying meteorological conditions on clouds (Barthlott and Hoose, 2018) since the aerosol is influenced through meteorology by air mass history as well as cloud and precipitation processes (Rosenfeld et al., 2014). Long-range transport is significant when investigating the characteristics and the spatial distribution of aerosols (e.g., Raatz and Shaw, 1984; Barrie, 1986; Freud et al., 2017; Wang et al., 2020; Lee et al., 2022). It is important to un-

derstand how different air masses can influence the aerosols and the cloud microphysics (e.g., Painemal et al., 2014; Orbe et al., 2015a; Fuchs et al., 2017; Cho et al., 2021). Investigating subarctic clouds is of particularly high interest due to the Arctic amplification effect, since the Arctic surface energy budget and Arctic warming feedback are affected by cloud-related radiative processes (e.g., Wendisch et al., 2019; Shupe at al., 2022).

Several observation efforts and experiments have been made to explore how air masses affect climate and the cloud macrophysical and microphysical properties (e.g., Hobbs and Rangno, 1998; Gultepe et al., 2000; Orbe et al., 2015b; Solomon and Shupe, 2019; Torres-Delgado et al., 2021). Hobbs and Rangno (1998) highlighted that air masses from the south resulted in the highest overall aerosol number concentration measured in altocumulus clouds over the Beaufort Sea. Gultepe et al. (2000) stated that Arctic clouds were affected by the air mass origin, which was strongly related to aerosol properties and dynamical and thermodynamical parameters. Gultepe and Isaac (2002) studied the cloud microphysics over the Arctic Ocean and found that there were differences in the number concentration, liquid water content and effective radius of Arctic clouds in air masses originating from the Arctic and Pacific oceans. After investigating the air mass origin seasonality, Orbe et al. (2015a) revealed that the Northern Hemisphere summer air mass origin response to increases in greenhouse gases (Orbe et al., 2015b). Fuchs et al. (2017) highlighted the impact of air mass origin and dynamics on cloud property changes in the southeast Atlantic during the biomass burning season based on a cluster analysis of 8 years of September data. Solomon and Shupe (2019) presented a case study of a sharp transition between high ice clouds and the formation of lower stratocumulus from Summit, Greenland, when a warm and moist air mass was advected to Greenland from lower latitudes. Iwamoto et al. (2021), using measurements from a high mountain site located in Japan, showed that the cloud droplet number concentrations were significantly higher in continental air masses than in air masses from the Pacific Ocean. Patel and Jiang (2021) combined measurements of aerosol properties from a site located in Lamont, Oklahoma, with cluster analysis of back trajectories to study aerosol characteristics and their influences on cloud condensation nuclei (CCN) under various air mass environments and suggested that information on the aerosol chemical composition and mixing state is more crucial at lower supersaturations. Torres-Delgado et al. (2021), using aerosol and cloud measurements from a site in a tropical montane cloud forest on the Caribbean island of Puerto Rico, suggested that air masses that arrived after passing over areas with anthropogenic emissions led to clouds with much higher cloud droplet concentrations. Cho et al. (2021) investigated wintertime cloud properties and radiative effects in connection with cold and warm air mass origins at Ny-Ålesund, Svalbard, using remote sensing measurements with cloud radar, ceilometer and microwave radiometer instruments and revealed that the effective radius of cloud particles in warm advection cases was approximately 5–10 µm larger than that of cold advection cases at all altitudes.

One of the few sites that enables long-term in situ observations of cloud and aerosol properties in Arctic and subarctic air masses is the Pallas Global Atmospheric Watch (GAW) station in northern Finland (e.g., Lihavainen et al., 2008; Hyvärinen et al., 2011; Anttila et al., 2012; Raatikainen et al., 2015; Gérard et al., 2019; Girdwood et al., 2020, 2022). However, after the initial case study (Lihavainen et al., 2008), which indicated a clear Twomey effect depending on air mass origin, no subsequent concerted study has investigated the effect of air mass origin on cloud microphysical properties at Pallas. In the Arctic, during autumn, the ultrafine aerosol number concentration and the occurrence of clean, natural Arctic background conditions are significantly increasing (Pernov et al., 2022). Subsequently, this allows us to focus in this work on quantifying the impact of air mass origin (e.g., clean Arctic vs. long-range-transported air from continental Europe) on the microphysical properties of low-level clouds and their patterns based on measurements at the Pallas GAW station. To our knowledge, this is the first study that was performed in a subarctic environment and connects extensive in situ cloud measurements to air mass origin. Size distribution is considered one of the most important parameters of the cloud system due to its impact on the dynamics and microstructures within the cloud (Igel and van den Heever, 2017a, b). Measuring cloud microphysical properties, such as the median volume diameter and liquid water content, is of high importance for the identification and description of clouds (Pruppacher and Klett, 2010; Rosenfeld and Ulbrich, 2003; Donovan et al., 2015), cloud radiative properties and lifetime (Albrecht, 1989; Small et al., 2009), and the probability for which clouds precipitate (Rosenfeld and Ulbrich, 2003; Chang et al., 2019). We used in situ low-level cloud measurements from two ground-based cloud spectrometers from 8 different years of campaigns to obtain the cloud droplet size distribution. A lidar ceilometer was used to monitor the cloud base. The FLEXible PARTicle (FLEXPART) dispersion model was used to analyze the air mass history. A description of the measurement site and the instrumentation, and how it was installed, is given in Sect. 2.1 and 2.2. Subsequently, in Sect. 2.3, a general overview of the campaigns is presented. In Sect. 2.4, we present how the backward trajectories were calculated. In Sect. 3, the optimal threshold of traveling air masses within a region to represent an air mass type is identified, and a detailed analysis is done to find out to what extent the air mass type influences the microphysical properties of the low-level clouds. Finally, in Sect. 4, we summarize our main conclusions.

2 Methodology

2.1 Sampling station

The measurements were conducted in subarctic Finland at the Pallas Atmosphere-Ecosystem Supersite (67°580′ N, 24°070′ E), hosted by the Finnish Meteorological Institute. The site where the ground-based cloud spectrometers were installed was the Sammaltunturi station, located on a hilltop, 565 m above sea level (a.s.l.) (Hatakka et al., 2003). The site where the ceilometer was installed was the Kenttärova station, 347 m a.s.l., located at the foot of the same hill (Fig. 1). A full description of the Pallas Atmosphere-Ecosystem Supersite can be found in Lohila et al. (2015).

2.2 Instrumentation

The instruments that were used in this study are listed in Table 1, together with the measured and derived parameters, their uncertainties and their location. During Pallas Cloud Experiments (PaCEs), we used ground-based in situ cloud spectrometers to monitor the cloud droplet size distribution, which has been recognized as a valid method for continuous cloud in situ measurements in the Aerosol, Clouds and Trace Gases Research Infrastructure (ACTRIS) network (Wandinger et al., 2018). Four microphysical parameters were derived from the measured size distribution (Droplet Measurement Technologies, 2009; Doulgeris et al., 2020): the cloud droplet number concentration (N_c; cm^{-3}), the median volume diameter (MVD; µm) and effective diameter (ED; µm) of cloud droplets, and the cloud liquid water content (LWC; $g\,m^{-3}$).

Two ground-based spectrometers were installed on the roof of Sammaltunturi station: the cloud, aerosol and precipitation spectrometer (CAPS) and the forward-scattering spectrometer probe (FSSP-100; hereafter called FSSP for simplicity) (Fig. 2). CAPS was made by Droplet Measurement Technologies (DMT), Boulder, CO, USA. FSSP-100 (model SPP-100, DMT) was initially manufactured by Particle Measuring Systems (PMS Inc., Boulder CO, USA) and later acquired by DMT. The CAPS probe includes three instruments: the cloud and aerosol spectrometer (CAS), the cloud imaging probe (CIP), and the hot-wire liquid water content (LWC_{hw}) sensor. Only CAS data were used during this work. The size range of the CAS extends from 0.51 to 50 µm and that of the FSSP from 0.5 to 47 µm in diameter. In both CAS and FSSP, the main measurement principle for the size detection is based on a conversion of the forward scattering of light into a size bin using Lorentz–Mie theory (Mie, 1908). Their main difference was that the CAS was fixed and always heading to the main wind direction of the station (southwest, ∼ 225), whereas the FSSP-100 was deployed on a rotating platform to continuously face the wind. A description of both ground setups, installation, limitations and the methodology that was used is documented in Doulgeris et al. (2020, 2022). The instrument that monitored the cloud base was a lidar ceilometer that was deployed at the Kenttärova site (model CT25K, Vaisala Oyj, 2002; Emeis et al., 2004), except in 2019 when it was replaced by a CL31 model, Vaisala Oyj. The meteorological variables were monitored by an automatic weather station (model Milos 500, Vaisala Oyj) that was deployed at the Sammaltunturi site. All the weather sensors that were used in this work were described in Hatakka et al. (2003). The temperature was measured at 570 m a.s.l. by a PT100 sensor, the horizontal visibility by a weather sensor (model FDP12P, Vaisala Oyj), the relative humidity by a HUMICAP (Vaisala Oyj), the barometric pressure by a BAROCAP (Vaisala Oyj) sensor, the wind direction by a heated wind vane and the wind speed by a heated cup (Vaisala Oyj).

2.3 Sampling campaigns

Measurements used in this study were conducted during the Pallas Cloud Experiments (PaCEs). A description of the dataset (microphysical properties of clouds along with meteorological variables) that was obtained during PaCEs is available in Doulgeris et al. (2022). The PaCEs were approximately 2-month-long field campaigns conducted in the Finnish subarctic region at the Sammaltunturi station during autumn and lasted approximately from the beginning of September until the end of November. The reason for this choice was that during autumn the Sammaltunturi station is frequently inside a cloud, which allowed us to perform ground-based, continuous in situ cloud measurements (Hatakka et al., 2003). An overview of each campaign, along with the availability of instruments and the hours of observations in cloud, is presented in Table 2. During PaCEs, all measurements were performed with a 1 Hz acquisition frequency. For the data analysis, averages per minute from each instrument were calculated when the measuring site was inside a cloud. Each cloud event was inspected separately. Afterwards, in situ cloud data were related to the air mass origin and classified accordingly. We only used measurements when the cloud spectrometers were facing the wind direction, as suggested by Doulgeris et al. (2020). Thus, since the CAS was fixed, data when the CAS was not facing the wind direction were disqualified from further analysis.

Fine particles at the Sammaltunturi site are expected to be dominated by sulfate and particulate organic matter in continental air masses, while particulate organic matter, sodium and chlorine are the main components in marine air masses (Lihavainen et al., 2008; Brus et al., 2013a). Also, episodes of elevated concentrations of SO_2 and H_2SO_4 are possible in air masses arriving from the Kola Peninsula, which is a large source of SO_2 emissions (Kyrö et al., 2014; Sipilä et al., 2021; Brus et al., 2013a, b). Elevated SO_2 concentrations and particle number concentrations in the accumulation mode (0.1–1 µm in diameter) of the mass size distribution are also expected from air masses that have traveled over continental Europe. Total aerosol particle number

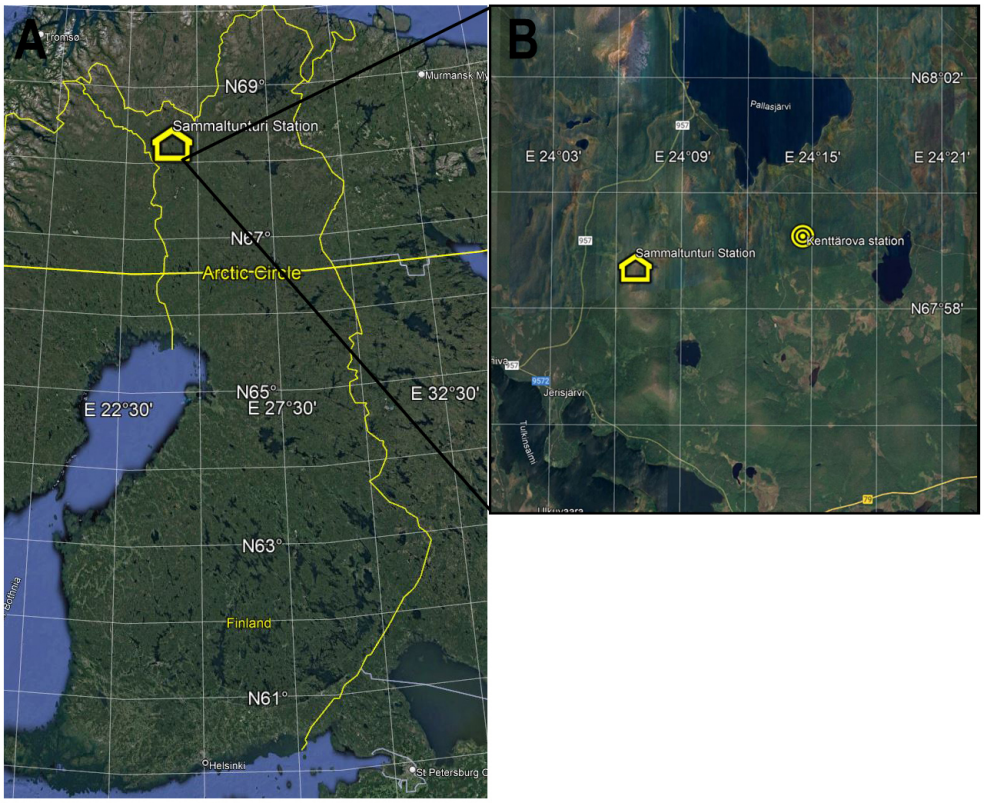

Figure 1. **(a)** Map of Finland showing the location of the Pallas Atmosphere-Ecosystem Supersite (yellow hut) and **(b)** map of the wider Pallas area showing the location of Sammaltunturi (yellow hut) and Kenttärova (yellow circles) stations (© Google Maps).

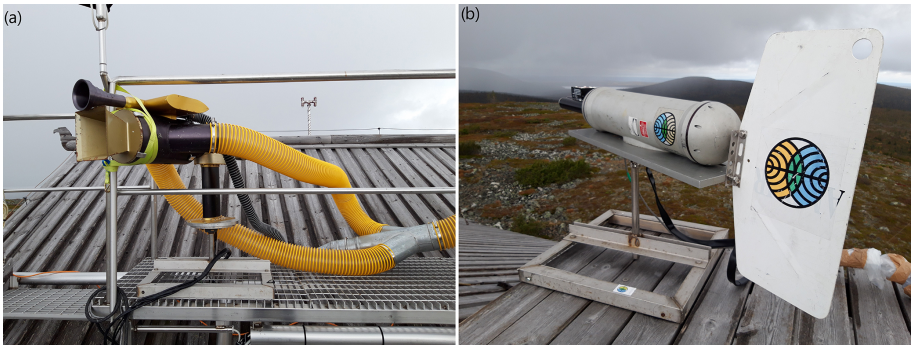

Figure 2. **(a)** CAPS and **(b)** FSSP-100 ground setups installed on the roof of Sammaltunturi station during PaCE 2017.

concentrations at Sammaltunturi are typically low (average of 700 cm^{-3}; in winter the daily averages may drop below 100 cm^{-3}) (Hatakka et al., 2003; Komppula et al., 2003). Generally, in Finnish Lapland, aerosol particle number concentrations are expected to be the highest in air masses arriving from the Kola Peninsula (more than 1000 cm^{-3}) and the lowest in marine air masses, especially in air originating from the Arctic Sea (often less than 100 cm^{-3}) (Lihavainen et al., 2008). Higher particle number concentrations in the accumulation mode are also expected in air masses which have traveled over continental Europe (Virkkula et al., 1997). In Sammaltunturi, cloud condensation nuclei (CCN) concentrations are smaller than 100 cm^{-3} for supersaturations from 0.1 % to 0.5 %. The aerosol particle population is dominated by the Aitken mode (30–100 nm in diameter), and a low hygroscopicity is expected (Paramonov et al., 2015).

2.4 Classification of air mass origin

Air mass origins were analyzed using the Lagrangian particle dispersion model FLEXPART version 10.4 (Seibert and Frank, 2004; Stohl et al., 2005; Pisso et al., 2019). FLEX-

Table 1. Instrumentation that was used during PaCE, along with measured and derived parameters, their sampling frequencies, accuracy of the instruments and the location where the instruments were installed.

Instrument	Measured, derived parameters	Sampling frequency	Accuracy	Location	References
CAS, DMT	Number size distribution of cloud droplets (0.51 to 50 µm); derived parameters N_c, LWC, ED, MVD	1 s	At ambient droplet concentrations of 500 cm^{-3}, 27 % undercounting 20 %–30 % oversizing	Sammaltunturi	Doulgeris et al. (2020, 2022), Baumgardner et al. (2001), Lance (2012)
FSSP, DMT	Number size distribution of cloud droplets (0.5 to 47 µm); derived parameters N_c, LWC, ED, MVD	1 s	N_c accuracy: 16 % sizing accuracy: ±3 µm LWC accuracy: 30 %–50 %	Sammaltunturi	Doulgeris et al. (2020, 2022), Brenguier (1989), Baumgardner et al. (2017), Baumgardner (1983)
Ceilometer CT25K, Vaisala	Cloud base altitude	60 s	±2 % ± 1/2× (resolution)	Kenttärova	Vaisala Oyj (2002), Emeis et al. (2004)
FD12P, Vaisala	Horizontal visibility	60 s	±10 % at 10–10 000 (m)	Sammaltunturi	Hatakka et al. (2003)
PT100 sensor, Vaisala	Temperature	60 s	±0.1 (°C)	Sammaltunturi	Hatakka et al. (2003)
HUMICAP sensor, Vaisala	Relative humidity	60 s	±0.8 (%) RH	Sammaltunturi	Hatakka et al. (2003)
BAROCAP sensor, Vaisala	Barometric pressure	60 s	±0.15 (%) (hPa)	Sammaltunturi	Hatakka et al. (2003)
Wind vane, Vaisala	Wind direction	60 s	±3 (°)	Sammaltunturi	Hatakka et al. (2003)
Heated cup, Vaisala	Wind speed	60 s	±0.17 ($m\,s^{-1}$)	Sammaltunturi	Hatakka et al. (2003)

Table 2. Overview of each campaign, including the starting and ending date, the availability of the ground cloud spectrometer probes and the ceilometer.

Year	Starting date	Ending date	CAS	FSSP	Ceilometer	Cloud observations CAPS (hours)	Cloud observations FSSP (hours)
2004	25 October	7 November	Not available	On-site	CT25K	–	42
2005	30 September	5 October	Not available	On-site	CT25K	–	45.4
2009	11 September	9 October	Not available	On-site	CT25K		34.2
2012	14 September	30 October	On-site	On-site from 9 October	CT25K	477.5	50
2013	14 September	28 November	On-site from 15 October	On-site	CT25K	483.5	492.6
2015	24 September	2 December	On-site from 6 October	On-site	CT25K	528.4	561.9
2017	18 September	29 November	On-site	Not available	CT25K	681.8	–
2019	20 September	24 November	On-site	Not available	CL31	479.6	–

PART was run backward in time to calculate potential emission sensitivity (PES) fields. PES in a particular grid cell is proportional to the air mass residence time in that cell and was calculated in units of seconds (Seibert and Frank, 2004; Pisso et al., 2019). ERA5 reanalysis by the European Centre for Medium-Range Weather Forecasts (ECMWF) was used as meteorological input fields for FLEXPART at 1 h temporal resolution and 0.25° resolution in latitude and longitude. In the vertical, ERA5 levels 50 to 137 were used, which corresponds approximately to the lowest 20 km above the surface. The model domain was from 125° W to 75° E and 10 to 85° N, which was large enough to contain 96 h simulations backward in time. FLEXPART runs were initiated at an hourly time resolution for the in-cloud measurement periods at Sammaltunturi. The retro plume release height was set to 560–660 m a.s.l., as the terrain height in ERA5 at the site was approximately 300 m a.s.l. The PES output resolution was set to 0.2° latitude and longitude with a 250 m height resolution up to 5 km and two additional output levels at 10 and 50 km.

The air mass source regions for the Sammaltunturi site were divided into five categories: "Arctic", "Eastern", "Southern", "Western" and "Local" (Fig. 3). The division

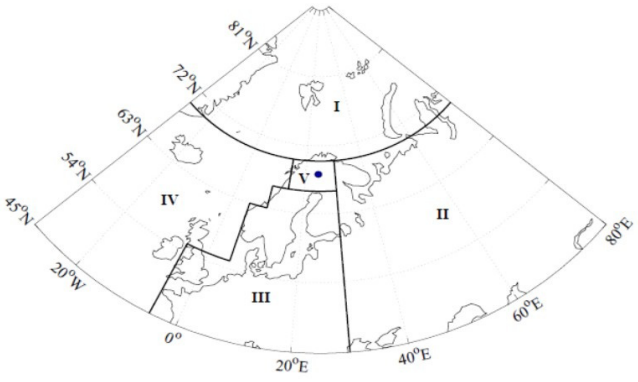

Figure 3. Map of the air mass regions: I (Arctic), II (Eastern), III (Southern), IV (Western) and V (Local). Figure was adopted from Asmi et al. (2011).

was based on previous studies that were conducted at Sammaltunturi (e.g., Aalto et al., 2003; Eneroth et al., 2005; Tunved et al., 2006; Asmi et al., 2011). Initially, the regions were classified using trajectory cluster analysis, following the method proposed by Eneroth et al. (2003). The choice of sectors roughly represents the characteristics of the region. The Arctic and Western regions represent marine areas, whereas the Eastern, Southern and Local regions represent continental areas. Figure 4 illustrates an example case for air masses arriving on 20 September 2012 at 11:00 UTC at Sammaltunturi. In Fig. 4a PES is summed up for the full duration of the 96 h backward simulation and for all output heights at each latitude–longitude grid cell. Figure 4b displays the vertical distribution of PES during the simulation. However, the information in Fig. 4b is not used in further analysis, but the fraction of PES in each source region is calculated based on the integrated data presented in Fig. 4a. For the case in Fig. 4a, this results in PES fractions of 42 % Local (area V), 35 % Southern (area III) and 23 % Western (area IV). Finally, Fig. 4c shows how the PES fractions evolve during 20 September 2012 at Sammaltunturi, with the case in Fig. 4a represented by the bar at 11:00 UTC. In Fig. 4c a clear change in air mass origin is observed at 18:00 UTC when the fraction of Arctic source region starts to increase, reaching up to 48 % at 22:00 UTC.

3 Results

3.1 Local meteorological conditions

Figure 5 shows the daily average temperatures at 570 m observed at the Sammaltunturi measuring site for days with "cloud events". The seasonal temperatures range from an average of 4.5 °C (SD 2.1 °C) in September to −5.3 °C (SD 1.8 °C) in November, and interannual variability is revealed. Days with "cloud events" were defined as the days when the station was at least 30 min immersed in a cloud. To identify the presence of a cloud at the station, four steps were followed. The droplet size distribution was checked from both cloud spectrometers; the relative humidity should be ∼ 100 %, and the horizontal visibility should be less than 1000 m, and a final inspection was performed visually using pictures recorded by an automatic weather camera installed on the roof of the station. During days with no cloud events, clouds could still exist at higher altitudes. Supercooled water droplets were expected at temperatures < 0 °C (usually during November and October of each campaign, in total 175 cloud events with temperature < 0 °C were sampled). Mixed-phase clouds, consisting of water vapor, ice particles and supercooled liquid droplets, are frequent at temperatures from −10 to −25 °C (Korolev et al., 2017; Filioglou et al., 2019); however, they can be present up to temperatures of 0 °C (Andronache, 2017). During September, the average temperature was > 0 °C; thus, the clouds were expected to consist of liquid hydrometeors only (liquid droplets, drizzle drops and raindrops). Wind speed ranges during the PaCEs were approximately 0 to 10 m s^{-1}, and the average wind speed during each campaign was around 7 m s^{-1}. These values were lower in comparison to the probe air speed of both cloud ground-based spectrometers (Doulgeris et al., 2022).

3.2 Identification of the air mass origin and its effect on the number concentration of cloud droplets

First, we examined which was the optimal threshold of the PES fraction within one region that should be used for a particular region to be representative of the air mass type. N_c was chosen to be used as a benchmark parameter. Figure 6 shows hourly N_c values depending on the PES fraction of the Arctic region (in the Arctic, during autumn, the ultrafine aerosol number concentration and the occurrence of clean, natural Arctic background conditions are significantly increasing; Pernov et al., 2022). The lowest values of N_c (< 30 cm^{-3}) were related to PES fractions > 80 %. When the PES fraction was between 70 % and 80 %, the values of N_c were varying between 5 and 80 cm^{-3}, and the highest values of N_c (> 30 cm^{-3}) were related to a PES fraction lower than 70 %.

To achieve a generalization of the large-scale air mass influence on microphysical cloud properties, the characteristics of all regions were intercompared. In Fig. 7 we summarize cloud N_c measurements from both CAS and FSSP. Each point represents a single PaCE campaign for different regions according to the classification criteria that were introduced previously in this section. We present each campaign and instrument to demonstrate that there were no obvious changes through years or possible malfunction of the instruments that were used and could produce biased results. Two different levels of the PES fraction were chosen to be further investigated: (i) when the PES fraction was more than 80 % within one region and (ii) when the PES fraction was between 70 % and 80 % within one region. For the first level, the highest

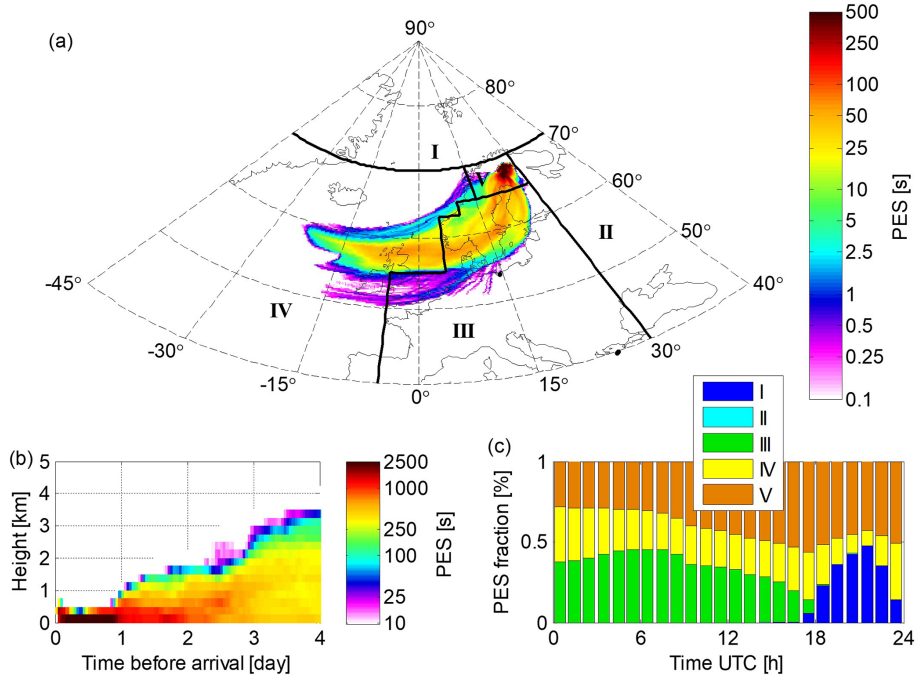

Figure 4. **(a)** Horizontal distribution of vertically integrated PES for air masses arriving at Sammaltunturi on 20 September 2012 11:00 UTC. Source regions are indicated with Roman numerals. **(b)** Vertical distribution of PES in panel **(a)** as a function of time before arrival at Sammaltunturi. **(c)** Timeline of the PES fraction for each source region for 20 September 2012.

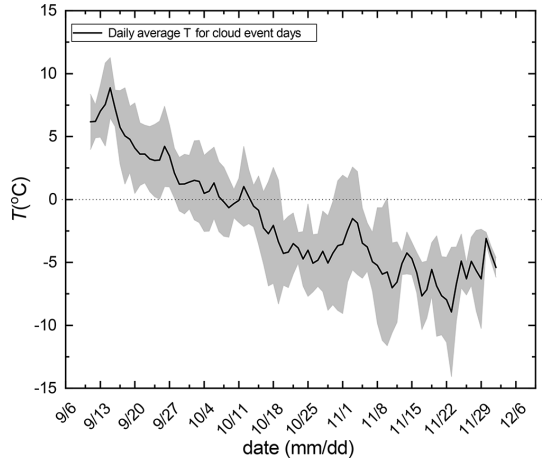

Figure 5. The daily average temperatures at the Sammaltunturi site for days with cloud events during all PaCE campaigns. The dotted line is used as a reference line for 0 °C temperature. The definition of a cloud event is provided in the text. The shaded area represents the corresponding standard deviations.

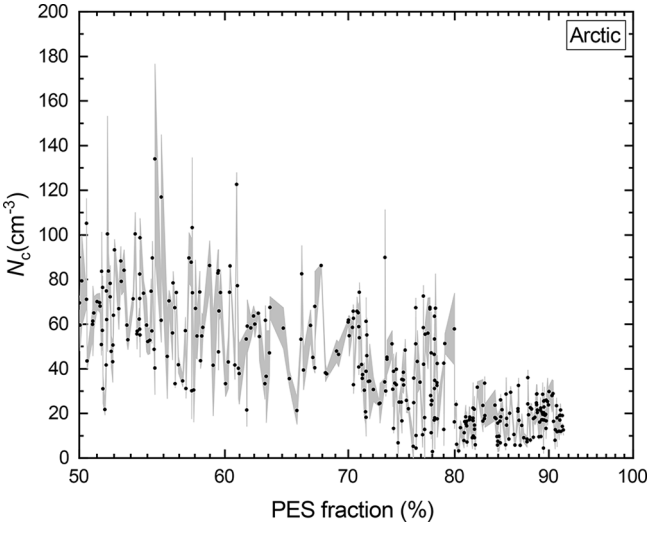

Figure 6. Hourly cloud droplet number concentration (N_c) versus the different potential emission sensitivity (PES) fraction for the Arctic region. The shaded area represents the corresponding standard deviations.

values of N_c (approximately 100–200 cm^{-3}) were clearly associated with Southern air masses, whereas the lowest ones (approximately 20 cm^{-3}) were observed in Arctic air masses. In general, marine air masses (Arctic, Western) arriving at Sammaltunturi resulted in lower values of N_c compared with continental air masses. However, there was also a difference (by a factor of approximately 2) between marine air masses: N_c values in air masses traveling over the Atlantic Ocean or the Norwegian Sea were higher than those in air masses arriving from the Arctic Sea. For aerosol populations, higher values of N_{CCN} are expected in more polluted air

masses (Southern and Eastern air masses, due to emissions from Europe and the Kola Peninsula) (Virkkula et al., 1997; Jaatinen et al., 2014; Sipilä et al., 2021). Averaged temperatures at Sammaltunturi for each air mass were −3.1 °C (SD 2.5 °C), −2.2 °C (SD 5.9 °C), 1.3 °C (SD 3.9 °C) and −2.8 °C (SD 2.01 °C) for the Arctic, Eastern, Southern and Western region respectively. Furthermore, there was no clear indication that there was any trend in N_c through different years of PaCEs. In this work, N_{CCN} measurements at different supersaturations were not conducted.

For a PES fraction between 70 % and 80 %, the impact of the air mass type on the N_c changed as the differences in N_c were less than for PES > 80 %. Clouds that were associated with Southern air masses had slightly higher values of N_c (approximately 60–80 cm^{-3}) in comparison with clouds from the other regions (approximately 20–60 cm^{-3}). As a result, for further analysis in this work, we decided to exclude measurements that were performed when the PES fraction was between 70 % and 80 %. Thus, we considered that > 80 % of the PES fraction within a particular region would be the optimal threshold to represent an air mass type during PaCEs. Using the > 80 % PES fraction from one source region as a criterion for further analysis left 492 h of in-cloud measurements with the CAS and 214 h of in-cloud measurements with the FSSP probe (from a total of 2004 h of in situ cloud data, 706 h belongs to non-mixed air mass origin), respectively, which ensured statistically robust results. Cloud observation related to Arctic, Eastern, Southern, Western and Local air masses were 118, 275, 152, 118 and 43 h, respectively. The observation hours related to each region for each PaCE are presented in Table S2 of the Supplement. Clouds that were related with local air masses were excluded due to a relatively small number of observations.

Based on the air mass origin classification, a statistical analysis was made to investigate the frequency of the air masses during cloud events at the measuring site. When the air masses were not mixed, the occurrence of clouds at the station related to continental and marine air masses in 31.9 % and 14.3 % of the cases, respectively. Focusing on each region separately, 29.6 % of the cloud's occurrence seemed to be related to Southern and Eastern air masses and 7.4 % were related to Arctic air masses, although the predominant air mass at Sammaltunturi was from the Arctic (Asmi et al., 2011).

3.3 Effect of the air mass origin on the cloud droplet size

In this section, we focused on investigating the size distribution of the cloud droplets and the derived parameters ED, MVD and LWC. ED and MVD are strongly dependent on the shape of the cloud droplet size distribution, while LWC is a function of both N_c and sizes of the cloud droplets. To achieve a generalization, size distributions of cloud droplets related to each air mass origin for all PaCE campaigns are presented in Fig. 8. Cloud droplet size distributions originating from marine regions (Arctic, Western) had a relatively broad shape with the presence of large (10–20 µm) droplets, whereas in continental air masses there was a clear absence of large cloud droplets. In general, the average size distribution showed a spectrum with more droplets at small size ranges when the masses were continental and more droplets in larger size ranges when the air masses were marine. Cloud droplets larger than 16.0 µm started to appear in clouds that were characterizes by Arctic and western air masses. On the other hand, clouds that were characterized by Eastern and Southern air masses had cloud droplets mainly in the range from 5 to 10 µm. Values of N_c for different sizes of the cloud droplets suggest that higher aerosol loadings lead to higher number concentrations of cloud droplets and smaller cloud droplet effective diameters. This result is consistent with the Twomey effect (Twomey, 1977), reported in several in situ observations (e.g., Twohy et al., 2005; Freud et al., 2008; Goren and Rosenfeld, 2014). In general, in a cloud system, it is expected that for a relatively constant LWC, the effective diameter of cloud droplets decreases as their number concentration increases.

We also investigated whether sizes of cloud droplets depend on the air temperature. For that reason, temperature bins of 4 °C range were created. Thus, the measurements were grouped into temperature bins of −10 to −6, −6 to −2, −2 to 2 and 2 to 6 °C. The mid-temperature value of each bin was used to create Fig. 9 which shows that cloud droplets appeared to be more prone to growing at temperatures larger than −2 °C. A hypothesis to explain such growth could be the collision–coalescence procedures that can take place in warm clouds (e.g., Xue et al., 2008; Pruppacher and Klett, 2010; Lohmann et al., 2016). In this study, all the sampled clouds are considered to be warm clouds; however those at warmer air temperatures seem to consist of larger droplets. Both MVD and ED showed a similar behavior. When the clouds were characterized by Arctic air masses, MVD and ED were approximately 15 µm within our temperature spectrum. The decrease of particle size for the "Arctic" subsample in the FSSP data above 0 °C was due to the relatively low number of observations in this temperature range (2 h of observation). The observation hours related to each temperature bin for each PaCE are presented in Table S3. For clouds related to Eastern air masses, MVD and ED were approximately 9 µm when the temperature was below 0 °C and showed approximately 6 µm larger hydrometeors in warmer clouds (above 0 °C). However, more observations from existing and wider temperature ranges are needed to statistically ensure those results.

The LWC of low-level clouds for the different air mass types is summarized for each PaCE campaign (Fig. 10a). The Arctic air masses were related to the lowest values of LWC (approximately 0.025 g m^{-3}), whereas the Southern air masses were related to the highest values of LWC (> 0.05 g m^{-3}). Western and Eastern air masses were related to LWC values of approximately 0.025 to 0.05 g m^{-3}. In this

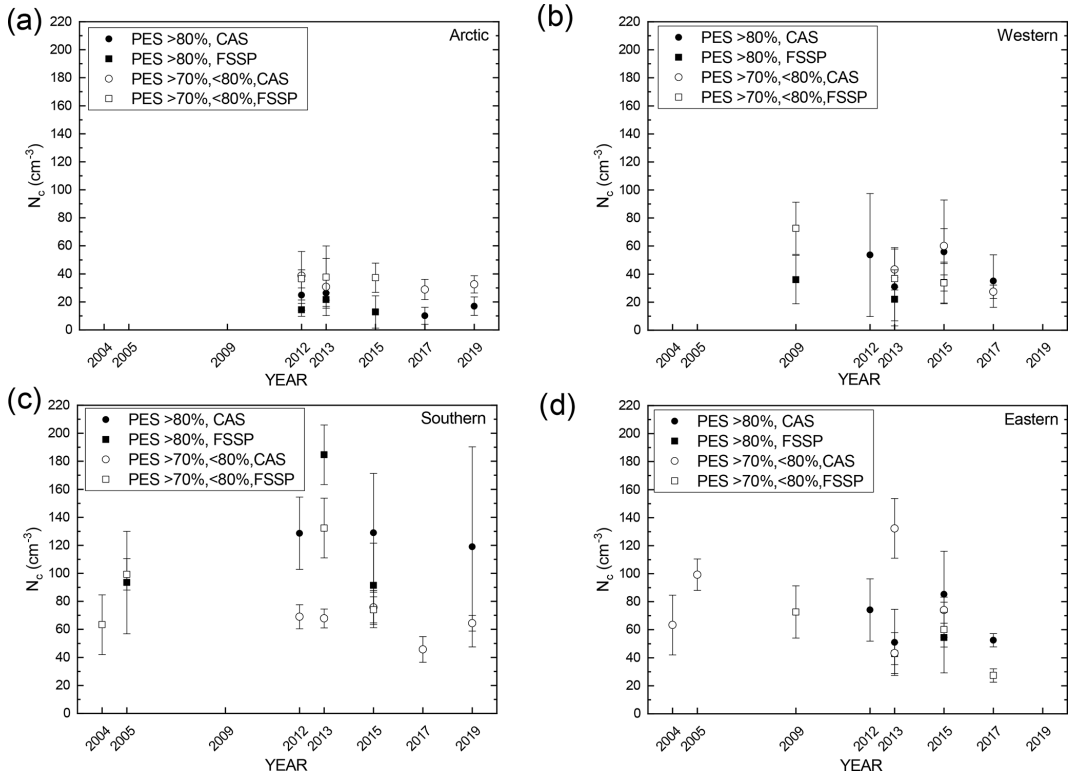

Figure 7. Cloud droplet number concentration (N_c) for each region and single PaCE campaign measured by the cloud and aerosol spectrometer (CAS) and the forward-scattering spectrometer probe (FSSP) where the PES fraction was within one region >80 % (full symbols) and the PES fraction was within one region from 70 % to 80 % (open symbols). Error bars indicate the corresponding standard deviation.

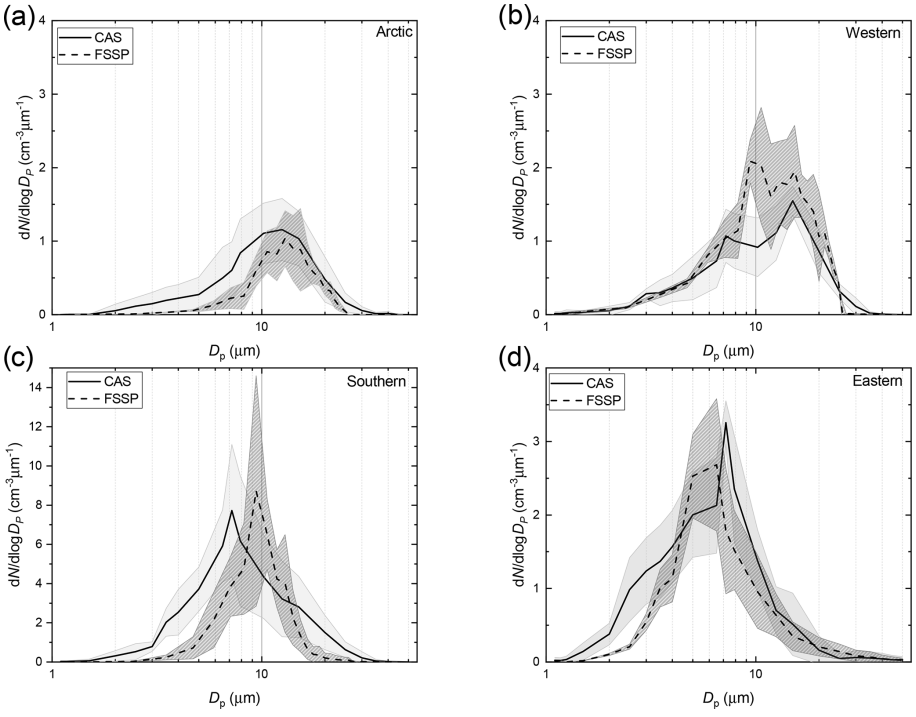

Figure 8. Cloud droplet size distribution associated with the **(a)** Arctic, **(b)** Western, **(c)** Southern and **(d)** Eastern region measured by the cloud and aerosol spectrometer (CAS) and the forward-scattering spectrometer probe (FSSP) during all PaCEs.

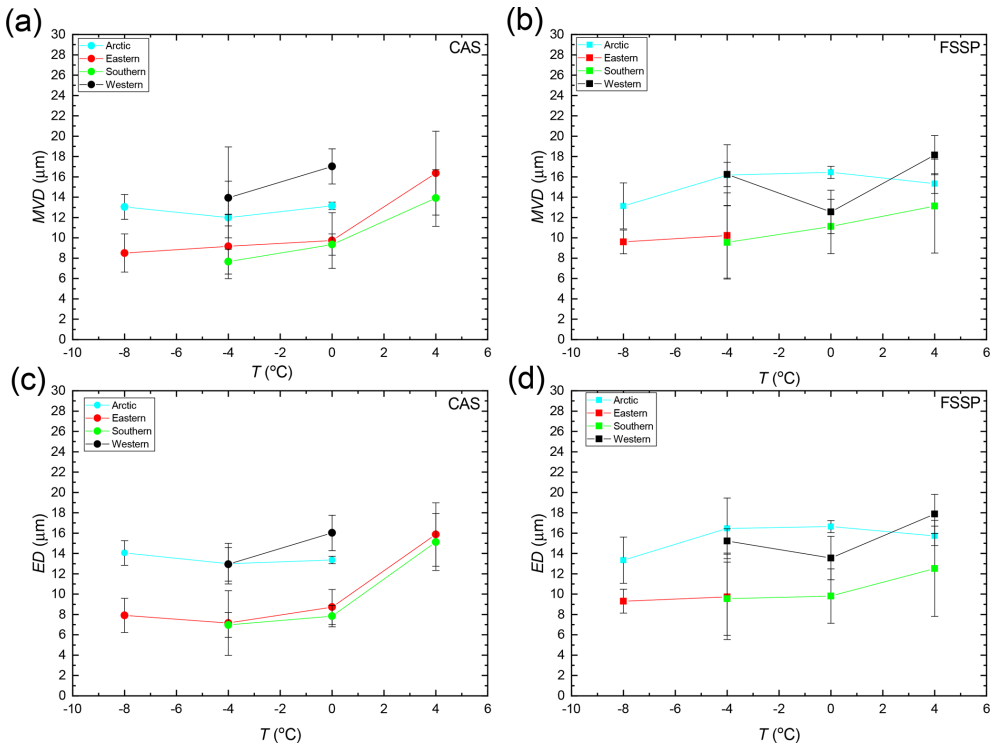

Figure 9. Hourly averages of median volume diameter (MVD) and effective diameter (ED) values versus temperature for all PaCE campaigns measured by the cloud and aerosol spectrometer (CAS) and the forward-scattering spectrometer probe (FSSP) where the PES fraction was within one region > 80 %. Solid lines were made to lead readers' eyes.

study, the LWC of continental air masses was, on average, larger than that of marine air masses. This is also reflected in the higher N_c of continental air masses (Fig. 7), as LWC is a function of both N_c and the size of cloud droplets. In Fig. 10b, the relation between the N_c and MVD is plotted. The points were divided into three different levels according to the measured LWC. The values of MVD ranged from ∼ 9 to 19 µm. MVD was larger for higher values of LWC and decreased with an increasing cloud droplet number concentration for each LWC category. The LWC values of the clouds we sampled (∼ 0.03 g m^{-3} for marine and ∼ 0.06 g m^{-3} for continental conditions) are comparable to those observed in several other in situ cloud studies (e.g., Gultepe and Isaac, 1997; Zhao et al., 2012; Lu et al., 2014; Guyot et al., 2015; Dionne et al., 2020).

3.4 Influence of the vertical position of the probe on the derived parameters

In this section, we focus on investigating how the derived parameters change with changes in the vertical position (altitude) of the sampling probe, H (m) (e.g., Martins et al., 2011; MacDonald et al., 2018; Alexandrov et al., 2020). Under theoretical adiabatic conditions, the vertical profile of LWC is expected to increase linearly with height above cloud base, with a constant gradient that is dependent on the temperature and pressure at cloud base (Brenguier, 1991). N_c is constant through the vertical profile of the cloud layer, while the size of the droplets increases with altitude (Pawlowska et al., 2006). Assuming homogenous mixing, this expectation of the cloud microphysical profile also holds for "scaled-adiabatic" conditions which include the entrainment of drier air (Boers et al., 2000). In reality, there are more processes to consider, which lead to departures from this ideal condition, particularly towards the cloud top (Pawlowska et al., 2006). As already discussed in Sect. 2.2, both ground-based spectrometers were fixed in one vertical position. Thus, there were cases that we sampled with different layers of a cloud in a range of 120 m from the cloud base. The ground-based spectrometers were placed at the Sammaltunturi, 210 m above the ceilometer (installed at the Kenttärova site). Kenttärova is located 4.3 km to the east of the hilltop station, Sammaltunturi. Since the Sammaltunturi station is on the top of an Arctic fell, cloud formation and properties could also be influenced by the local topography via changes in turbulence or orographic flows. The ceilometer's resolution in estimation of the cloud base was 30 m.

In Fig. 11, a statistical description of MVD is presented, derived from both cloud spectrometers at five different altitudes above cloud base. The distance of the cloud spectrometer was relative to the cloud base. From this analysis, it is apparent that there was no strong dependency between the ver-

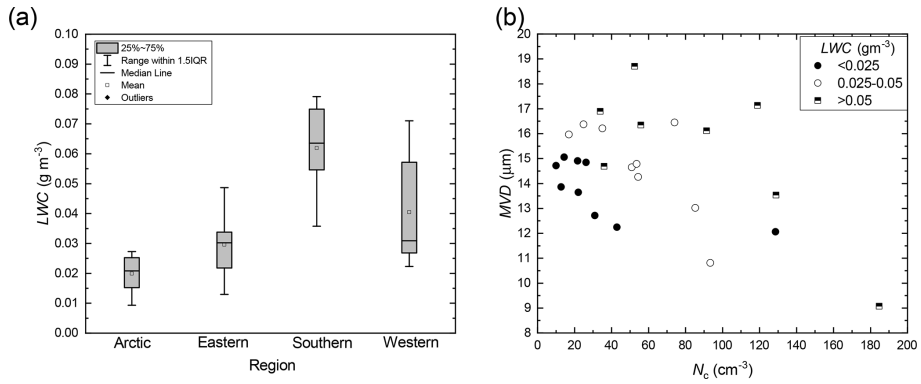

Figure 10. **(a)** Statistical description of liquid water content (LWC) for each region measured by the cloud and aerosol spectrometer (CAS) and the forward-scattering spectrometer probe (FSSP) where PES was within one region > 80 %. **(b)** Median volume diameter (MVD) as a function of total cloud droplet number concentration (N_c) for three different categories of LWC. Each point represents a single PaCE campaign for different regions.

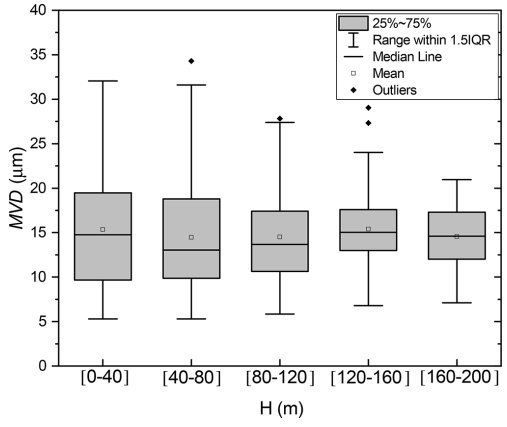

Figure 11. Statistical description of hourly averages of median volume diameter (MVD) measured by the cloud and aerosol spectrometer (CAS) and the forward-scattering spectrometer probe (FSSP) where PES was within one region > 80 % for five different levels of the position of the probes inside the cloud (H) (relative distance of the cloud ground-based spectrometer). Cloud base was measured at the Kenttärova station.

tical position of CAS and FSSP in the cloud and the derived sizing parameters. It is expected that number concentration provides a robust signal and can clearly be linked to air mass origin, whereas MVD and ED have some extra uncertainties depending on the altitude with respect to cloud base.

4 Summary and conclusions

Our main goal during this work was to quantify the effect of air mass origin on cloud microphysical properties in a clean subarctic environment. Thus, the impact of different air masses on cloud properties in the subarctic Finland was investigated based on data from eight Pallas Cloud Experiments (PaCEs) made during 2004–2019. For measuring the cloud microphysical properties, we deployed two cloud ground-based spectrometer probes: the cloud and aerosol spectrometer and the forward-scattering spectrometer probe. For performing the air mass source classification, the FLEXPART model was used with ERA5 meteorology. The air mass source regions were categorized into Arctic, Eastern, Southern, Western and Local sectors, with the Arctic and Western sectors representing marine air masses and the Eastern, Southern and Local sectors representing continental air masses.

Our analysis demonstrated that different air mass types had significant impacts on cloud microphysics. When 80 % of the potential emission sensitivity fraction was within a region, the observations were considered representative of that air mass type. Continental air masses led to the highest cloud droplet number concentrations ($\sim$ 100–200 cm^{-3}) and marine air masses to the lowest ones ($\sim$ 20 cm^{-3}). The lowest values of cloud droplet concentration were related to clean Arctic air masses. We observed a clear relationship between air mass origin and cloud droplet number concentration. This connection is expected to be a robust signal as according to theoretical considerations (Brenguier 1991; Pawlowska et al., 2006), the measurements of cloud droplet number concentration do not depend on the vertical position of the cloud spectrometer within the cloud layer. In general, the median volume diameter and effective diameter of cloud droplets were found to be influenced by the cloud droplet number concentration: clouds associated with marine air masses had larger cloud droplets (ranging from 15 to 20 µm) in comparison with continental clouds (ranging from 8 to 12 µm). These results are in agreement with the Twomey effect (Twomey, 1977). The above differences that were observed in cloud microphysical properties when the air masses were related to different regions show the need to investigate how the aerosol loading and meteorology of different air masses along with local meteorological parameters

change the cloud microphysics and to what scale. Furthermore, there was an indication that cloud droplets in clouds in warmer air (from −2 to 6 °C) were more prone to growing. However, all-year-round in situ cloud measurements in the area are of high importance to confirm such temperature dependency of droplet sizes. Specifically, a large dataset containing a wider temperature range needs to be obtained.

Data availability. The cloud probes and meteorological data used here are available in the Finnish Meteorological Institute (FMI) open data repository for each campaign and each cloud spectrometer ground setup individually (Doulgeris et al., 2021: https://doi.org/10.23728/fmi-b2share.988739d21b824c709084e88ed6c6d54b, Doulgeris et al., 2022: https://doi.org/10.5194/essd-14-637-2022). The FLEXPART simulations and the ceilometer dataset are available upon request to the corresponding author (konstantinos.doulgeris@fmi.fi).

Supplement. The supplement related to this article is available online at: https://doi.org/10.5194/acp-23-2483-2023-supplement.

Author contributions. KMD wrote the paper with contributions from all co-authors. HL planned and coordinated PaCE 2004, 2005 and 2009. HL and DB planned and coordinated PaCE 2012 and 2013. KMD and DB planned and coordinated PaCE 2015, 2017 and 2019. KMD and DB processed, analyzed and quality-controlled the dataset. VV carried out the FLEXPART simulations. EJO'C provided the ceilometer data. VMK reviewed and edited the manuscript.

Competing interests. The contact author has declared that none of the authors has any competing interests.

Disclaimer. Publisher's note: Copernicus Publications remains neutral with regard to jurisdictional claims in published maps and institutional affiliations.

Acknowledgements. This work was supported by the Koneen Säätiö (grant no. 46-6817) and the Academy of Finland Flagship funding (grant no. 337552). This project has also received funding from the European Union, H2020 Research and Innovation program (ACTRIS-IMP, the European Research Infrastructure for the observation of Aerosol, Clouds, and Trace gases (grant no. 871115)). The authors wish to acknowledge CSC – IT Center for Science, Finland, for computational resources. The authors would also like to thank all the people who have helped in PaCE campaign measurements throughout the years.

Financial support. This research has been supported by the Academy of Finland (grant no. 337552), the KONE Foundation (grant no. 46-6817) and Horizon 2020 (ACTRIS IMP (grant no. 871115)).

Review statement. This paper was edited by Matthias Tesche and reviewed by two anonymous referees.

References

Aalto, T., Hatakka, J., and Viisanen, Y.: Influence of air mass source sector on variations in CO_2 mixing ratio at a boreal site in northern Finland, Boreal Environ. Res., 8, 285–393, 2003.

Albrecht, B. A.: Aerosols, cloud microphysics, and fractional cloudiness, Science, 245, 1227–1230, 1989.

Alexandrov, M. D., Miller, D. J., Rajapakshe, C., Fridlind, A., van Diedenhoven, B., Cairns, B., Ackerman, A., and Zhang, S: Vertical profiles of droplet size distributions derived from cloud-side observations by the research scanning polarimeter: Tests on simulated data, Atmos. Res., 239, 104924, https://doi.org/10.1016/j.atmosres.2020.104924, 2020.

Andronache, C.: Mixed-phase Clouds: Observations and Modeling, Elsevier, Saint Louis, proQuest Ebook Central, https://ebookcentral.proquest.com/lib/fmi/detail.action?docID=5064425 (last access: 16 January 2023), 2017.

Anttila, T., Brus, D., Jaatinen, A., Hyvärinen, A.-P., Kivekäs, N., Romakkaniemi, S., Komppula, M., and Lihavainen, H.: Relationships between particles, cloud condensation nuclei and cloud droplet activation during the third Pallas Cloud Experiment, Atmos. Chem. Phys., 12, 11435–11450, https://doi.org/10.5194/acp-12-11435-2012, 2012.

Asmi, E., Kivekäs, N., Kerminen, V.-M., Komppula, M., Hyvärinen, A.-P., Hatakka, J., Viisanen, Y., and Lihavainen, H.: Secondary new particle formation in Northern Finland Pallas site between the years 2000 and 2010, Atmos. Chem. Phys., 11, 12959–12972, https://doi.org/10.5194/acp-11-12959-2011, 2011.

Barrie, L. A.: Arctic air pollution: an overview of current knowledge, Atmos. Environ., 20, 643–663, 1986.

Barthlott, C. and Hoose, C.: Aerosol effects on clouds and precipitation over central Europe in different weather regimes, J. Atmos. Sci., 75, 4247–4264, https://doi.org/10.1175/JAS-D-18-0110.1, 2018.

Baumgardner, D.: An analysis and comparison of five water droplet measuring instruments, J. Appl. Meteorol., 22, 891–910, https://doi.org/10.1175/1520-0450(1983)022<0891:AAACOF>2.0.CO;2, 1983.

Baumgardner, D., Jonsson, H., Dawson, W., O'Connor, D., and Newton, R.: The cloud, aerosol and precipitation spectrometer (CAPS): A new instrument for cloud investigations, Atmos. Res., 59–60, 251–264, https://doi.org/10.1016/S0169-8095(01)00119-3, 2001.

Baumgardner, D., Abel, S. J., Axisa, D., Cotton, R., Crosier, J., Field, P., Gurganus, C., Heymsfield, A., Korolev, A., Krämer, M., Lawson, P., McFarquhar, G., Ulanowski, Z., and Um, J.: Cloud Ice Properties: In Situ Measurement Challenges, Meteor. Mon., 58, 9.1–9.23, https://doi.org/10.1175/AMSMONOGRAPHS-D-16-0011.1, 2017.

Boers, R., Russchenberg, H., Erkelens, J., Venema, V., van Lammeren, A., Apituley, A., and Jongen, S.: Ground-based remote

sensing of stratocumulus properties during CLARA, 1996, J. Appl. Meteorol., 39, 169–181, 2000.

Boucher, O., Randall, D., Artaxo, P., Bretherton, C., Feingold, G., Forster, P., Kerminen, V.-M., Kondo, Y., Liao, H., Lohmann, U., Rasch, P., Satheesh, S. K., Sherwood, S., Stevens, B., and Zhang, X. Y.: Chapter 7 – Clouds and aerosols, in: Climate Change 2013: The Physical Science Basis. Contribution of Working Group I to the Fifth Assessment Report of the Intergovernmental Panel on Climate Change, edited by: Stocker, T. F., Qin, D., Plattner, G.-K., Tignor, M., Allen, S. K., Doschung, J., Nauels, A., Xia, Y., Bex, V., and Midgley, P. M., Cambridge University Press, Cambridge, 571–657, https://doi.org/10.1017/CBO9781107415324.016, 2013.

Brenguier, J. L.: Coincidence and Dead-Time Corrections for Particles Counters. Part II: High Concentration Measurements with an FSSP, J. Atmos. Ocean. Tech., 6, 585–598, https://doi.org/10.1175/1520-0426(1989)006<0585:CADTCF>2.0.CO;2, 1989.

Brenguier, J. L.: Parameterization of the condensation process – A theoretical approach, J. Atmos. Sci., 48, 264–282, 1991.

Brus, D., Neitola, K., Asmi, E., Aurela, M., Makkonen, U., Svensson, J., Hyvärinen, A.-P., Hirsikkoa, A., Hakola, H., Hillamo, R., and Lihavainen, H.: Pallas cloud experiment, PACE 2012, AIP Conf. Proc., 1527, 964, https://doi.org/10.1063/1.4803433, 2013a.

Brus, D., Asmi, E., Raatikainen, T., Neitola, K., Aurela, M., Makkonen, U., Svensson, J., Hyvärinen, A.-P., Hirsikkoa, A., Hakola, H., Hillamo, R., and Lihavainen, H: Ground-based observations of aerosol and cloud properties at sub-arctic Pallas GAW-station, PAllas Cloud Experiment (PACE 2012) report series in aerosol science no. 142, in: Proceedings of FCoE in 'Physics, Chemistry, Biology and Meteorology of Atmospheric Composition and Climate Change' Annual Meeting, Helsinki, 2013, Proceedings_FCoE_2013, 187–191, http://www.faar.fi/wp-content/uploads/2020/04/RS142_Proceedings_FCoE_2013.pdf (last access: 16 January 2023), 2013b.

Chang, Y., Guo, X., Tang, J., and Lu, G.: Aircraft measurement campaign on summer cloud microphysical properties over the Tibetan Plateau, Sci. Rep., 9, 4912, https://doi.org/10.1038/s41598-019-41514-5, 2019.

Cho, Y., Park, S.-J., Kim, J.-H., Yeo, H., Nam, J., Jun, S.-Y., Kim, B.-M., and Kim, S.-W.: Investigating Wintertime Cloud Microphysical Properties and Their Relationship to Air Mass Advection at Ny-Ålesund, Svalbard Using the Synergy of a Cloud Radar–Ceilometer–Microwave Radiometer, Remote Sens., 13, 2529, https://doi.org/10.3390/rs13132529, 2021.

Devenish, B. J., Bartello, P., Brenguier, J.-L., Collins, L. R., Grabowski, W. W., Jzermans, R. H. A., Malinowski, S. P., Reeks, M. W., Vassilicos, J. C., Wang, L.-P., and Warhaft, Z.: Droplet growth in warm turbulent clouds, Q. J. Roy. Meteor. Soc., 138, 1401–1429, https://doi.org/10.1002/qj.1897, 2012.

Dionne, J., von Salzen, K., Cole, J., Mahmood, R., Leaitch, W. R., Lesins, G., Folkins, I., and Chang, R. Y.-W.: Modelling the relationship between liquid water content and cloud droplet number concentration observed in low clouds in the summer Arctic and its radiative effects, Atmos. Chem. Phys., 20, 29–43, https://doi.org/10.5194/acp-20-29-2020, 2020.

Donovan, D. P., Klein Baltink, H., Henzing, J. S., de Roode, S. R., and Siebesma, A. P.: A depolarisation lidar-based method for the determination of liquid-cloud microphysical properties, Atmos. Meas. Tech., 8, 237–266, https://doi.org/10.5194/amt-8-237-2015, 2015.

Doulgeris, K.-M., Komppula, M., Romakkaniemi, S., Hyvärinen, A.-P., Kerminen, V.-M., and Brus, D.: In situ cloud ground-based measurements in the Finnish sub-Arctic: intercomparison of three cloud spectrometer setups, Atmos. Meas. Tech., 13, 5129–5147, https://doi.org/10.5194/amt-13-5129-2020, 2020.

Doulgeris, K.-M., Lihavainen, H., Hyvärinen, A.-P., Kerminen, V.-M., and Brus, D.: Data set for Doulgeris et al. 2021: In-situ microphysical characterization of low-level clouds in the Finnish sub-Arctic, extensive dataset, Finnish Meteorological Institute [data set], https://doi.org/10.23728/fmi-b2share.988739d21b824c709084e88ed6c6d54b, 2021.

Doulgeris, K. M., Lihavainen, H., Hyvärinen, A.-P., Kerminen, V.-M., and Brus, D.: An extensive data set for in situ microphysical characterization of low-level clouds in a Finnish sub-Arctic site, Earth Syst. Sci. Data, 14, 637–649, https://doi.org/10.5194/essd-14-637-2022, 2022.

Droplet Measurement Technologies (DMT): Manual: Particle Analysis and Display System (PADS) Image Probe Data Reference Manual DOC-0201 Rev A-2 PADS 2.5.6, DMT, Boulder, Colorado, USA, 2009.

Emeis, S., Münkel, C., Vogt, S., Müller, W. J., and Schäfer, K.: Atmospheric boundary-layer structure from simultaneous SODAR, RASS and ceilometer measurements, Atmos. Environ., 38, 273–286, 2004

Eneroth, K., Kjellström, E. and Holmén, K.: A trajectory climatology for Svalbard; investigating how atmospheric flow patterns influence observed tracer concentrations, Phys. Chem. Earth, 28, 1191–1203, https://doi.org/10.1016/j.pce.2003.08.051, 2003.

Eneroth, K., Aalto, T., Hatakka, J., Holmen, K., Laurila, T., and Viisanen, Y.: Atmospheric transport of carbon dioxide to a baseline monitoring station in northern Finland, Tellus B, 57, 366–374, https://doi.org/10.1111/j.1600-0889.2005.00160.x, 2005.

Filioglou, M., Mielonen, T., Balis, D., Giannakaki, E., Arola, A., Kokkola, H., Komppula, M., and Romakkaniemi, S.: Aerosol Effect on the Cloud Phase of Low-Level Clouds Over the Arctic, J. Geophys. Res.-Atmos., 124, 7886–7899, https://doi.org/10.1029/2018JD030088, 2019.

Freud, E., Rosenfeld, D., Andreae, M. O., Costa, A. A., and Artaxo, P.: Robust relations between CCN and the vertical evolution of cloud drop size distribution in deep convective clouds, Atmos. Chem. Phys., 8, 1661–1675, https://doi.org/10.5194/acp-8-1661-2008, 2008.

Freud, E., Krejci, R., Tunved, P., Leaitch, R., Nguyen, Q. T., Massling, A., Skov, H., and Barrie, L.: Pan-Arctic aerosol number size distributions: seasonality and transport patterns, Atmos. Chem. Phys., 17, 8101–8128, https://doi.org/10.5194/acp-17-8101-2017, 2017.

Fuchs, J., Cermak, J., Andersen, H., Hollmann, R., and Schwarz, K.: On the influence of air mass origin on low-cloud properties in the Southeast Atlantic, J. Geophys. Res.,-Atmos., 122, 11076–11091, https://doi.org/10.1002/2017JD027184, 2017.

Gérard, V., Noziere, B., Fine, L., Ferronato, C., Singh, D., K., Frossard, A., Cohen, R. C. Asmi, E., Lihavainen, H., Kivekäs, N., Aurela, M., Brus, D., Frka, S., and Cvitešić Kušan, A.: Concentrations and Adsorption Isotherms for Amphiphilic Surfactants in PM_1 Aerosols from Different Re-

gions of Europe, Environ. Sci. Technol., 53, 12379–12388, https://doi.org/10.1021/acs.est.9b03386, 2019.

Girdwood, J., Smith, H., Stanley, W., Ulanowski, Z., Stopford, C., Chemel, C., Doulgeris, K.-M., Brus, D., Campbell, D., and Mackenzie, R.: Design and field campaign validation of a multi-rotor unmanned aerial vehicle and optical particle counter, Atmos. Meas. Tech., 13, 6613–6630, https://doi.org/10.5194/amt-13-6613-2020, 2020.

Girdwood, J., Stanley, W., Stopford, C., and Brus, D.: Simulation and field campaign evaluation of an optical particle counter on a fixed-wing UAV, Atmos. Meas. Tech., 15, 2061–2076, https://doi.org/10.5194/amt-15-2061-2022, 2022.

Goren, T. and Rosenfeld, D.:Decomposing aerosol cloud radiative effects into cloud cover, liquid water path and Twomey components in marine stratocumulus, Atmos. Res., 138, 378–393, https://doi.org/10.1016/j.atmosres.2013.12.008, 2014.

Gultepe, I. and Isaac, G. A.: Liquid water content and temperature relationship from aircraft observations and its applicability to GCMs, J. Climate, 10, 447–452, https://doi.org/10.1175/1520-0442(1997)010<0446:LWCATR>2.0.CO;2, 1997.

Gultepe, I. and Isaac, G. A.: Effects of air mass origin on Arctic cloud microphysical parameters for April 1998 during FIRE.ACE, J. Geophys. Res., 107, SHE 4-1–SHE 4-12, https://doi.org/10.1029/2000JC000440, 2002.

Gultepe, I., Isaac, G., Hudak, D., Nissen, R., and Strapp, W.: Dynamical and microphysical characteristics of Arctic clouds during BASE, J. Climate, 13, 1225–1254, 2000.

Guyot, G., Gourbeyre, C., Febvre, G., Shcherbakov, V., Burnet, F., Dupont, J.-C., Sellegri, K., and Jourdan, O.: Quantitative evaluation of seven optical sensors for cloud microphysical measurements at the Puy-de-Dôme Observatory, France, Atmos. Meas. Tech., 8, 4347–4367, https://doi.org/10.5194/amt-8-4347-2015, 2015.

Hatakka, J., Aalto, T., Aaltonen, V., Aurela, M., Hakola, H., Komppula, M., Laurila, T., Lihavainen, H., Paatero, J., Salminen, K., and Viisanen Y.: Overview of the atmospheric research activities and results at Pallas GAW station, Boreal Environ. Res., 8, 365–384, 2003.

Hobbs, P. V. and Rangno, A. L.: Reply to "Comments by Alan M. Blyth and John Latham on 'Cumulus glaciation papers by P. V. Hobbs and A. L. Rangno'", Q. J. Roy. Meteor. Soc., 124, 1009–1011, 1998.

Hyvärinen, A.-P., Kolmonen, P., Kerminen, V.-M., Virkkula, A., Leskinen, A., Komppula, M., Hatakka, J., Burkhart, J., Stohl, A., Aalto, P., Kulmala, M., Lehtinen, K., Viisanen, Y., and Lihavainen, H.: Aerosol black carbon at five background measurement sites over Finland, a gateway to the Arctic, Atmos. Environ., 45, 4042–4050, 2011.

Igel, A. L. and van den Heever, S. C.: The Importance of the Shape of Cloud Droplet Size Distributions in Shallow Cumulus Clouds. Part I: Bin Microphysics Simulations, J. Atmos. Sci., 74, 249–258, https://doi.org/10.1175/JAS-D-15-0382.1, 2017a.

Igel, A. L. and van den Heever, S. C.: The Importance of the Shape of Cloud Droplet Size Distributions in Shallow Cumulus Clouds. Part II: Bulk Microphysics Simulations, J. Atmos. Sci., 74, 259–273, https://doi.org/10.1175/JAS-D-15-0383.1, 2017b.

Iwamoto, Y., Watanabe, A., Kataoka, R., Uematsu, M., and Miura, K.: Aerosol–Cloud Interaction at the Summit of Mt. Fuji, Japan: Factors Influencing Cloud Droplet Number Concentrations, Appl. Sci., 11, 8439, https://doi.org/10.3390/app11188439, 2021.

Jaatinen, A., Romakkaniemi, S., Anttila, T., Hyvärinen, A.-P., Hao, L. Q., Kortelainen, A., Miettinen, P., Mikkonen, S., Smith, J. N., Virtanen, A., and Laaksonen, A.: The third Pallas Cloud Experiment: Consistency between the aerosol hygroscopic growth and CCN activity, Boreal Environ. Res., 19, 368–382, 2014.

Komppula, M., Lihavainen, H., Hatakka, J., Paatero, J., Aalto, P., Kulmala, M., and Viisanen, Y.: Observations of new particle formation and size distributions at two different heights and surroundings in subarctic area in northern Finland, J. Geophys. Res., 108, 4295, https://doi.org/10.1029/2002JD002939, 2003.

Korolev, A., McFarquhar, G., Field, P. R., Franklin, C., Lawson, P., Wang, Z., Williams, E., Abel, S. J., Axisa, D., Borrmann, S., Crosier, J., Fugal, J., Krämer, M., Lohmann, U., Schlenczek, O., Schnaiter, M., and Wendisch, M.: Mixed-Phase Clouds: Progress and Challenges, Meteorol. Mon., 58, 5.1–5.50, 2017.

Kyrö, E.-M., Väänänen, R., Kerminen, V.-M., Virkkula, A., Petäjä, T., Asmi, A., Dal Maso, M., Nieminen, T., Juhola, S., Shcherbinin, A., Riipinen, I., Lehtipalo, K., Keronen, P., Aalto, P. P., Hari, P., and Kulmala, M.: Trends in new particle formation in eastern Lapland, Finland: effect of decreasing sulfur emissions from Kola Peninsula, Atmos. Chem. Phys., 14, 4383–4396, https://doi.org/10.5194/acp-14-4383-2014, 2014.

Lance, S.: Coincidence Errors in a Cloud Droplet Probe (CDP) and a Cloud and Aerosol Spectrometer (CAS), and the Improved Performance of a Modified CDP, J. Atmos. Ocean. Tech., 29, 1532–1541, https://doi.org/10.1175/JTECH-D-11-00208.1, 2012.

Lee, H. J., Jo, Y. J., Kim, S., Kim, D., Kim, J., Choi, D., Jo, H., Bak, J., Park, S., Jeon, W., and Kim, C.-H.: Transboundary aerosol transport process and its impact on aerosol-radiation-cloud feedbacks in springtime over Northeast Asia, Sci. Rep., 12, 4870, https://doi.org/10.1038/s41598-022-08854-1, 2022.

Lihavainen, H., Kerminen, V.-M., Komppula, M., Hyvärinen, A.-P., Laakia, J., Saarikoski, S., Makkonen, U., Kivekäs, N., Hillamo, R., Kulmala, M., and Viisanen, Y.: Measurements of the relation between aerosol properties and microphysics and chemistry of low level liquid water clouds in Northern Finland, Atmos. Chem. Phys., 8, 6925–6938, https://doi.org/10.5194/acp-8-6925-2008, 2008.

Lohila, A., Penttilä, T., Jortikka, S., Aalto, T., Anttila, P., Asmi, E., Aurela, M., Hatakka, J., Hellén, H., Henttonen, H., Hänninen, P., Kilkki, J., Kyllönen, K., Laurila, T., Lepistö, A., Lihavainen, H., Makkonen, U., Paatero, J., Rask, M., Sutinen, R., Tuovinen, J.-P., Vuorenmaa, J., and Viisanen, Y.: Preface to the special issue on integrated research of atmosphere, ecosystems and environment at Pallas, Boreal Environ. Res., 20, 431–454, 2015.

Lohmann, U., Lüönd, F., and Mahrt, F.: Microphysical processes in warm clouds, in: An Introduction to Clouds: From the Microscale to Climate, Cambridge University Press, Cambridge, 186–217, https://doi.org/10.1017/CBO9781139087513.008, 2016.

Lu, C., Liu, Y., Niu, S., and Endo, S.: Scale dependence of entrainment-mixing mechanisms in cumulus clouds, J. Geophys. Res.-Atmos., 119, 13877–13890, 2014.

MacDonald, A. B., Dadashazar, H., Chuang, P. Y., Crosbie, E., Wang, H., Wang, Z., Jonsson, H. H., Flagan, R. C., Seinfeld, J. H., and Sorooshian, A.: Characteristic Vertical Profiles of Cloud Water Composition in Marine Stratocumulus Clouds and Re-

lationships With Precipitation, J. Geophys. Res.-Atmos., 123, 3704–3723, https://doi.org/10.1002/2017JD027900, 2018

Martins, J. V., Marshak, A., Remer, L. A., Rosenfeld, D., Kaufman, Y. J., Fernandez-Borda, R., Koren, I., Correia, A. L., Zubko, V., and Artaxo, P.: Remote sensing the vertical profile of cloud droplet effective radius, thermodynamic phase, and temperature, Atmos. Chem. Phys., 11, 9485–9501, https://doi.org/10.5194/acp-11-9485-2011, 2011.

McFarquhar, G. M., Bretherton, C., Marchand, R., Protat, A., DeMott, P. J., Alexander, S. P., Roberts, G. C., Twohy, C. H., Toohey, D., Siems, S., Huang, Y., Wood, R., Rauber, R. M., Lasher-Trapp, S., Jensen, J., Stith, J., Mace, J., Um, J., Järvinen, E., Schnaiter, M., Gettelman, A., Sanchez, K. J., McCluskey, C. S., Russell, L. M., McCoy, I. L., Atlas, R., Bardeen, C. G., Moore, K. A., Hill, T. C. J., Humphries, R. S., Keywood, M. D., Ristovski, Z., Cravigan, L., Schofield, R., Fairall, C., Mallet, M. D., Kreidenweis, S. M., Rainwater, B., D'Alessandro, J., Wang, Y., Wu, W., Saliba, G., Levin, E. J. T., Ding, S., Lang, F., Truong, S. C., Wolff, C., Haggerty, J., Harvey, M. J., Klekociuk, A., and McDonald, A.: Observations of clouds, aerosols, precipitation, and surface radiation over the Southern Ocean: An overview of CAPRICORN, MARCUS, MICRE and SOCRATES, B. Am. Meteorol. Soc., 102, E894–E928, https://doi.org/10.1175/BAMS-D-20-0132.1, 2020.

Mie, G.: Beiträge zur Optik trüber Medien, speziell kolloidaler Metallösungen, Ann. Phys.-Berlin, 330, 377–445, 1908.

Morrison, H., van Lier-Walqui, M., Fridlind, A. M., Grabowski, W. W., Harrington, J. Y., Hoose, C., Korolev, A., Kumjian, M. R., Milbrandt, J. A., Pawlowska, H., Posselt, D. J., Prat, O. P., Reimel, K. J., Shima, S.-I., Van Diedenhoven, B., and Xue, L.: Confronting the challenge of modeling cloud and precipitation microphysics, J. Adv. Model. Earth Sy., 12, e2019MS001689, https://doi.org/10.1029/2019MS001689, 2020.

Orbe, C., Newman, P. A., Waugh, D. W., Holzer, M., Oman, L. D., Li, F., and Polvani, L. M.: Airmass Origin in the Arctic. Part I: Seasonality, J. Climate, 28, 4997–5014, https://doi.org/10.1175/JCLI-D-14-00720.1, 2015a.

Orbe, C., Newman, P. A., Waugh, D. W., Holzer, M., Oman, L. D., Li, F., and Polvani, L. M.: Air-mass Origin in the Arctic. Part II: Response to Increases in Greenhouse Gases, J. Climate, 28, 9105–9120, https://doi.org/10.1175/JCLI-D-15-0296.1, 2015b.

Paramonov, M., Kerminen, V.-M., Gysel, M., Aalto, P. P., Andreae, M. O., Asmi, E., Baltensperger, U., Bougiatioti, A., Brus, D., Frank, G. P., Good, N., Gunthe, S. S., Hao, L., Irwin, M., Jaatinen, A., Jurányi, Z., King, S. M., Kortelainen, A., Kristensson, A., Lihavainen, H., Kulmala, M., Lohmann, U., Martin, S. T., McFiggans, G., Mihalopoulos, N., Nenes, A., O'Dowd, C. D., Ovadnevaite, J., Petäjä, T., Pöschl, U., Roberts, G. C., Rose, D., Svenningsson, B., Swietlicki, E., Weingartner, E., Whitehead, J., Wiedensohler, A., Wittbom, C., and Sierau, B.: A synthesis of cloud condensation nuclei counter (CCNC) measurements within the EUCAARI network, Atmos. Chem. Phys., 15, 12211–12229, https://doi.org/10.5194/acp-15-12211-2015, 2015.

Painemal, D., Kato, S., and Minnis, P.: Boundary layer regulation in the southeast Atlantic cloud microphysics during the biomass burning season as seen by the A-train satellite constellation, J. Geophys. Res.-Atmos., 119, 11288–11302, https://doi.org/10.1002/2014JD022182, 2014.

Patel, P. N. and Jiang, H. J.: Cloud condensation nuclei characteristics at the Southern Great Plains site: role of particles size distribution and aerosol hygroscopicity, Environ. Res. Commun., 3, 075002, https://doi.org/10.1088/2515-7620/ac0e0b, 2021.

Pawlowska, H., Grabowski, W. W., and Brenguier, J.-L.: Observations of the width of cloud droplet spectra in stratocumulus, Geophys. Res. Lett., 33, L19810, https://doi.org/10.1029/2006GL026841, 2006.

Pernov, J. B., Beddows, D., Thomas, D. C., Dall'Osto, M., Harrison, R. M., Schmale, J., Skov, H., and Massling, A.: Increased aerosol concentrations in the High Arctic attributable to changing atmospheric transport patterns, npj Climate and Atmospheric Science, 5, 62, https://doi.org/10.1038/s41612-022-00286-y, 2022.

Pisso, I., Sollum, E., Grythe, H., Kristiansen, N. I., Cassiani, M., Eckhardt, S., Arnold, D., Morton, D., Thompson, R. L., Groot Zwaaftink, C. D., Evangeliou, N., Sodemann, H., Haimberger, L., Henne, S., Brunner, D., Burkhart, J. F., Fouilloux, A., Brioude, J., Philipp, A., Seibert, P., and Stohl, A.: The Lagrangian particle dispersion model FLEXPART version 10.4, Geosci. Model Dev., 12, 4955–4997, https://doi.org/10.5194/gmd-12-4955-2019, 2019.

Pruppacher, H. R. and Klett, J. D.: Microphysics of Clouds and Precipitation, 2nd edn., Springer, Dordrecht, Netherlands, ISBN 978-0-7923-4211-3, ISBN 978-0-306-48100-0, https://doi.org/10.1007/978-0-306-48100-0, 2010.

Raatikainen, T., Brus, D., Hyvärinen, A.-P., Svensson, J., Asmi, E., and Lihavainen, H.: Black carbon concentrations and mixing state in the Finnish Arctic, Atmos. Chem. Phys., 15, 10057–10070, https://doi.org/10.5194/acp-15-10057-2015, 2015.

Raatz, W. E. and Shaw, G. E.: Long-range tropospheric transport of pollution aerosols into the Alaskan Arctic, J. Appl. Meteorol. Clim., 23, 1052–1064, 1984.

Rosenfeld, D. and Ulbrich, C. W.: Cloud Microphysical Properties, Processes, and Rainfall Estimation Opportunities, Meteor. Mon., 30, 237–237, https://doi.org/10.1175/0065-9401(2003)030<0237:CMPPAR>2.0.CO;2, 2003.

Rosenfeld, D., Sherwood, S., Wood, R., and Donner, L.: Climate effects of aerosol-cloud interactions, Science, 343, 379–380, https://doi.org/10.1126/science.1247490, 2014.

Seibert, P. and Frank, A.: Source-receptor matrix calculation with a Lagrangian particle dispersion model in backward mode, Atmos. Chem. Phys., 4, 51–63, https://doi.org/10.5194/acp-4-51-2004, 2004.

Sherwood, S., Webb, M. J., Annan, J. D., Armour, K. C., Forster, P. M., Hargreaves, J. C., Hegerl, G., Klein, S. A., Marvel, K. D., Rohling, E. J., Watanabe, M., Andrews, T., Braconnot, P., Bretherton, C. S., Foster, G. L., Hausfather, Z., von der Heydt, A. S., Knutti, R., Mauritsen, T., Norris, J. R., Proitosescu, C., Rugenstein, M., Schmidt, G. A., Tokarska, K. B., and Zelinka, M. D.: An assessment of Earth's climate sensitivity using multiple lines of evidence, Rev. Geophys., 58, e2019RG000678, https://doi.org/10.1029/2019RG000678, 2020.

Shupe, M. D., Rex, M., Blomquist, B., Persson, P. O. G., Schmale, J., Uttal, T., Althausen, D., Angot, H., Archer, S., Bariteau, L., Beck, I., Bilberry, J., Bucci, S., Buck, C., Boyer, M., Brasseur, Z., Brooks, I. M., Calmer, R., Cassano, J., Castro, V., Chu, D., Costa, D., Cox, C. J., Creamean, J., Crewell, S., Dahlke, S., Damm, E., de Boer, G., Deckelmann, H., Dethloff, K., Dütsch, M., Ebell, K., Ehrlich, A., Ellis, J., Engelmann, R., Fong, A. A.,

Frey, M. M., Gallagher, M. R., Ganzeveld, L., Gradinger, R., Graeser, J., Greenamyer, V., Griesche, H., Griffiths, S., Hamilton, J., Heinemann, G., Helmig, D., Herber, A., Heuzé, C., Hofer, J., Houchens, T., Howard, D., Inoue, J., Jacobi, H.-W., Jaiser, R., Jokinen, T., Jourdan, O., Jozef, G., King, W., Kirchgaessner, A., Klingebiel, M., Krassovski, M., Krumpen, T., Lampert, A., Landing, W., Laurila, T., Lawrence, D., Lonardi, M., Loose, B., Lüpkes, C., Maahn, M., Macke, A., Maslowski, W., Marsay, C., Maturilli, M., Mech, M., Morris, S., Moser, M., Nicolaus, M., Ortega, P., Osborn, J., Pätzold, F., Perovich, D. K., Petäjä, T., Pilz, C., Pirazzini, R., Posman, K., Powers, H., Pratt, K. A., Preußer, A., Quéléver, L., Radenz, M., Rabe, B., Rinke, A., Sachs, T., Schulz, A., Siebert, H., Silva, T., Solomon, A., Sommerfeld, A., Spreen, G., Stephens, M., Stohl, A., Svensson, G., Uin, J., Viegas, J., Voigt, C., von der Gathen, P., Wehner, B., Welker, J. M., Wendisch, M., Werner, M., Xie, Z. Q., Yue, F.: Overview of the MOSAiC expedition: Atmosphere, Elementa: Science of the Anthropocene, 10, 00060, https://doi.org/10.1525/elementa.2021.00060, 2022.

Sipilä, M., Sarnela, N., Neitola, K., Laitinen, T., Kemppainen, D., Beck, L., Duplissy, E.-M., Kuittinen, S., Lehmusjärvi, T., Lampilahti, J., Kerminen, V.-M., Lehtipalo, K., Aalto, P. P., Keronen, P., Siivola, E., Rantala, P. A., Worsnop, D. R., Kulmala, M., Jokinen, T., and Petäjä, T.: Wintertime subarctic new particle formation from Kola Peninsula sulfur emissions, Atmos. Chem. Phys., 21, 17559–17576, https://doi.org/10.5194/acp-21-17559-2021, 2021.

Small, J. D., Chuang, P. Y., Feingold, G., and Jiang, H.: Can aerosol decrease cloud lifetime?, Geophys. Res. Lett., 36, L16806, https://doi.org/10.1029/2009GL038888, 2009.

Solomon, A. and Shupe, M. D.: A Case Study of Airmass Transformation and Cloud Formation at Summit, Greenland, J. Atmos. Sci., 76, 3095–3113, https://doi.org/10.1175/JAS-D-19-0056.1, 2019.

Stohl, A., Forster, C., Frank, A., Seibert, P., and Wotawa, G.: Technical note: The Lagrangian particle dispersion model FLEXPART version 6.2, Atmos. Chem. Phys., 5, 2461–2474, https://doi.org/10.5194/acp-5-2461-2005, 2005.

Torres-Delgado, E., Baumgardner, D., and Mayol-Bracero, O. L.: Measurement report: Impact of African aerosol particles on cloud evolution in a tropical montane cloud forest in the Caribbean, Atmos. Chem. Phys., 21, 18011–18027, https://doi.org/10.5194/acp-21-18011-2021, 2021.

Tunved, P., Hansson, H. C., Kerminen, V. M., Strom, J., Dal Maso, M., Lihavainen, H., Viisanen, Y., Aalto, P. P., Komppula, M., and Kulmala, M.: High natural aerosol loading over boreal forests, Science, 312, 261–263, https://doi.org/10.1126/science.1123052, 2006.

Twohy, C. H., Petters, M. D., Snider, J. R., Stevens, B., Tahnk, W., Wetzel, M., Russell, L., and Burnet, F.: Evaluation of the aerosol indirect effect in marine stratocumulus clouds: Droplet number, size, liquid water path, and radiative impact, J. Geophys. Res., 110, D08203, https://doi.org/10.1029/2004JD005116, 2005.

Twomey, S.: The Influence of Pollution on the Shortwave Albedo of Clouds, J. Atmos. Sci., 34, 1149–1152, https://doi.org/10.1175/1520-0469(1977)034<1149:TIOPOT>2.0.CO;2, 1977.

Vaisala Oyj: Ceilometer CT25K: User's Guide, Vaisala Oyj, Vantaa, Finland, 2002.

Virkkula, A., Hillamo, R. E., Kerminen, V.-M., and Stohl, A.: The influence of Kola Peninsula, continental European and marine sources on the number concentrations and scattering coefficients of the atmospheric aerosol in Finnish Lapland, Boreal Environ. Res., 2, 317–336, ISSN 1239-6095, 1997.

Wandinger, U., Apituley, A., Blumenstock, T., Bukowiecki, N., Cammas, J.-P., Connolly, P., De Mazière, M., Dils, B., Fiebig, M., Freney, E., Gallagher, M., Godin-Beekmann, S., Goloub, P., Gysel, M., Haeffelin, M., Hase, F., Hermann, M., Herrmann, H., Jokinen, T., Komppula, M., Kubistin, D., Langerock, B., Lihavainen, H., Mihalopoulos, N., Laj, P., Lund Myhre, C., Mahieu, E., Mertes, S., Möhler, O., Mona, L., Nicolae, D., O'Connor, E., Palm, M., Pappalardo, G., Pazmino, A., Petäjä, T., Philippin, S., Plass-Duelmer, C., Pospichal, B., Putaud, J.-P., Reimann, S., Rohrer, F., Russchenberg, H., Sauvage, S., Sellegri, K., Steinbrecher, R., Stratmann, F., Sussmann, R., Van Pinxteren, D., Van Roozendael, M., Vigouroux, C., Walden, C., Wegene, R., and Wiedensohler, A.: ACTRIS-PPP Deliverable D5.1: Documentation on technical concepts and requirements for ACTRIS Observational Platforms, https://www.actris.eu/sites/default/files/Documents/ACTRIS PPP/Deliverables/ACTRIS PPP_WP5_D5 1_Documentation on technical concepts and requirements for ACTRIS observational platforms.pdf (last access: 21 January 2023), 2018.

Wang, Y., Zheng, X., Dong, X., Xi, B., Wu, P., Logan, T., and Yung, Y. L.: Impacts of long-range transport of aerosols on marine-boundary-layer clouds in the eastern North Atlantic, Atmos. Chem. Phys., 20, 14741–14755, https://doi.org/10.5194/acp-20-14741-2020, 2020.

Wendisch, M., Macke, A., Ehrlich, A., Lüpkes, C., Mech, M., Chechin, D., Dethloff, K., Velasco, C. B., Bozem, H., Brückner, M., Clemen, H., Crewell, S., Donth, T., Dupuy, R., Ebell, K., Egerer, U., Engelmann, R., Engler, C., Eppers, O., Gehrmann, M., Gong, X., Gottschalk, M., Gourbeyre, C., Griesche, H., Hartmann, J., Hartmann, M., Heinold, B., Herber, A., Herrmann, H., Heygster, G., Hoor, P., Jafariserajehlou, S., Jäkel, E., Järvinen, E., Jourdan, O., Kästner, U., Kecorius, S., Knudsen, E. M., Köllner, F., Kretzschmar, J., Lelli, L., Leroy, D., Maturilli, M., Mei, L., Mertes, S., Mioche, G., Neuber, R., Nicolaus, M., Nomokonova, T., Notholt, J., Palm, M., van Pinxteren, M., Quaas, J., Richter, P., Ruiz-Donoso, E., Schäfer, M., Schmieder, K., Schnaiter, M., Schneider, J., Schwarzenböck, A., Seifert, P., Shupe, M. D., Siebert, H., Spreen, G., Stapf, J., Stratmann, F., Vogl, T., Welti, A., Wex, H., Wiedensohler, A., Zanatta, M., and Zeppenfeld, S.: The Arctic Cloud Puzzle: Using ACLOUD/PASCAL Multiplatform Observations to Unravel the Role of Clouds and Aerosol Particles in Arctic Amplification, B. Am. Meteorol. Soc., 100, 841–871, https://doi.org/10.1175/BAMS-D-18-0072.1, 2019.

Xue, Y., Wang, L., and Grabowski, W. W.: Growth of Cloud Droplets by Turbulent Collision–Coalescence, J. Atmos. Sci., 65, 331–356, https://doi.org/10.1175/2007JAS2406.1, 2008.

Zhao, C. F., Xie, S. C., Klein, S. A., Protat, A., Shupe, M. D., McFarlane, S. A., Comstock, J. M., Delanoe, J., Deng, M., Dunn, M., Hogan, R. J., Huang, D., Jensen, M. P., Mace, G. G., McCoy, R., O'Connor, E. J., Turner, D. D., and Wang, Z. E.: Toward understanding of differences in current cloud retrievals of ARM ground-based measurements, J. Geophys. Res.-Atmos., 117, D10206, https://doi.org/10.1029/2011jd016792, 2012.

ILMATIETEEN LAITOS
METEOROLOGISKA INSTITUTET
FINNISH METEOROLOGICAL INSTITUTE

FINNISH METEOROLOGICAL INSTITUTE
Erik Palménin aukio 1
P.O. Box 503
FI-00560 HELSINKI
tel. +358 29 539 1000
WWW.FMI.FI

FINNISH METEOROLOGICAL INSTITUTE
CONTRIBUTIONS No. 186
ISBN 978-952-336-170-6 (print)
ISBN 978-952-336-171-3 (online)
ISSN 0782-6117 (print)
ISSN 2814-5658 (online)
https://doi.org/10.35614/isbn.9789523361713

Helsinki 2023
Edita Prima Oy